Self-assembly of oligopyrenotides - from DNA to supramolecular polymers

Inauguraldissertation
der Philosophisch-naturwissenschaftlichen Fakultät
der Universität Bern

vorgelegt von

Nussbaumer Alina Laura
von Mümliswil-Ramiswil SO

Leiter der Arbeit:
Prof. Dr. Robert Häner
Departement für Chemie und Biochemie der Universität Bern

Self-assembly of oligopyrenotides - from DNA to supramolecular polymers

Inauguraldissertation
der Philosophisch-naturwissenschaftlichen Fakultät
der Universität Bern

vorgelegt von

Nussbaumer Alina Laura
von Mümliswil-Ramiswil SO

Leiter der Arbeit:
Prof. Dr. Robert Häner
Departement für Chemie und Biochemie der Universität Bern

Von der Philosophisch-naturwissenschaftlichen Fakultät angenommen.

Der Dekan

Bern, 23.3.2012

Prof. Dr. S. Decurtins

Für meine Eltern Anita und Christoph Nussbaumer-Wyler
und meine Grosseltern Annamarie und Toni Wyler-Gloor

labor vincit
omnia
alle besiegt
das Labor

Mani Matter

Acknowledgments

First of all I would like to thank Prof. Robert Häner for giving me the opportunity to work in his research group. I appreciated the interesting discussions during the last four years and his great support. With his guidance I have been able to acquire a diverse knowledge in DNA and supramolecular chemistry, as well as in teaching, presenting and writing.

Special thanks go to Prof. Markus Albrecht and Prof. Thomas Wandlowski having accepted to read and judge my PhD thesis and to give their expert opinion as a co-examinator and co-referee of my work.

Sincere thanks go to Dr. Vladimir Malinovskii for his support and the helpful discussions. Many thanks go to Dr. Oleg Khorev, who was always ready to help, if it was required. Thanks go to Dr. Daniel Studer for performing transmission electron microscopy measurements. I thank Ettore Castiglioni from the University of Brescia for performing LD experiments. I owe a lot to Dr. Alexander Rudnev from the group of Prof. Thomas Wandlowski for his valuable contribution to this work, doing AFM measurements. I am very thankful to Dr. Fabio Simona from the group of Prof. Michele Cascella for giving me an interesting insight in computational chemistry and for performing calculations.

Special thanks go to all the past and current members of the Häner group for the great time we spent together.

I am grateful to the staff of the Departement of Chemistry and Biochemistry of the University of Bern. I thank the team of the “Ausgabe”, the secretaries Rosmarie Rohner and Patricia Brunold, the “Werkstatt”, Rosa Herren, the library and many more for administrative and material concerns.

I am thankful to the group of Prof. Samuel Leutwyler for the coffee breaks full of inspiration. During the four last years I met many interesting and nice people from all over the world. I am very grateful for many happy times, we spent together.

I am very grateful to Alan Greiner and Anne Bürki for carefully reading my dissertation.

Last but not least I thank my family for their love and important support. I thank my grandfather Toni Wyler. In his laboratory I started to be interested in science.

Table of Contents:

Abstract 1

1. Introduction 3

1.1 DNA double helix – an example of strict self-assembly in nature 4

1.2 Supramolecular chemistry – self-assembly in synthetic chemistry 8

1.2.1 Supramolecular polymers 10

1.2.2 Mechanism for the formation of supramolecular polymers 14

1.3 Supramolecular chirality in artificial systems 16

1.3.1 Amplification of chirality 18

1.4 Templated self-assembly 20

1.2 References 24

2. Aim of the work 27

2.2 References 29

3. Amplification of chirality by supramolecular polymerization of pyrene oligomers

3.1 Abstract 30

3.2 Introduction 30

3.3 Results and Discussion 31

3.3.1 Synthesis 31

3.3.2 Influence of salt on the organization of pyrene oligomers 32

3.3.3 Amplification of chirality / Sergeant-and-Soldiers experiment 35

3.3.4 Kinetics of the formation of supramolecular polymers 40

3.3.5 Mechanism for the formation of supramolecular polymers 41

3.3.6 Sample preparation and formation of supramolecular polymers 42

3.3.7 Limits of the chiral information 43

3.3.6 Methods to characterize the formed long aggregates 44
3.4 Conclusions 46
3.5 Experimental part 46
3.5 References 51

4. Atomic force microscopy: A tool to study supramolecular polymerization

4.1 Abstract 55
4.2 Introduction 55
4.3 Results and discussion 57
4.3.1 Visualization of supramolecular polymers 57
4.3.2 Formation of supramolecular polymers 61
4.3.3 Cooperative and non-cooperative formation of polymers 63
4.4 Conclusions 64
4.5 Experimental part 65
4.6 References 66

5. Stereochemical control of supramolecular pyrene polymers

5.1 Abstract 67
5.2 Introduction 68
5.3 Results and Discussion 70
5.3.1 Cytidine modified oligomers 72
5.3.2 Guanosine modified oligomers 78
5.3.3 Thymidine modified oligomers 84
5.3.4 Adenosine modified oligomers 89
5.3.5 Supramolecular polymers 94
5.3.6 Helical chirality of polymers 95
5.3.7 Amplification of chirality 97
5.3.8 The effect of Watson-Crick complementary bases 100

5.4 Conclusions 105

5.5 Experimental part 106

5.6 References 109

6. Towards new DNA-based nanostructures connected via artificial sticky ends

6.1 Abstract 112

6.2 Introduction 112

6.3 Results and Discussion 114

6.4 Conclusions 124

6.5 Experimental part 124

6.6 References 128

7. Assembly of porphyrin ligands on oligopyrenotide helical scaffolds

7.1 Abstract 129

7.2 Introduction 129

7.3 Results and Discussion 131

7.4 Conclusions 140

7.5 Experimental part 141

7.6 References 143

8. Porphyrin derivatives –towards non-nucleosidic building block for the incorporation into DNA

8.1 Abstract 146

8.2 Introduction 146

8.3 Results and discussion 150

8.3.1 Synthesis of the non-nucleosidic building block 150

8.3.2 Spectroscopic studies of the new synthesized building blocks 155

8.3.3 Synthesis of oligonucleotides 156

8.3.4 Spectroscopic studies of oligomer 1 and 2 156

8.3.4 Synthesis of non-nucleosidic porphyrin building block with alkynyl linker 158

8.4 Conclusions 161

8.5 Experimental part 162

8.6 References 174

9. Conclusions 176

10. Outlook 178

11. Appendix

11.1 Abbreviations 180

11.2 CV 182

Abstract

For the construction of large, complex structures nature takes advantage of spontaneous self-assembly of units into intact machinery with highly sophisticated functions. Supramolecular chemistry is one field of chemistry which makes use of the power of self-assembly to design functional nanostructures, which are held together mainly through non-covalent interactions as, for example, hydrogen bonding, van der Waals forces, and $\pi-\pi$ interactions.

Due to the self-assembling into a defined double helix, DNA is one of the most prominent and exploited biological molecules, which is used to build multidimensional nanostructures and nanomaterials. Further, DNA can be used as a scaffold for the placement of functional molecules at defined positions. We are interested in exploring the limits of modifications and possible simplification of DNA. For the present research, we asked the basic questions whether oligomers of simple polyaromatic hydrocarbons linked by a phosphodiester backbone would assemble in defined and organized structures or nanomaterials.

In this thesis it will be shown, that oligomers of seven pyrene units connected *via* flexible phosphodiester linkers organize and assemble into supramolecular polymers. Furthermore strong amplification of chirality was observed by adding minute amounts of pyrene oligomers modified with a natural base thereby the helical sense of the polymers can be shifted to an *M*-helix or a *P*-helix. Depending on the nucleotide, the self-assembly of the pyrene oligomers can be switched from a cooperative to a non-cooperative mechanism (Scheme 1). Atomic force microscopy experiments confirmed the proposed model of supramolecular polymerization. This technique provides a fast and reliable tool to obtain structure information under various experimental conditions.

The designed artificial supramolecular polymers can serve as templates to organize additional functional molecules such as porphyrins, thereby allowing the formation of chiral supramolecular assemblies. The organization of cationic porphyrins on supramolecular oligopyrenotides show characteristics similar to poly-d(A-T). This and other findings highlight structural similarities between DNA and the presented supramolecular polymers.

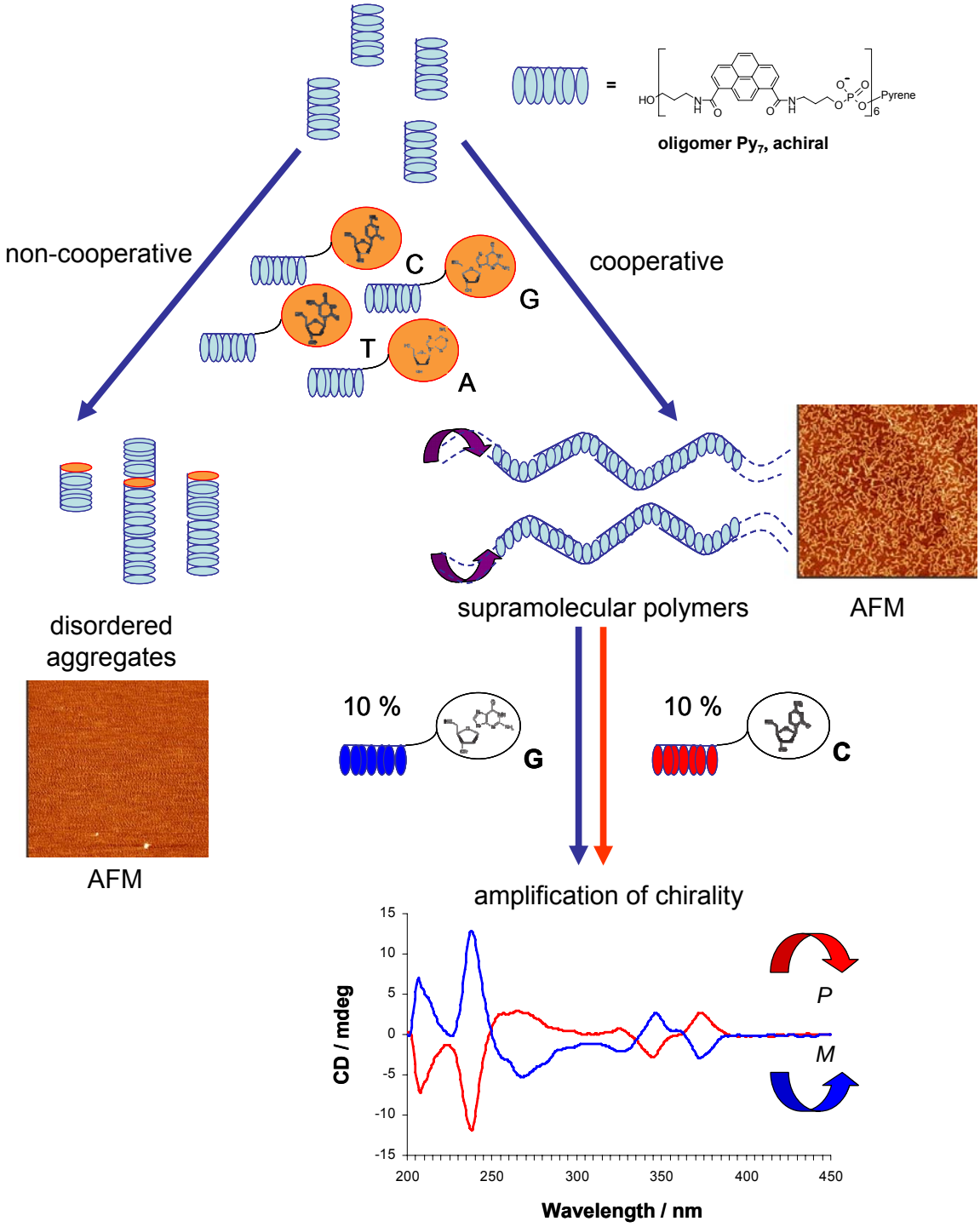

Scheme 1. Supramolecular polymerization of oligopyrenotides and the influence of a single nucleotide on their aggregation properties.

1. Introduction

The inspiration by nature and the desire to mimic it have long been driving forces in research, and are still motivating chemists, not only in the hope of further understanding biological systems and exploiting their elegant functions, but also for the designing of new compounds or structures, which can find applications in different areas including medicine, diagnostics and materials sciences.

One approach to the synthesis of new compounds or materials relies upon the stepwise formation of covalent bonds. However, such a process is burdened with several limitations when applied to the construction of large and complex molecules. [1]

To construct larger structures with more complexity, nature takes advantage of spontaneous self-assembly of units into intact machineries with highly sophisticated functions. Nature makes use of weak interactions between small molecules. Hydrogen bonds, van der Waals forces, $\pi-\pi$ interactions and hydrophobic interactions, govern the assembly of everything from protein and DNA folding, to the formation of protein aggregates and many more processes which are essential for life. [2] Therefore, the understanding of self-assembly is crucial to obtain insight into processes which take part in living systems. The spontaneous, and the reversible association of molecules to form larger, more complex entities according to the intrinsic information contained in the molecules themselves, are characteristics of self-assembly. [3]

Self-assembly is also emerging as a new strategy in chemical synthesis, with the potential of generating non-biological structures with complexity and new functions. The process of defined self-assembly leads to new possibilities in designing nanostructures with dimensions in the range of 1 to 100 nanometers. [4,5] The reversibility of the self-assembly process makes it possible to form systems with a thermodynamically most favourable structure and with the potential of self-repair and correction of defects, as in biological systems. [3]

In 1991 Lindsey introduced a definitive classification scheme for various types of self-assembly across biochemistry and chemistry. [6] Lindsay's scheme divides self-assembly into seven broad, overlapping classes. Here, two class of self-assembly are mentioned, which are important for this work:

Class 1: Strict Self-assembly. In this process the final product is produced spontaneously when the components are mixed together under a given set of conditions of temperature, pH, concentration, *etc*. The formation of the product is reversible and represents the thermodynamic minimum for the system. All the information necessary for the assembly to occur is coded into the constituent parts.
Class 6: Directed self-assembly or templated self-assembly. In these processes a template is involved, whether or not it ends up in the final structure. [3,6]

1.1 DNA double helix – an example of strict self-assembly in nature

A famous example of a strict self-assembly process is the formation of a DNA double helix, by the spontaneous association of two single strands. (Figure 1). The self-assembly is a cooperative interplay process of hydrogen bonding, π- stacking, electrostatic and hydrophobic interactions controlled by precise basepairing rules (complementary nucleobase pairs guanosine/cytidine and adenosine/thymidine). The assembly into a DNA double helix is a two stage process consisting firstly of a nucleation phase followed by a cascade propagation sequence. [3,7]

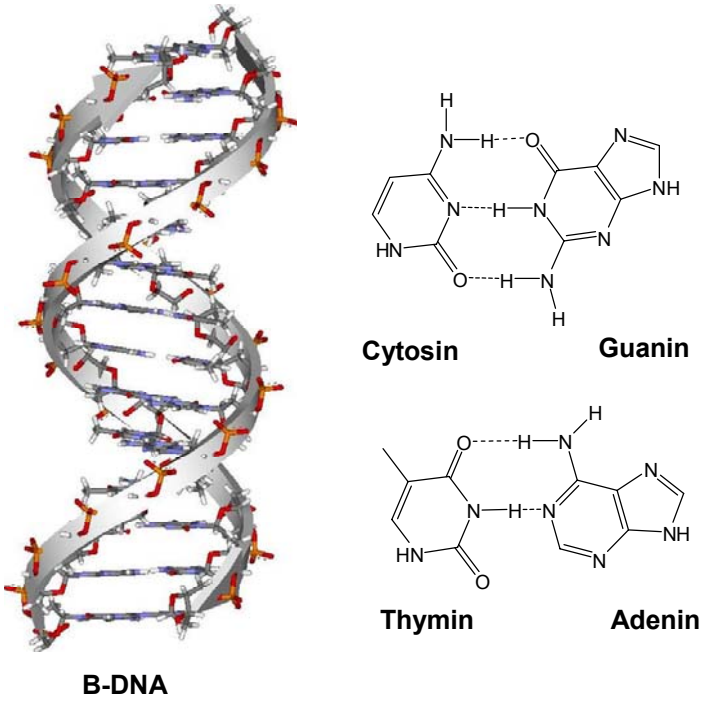

Figure 1. Structure of B-DNA and the complementary nucleobase pairs.

Due to the self-assembling properties of DNA and the different controlling interactions, DNA is one of the most prominent and exploited biological molecules, which is used to build multidimensional nanostructures and nanomaterials. [8,9,10]

A number of basic structural motifs have been designed to convert DNA molecules into 2D and 3D structures (Figure 2). By assembling four DNA strands into four-way junctions with single-stranded “sticky ends” at the periphery for hybridization, it was possible to create geometric objects (**2A**). For more rigid structures DNA doublecrossover motifs were introduced, which contain two double helices connected to each other twice through crossover points (**2B**). [11,12] Planar tiles are formed from several parallel helices joined by crossover junctions and were used to synthesize, for example, DNA nanotubes (**2C**). [13] In a DNA origami a single continous strand of DNA is systematically folded using smaller strands, “stapling strands” (**2D**). [14]

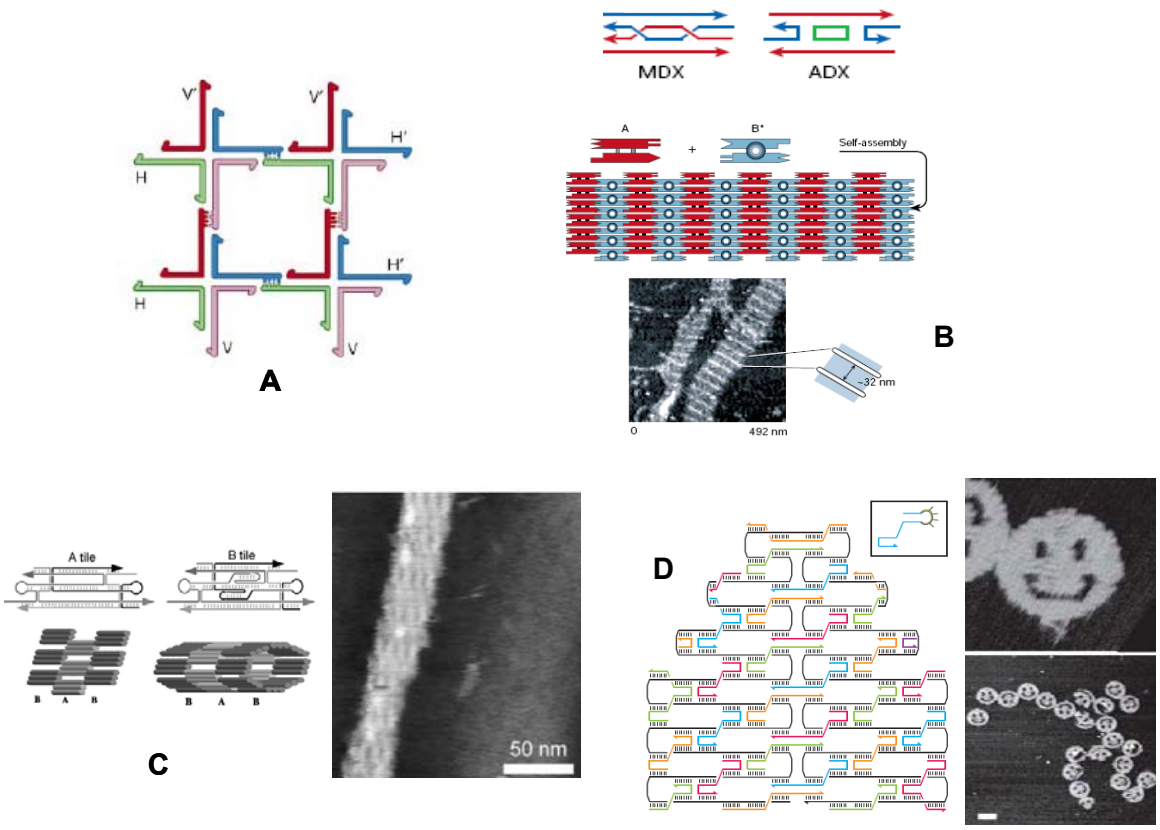

Figure 2. (**A**) Four-way junctions with sticky ends, [11,12] (**B**) DNA doublecrossover motif, [11,12] (**C**) planar tiles motif, [13] (**D**) DNA origami. [14]

The designed two-dimensional DNA structures provide the opportunity to template the positioning of materials like nanoparticles or even proteins. [7]

Further, DNA can be used as a scaffold for the placement of functional molecules at defined positions. The defined DNA double helix allows the construction of distinct molecular architectures with defined size and shape. Multimeric complexes and organized arrays of chromophores exhibit properties which differ significantly from those of the individual or unordered monomers. [15] Designed DNA/chromophores assembly can lead to novel materials and diagnostic tools.

Different strategies to attach chromophores to the DNA scaffold have been explored. Here only some selected examples are shown to illustrate the different approaches for attaching functional molecules (Figure 3). One strategy is the postsynthetic modification of DNA, in which a functional group of the label reacts with the complementary functional group on the DNA. For example, click chemistry for the postsynthetic modification of oligonucleotides with porphyrin molecules via the copper (I)-catalysed Huisgen 1,3-dipolar cycloaddition, has been used recently (**3A**). [16] In another approach a porphyrin-maleimide was reacted with a thiol group, which was introduced into DNA, to give conjugate **3B**.[17]

A second strategy is the incorporation of chromophores during the oligonucleotide synthesis. It leads to several possibilities concerning the number and placement of the functional molecules. For example, artificial molecules can be attached at the base, the sugar moiety or the base can be replaced completely.[15]

Example **3C** shows RNA, which is modified at the 2′-*O*-sugar residues with up to 5 pyrene moieties in one strand.[18] In example **3D**, functional molecules like pyrene and phenothiazine have been covalently attached to the 5-position of uridines. Optical properties of DNA duplexes that have been functionalized by five adjacent chromophores with mixed sequences are presented. [19]

An additional approach is the complete replacement of the nucleobase with different chromophores, for example with biphenyl and bipyridyl **3E** [20] or with pyrene and perylene **3F** [21].

Chromophores, which are nor attached at the base nor at the sugar moiety are non-nucleosidic building blocks, which can be incorporated during the oligonucleotide synthesis. In example **3G** the authors describe the incorporation of several methyl red dyes as a nucleoside analogs into DNA.[22]

Pyrene is an additional example, which was used as nucleoside analogs **3H**. Here the pyrene building block is connected via a trihydroxypropyl linker. [23]

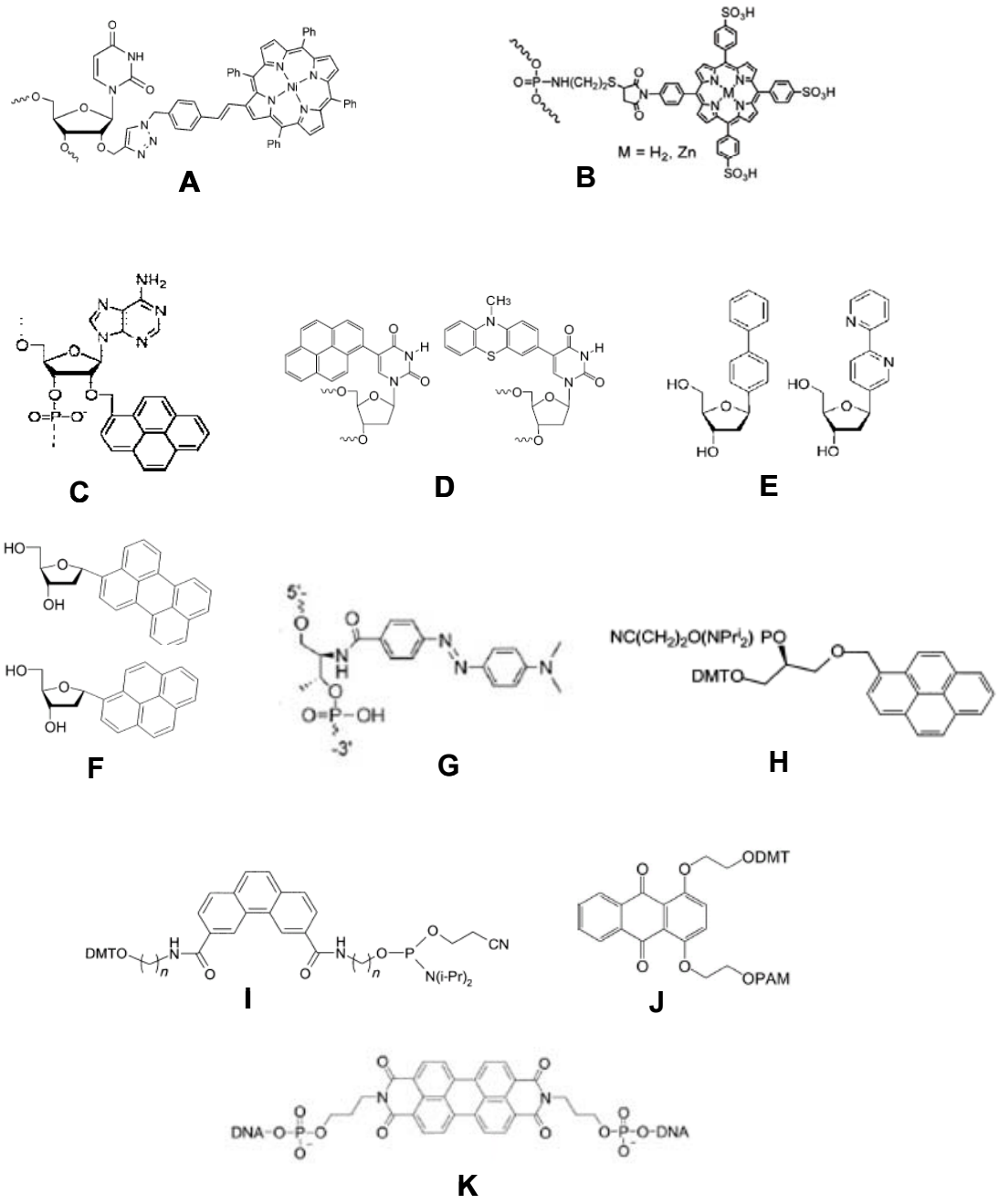

Figure 3. Selected examples of chromophore/DNA conjugates: **A** [16], **B** [17], **C** [18], **D** [19], **E** [20], **F** [21], **G** [22], **H** [23], **I**[24], **J**[25], and **K**[26].

The incorporation of non-nucleosidic building blocks into a DNA scaffold, and the application of these modified nucleic acids in diagnostics and in materials science, is as well one of the research interests of the Häner group. Functional molecules as, for example, phenanthrene **3I** [24], anthraquinone **3J** [25], perylene diimide **3K** [26] have been incorporated using standard oligonucleotide synthesis.
All these different types of modification have in common that the precise control over the association and structural organization of the synthesized functional molecules lies in the nature of DNA and is directed through the formation of a double helix.

1.2 Supramolecular chemistry – self-assembly in synthetic chemistry

Supramolecular chemistry is the branch of chemistry associated with the study of complex molecular systems formed from several discrete chemical components. While the individual blocks contain strong covalent bonds, the multicomponent aggregate is likely to be held together by weaker non-covalent interactions. [27] Hydrogen bonding, van der Waals forces, π-π interactions, hydrophobic effects, and ion-ion interactions are examples of non-covalent interactions used in supramolecular chemistry. Due to these reversible interactions the structures may dissociate and reform in response to different stimuli like temperature, pH, solvent, *etc*. The self-assembly of these components gives rise to new entities with different properties that often behave in novel and unexpected ways. [27,28]
The origin of the expression “supramolecular” can be traced back to the beginning of the 20th century. In 1909, in the *Century dictionary*, it was defined as: *“Composed of an aggregation of molecules; of greater complexity than the molecule.”* Even though this expression and concept was used afterwards by other scientists, supramolecular chemistry gained a wider scientific currency following the award of the 1987 Nobel Prize in chemistry to Donald Cram, Jean-Marie Lehn and Charles Pederson for their “*development and use of molecules with structure-specific interactions of high selectivity*”. The definition of supramolecular chemistry Lehn gave in his Nobel Lecture was: ”*the chemistry beyond the molecule bearing on the organized entities of higher complexity that result from the association of two or more chemical species held together by intermolecular forces.*” [27,28]

Many examples of supramolecular phenomena can be found in the chemistry of life. Supramolecular chemical principles like molecular recognition, self-assembly and self-organization, are inspired by the reversible, highly specific, intermolecular processes in nature. In supramolecular chemistry different approaches exist to mimic biological systems for example enzymes, which have specific binding sites for their substrates to covert them catalytically to other molecules. The creation of artificial membranes and transmembrane channels, as well micelles, is another important task in supramolecular chemistry (Scheme 1). [27]

Jean-Marie Lehn devided supramolecular objects into two broad, partially overlapping classes: (1) Supermolecules, which are well-defined oligomolecular species resulting from specific intermolecular association of a few components. This involves host-guest chemistry, helicates and catenanes, rotaxanes. (2) Supramolecular assemblies, which are formed by the spontaneous self-assembly and self-organization of a large number of components into a large architecture having more or less well-defined microscopic organization and macroscopic characteristics depending on its nature. Films, layers, membranes, vesicles, micelles, gels, solids, liquid crystals, supramolecular polymers, *etc*. are part of the second class. [28, 29]

These systems with well-defined functional architectures give access to advanced supramolecular materials and provide an approach to nanoscience and nanotechnology.

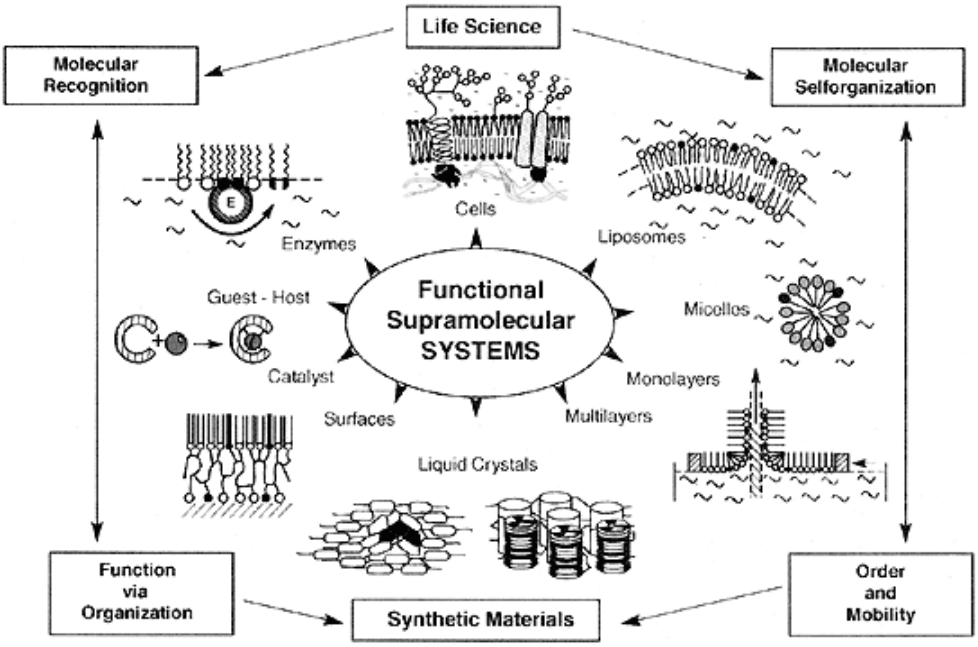

Figure 4. Functional supramolecular systems in nature and as synthetic materials. [30]

1.2.1 Supramolecular polymers

Supramolecular polymers form the most recent branch in supramolecular chemistry. In the last two decades, the topic of supramolecular polymers has rapidly developed into a separate field of research that has promising prospects for the development of new materials. Supramolecular polymers are dynamic polymeric arrays of monomer units, held together by noncovalent interactions. Principally, the spontaneous self-association of monomeric units towards the formation of polymeric structures may appear as a reversible or irreversible process, depending on conditions such as concentrations of monomers, temperature, pH, solvent polarity, ionic strength, etc. This results in materials that are able to respond to external stimuli in a way that is not possible for traditional macromolecules. Importantly, non-covalent synthesis allows creating nanostructures without defects under reversible conditions, due to self-healing or self-sorting effects. [31, 32, 33, 34]

Several examples can be found using hydrogen bonding interactions owing to their moderate strength, selectivity and directionality. To increase the strength of the interactions, systems with multiple hydrogen bonds in row, which act in a cooperative way, were designed. Here some selected examples of supramolecular polymers are presented for illustration.

The group of Lehn found a system based on difunctional diaminopyridines and difunctional uracil derivatives, which form supramolecular polymers by triple hydrogen bonding (**5A**) (Figure 5). The described system exhibits liquid crystallinity. [28, 32]

In recent work performed by Meijer and co-workers, 2-ureido-4-pyrimidone units that dimerize strongly in a self-complementary array of four cooperative hydrogen bonds, were used as the associating end group in reversible self-assembling polymer systems. The molar mass of these polymers was found to be very high as a result of self-complementarity, the lack of side reaction during polymerization, and the high dimerization constant. The reversibilty of this system makes the control over properties, such as viscosity, chain length, and composition by temperature, solvents or the addition of monofunctional compounds tunable (**5B**). [32, 34, 35] Example **5C**, from the laboratory of Meijer, is a π-conjugated oligo(p-phenylene vinylene) using ureido-s-triazine to form dimers through, again, complementary hydrogen bonding. They assemble to helical stacks in apolar medium. [36, 37]

Another interesting example based on hydrogen bonding was developed by the group of Rebek Jr. They used the hydrogen bonding between urea functionalized calixarenes to form supramolecular polymers.[38] These calixarenes are known to form very stable dimeric capsules which bind solvent molecules inside the cavity. The association of bifunctional molecules consisting of two covalently connected calixarene moieties results in the formation of polycaps. In addition to the hydrogen bonding, the supramolecular polymerization occurs via the encapsulation of a small guest molecule as, for example, benzene (**5D**). [32, 34, 38]

Gotarelli and Spada et al. used the G-quartet as the basic unit to form helical columns/ polymer structures (**5E**). In addition to to the hydrogen bonding within the G-quartets, the columnar stacks were stabilized by the addition of potassium ions, which bind to the inner carbonyl groups of the stacks. [39]

Other examples make use of the $\pi-\pi$ aromatic stacking. Units with an aromatic system as a core tend to aggregate in either polar or apolar solvents into rod-like or worm-like polymers. Additionally, hydrogen bonding can occure in those systems to compensate the lack of directionality in aromatic stacking interactions.

Nonracemic helicene has been shown to form supramolecular polymers, and the helical shape of their rigid cores renders these columns helical (**5F**). [32, 40]

Meijer et al. repoted that C_3-symmetrical disk-shaped molecules form polymeric structures through π-π stacking interactions together with hydrogen bonding in water [41] and polar solvents, as well in apolar solvents (**5G**). [32]

The next example shows that polymer-like structures can assemble as a next step into higher order assemblies like nanotubes. Fukushima and Aida et al. reported that an achiral amphiphilic hexa-*peri*-hexabenzocoronene self-assembles into a helical coil and further into nanotubes (**5H**). [42]

The last example is a phthalocyanine derivative bearing four crown ether moieties with optical active tails. They assemble into long columns driven by π-π stacking interactions in chloroform, resulting in fibers. The fibers can further assemble in superhelices. The helicity of these aggregates can be turned off by the addition of potassium salt, which interacts with the crown ether rings. The fibers stay intact (**5I**). [43]

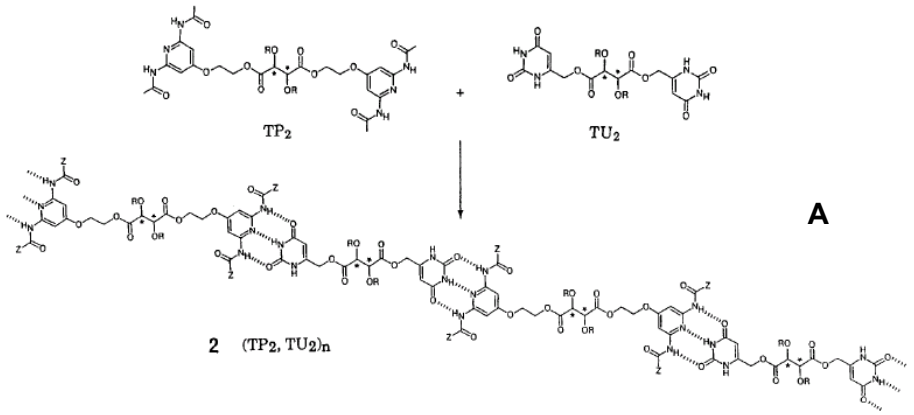
TP2
TU2
2 (TP2, TU2)n

A

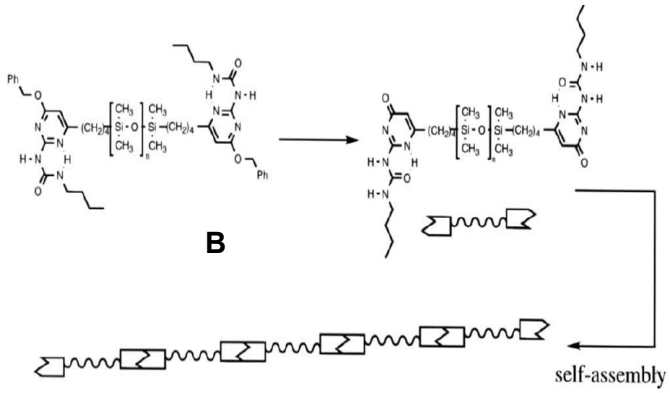
self-assembly

B

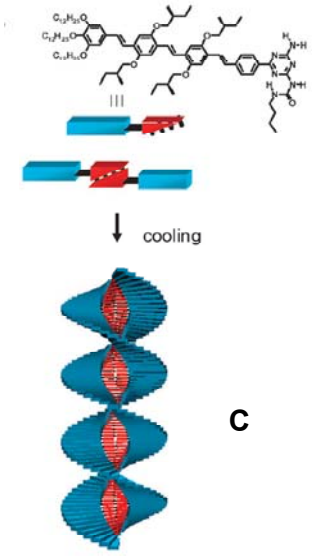
cooling

C

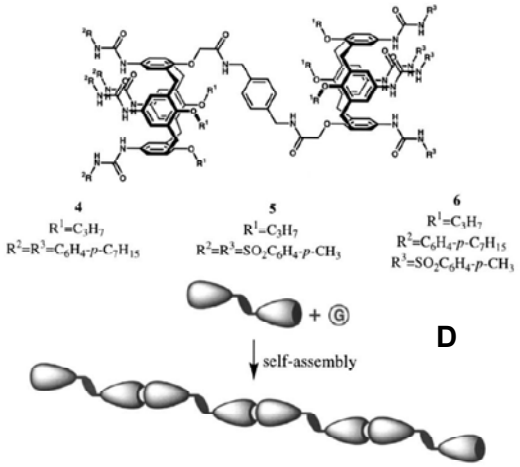
4
R1=C3H7
R2=R3=C6H4-p-C7H15
5
R1=C3H7
R2=R3=SO2C6H4-p-CH3
6
R1=C3H7
R2=C6H4-p-C7H15
R3=SO2C6H4-p-CH3
+ G
self-assembly

D

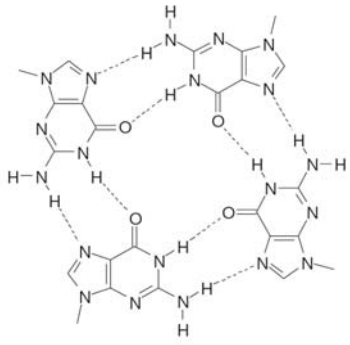

E

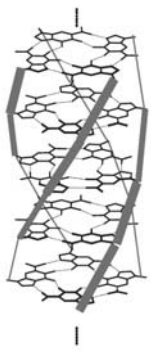

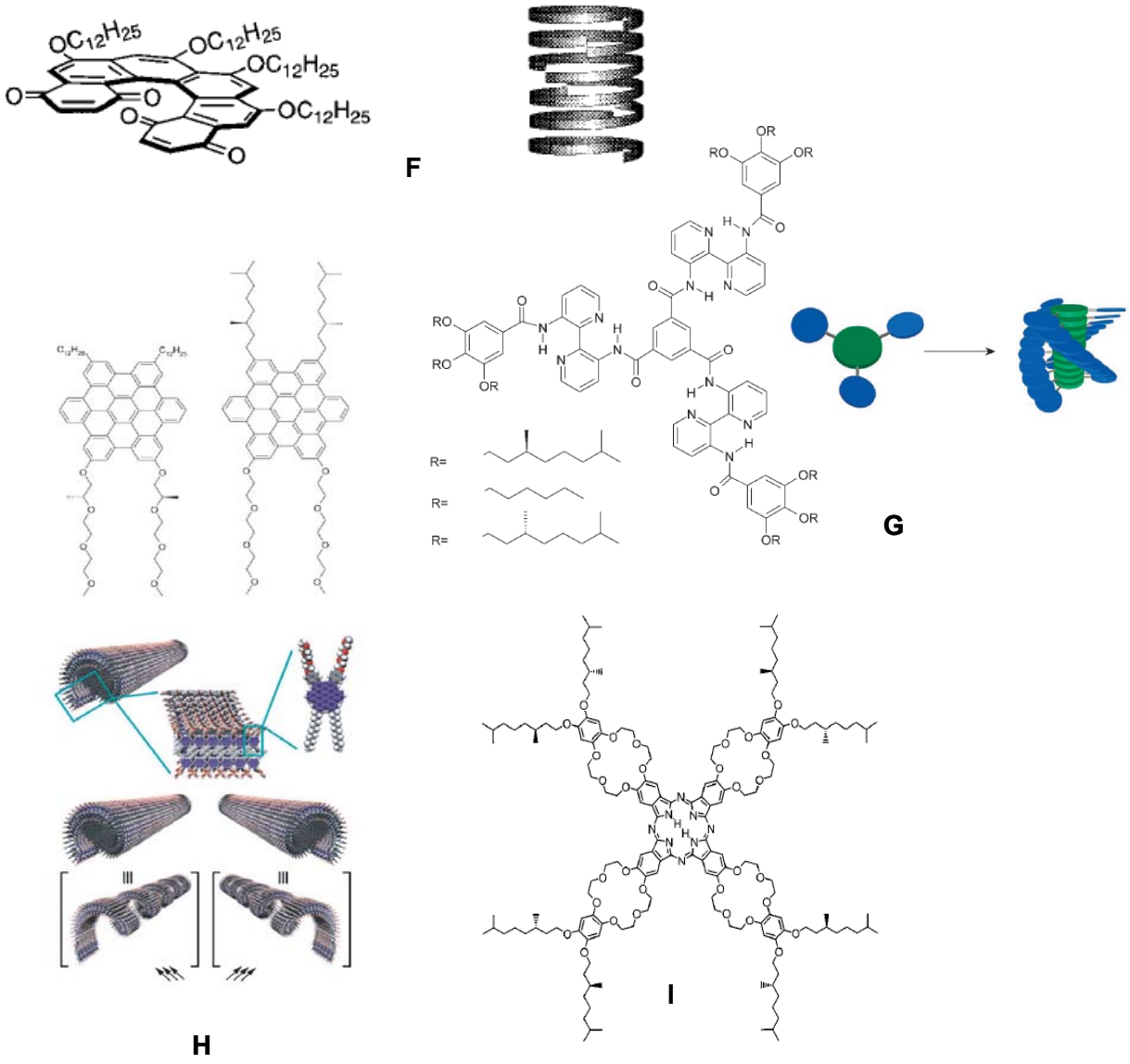

Figure 5. Several selected examples of structures forming supramolecular polymers: (**A**)difunctional diaminopyridines and difunctional uracil derivatives forming hydrogen bonds [28] (**B**) 2-ureido-4-pyrimidone motif [35] (**C**) oligo(p-phenylene vinylene) modified with ureido-s-triazine [37] (**D**) urea functionalized calixarenes [38] (**E**) G-quartet [39] (**F**) helicene [40] (**G**) C_3-symmetrical disk-shaped molecules [32] (**H**) hexa-*peri*-hexabenzocoronene [42] (**I**) phthalocyanine derivative [43].

Despite their short history, supramolecular polymers are already beginning to find commercial use and applications. They can have interesting mechanical properties, like the supramolecular polymers created with the ureidopyrimidone (**5B**) unit. These supramolecular polymers find applications as superglues, hotmelts and novel thermoplastic elastomers. [32]

The graphitic nanotubes (**5H**) described by Fukushima and Aida et al. are redox active and show, upon oxidation, an electrical conductivity. Due to the electonic properties, this system can find applications in supramolecular electronics. [42]

1.2.2 Mechanism for the formation of supramolecular polymers

There are three main growth mechanisms for supramolecular polymerization, namely isodesmic, ring-chain, and cooperative grows.

The first described mechanism, the **isodesmic growth**, is represented by the reversible formation of a single noncovalent bond. In this model, it is assumed that any monomer addition to another monomer or a polymer occurs with the same free energy changes. Thus, interaction is *identical* at any step of the polymerization process and is characterized by a single binding constant (K) during the assembly pathway. The reaction is non-cooperative. [44, 45]

An example for isodesmic growth can be found in the system developed by Rebek Jr. et al. (**5D**) (Figure 5), which is based on the encapsulation of guest molecules by calixarene moieties. In chloroform, polymeric structures were formed by encapsulation of solvent molecules. Upon addition of *p*-difluorobenzene, the encapsulated solvent was replaced by the guest molecule due to the higher association constant and the polymeric porperty was maintained. Addition of dimeric capsules showed depolymerization of the supramolecular polymer and the formation of discrete oligomeric complexes. This could be confirmed by NMR spectroscopy. [46]

From early investigations with protein polymers, it was noted that in this case polymerization doesn't follow the same characteristics as in an isodesmic growth model. Here it was found that polymerization takes place only above a critical total concentration. The polymer coexists in an equilibrium with a significant amount of monomer that remain in the solution. Once the polymer is formed, its molecular weight is

rather large, even the total concentration is near the critical value. By further increasing the total concentration, only the polymer concentration increases, while the concentration of monomer units stays constant. Another model was postulated, the **nucleation-elongation** polymerization, which occurs in a cooperative way. The first step is the formation of a nucleus, which is energetically less favored. It is followed by the elongation step, which is characteristic by a sharp transition upon cooling. [44, 45]

An example is the supramolecular polymerization of the oligo(p-phenylenevinylene) (**5C**) derivatives, which was studied in more detail by Meijer et al. It was found that the self-assembly into helical fibrillar structures followed clearly a nucleation-growth pathway. A clear transition from monomers into helical aggregates was observed by optical techniques upon slow cooling. [47]

The third mechanism is the **ring-chain supramolecular polymerization** process. They are characterized by the fact that linear oligomers and polymers are in equilibrium with their cyclic counterpart. Here we will concentrate on the first two described mechanism (Figure 6). [44, 45]

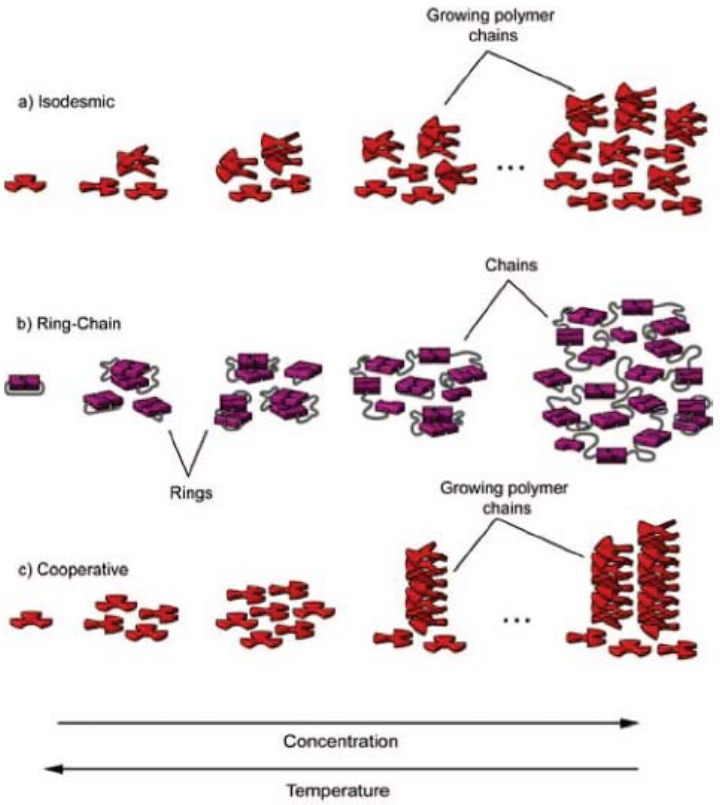

Figure 6. Schematic presentation of the three main growth mechanisms for supramolecular polymers. [45]

1.3 Supramolecular chirality in artificial systems

The term chirality originates from the Greek *hkeir*, which means *hand* and describes objects that exist as a pair of non-superimposable mirror images, which are called enantiomers.

In configurational chirality, the chirality arises directly from the arrangement of the covalent structure of the molecule. Point chirality, which is considered as the most fundamental form, originates from the different substituents bonded three dimensionally to a central atom, the chiral center. In case there are *n* chiral centeres in a molecule, 2^n stereoisomers are possible. Stereisomers, which are not mirror images of one another, are called diastereomers. [48]

Not only covalently bonded molecules with defined configuration and conformation, but also noncovalently interacting supramolecular assemblies with the properties of conformational flexibilities, reversibility, self-correction and self-recognition, can form chiral structures or architectures. [49,50]

Supramolecular chirality arises from the rearrangement of part or all of the assembly which cancel from it any elements of symmetry of second order. Supramolecular chirality may occur via (**A**) diastereoselective aggregation, which regards the self-assembly of chiral units with stereogenic centers. When those chiral components associate, a structure of higher degree of asymmetry is formed, leading to diastereomeric structures. (**B**) A second approach is based on the aggregation of achiral building blocks, where only racemic enatiomeric assemblies are possible. An imbalance can be induced through a chiral inductor and asymmetric information transfer. (**C**) The chirality memory effect is the third case leading to chiral aggregates. It has the advantage of creating a chiral supramolecular enantioriched structure by adding a chiral building block to the racemic enantiomeric starting mixture. Because of the slow kinetics of association and dissociation of the assembly, the chiral templating components can be replaced by achiral ones without changing the chirality level of the supramolecular system. It must be mentioned that these systems are not under thermodynamic control and can racemize slowly by means of reassembly. [50]

Approach (**A**) and (**C**) can be demonstrated with the system found by Reinhoudt and co-workers (Figure 7). [51] It was shown that calix[4]arene dimelamines mixed either with barbiturates or with cyanurates in a 1:2 ratio in apolar solvents such as chloroform,

toluene, or benzene, form double rosette assemblies. In principle, the assemblies can exist in three different isomeric forms: with D_3, C_{3h}, or C_3 symmetry. The D_3-symmetry exists as a pair of enantiomers. Chiral centers present either in the dimelamine components of calix[4]arene or the cyanurate components can induce diastereomerically pure structures.

Further it was found that the described system has a chiral memory effect. The substitution of chiral barbiturates with achiral cyanurates shows still very intense CD spectra, which can be explained by the fact that the assembly has preserved the chiral information. The half-life to racemization is more than four days at room temperature. [52]

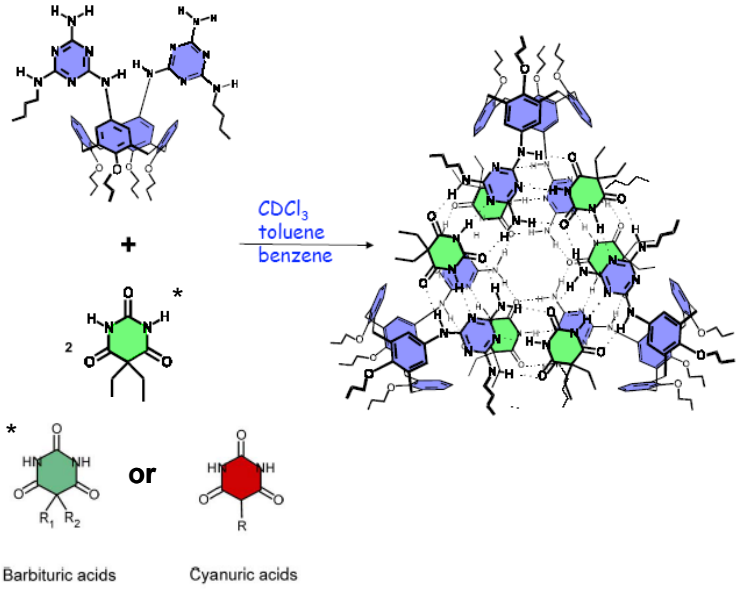

Figure 7. Calix[4]arene-based double-rosette assemblies. [51]

(**D**) Entrapment of chiral guests within self-assembled capsules provides a fourth method for the design of chiral supramolecular aggregates. Inouye et al. found that synthetic polymers, poly-and oligo(*meta*-ethynylpyridine)s, are guided to helical structures by hydrogen-bonding interactions with the encapsulated saccharide guest. CD studies revealed that chirality was transferred to the helical sense of the polymers. [53]

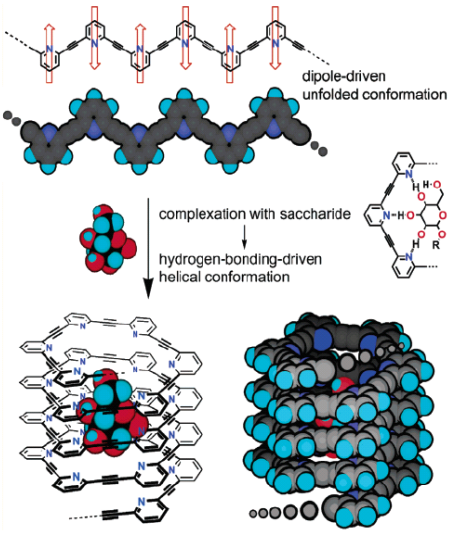

Figure 8. Conformation change of poly(*meta*-ethynylpyridine) driven by the complexation with saccharide. [53]

Helical chirality can be found many times in nature, for example in DNA, α-helix of proteins, and polysaccharides, as well as in synthetic systems like oligomers, polymers and nonplanar single molecules like helicenes. Here, the chirality arises from the unidirectional nature of the twist propagation along the long axis of the molecules or assembly. There is no need for point-chiral centers or chiral building blocks; cases where the extended molecules are achiral can occur. In this case the corresponding racemization equilibrium can be shifted toward one particular enantiomer by external chiral influences. [49]

The most common technique for examining chiral systems is CD-spectroscopy. It is generally accepted that a positive Cotton effect in the CD spectra (coming from the low energy wavelength) reveals a positive chirality (*P*), and a negative Cotton effect corresponds to a negative chirality (*M*). [49]

1.3.1 Amplification of chirality

Chiral amplification is a unique process from which a small chiral bias is significantly enhanced through cooperating units. This phenomenon is interesting in connection with the origin of biomolecular homochirality in nature, and for the development of methods to

produce optically active compounds. [36] Amplification of chirality is a phenomenon which was discovered by the pioneering work by Mark Green and co-workers studying polyisocyanates, a class of polymers. Polyisocyanates adopt a helical conformation without a preference for helical sense. The dynamic polymers are composed of right- and left-handed helical conformations separated by helical reversals. [54, 55, 56]

The polyisocyanates were made optically active by a single stereospecific deuteration at the α or β position of the side chain (Figure 9), leading to a large circular dichroism spectrum, which is caused by a large excess of one helical sense. [57]

It is interesting that copolymerization of chiral monomers in poly(n-hexylisocyanate) led to the observation that only minute amounts of chiral seed compound were required to change the equilibrium and render the polymer homochiral. [57]

Mixing enatiomeric monomers in different ratios created polyisocyanates, whose optical activity showed nonlinear effects that were dependent on the enantiomeric excess. [57]

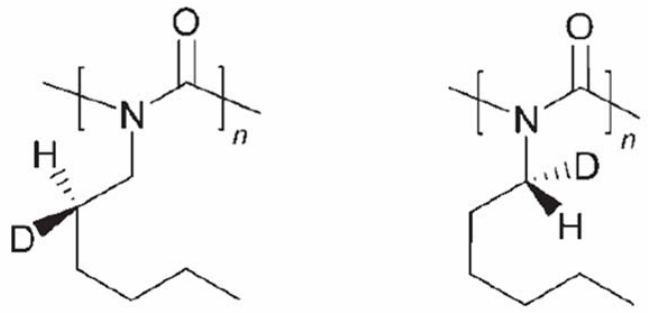

Figure 9. Structural formulas of specifically deuterated poly(n-hexylisocyanate). [51]

The two observed effects mentioned, which influence amplification of chirality, are referred to as the “sergeants-and-soldiers” principle and the “majority-rules” principle. The “sergeants-and-soldiers” principle implies a control of the helicity of large numbers of cooperative achiral units (the soldiers) by a few chiral units (the sergants). In the “majority-rules” principle a slight excess of one enatiomer leads to a strong bias toward the helicity of that enantiomer. [54, 55, 56, 57]

Not only in covalently linked polymers, but also in noncovalent supramolecular assemblies, amplification of chirality is observed and many examples can be found. [57]

The C_3-symmetrical disk-shaped molecules designed by Meijer and co-workers showe strong amplification of chirality (**5G**) (Figure 5).The disk-shaped molecules are modified with long aliphatic chains on the periphery, either with a chiral center or not. “Sergeants-and-soldiers” experiments as well as majority-rules experiments showed nonlinear response of the CD effect. [57]

Within the assembly of hexa-*peri*-hexabenzocoronene (**5H**) (Figure 5) into nanotubes, amplification of chirality was observed as well. It was found that the stereocenter should be located in the oligo(ethylene oxide) side chain and not in the alkyl substituents to show a preference for one of the two helicities. [57]

1.4 Templated self-assembly

Due to its well defined and organized structure, DNA finds application as a template for organizing ligands in a controlled manner. It can lead to chiral supramolecular assemblies.

For example, Armitage et al. [58] described the assembly of cationic cyanine dyes into helical supramolecular polymers using DNA as a template.

Among the different ligands, cationic porphyrins are probably belonging to the most studied molecules, which have been exploited in the context with DNA and its use as a template. In this section the interaction of porphyrin as a ligand with the DNA scaffold is desribed in more detail.

In 1979 it was discovered by Fiel and co-workers [59] that porphyrins are capable of intercalating to DNA.

The main observations were: (1) the stabilization of the DNA double helix against thermal denaturation; (2) A hypochromic effect in the absorption spectra was observed for DNA and in the Soret band of porphyrin; (3) The increase of viscosity reflected an icrease of the chain length of DNA; (4) further, it was observed that the binding of the porphyrin results in an unwinding of DNA, and, (5), also induced circular dichroism features were observed. X-ray structures revealed that the phenyl groups of the porphyrin are nearly perpendicular to the plane of the porphyrin ring and thus might be expected to provide steric hindrance for intercalation. It was clear that further studies

about the interaction of porphyrin to DNA would provide interesting information about the flexibility and structure of DNA. [59]

Studies carried out by Pasternack et al. [60, 61, 62, 63] using cationic porphyrins, but also metalloporphyrins, helped to clarify the binding mode to DNA. The findings were confirmed by many other research groups using additional techniques. For example, nuclear magnetic resonance was used by Marzilli and co-workers. [64] Kelly at al. [65] demonstrated by fluorescence and topoisomerase studies the differences between binding modes.

It was shown that tetrakis(4-N-methyl-pyridyl)porphine (H_2TMPyP) and its metal derivatives interact differently with GC regions of DNA than with AT regions. Specifically, porphyrins can intercalate in GC regions, whereas at AT regions they either partially intercalate or bind in the outside or groove binding mode (Figure 10).

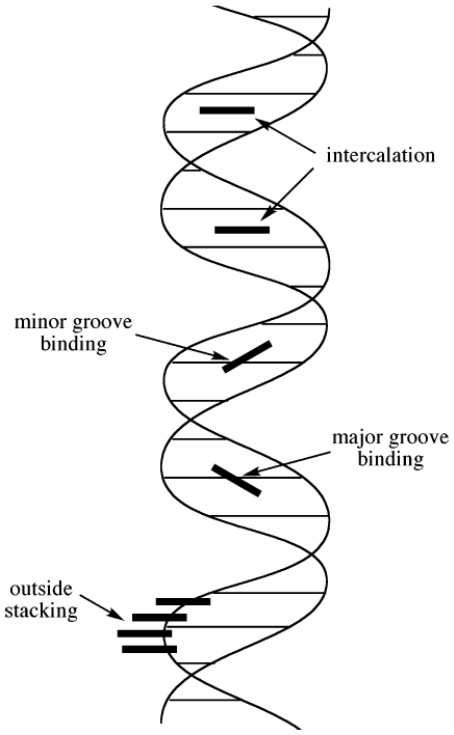

Figure 10. Illustration of different porphyrin-DNA interactions or binding modes. [49]

Table 1. Spectroscopic features of intercalation and outside binding mode of porphyrin-DNA interactions: [60, 61, 62, 63, 65]

	Intercalation	Outside binding
Absorbance (λ_{max}, nm)	Large bathochromic shifts of the Soret band (>15 nm)	Small red shifts (<8 nm)
H (%)	>35%	small hypochromism
$\Delta\varepsilon$ at Soret band ($M^{-1}cm^{-1}$)	Negative CD signal	Positive CD-signal
Fluorescence (λ_{max}, nm)	655 and 715 nm	669 and 730 nm
preferred DNA sequence	GC	AT

Additionally, a third binding mode was described, which is the outside binding with self-stacking on a DNA surface, using the DNA as a template for the organized helical assembly. Because self-stacking can change with the various conditions such as salt and the ratio of porphyrin to the DNA, simple spectral signatures are difficult to define and categorize. [66]

The type of interaction with DNA depends on the nature of the interacting porphyrin. Those porphyrins without axial ligands, such as the metal free, copper(II) and nickel(II) derivatives, intercalate into DNA. The metalloporphyrins which maintain axial ligands such as Fe(III), Co(III), Mn(III) and Zn(II) do not intercalate, because the axial ligands prevent the porphyrins from inserting between closely stacked base pairs. Furthermore porphyrins, like tetrakis(2-N-methylpyridyl)porphine, with a very large barrier to rotate the peripheral N-methyl pyridine, do not intercalate as well. [60, 61, 67]

Since the postulation of the different binding modes, the interaction of porphyrins with DNA is still under investigation by many research groups.

Porphyrins, in addition to their chemical and photochemical properties, have been known to accumulate spontaneously in malignancies. Photodynamic treatment is an example; it is used for the treatment of several types of cancer, taking advantage of both porphyrin

accumulation and photosensitization properties. [68] In general, photocleavage of DNA prompted by porphyrin has received considerable attention. [69] Further, the production of chiral supramolecular assemblies is of interest in order to design new nanomaterials. [46]

1.2 References

[1] D.S. Lawrence, T.Jiang, M. Levett, *Chem.Rev.***1995**, *95*, 2229-2260.

[2] R.F Service, *Science* **2005**, *309*, 95.

[3] J.W. Steed, J.L Atwood, *Supramolecular Chemistry*, John Wiley&Sons, **2009**.

[4] G.M. Whitesides, J. P. Mathias, C. T. Seto, *Science* **1991**, *254*, 1312-1319.

[5] G.M. Whitesides, B. Grzybowski, *Science* **2002**, *295*, 2418-2421.

[6] J.S. Lindsey, *New J. Chem*. **1991**, *15*, 153-180.

[7] F.A. Aldaye, A.L. Palmer, H.F. Sleiman, *Science* **2008**, *321*, 1795-1799.

[8] F.A. Aldaye, H.F. Sleiman, *Pure Appl.Chem.* **2009**, *81*, 2157-2181.

[9] Y.H. Roh, R.C.H. Ruiz, S. Peng, J.B. Lee, D. Luo, *Chem.Soc.Rev* **2011**.

[10] M.Endo, H. Sugiyama, *ChemBioChem* **2009**, *10*, 2420-2443.

[11] N.C. Seeman, *Nature* **2003**, *421*, 427-431.

[12] N.C. Seeman, A.M. Belcher, *PNAS* **2002**, *99*, 6451-6455.

[13] D.Liu, S.H. Park, J.H. Reif, T.H. LaBean, *PNAS* **2004**, *101*, 717-722.

[14] P.W.K. Rothemund, *Nature* **2006**, *440*, 297-302.

[15] V. L. Malinovskii, D. Wenger, R. Häner, *Chem.Soc.Rev.* **2010**, *39*, 410-422.

[16] A.W.I. Stephenson, N. Bomholt, A.C. Partridge, V. V. Filichev, *ChemBioChem* **2010**, *11*, 1833-1839.

[17] M. Endo, M. Fujitsuka, T. Majima, *J.Org.Chem.* **2008**, *73*, 1106-1112.

[18] M. Nakamura, Y. Murakami, K. Sasa, H. Hayashi, K. Yamana, *JACS* **2008**, *130*, 6904–6905.

[19] E. Mayer-Enthart, C. Wagner, J. Barbaric, H.-A. Wagenknecht, *Tetrahedron* **2007**, *63*, 3434–3439.

[20] J. N. Wilson, J. Gao, E. T. Kool, *Tetrahedron* **2007**, *63*, 3427–3433.

[21] Ch. Brotschi, G. Mathis, Ch.J. Leumann, *Chem.Eur.J.* **2005**, *11*, 1911-1923.

[22] H. Kashida, M. Tanaka, S. Baba, T. Sakamoto, G. Kawai, H. Asanuma, M. Komiyama, *Chem.Eur.J.* **2006**, *12*, 777-784.

[23] U.B. Christensen, E.B. Pedersen, *Nucleic Acids Research* **2002**, *30*, 4918-4925.

[24] S. M. Langenegger, R. Häner, *Chemistry & Biodiversity* **2004**, *1*, 259-264.

[25] N. Bouquin, V. L. Malinovskii, R. Häner, *Eur. J. Org. Chem.* **2008**, 2213–2219.

[26] N. Bouquin, V. L. Malinovskii, R. Häner, *Chem. Commun.* **2008**, 1974–1976.

[27] P.J. Cragg, *Supramolecular Chemistry –from Biological Inspiration to Biomedical Applications*, Springer, **2010**.

[28] J. M. LEHN, *Polymer International* **2002**, *51*, 825-839.

[29] J. M. LEHN, *Supramolecular Chemistry - Concepts and Perspectives*, VCH, Weinheim **1995**.

[30] http://www.chem.wisc.edu/courses/801/Spring00/Ch1_2.html

[31] A. W. Bosman, R. P. Sijbesma, E. W. Meijer, *Mat.Today* **2004**, *7*, 34-39.

[32] L. Brunsveld, B. J. B. Folmer, E. W. Meijer, R. P. Sijbesma, *Chem.Rev.* **2001**, *101*, 4071-4097.

[33] T. F. A. Greef, E. W. Meijer, *Nature* **2008**, *453*, 171-173.

[34] J. S Moore, *Current Opinion in Colloid & Interface Science* **1999**, *4*, 108-116.

[35] R. P. Sijbesma, F. H. Beijer, L. Brunsveld, B. J. B. Folmer, J. H. K. Ky Hirschberg, R. F. M. Lange, J. K. L. Lowe, E. W. Meijer, *Science* **1997**, *278*, 1601-1604.

[36] K. Maeda, E. Yashima, *Top.Curr.Chem.* **2006**, *265*, 47-88.

[37] C.C Lee, Ch. Grenier, E.W. Meijer, A.P.H.J. Schenning, *Chem.Soc.Rev.* **2009**, *38*, 671-683.

[38] R. K. Castellano, J. Rebek, Jr., *J. Am. Chem. Soc.* **1998,** *120,* 3657-3663.

[39] G.Gottarelli, G. P. Spada, *The Chemical Record* **2004**, *4*, 39–49.

[40] C. Nuckolls, T. J. Katz, G. Katz, P. J. Collings, L. Castellanos, *J. Am. Chem. Soc.* **1999**, *121,* 79-88.

[41] P. Besenius, G. Portale, P.H.H. Bomans, H. M. Janssen, A.R.A. Palmans, E.W. Meijer, *PNAS* **2011**, *107*, 17888-17893.

[42] J. P. Hill, W. Jin, A. Kosaka, T. Fukushima, H. Ichihara, T. Shimomura, K. Ito, T. Hashizume, N. Ishii, T. Aida, *Science* **2004**, 304, 1481-1483.

[43] H. Engelkamp, S. Middelbeek, R. J. M. Nolte, *Science* **1999**, 284, 785-788.

[44] D. Zhao, J.S. Moore, *Org. Biomol.Chem.* **2003**, *1*, 3471-3491.

[45] T. F. A. de Greef, M. M. J. Smulders, M. Wolffs, A. P. H. J. Schenning, R. P. Sijbesma, E. W. Meijer, *Chem.Rev.* **2009**, *109*, 5687-5754.

[46] R. K. Castellano, D.M. Rudkevich, J. Rebek, Jr., *PNAS* **1997,** *94,* 7132-7137.

[47] P. Jonkheijm, P. van der Schoot, A.P.H.J. Schenning, E.W. Meijer, *Science* **2006**, *313*, 80-83.

[48] K.P.C. Vollhardt, N.E. Schore, *Organische Chemie*, VCH, Weinheim **2000**.

[49] G. A. Hembury, V. V. Borovkov, Y. Inoue, *Chem.Rev.* **2008**, *108*, 1-73.

[50] A. Scarso, J. Rebek Jr., *Top.Curr.Chem.* **2006**, *265*, 1-46.

[51] L.J. Prins, R. Hulst, P. Timmerman, D.N. Reinhoudt, *Chem.Eur.J.* **2002**, *8*, 2288-2301.

[52] L.J. Prins, F. De Jong, P. Timmerman, D.N. Reinhoudt, *Nature* **2000**, *408*, 181-184.

[53] M.Inouye, M. Waki, H. Abe, *J. Am. Chem. Soc.* **2004**, *126,* 2022-2027.

[54] M. M. Green, N. C. Peterson, T. Sato, A. Teramoto, R. Cook, S. Lifson, *Science* **1995**, *268*, 1860-1866.

[55] M. M. Green, J. W. Park, T. Sato, A. Teramoto, S. Lifson, R. L. B. Selinger, J. V. Selinger, *Angew.Chem.-Int.Ed.* **1999**, *38*, 3139-3154.

[56] M. M. Green, K. S. Cheon, S. Y. Yang, J. W. Park, S. Swansburg, W. H. Liu, *Acc.Chem.Res.* **2001**, *34*, 672-680.

[57] A. R. A. Palmans, E. W. Meijer, *Angew.Chem.Int.Ed.* **2007**, *46*, 8948-8968.

[58] K. C. Hannah, B. A. Armitage, *Acc.Chem.Res.* **2004**, *37*, 845-853.

[59] R. J. Fiel, J. C. Howard, E. H. Mark, N. Datta Gupta, *Nucl.Acids Res.* **1979**, *6*, 3093-3118.

[60] R. F. Pasternack, E. J. Gibbs, J. J. Villafranca, *Biochemistry* **1983**, *22*, 2406-2414.

[61] R. F. Pasternack, E. J. Gibbs, *Metal Ions in Biological Systems, Vol 33* **1996**, *33*, 367-397.

[62] R. F. Pasternack, E. J. Gibbs, D. Bruzewicz, D. Stewart, K. S. Engstrom, *J.Am.Chem.Soc.* **2002**, *124*, 3533-3539.

[63] R. F. Pasternack, *Chirality* **2003**, *15*, 329-332.

[64] L. G. Marzilli, *New J.Chem.* **1990**, *14*, 409-420.

[65] J. M. Kelly, M. J. Murphy, D. J. Mcconnell, C. Ohuigin, *Nucl.Acids Res.* **1985**, *13*, 167-184.

[66] J. Manono, P.A. Marzilli, L.G. Marzilli, *Inorg.Chem.* **2009**,*48*, 5636-5647.

[67] D. R. McMillin, A. H. Shelton, S. A. Bejune, P. E. Fanwick, R. K. Wall, *Coord.Chem.Rev.* **2005**, *249*, 1451-1459.

[68] X.Zheng, R.K. Pandey, *Anti-cancer Agents in Medicinal Chemistry* **2008**, *8*, 241-268.

[69] B. Meunier, *Chem.Rev.* **1992**, *92*, 1411-1456.

2. Aim of the work

Among the non-nucleosidic building blocks which have been incorporated into a DNA scaffold by the Häner group, pyrene is one. Different linkers as triazol [1], alkynyl [2] or carboxamide [3, 4] have been attached to the pyrene moiety for the incorporation, using standard oligonucleotide synthesis (Figure 1).

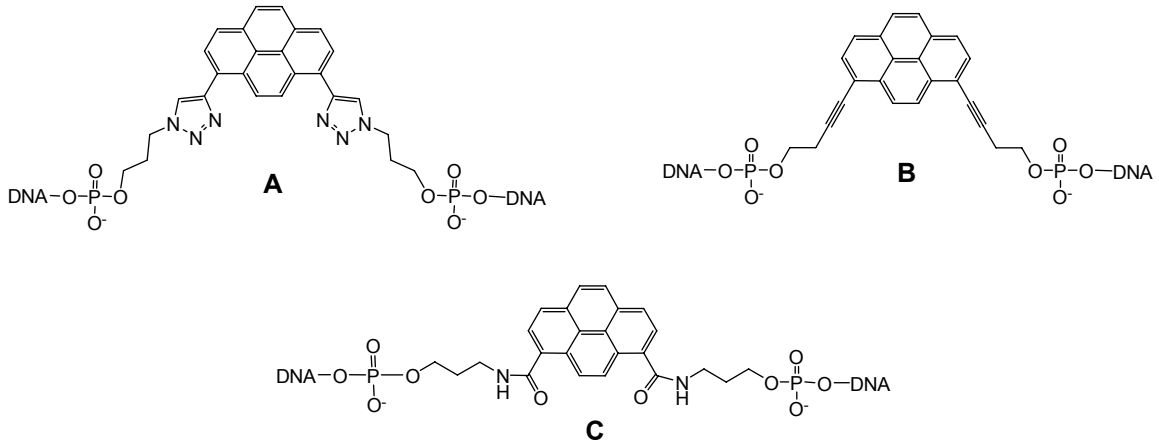

Figure 1. Non-nucleosid pyrene building blocks with different linkers **A** [1], **B** [2], **C** [3,4] for the incorporation into a DNA scaffold.

Pyrene appears attractive because they have an extended π-system, which brings favorable stacking properties, and are sensitive towards structural changes, which are reflected in changed photophysical properties. [5]

Recent results of Häner et al. have shown that an entirely artificial section of pyrene (**1C**) units, embedded in a double-stranded DNA molecule, adopt helical organization. Due to the negatively charged phosphate backbone and the two DNA stem attached on both sides of the pyrene section, the solubility in aqueous media is guaranteed. The performed studies included artificial sections of a range from 2 to 14 pyrene units. Helical organization, as shown by fluorescence and CD spectroscopy, takes place in a hybrid with 12 or 14 achiral pyrene building blocks, but not within the respective single strands nor in hybrids containing less then 10 pyrene residues. Further, it was shown that the interstrand stacking of the 14 pyrene units lead to a stabilization of the duplex. [3, 4]

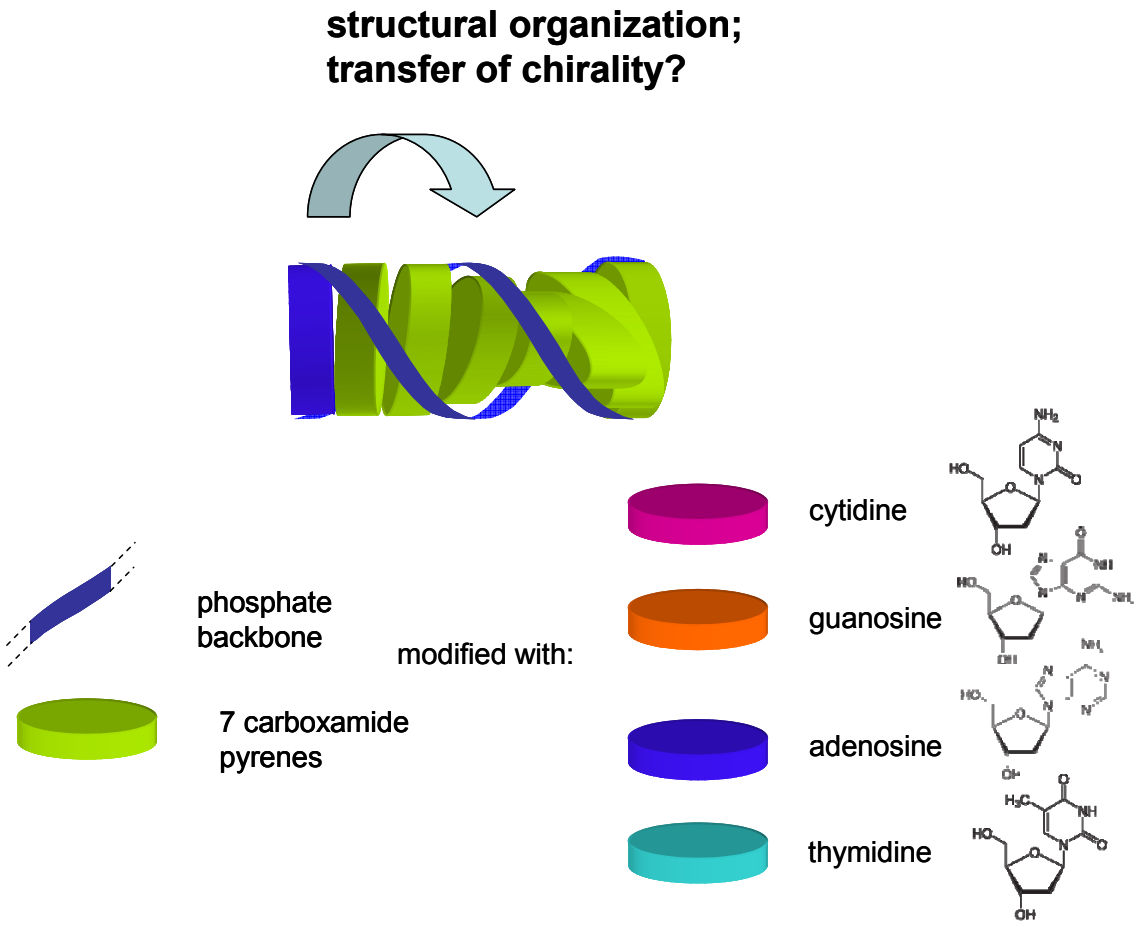

Figure 2. Oligopyrenotides modified with the four nucleotides A, G, C, T.

The reduction of the DNA part from a tri-segmental oligomer to a bi-segmental oligomer with only one DNA stem didn't change the structural behaviour of the 14 pyrene units.
In this approach the DNA brings the pyrene strand in close proximity, supporting their structural organization. It was concluded that aromatic oligopyrene amphiphilic blocks have intrinsic properties to *directional self-association*.
These findings prompted us to do further investigations to explore if the pyrene units still adopt a defined structure and if transfer of chirality occurs from the nucleotide to the pyrene stacks, when the DNA part is reduced to the minimum of one base pair.

References

[1] S. Werder, V.L. Malinovskii, R. Häner, *Org. Lett.* **2008**, *10*, 2011-2014.

[2] H. Bittermann, D. Siegemund, V. L. Malinovskii, R. Häner, *J.Am.Chem.Soc.* **2008**, *130*, 15285–15287

[3] V. L. Malinovskii, F. Samain, R. Häner, *Angew.Chem. Int. Ed.* **2007**, *46*, 4464-4467.

[4] R. Häner, F. Samain, V.L. Malinovskii, *Chem.Eur.J.* **2009**, *15*, 5701-5708.

[5] V. L. Malinovskii, R. Häner, *Eur. J. Org. Chem.* **2006**, 3550–3553.

3. Amplification of chirality by supramolecular polymerization of pyrene oligomers

Published: Alina L. Nussbaumer, Daniel Studer, Vladimir L.Malinovskii and Robert Häner;
Angew.Chem.Int.Ed. **2011**, *50*, 5490-5494

3.1 Abstract

In this chapter, it is reported that short achiral oligomers of pyrenes (**Py_7**) units connected *via* flexible phosphodiester linkers show strong amplification of chirality by adding small amount of chiral oligopyrenes modified with the base cytosine (**Py_7-C**). These findings can be explained with the formation of supramolecular polymers in aqueous environment. The formation of the supramolecular polymers occur via a nucleation-elongation mechanism, whereas the self-association of oligomer **Py_7-C** alone follows a isodesmic model. Further proof for the proposed model was found by gel-electrophoreses and transmission electron microscopy (TEM). To the best of our knowledge, this represents the first example of supramolecular polymerization observed with oligomeric building blocks that are not pre-organized.

3.2 Introduction

Over the past two decades, the field of supramolecular polymers[1-3] has emerged as a separate area of materials research. As in other areas of supramolecular chemistry,[4,5] the structure and functional properties of supramolecular polymers largely depend on the nature of the non-covalent interactions existing between the individual units.[6-9] Therefore, the macroscopic properties of the system formed are highly dependent on the supramolecular organization and not solely defined by the properties of the molecular

components.[10-16] While the formation of supramolecular polymers *via* hydrogen bonding was explored rather intensively, systems based on aromatic stacking have thus far been reported to a lesser extent.[17-22] The reason for this may be partly found in the relatively limited directionality of aromatic stacking interactions in comparison to hydrogen bonding.[15,19,23,24] Strength and directionality of aromatic interactions may be significantly enhanced by either using templates,[25-29] or by applying geometrical restrictions to pre-organize the individual aromatic units and, thus, reducing unfavorable entropic terms of the supramolecular assembly process.[24,30-35] A further approach consists in the covalent linking of individual units to oligomeric building blocks.

3.3 Results and Discussion

3.3.1 Synthesis

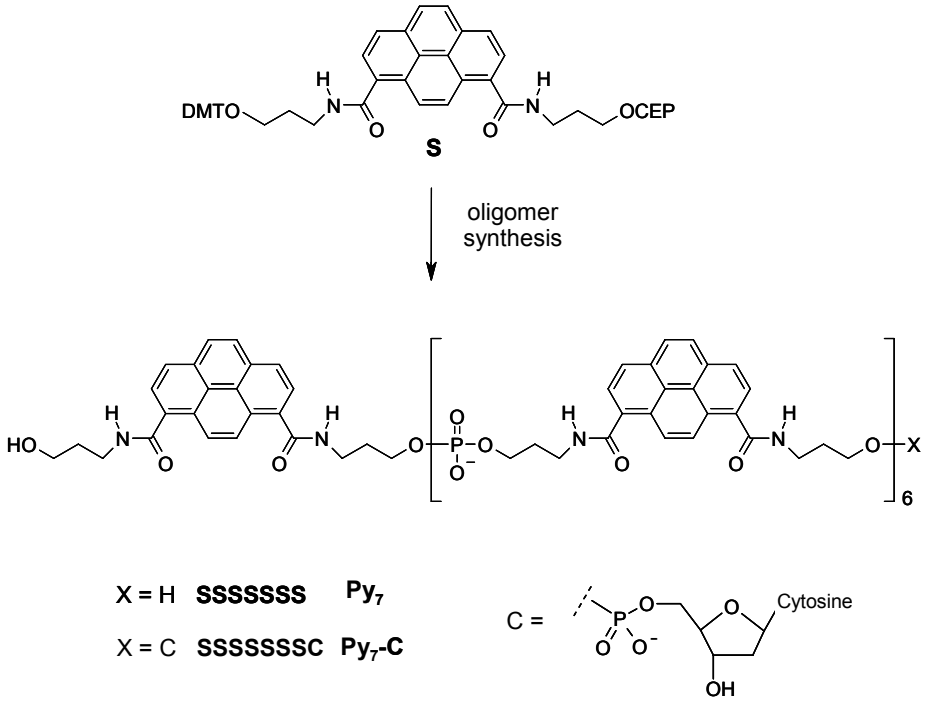

Scheme 1. Synthesis of oligomeric pyrene strands **Py_7** (*achiral*) and **Py_7-C** (*chiral*, bearing a 2'-deoxycytidine); CEP = 2-cyanoethyl-*N*,*N*-diisopropylphosphoramidite, DMT = 4,4'-dimethoxytrityl.

The synthesis of oligomers is shown in Scheme 1. Using phosphoramidite **S**,[36-41] oligomers **Py$_7$** and **Py$_7$-C** were assembled on a pyrene-derived polystyrene solid support *via* automated phosphoramidite chemistry.[42] Choice of the number of pyrene units was based on our previous studies showing that sections of seven pyrenes lead to helically organized structures in a DNA framework.[43-46] Oligomer **Py$_7$** is achiral while oligomer **Py$_7$-C**, which contains a terminally attached 2'-deoxycytidine, is chiral.

3.3.2 Influence of salt on the organization of pyrene oligomers

Temperature dependent UV/Vis and fluorescence measurement of **Py$_7$** in water showed no remarkable change in its spectroscopic properties (Figure 1). Gradual changes in the intensities of fluorescence show no formation of big aggregates with specific organization.

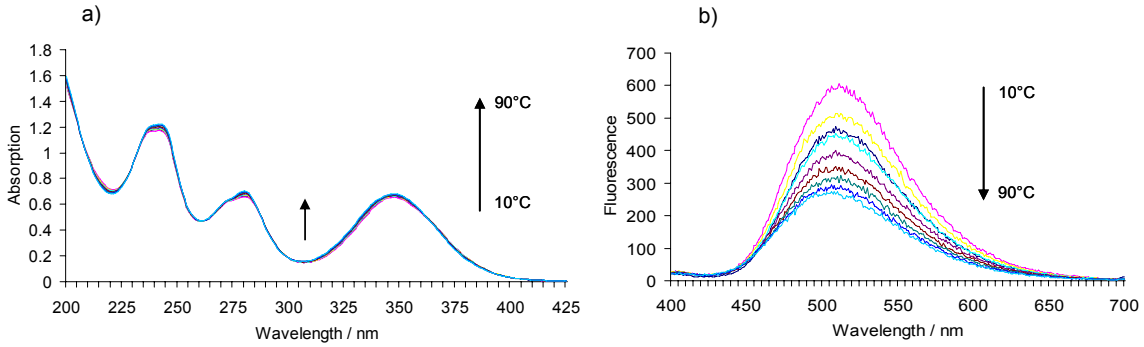

Figure 1. Absorbance and fluorescence spectra of oligomer **Py$_7$**: a) variable temperature UV/Vis; b) variable temperature fluorescence spectra; conditions are: water; 5 µM oligomer concentration.

Further investigation by UV/Vis and fluorescence spectroscopy (Figure 2) showed that high salt concentration has a pronounced influence on the stacking of the pyrene residues of oligomer **Py$_7$** as indicated by a pronounced hypochromism, the appearance of vibronic structures in UV/Vis (I_{355}/I_{345}, I_{280}/I_{270}, I_{245}/I_{235}), as well as in the excitation spectrum and a shift in the excimer fluorescence ($\Delta\lambda_{em}$= -12 nm). The appearance of vibronic structures is due to conformational restrictions. It shows that the pyrene units are not in a bulk, but that a bigger fraction of pyrene units are organized in the same manner. Blue shift in fluorescence spectra is an indication that a preferred sandwich-type

conformation of the pyrene units is restricted. The blue shift arises with the twisting of the pyrene units.

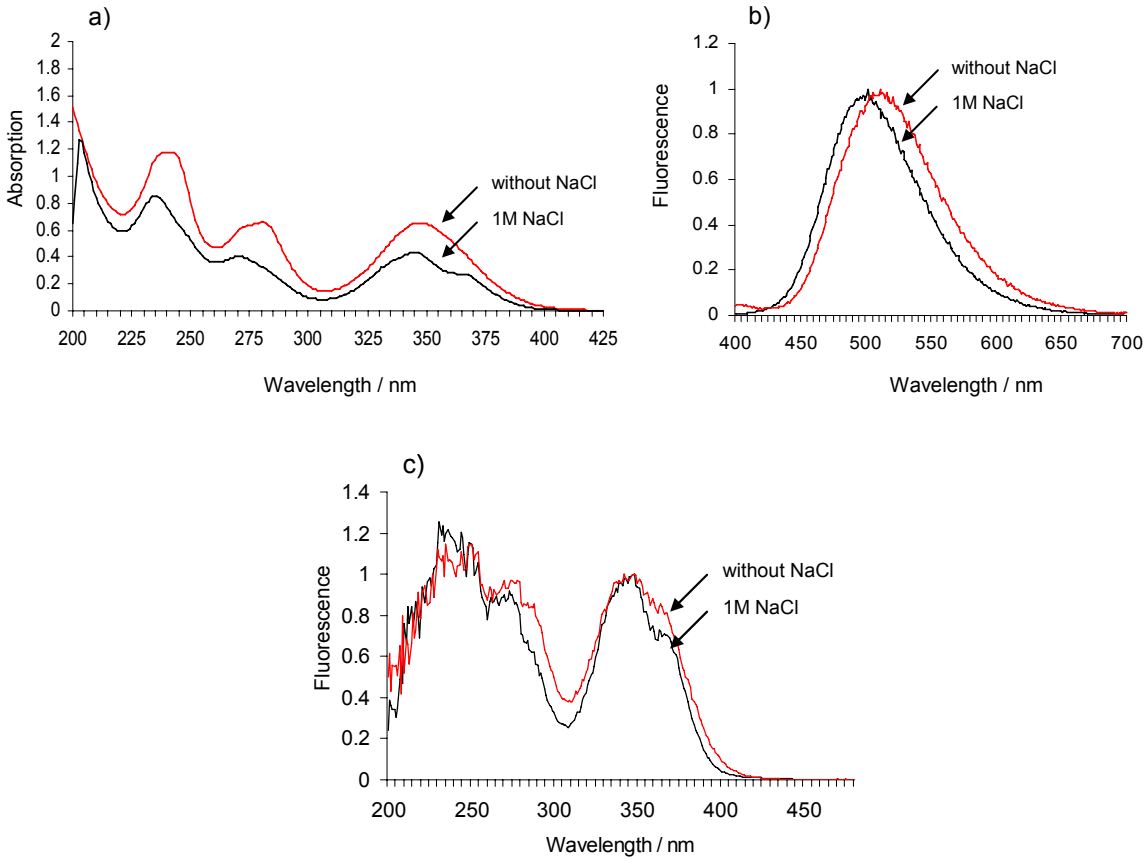

Figure 2. Absorbance and fluorescence spectra of oligomer **Py_7**: a) UV/Vis, influence of NaCl; hypochromism: H_{245} = 31%, H_{284} = 43%, H_{354} = 32%; b) fluorescence normalized spectra; λ_{max}= 500 vs. 512 nm; c) excitation normalized spectra, conditions are: pH = 7.0, phosphate buffer, 1 M NaCl, 20°C; 5 μM oligomer concentration.

Upon increasing the temperature, these effects disappear (Figure 3), indicating a significant loss of stacking interactions between pyrenes at high temperature. Thus, under conditions of high ionic strength, pyrene oligomer **Py_7** adopts a structure in which the pyrene units are conformationally restricted and twisted.[41,47-51]

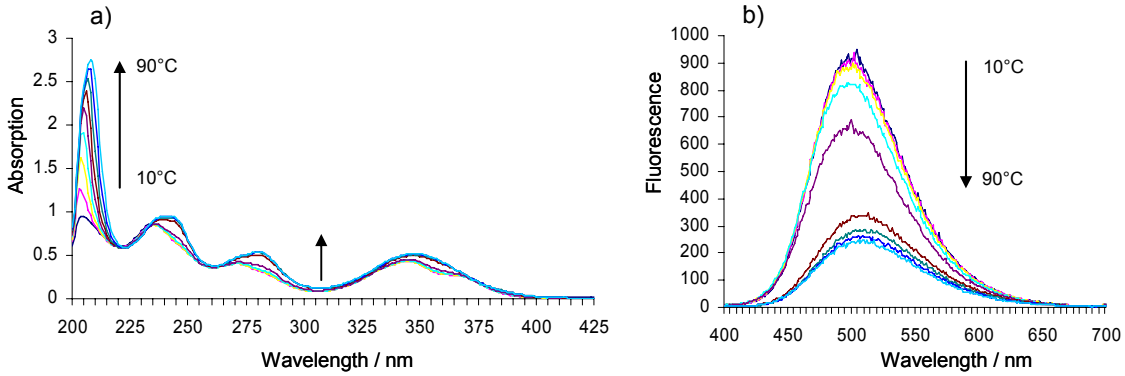

Figure 3. Absorbance and fluorescence spectra of oligomer **Py_7**: a) variable temperature UV/Vis; b) variable temperature fluorescence spectra; unless otherwise indicated, conditions are: pH = 7.0, phosphate buffer, 1 M NaCl, 5 µM oligomer concentration.

It is noteworthy that the vibronic structures in the UV/Vis spectra are more pronounced for the achiral oligomer **Py_7** than for the chiral oligomer **Py_7-C** (Figure 4) or for systems in which pyrene residues were conjugated to longer DNA parts.[43,44]

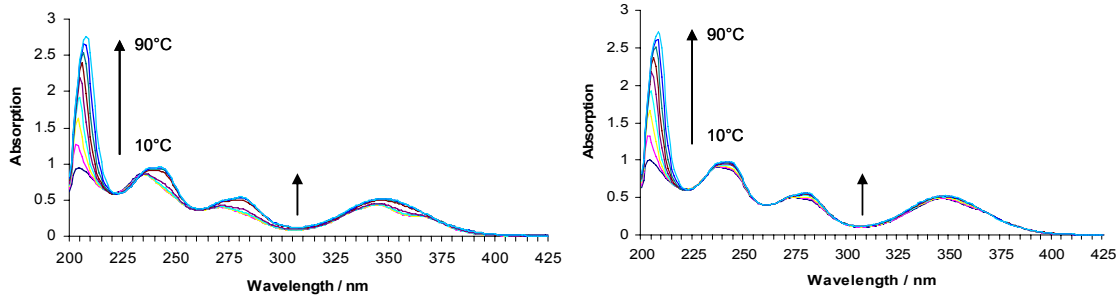

Figure 4. Temperature variable absorbance spectra of oligomer **Py_7** (left) and **Py_7-C** (right), conditions are: pH = 7.0, phosphate buffer, 1 M NaCl, 5 µM oligomer concentration.

Further, a sharp transition in fluorescence intensity (between 50 – 60 °C) is observed for **Py_7** only, but not for **Py_7-C**, supporting a much less defined aggregation of **Py_7-C** compared to **Py_7**. The vibronic bands in excitation spectra at low temperature further clarify the high packing of emitting pyrenes (Figure 5). This suggests that the degree of

stacking in **Py_7** is higher than in **Py_7-C** or in the previous described systems, meaning that a higher fraction of pyrene units adopt the same conformation.

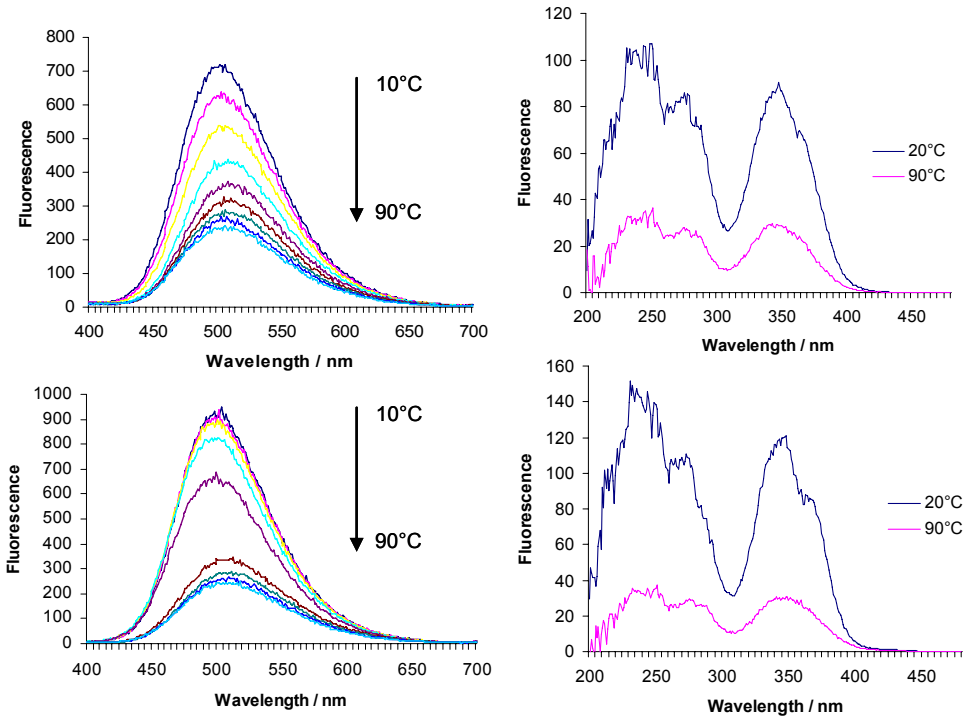

Figure 5. Temperature variable fluorescence spectra (left) and excitation spectra (em. at 500 nm) at 20°C and 90°C of oligomer **Py_7-C** (top) and oligomer **Py_7** (10 mM phosphate buffer, 1 M NaCl, pH 7.0).

3.3.3 Amplification of chirality / Sergeant-and-soldiers experiment

CD spectroscopy reveals no distinct signals for either of the two oligomers alone (Figure 6, top). However, if **Py_7-C** and **Py_7** are mixed in a 1:1-ratio a non-racemic, helical structure is formed as indicated by the appearance of strong Cotton effects. This observation can only be explained by the interaction between strands of **Py_7-C** and **Py_7** or, in other words, the formation of mixed aggregates of the two strands. The CD signals disappear with increasing temperature (Figure 6, bottom).

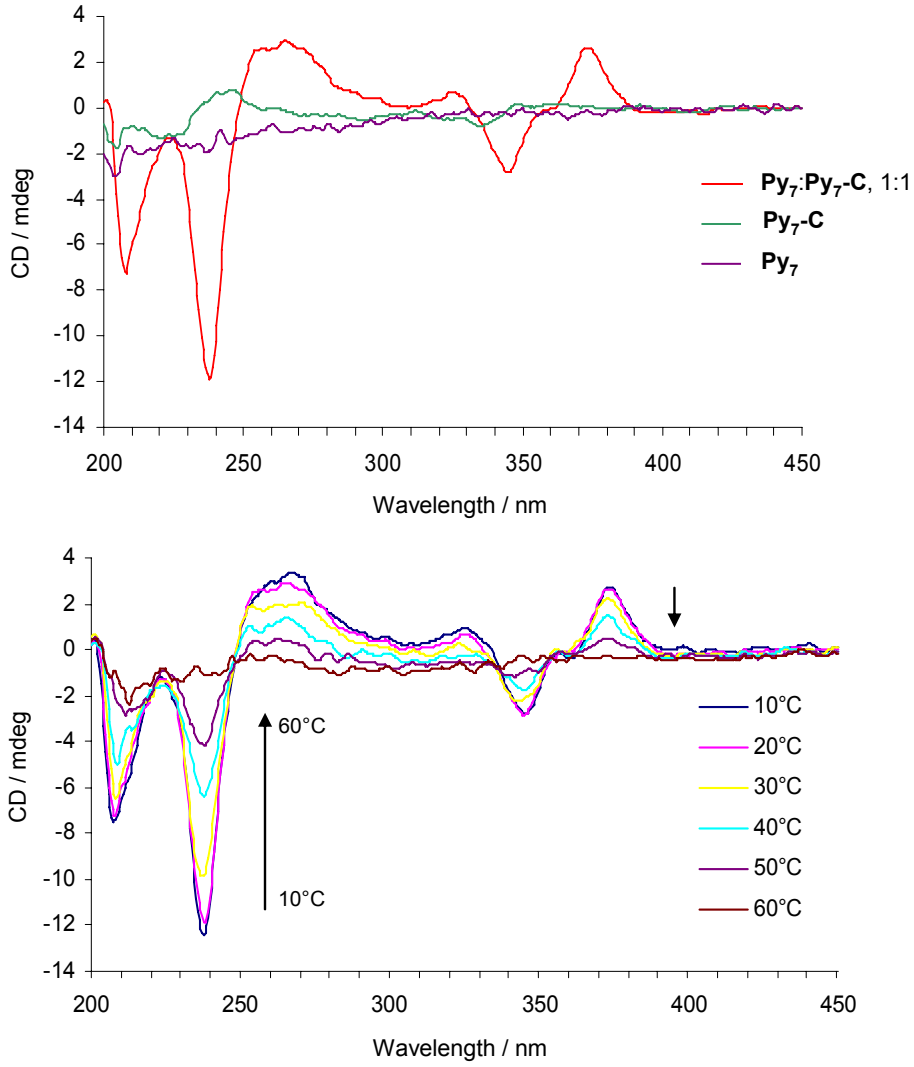

Figure 6. CD spectra of oligomers **Py_7** and **Py_7-C**; top: **Py_7** and **Py_7-C** alone and as a 1:1 mixture at 20 °C; bottom: variable temperature CD spectra of a 1:1 mixture of **Py_7** and **Py_7-C** (1 M NaCl, pH=7.0 phosphate buffer; 5 μM total oligomer conc.)

Intensities of the signals in LD experiments were at the level below 0.001, the overall shape was similar to the shape of UV/Vis, and the signals were not stable within time. Such observations support the polymeric nature of products, but clearly rule out the LD effects during CD experiment. The shape of CD signals observed in this study is clearly an example of exciton coupled chromophores, whereas LD shape is similar to the absorbance spectra.

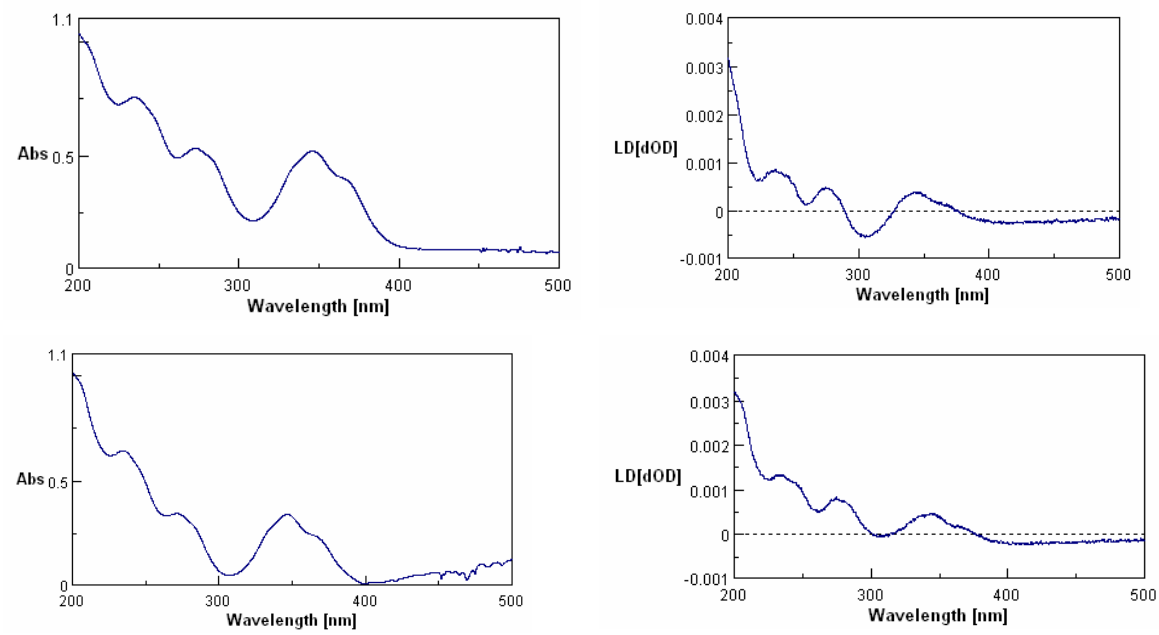

Figure 7. Examples of LD experiments: absorbance spectra (left) and LD data (right) for the **Py_7**:**Py_7-C**, 50:50 mixture (top), and 90:10 (buttom) at 20°C. (10 mM phosphate buffer, 1M NaCl, pH 7.0).

The appearance of a CD active structure formed by a 1:1-mixture of **Py_7** and **Py_7-C** prompted us to investigate the behavior of different ratios of the two oligomers. Figure 8 shows the CD spectra obtained with various compositions of the two oligomers.

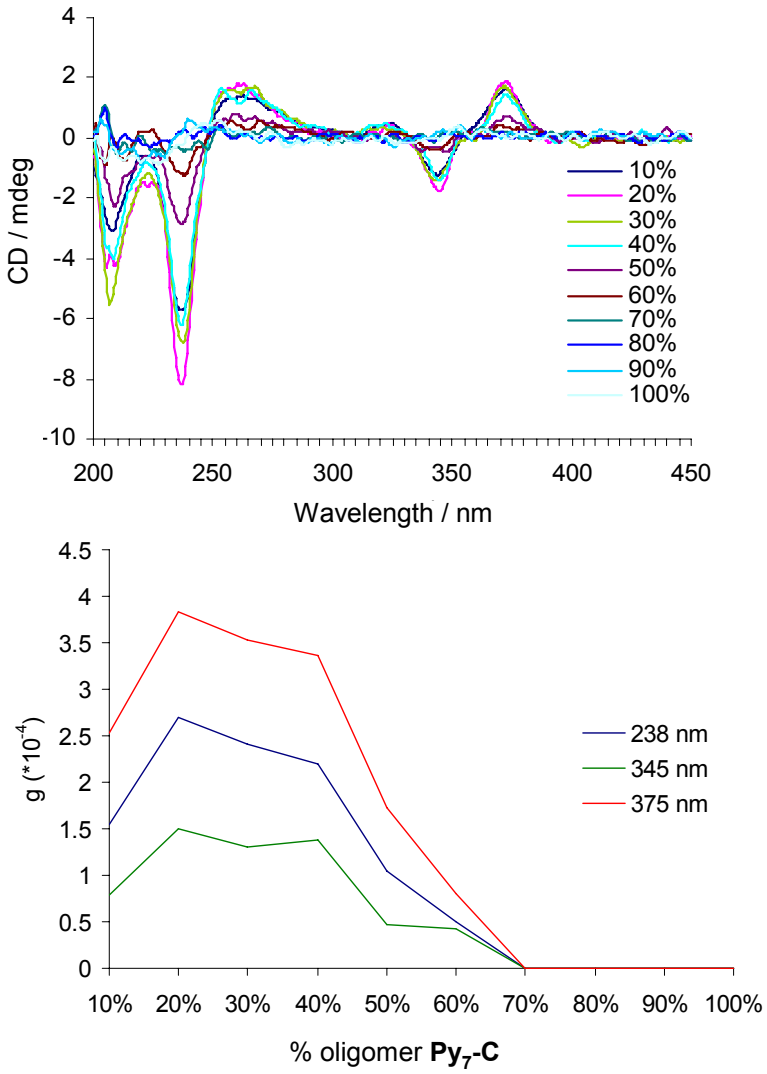

Figure 8. Top: CD spectra obtained with various ratios of the two oligomers **Py_7** and **Py_7-C**; 2.5 μM total oligomer conc.; bottom: data presented as anisotropy g-factor for the most intense signals.

The observed amplification of chirality[53-58] is compatible with the formation of *supramolecular polymers*[59] by assembly of individual pyrene oligomers. The high degree of anisotropy cannot be the result of formation of hetero-dimeric complexes (i.e. a duplex formed by one **Py_7** and one **Py_7-C**) since, in such case, the maximum effect should be observed at high concentrations of the chiral oligomer, which is opposite to our observation. The findings are in agreement with the formation of supramolecular polymers obeying the "sergeants-and-soldiers" rules.[60-63]

As illustrated in Scheme 2, the following model was proposed. High ionic strength favors aromatic stacking between pyrene units, both intra- and intermolecularly. Intermolecular stacking leads to formation of extended aggregates of the oligomers. In the absence of chiral information, i.e. in a solution containing only oligomer **Py_7**, a racemic mixture of helical, supramolecular polymers (*P* and *M*)[64-66] are formed. Upon addition of small amounts of **Py_7-C**, the chiral oligomer is integrated into the dynamic polymers and the solution slowly equilibrates, eventually resulting in an excess of the thermodynamically favored supramolecular helices (*P*-helix, see Figures 6 and 8).

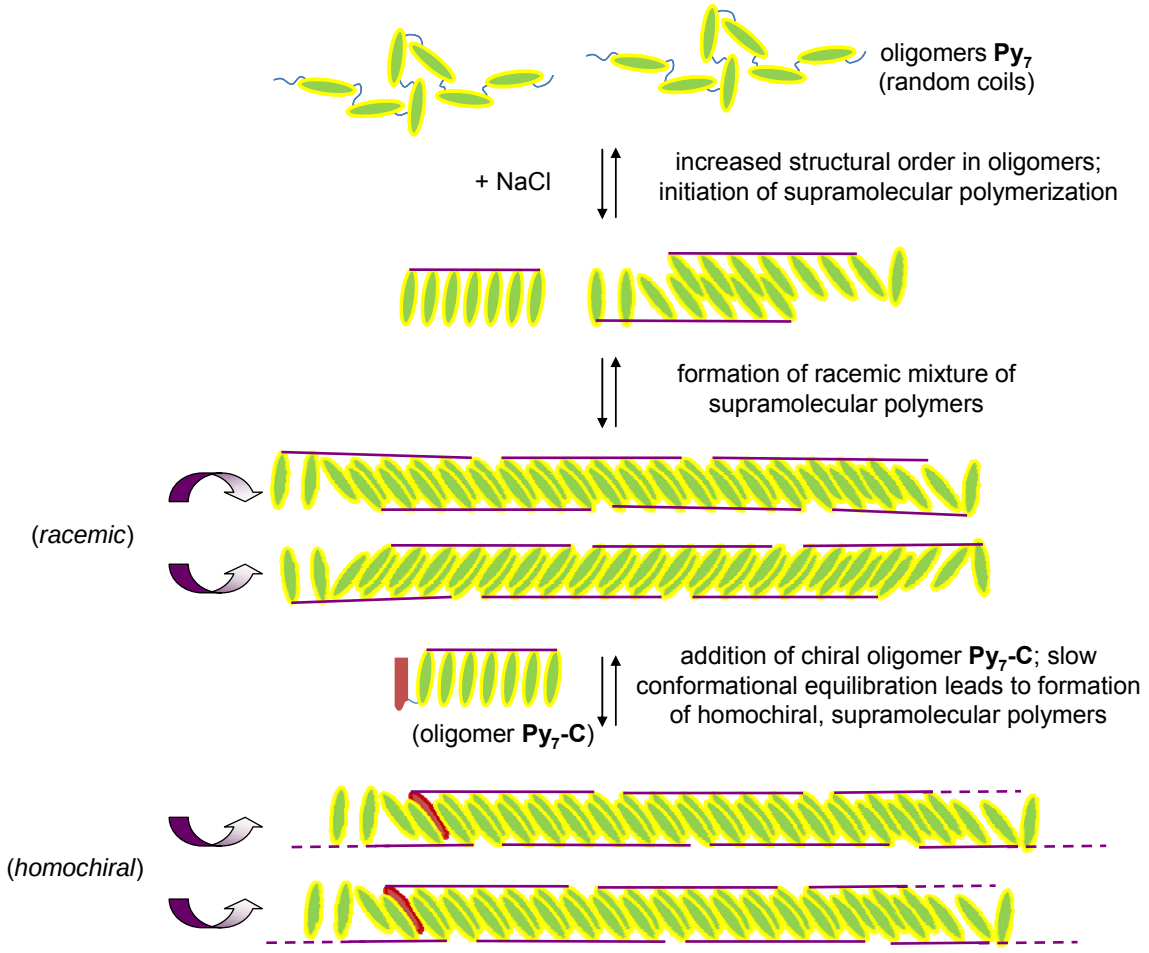

Scheme 2. Schematic illustration of supramolecular polymer formation: high ionic strength is accompanied by pyrene stacking and interaction between individual achiral oligomers **Py_7**. This leads to a racemic mixture of supramolecular helical polymers. Addition of a small quantity of a chiral *inductor* shifts the equilibrium in favor of the thermodynamically preferred *P*-helix.

3.3.4 Kinetics of the formation of supramolecular polymers

The development of the supramolecular polymers by aggregation and packing of the pyrene oligomers seems to be a rather slow process. Even though pronounced aggregation of pyrenes within **Py_7** is rapidly initiated after addition of NaCl to the water solution (Figure 2), further decrease of absorbance within days/weeks can be observed. This is due to the increasing fraction of aggregated pyrenes and the narrowing populations of conformational isomers, meaning the development of a defined geometry within the aggregates. Restricted conformational freedom of pyrenes through packing within the aggregates is then manifested by the appearance of vibronic bands.
The development of supramolecular polymers is accompanied by an increase of total intensity of pyrene excimer signal.

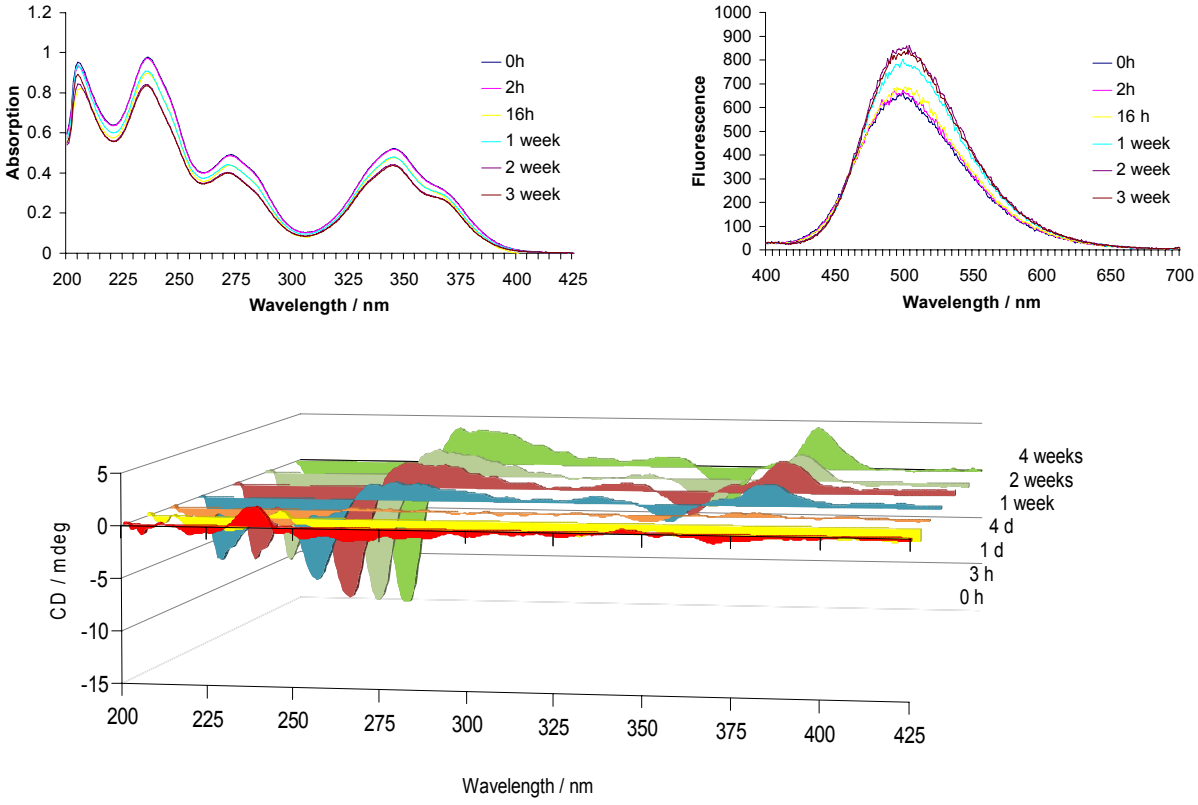

Figure 9. Spectroscopic “signatures” of pyrene polymerization at high ionic strength (1M NaCl): a) UV/Vis (top, left) of **Py_7**; b) fluorescence (top, right) of **Py_7** and c) CD (bottom) of **Py_7** with 10% of **Py_7-C**.

The described observations are independent of the presence or absence of chiral information. Development of the observed anisotropy is a relatively slow process too, as maximum anisotropy is obtained over a time range of several days (Figure 9).
The rather slow kinetics observed for the present system are a result of slow conformational changes towards the most stable isomer of the extended polymers, and not surprising in view of the slow processes reported for supramolecular systems that are primarily based on aromatic stacking and/or hydrophobic interactions.[24,52]
Reversibility of the system could be confirmed. After heating, the CD-signal disappeared, but it could be recovered within the same time scale during which anisotropy was developed initially.

3.3.5 Mechanism for the formation of supramolecular polymers

As described, the chiral induction does not grow linearly with the molar fraction of chiral oligomer, which is a characteristic of chiral amplification.[54-56] Even more remarkably, a gradual reduction of the fraction of chiral oligomer led to an increase of the CD signals. The highest anisotropy factor (g) value was reached with the 80:20-mixture of (achiral) **Py_7** and (chiral) **Py_7-C** oligomer, which is unexpected in view of previously described systems.[55,56,61,67,68] Temperature dependent analysis (Figure 10) shows that the polymerization of **Py_7** proceeds in a nucleated process, whereas aggregation of **Py_7-C** follows an isodesmic pattern.[69]
While assembly of **Py_7** is cooperative, the cytidine-bearing **Py_7-C** behaves in a non-cooperative way, preventing formation of long polymers. This explains why *smaller* fractions of **Py_7-C** lead to a *higher* degree of anisotropy; when only **Py_7-C** is present, the formation of long, conformationally defined polymers is not possible. In contrast, **Py_7** alone forms long, but racemic supramolecular polymers (*M*- and *P*-type). Mixtures of the two oligomers with a ratio of less than 70% **Py_7-C** lead to the formation of supramolecular polymers with a preferred helical sense (*P*-type). Increased amounts of **Py_7-C** (>70%) prevent the formation of nuclei of appropriate length, therefore suppressing the supramolecular polymerization. Another possibility may reside in the induction of helical reversals[60,70] by **Py_7-C** which would be observed as an overall racemization at high fraction of **Py_7-C**.

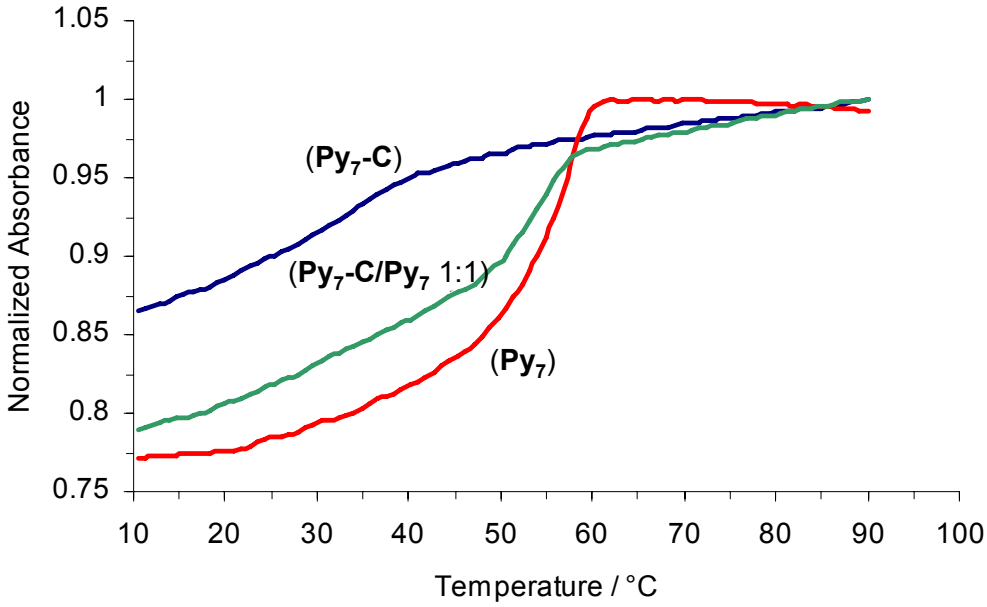

Figure 10. Cooperative (**Py_7**) and non-cooperative (**Py_7-C**) aggregation behavior of the two oligomers and their 1:1 mixture; cooling curves from 90 to 10 °C are shown; absorbance was measured at 354 nm.

3.3.6 Sample preparation and formation of supramolecular polymers

Due to the dynamic nature of supramolecular systems, they can undergo spontaneous and continuous assembly and disassembly processes in a given set of conditions. The final products are governed by thermodynamics and kinetics and may vary from a one defined system (thermodynamically controlled), because some of them are kinetically trapped (kinetically controlled). While performing the experiments we gave attention to the thermodynamically controlled products, the distribution of products or conformational reorganization within each system being followed during days and weeks till spectroscopic properties were stable.

During the performance of the experiments, it was found that, for example, preheating of the mixed oligomers **Py_7** and **Py_7-C** had an influence on the development of the signal intensity. The development of anisotropy showed less intense signals, when the samples were heated to 90°C before recording compared to the samples without preheating.

Some of the formed products may be kinetically trapped and do not contribute to the formation of the supramolecular polymers.

Further, it was found that the concentration of the synthesized oligomers is crucial for the formation of supramolecular polymers. For example, experiments with 10 % **Py_7-C** once performed with the concentration of 2 µM and once with 5 µM, showed different intensities in anisotropy g-factor. In literature [71], it was found that polymerization take place only above a critical total concentration, which could be an explanation for these observations.

3.3.7 Limits of the chiral information

Further studies have been carried out in order to detect the limit of chiral information, which is required to observe the amplification of chirality phenomena. Experiments adding 0.1%, 0.5% and 1% of **Py_7-C** to the preformed supramolecular polymers were performed. The results showed that 0.1% and 0.5% seem not to be enough for the induction of CD response. When 1% of **Py_7-C** was added, anisotropy could be observed (shown in Figure 11). Unfortunately the results were not stable.

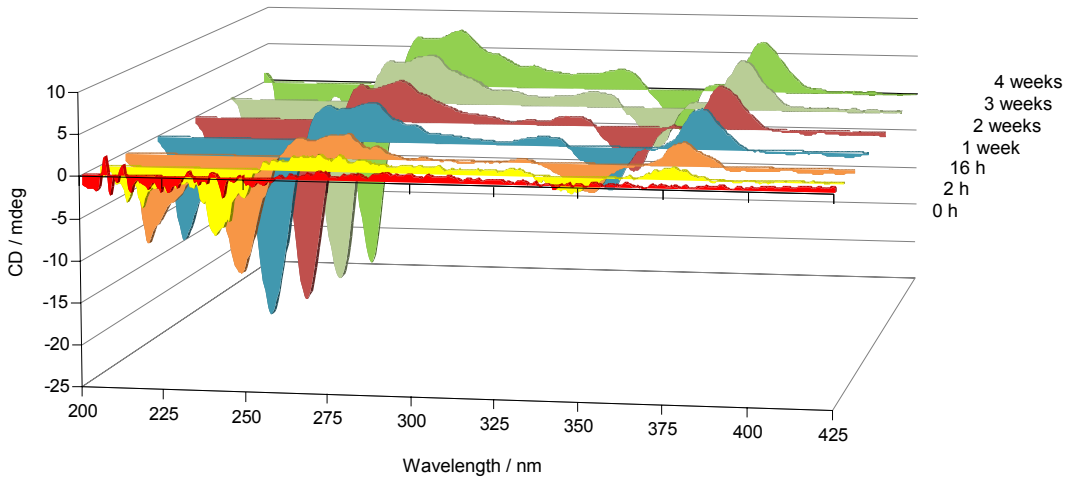

Figure 11. Time course of the development of CD signal intensities after addition of 1% of chiral oligomer **Py_7-C** to a 5 µM solution of achiral oligomer **Py_7**; pH = 7.0, phosphate buffer, 1 M NaCl, 7 µM oligomer concentration.

It should be noted that 1% of chiral information corresponds to a concentration range of about 10^{-8} μM, and so the effect can be cancelled by impurities either from a not completely successful synthesis or impurities in the buffer. The equilibration time of the achiral oligomer **Py_7** forming stable supramolecular polymers, as well the concentration of the oligomers **Py_7**, can be important for the amplification of chirality. Once the stable structure is formed a minute amount of chiral building block is enough to turn the whole system into one preferred helical sense.

3.3.6 Methods to characterize the formed long aggregates

Agarose gel electrophoresis were performed and provided support for the formation of extended aggregates.

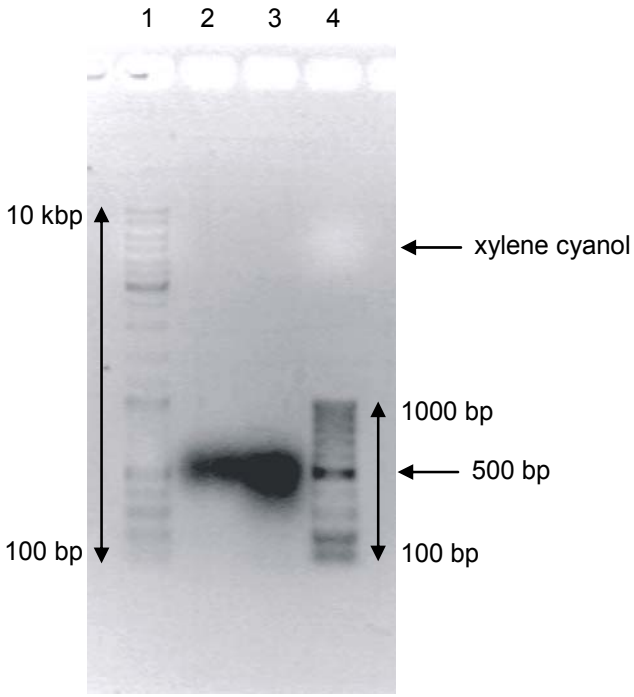

Figure 12. Electrophoretic mobility (1% agarose) of oligopyrene **Py_7** after equilibration; lane 1: DNA-ladder (0.1-10 kbp; steps of 100 bp); lane 2: oligomer **Py_7** alone; lane 3: a 99:1-mixture of **Py_7** and **Py_7-C**; lane 4: DNA-ladder (0.1-1 kbp; steps of 100 bp).

Oligopyrene **Py_7** forms large aggregates which possess approximately the same migration velocity as double stranded DNA of approx. 500 base pairs length (Figure 12). Even if a direct correlation between migration velocity of DNA and the phosphodiester-linked pyrene oligomers is not possible, this is clear evidence that **Py_7** forms aggregates of dozens of oligomers.

Further support for supramolecular polymer formation was obtained by transmission electron microscopy (TEM, Figure 13, left). The supramolecular polymers were adsorbed on a grid coated with carbon foil using positively charged polylysine. The obtained pictures revealed extended structures of a relatively uniform thickness (4-6 nm) and variable length (up to 200 nm). Furthermore, electron spectroscopic imaging (Figure 13 middle) showed that the linear structures possess phosphorus content, providing substantial evidence that the observed structures are representing aggregates of phosphodiester-linked pyrene oligomers. On the right (Figure 13) the phosphorus signal is overlaid with the bright field TEM image.

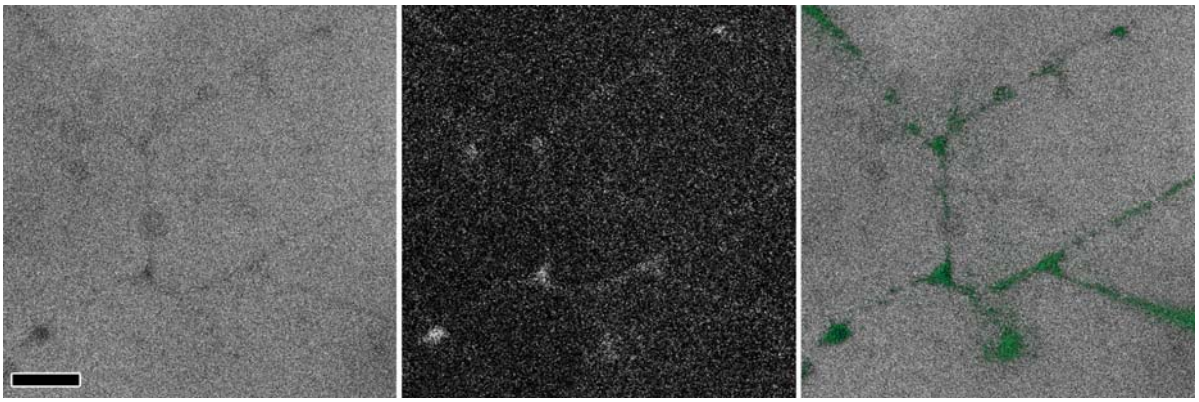

Figure 13. Transmission electron microscopy (TEM) of equilibrated solutions of oligomer **Py_7** (1 M NaCl; 5 µM total oligomer conc., no phosphate buffer); left: brightfield TEM image; middle: phosphorus map; right: overlay of phosphorus map with bright field image; scale bar: 50nm.

Further Cryo-TEM was used to characterize the formed supramolecular polymers. This technique makes it possible to image the molecules which are suspended in a solution.

Partially long structures could be observed. Due to the low resolution of these images, however, a separate study involving AFM was conducted (see next chapter).

3.4 Conclusions

In conclusion, chiral amplification was observed with short pyrene oligomers containing a flexible phosphodiester backbone in aqueous conditions. Highest anisotropy factors were found in the presence of lesser quantities of the chiral inductor, a pyrene oligomer containing a single 2'-deoxycytidine **Py_7-C**. Temperature dependent measurements showed that **Py_7** assemble via a nucleation-elongation mechanism, which is characteristic for supramolecular polymers. Self-association of **Py_7-C** followed an isodesmic mechanism.

Data obtained from UV/Vis, fluorescence and CD spectroscopy, as well as gel mobility experiments and electron microscopy, support a model in which pyrene oligomers form helical, supramolecular polymers through interstrand stacking interactions. The oligomers described herein represent a new type of oligomeric building blocks that form supramolecular polymers.

3.5 Experimental part

Synthesis of the pyrene building block

The required pyrene building block was synthesized according to a published procedure.[72] Nucleoside phosphoramidites from *Transgenomic* (Glasgow, UK) were used for oligomer synthesis. Oligomers were prepared *via* automated oligonucleotide synthesis by a standard synthetic procedure ('trityl-off' mode) on a 394-DNA/RNA synthesizer (*Applied Biosystems*). Cleavage from the solid support and final deprotection was done by treatment with 30% NH_4OH solution at 55°C overnight. All oligomers were purified by reverse phase HPLC (LiChrospher 100 *RP-18,* 5µm, Merck), eluent *A* = $(Et_3NH)OAc$ (0.1 M, pH 7.4); eluent *B* = MeCN; elution at 30°C; gradient 5 – 50% B over 39 min.

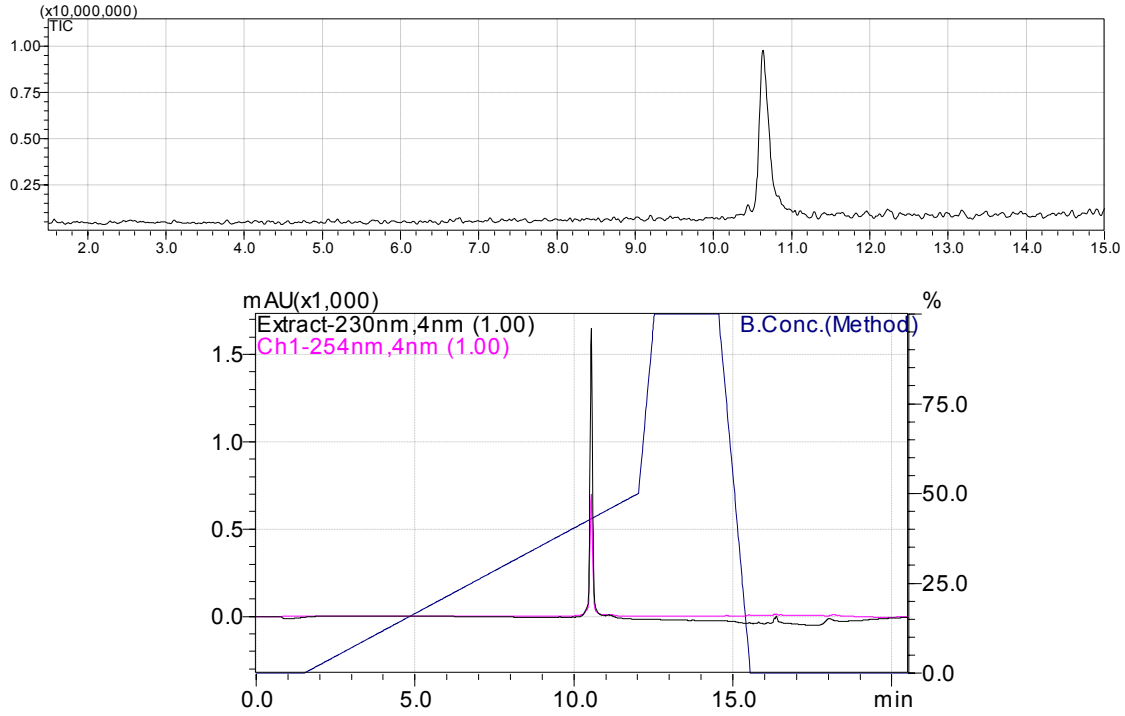

Figure 14. LC-MS data of oligomer **Py_7**; total ion chromatogram (top) and chromatogram using detection wavelength at 230 nm and 254 nm.

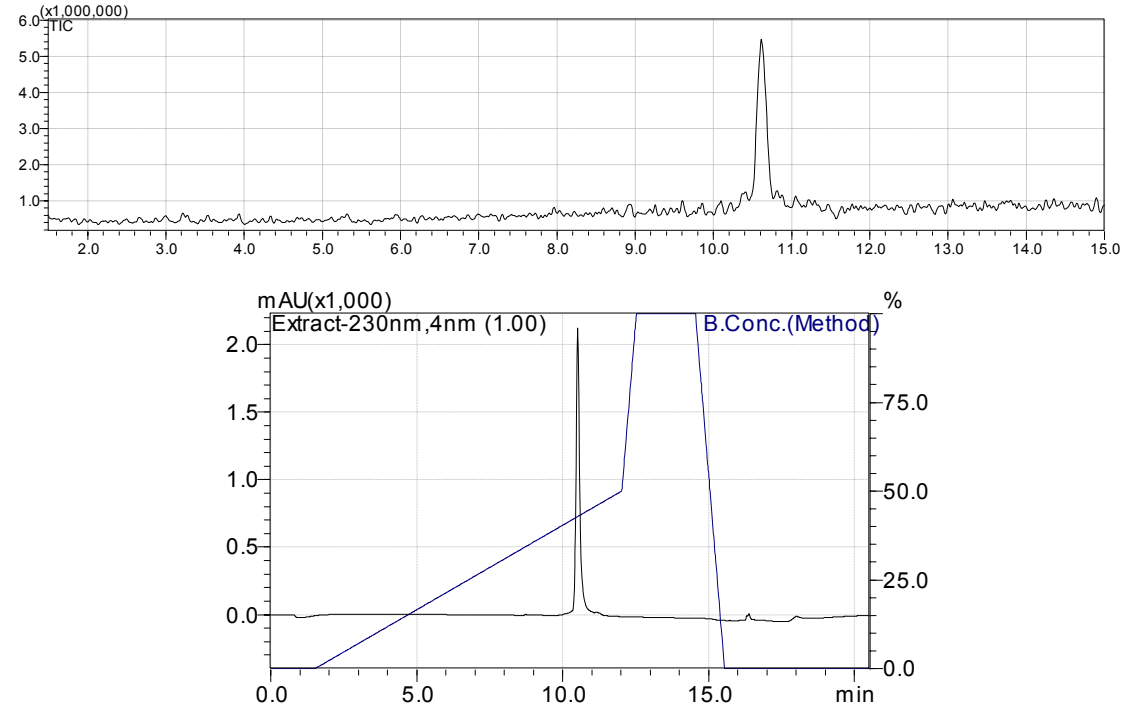

Figure 15. LC-MS data of oligomer **Py_7-C;** total ion chromatogram (top) and chromatogram using detection wavelength at 230 nm and 254 nm.

Spectroscopic methods

Unless otherwise indicated, all experiments were performed in sodium phosphate buffer (10 mM, 1M NaCl, pH 7.0) for 5 μM oligomer concentration, ε_{350}= 20'000 $dm^3 \times mole^{-1} \times cm^{-1}$ was used for pyrene units.

Temperature dependent UV/VIS spectra were collected with an optic path of 1 cm over the range of 200-500 nm at 10-90 ºC with a 10 ºC interval on *Varian Cary-100 Bio*-UV/VIS spectrophotometer equipped with a *Varian Cary*-block temperature controller. The cell compartment was flushed with N_2.

Thermal melting experiments were carried out on *Varian Cary-100 Bio*-UV/VIS spectrophotometer equipped with a *Varian Cary*-block temperature controller and data were collected with Varian WinUV software at 354 nm (cooling-ramp in the temperature range of 10-90°C, temperature gradient of 0.5°C/min). Data are normalized at maximum of absorbance (at high temperature).

Temperature dependent fluorescence data were collected on a *Varian Cary Eclipse* fluorescence spectrophotometer equipped with a *Varian Cary*-block temperature controller (excitation at 350 nm; excitation and emission slit width of 2.5 nm) using 1 cm x 1 cm quartz cuvettes. *Varian Eclipse* software was used to investigate the fluorescence of the oligopyrenes at a wavelength range of 370-700 nm in the temperature range of 10-90 °C, and the excitation at a wavelength range of 200-480 nm (emission at 500 nm, excitation slit width of 2.5, emission slit width of 1.5 nm).

CD spectra were recorded on a *JASCO J-715* spectrophotometer using quartz cuvettes with an optical path of 1 cm. (Scanning speed: 100 nm/min; data pitch: 0.5 nm; band width: 1.0 nm; response: 1 sec); LD measurements: optical path 10 mm, scanning speed 50 nm/min, SBW 1nm, integration time 1 sec.

The calculation of the g-factor was done with the equation G = CD(mdeg)/(32980*Abs) using the absorbance and CD values in mdeg recorded by the *JASCO-J-715*.

"Sergeant-and-soldiers" experiment. All samples were mixed on the same day in the corresponding ratio of **Py_7** and **Py_7-C** building block. To start the experiment from the same point, the samples were heated up to 60° C. Before heating at 60°C, and directly

after, measurements were performed. Data points were taken after 1 hour , 2 hours , 1 day , 2 days and then every week until one month had passed. The experiments were performed in sodium phosphate buffer (10 mM, 1M NaCl, pH 7.0) for 2.5 μM building block concentration.

Agarose gels were performed using 1×TAE buffer with 1% agarose. To the commercially available markers (GeneRuler DNA ladder mix, ready to use, and GeneRuler 100bp DNA ladder, ready to use, from Fermentas life sciences), ethidiumbromide (5 ng/mol) was added for visualization. A sample volume of 5μl (concentration: 5μM in 10 mM phosphate buffer, 1M NaCl, pH 7.0) of the samples were loaded. Gels were run at a voltage of 100 V. Due to the strong fluorescent properties of the pyrenyl derivatives, and to exclude possible disturbance of the formed aggregates, ethidiumbromide was only added to the DNA ladder and not to the preformed supramolecular polymers.

cryoTEM C-flat holey carbon films (CF-4/2-2C; EMS, Hatfield PA, US) were loaded with a drop of **Py_7** then blotted and immediately plunge frozen in liquefied propane (110K) according to Adrian and co-workers. [73] The frozen sample was transferred under liquid nitrogen into a Gatan cryoholder (Gatan 626, Gatan, Warrendale PA, US). At 100K the sample was investigated in a Tecnai F20 electron microscope (FEI, Eindhoven, NL). Images were taken with a 2kx2k Gatan CCD camera.

TEM For ESI (electron spectroscopic imaging), the samples were negatively stained as described by Harris. [74] In short, a carbon foil coated 400mesh grid was glow discharged, then a drop of 0.01% of polylysine (Sigma) was applied to the grid. After 10s the drop was removed with the help of a filterpaper. Adsorption of **Py_7** was performed by supplying a drop of the solution onto the grid for 60s. Then the sample was air dried for 2 minutes and a drop of negative stain (2% uranyl acetate in bidistilled water; Fluka, Buchs, CH) was applied. With the help of a filter paper the stain was removed so that a thin liquid phase remained. The sample was thereafter dried and investigated in the Tecnai F20 electron microscope. For the ESI imaging no phosphate buffer was added to the sample.

Mass spectrometry of oligomers was performed with a Sciex QSTAR pulsar (hybrid quadrupole time-of-flight mass spectrometer, *Applied Biosystems*). ESI-TOF MS (negative mode, CH_3CN/H_2O/TEA) data of compounds are presented in Table 1.

Table 1. Mass spectrometry data of synthesized oligomers (ESI-TOF MS, negative mode, CH_3CN/H_2O/TEA).

	Oligonucleotide	Molecular Formula	Calc. average mass	Found mass
1	SSS SSS S	$C_{168}H_{156}N_{14}O_{40}P_6$	3197.0	3203.0
2	(5') SS SSS SSC	$C_{177}H_{167}N_{17}O_{46}P_7$	3485.0	3492.0

3.5 References

[1] L. Brunsveld, B. J. B. Folmer, E. W. Meijer, R. P. Sijbesma, *Chem.Rev.* **2001**, *101*, 4071-4097.

[2] J. M. LEHN, *Polymer International* **2002**, *51*, 825-839.

[3] S. Mann, *Nature Mat.* **2009**, *8*, 781-792.

[4] J. M. LEHN, *Supramolecular Chemistry - Concepts and Perspectives*, VCH, Weinheim **1995**.

[5] G. M. Whitesides, J. P. Mathias, C. T. Seto, *Science* **1991**, *254*, 1312-1319.

[6] J. S. Lindsey, *New J.Chem.* **1991**, *15*, 153-180.

[7] V. Percec, M. Glodde, T. K. Bera, Y. Miura, I. Shiyanovskaya, K. D. Singer, V. S. K. Balagurusamy, P. A. Heiney, I. Schnell, A. Rapp, H. W. Spiess, S. D. Hudson, H. Duan, *Nature* **2002**, *419*, 384-387.

[8] H. J. Schneider, *Angew.Chem.Int.Ed.* **2009**, *48*, 3924-3977.

[9] D. Pijper, B. L. Feringa, *Soft Matter* **2008**, *4*, 1349-1372.

[10] A. W. Bosman, R. P. Sijbesma, E. W. Meijer, *Mat.Today* **2004**, *7*, 34-39.

[11] J. D. Badjic, A. Nelson, S. J. Cantrill, W. B. Turnbull, J. F. Stoddart, *Acc.Chem.Res.* **2005**, *38*, 723-732.

[12] J. E. Anthony, *Chem.Rev.* **2006**, *106*, 5028-5048.

[13] E. R. Kay, D. A. Leigh, F. Zerbetto, *Angew.Chem.Int.Ed.* **2007**, *46*, 72-191.

[14] L. C. Palmer, S. I. Stupp, *Acc.Chem.Res.* **2008**, *41*, 1674-1684.

[15] T. Rehm, C. Schmuck, *Chem.Commun.* **2008**, 801-813.

[16] M. R. Wasielewski, *Acc.Chem.Res.* **2009**, *42*, 1910-1921.

[17] A. R. A. Palmans, J. A. J. M. Vekemans, E. E. Havinga, E. W. Meijer, *Angew.Chem.Int.Ed.* **1997**, *36*, 2648-2651.

[18] F. J. M. Hoeben, P. Jonkheijm, E. W. Meijer, A. P. H. J. Schenning, *Chem.Rev.* **2005**, *105*, 1491-1546.

[19] T. F. A. Greef, E. W. Meijer, *Nature* **2008**, *453*, 171-173.

[20] A. Lohr, F. Wurthner, *Angew.Chem.Int.Ed.* **2008**, *47*, 1232-1236.

[21] X. L. Feng, W. Pisula, L. J. Zhi, M. Takase, K. Mullen, *Angew.Chem.Int.Ed.* **2008**, *47*, 1703-1706.

[22] V. L. Malinovskii, D. Wenger, R. Häner, *Chem.Soc.Rev.* **2010**, *39*, 410-422.

[23] J. D. Hartgerink, E. R. Zubarev, S. I. Stupp, *Curr.Opin.Solid State Mat.Sci.* **2001**, *5*, 355-361.

[24] E. A. Meyer, R. K. Castellano, F. Diederich, *Angew.Chem.Int.Ed.* **2003**, *42*, 1210-1250.

[25] K. C. Hannah, B. A. Armitage, *Acc.Chem.Res.* **2004**, *37*, 845-853.

[26] P. G. A. Janssen, A. Ruiz-Carretero, D. Gonzalez-Rodriguez, E. W. Meijer, A. P. H. J. Schenning, *Angew.Chem.Int.Ed.* **2009**, *48*, 8103-8106.

[27] P. G. A. Janssen, S. Jabbari-Farouji, M. Surin, X. Vila, J. C. Gielen, T. F. A. de Greef, M. R. J. Vos, P. H. H. Bomans, N. A. J. M. Sommerdijk, P. C. M. Christianen, P. Leclere, R. Lazzaroni, P. van der Schoot, E. W. Meijer, A. P. H. J. Schenning, *J.Am.Chem.Soc.* **2009**, *131*, 1222-1231.

[28] R. Iwaura, M. Ohnishi-Kameyama, T. Iizawa, *Chem.Eur.J.* **2009**, *15*, 3729-3735.

[29] H. Kitagishi, K. Oohora, T. Hayashi, *Biopolymers* **2009**, *91*, 194-200.

[30] S. H. Gellman, *Acc.Chem.Res.* **1998**, *31*, 173-180.

[31] D. J. Hill, M. J. Mio, R. B. Prince, T. S. Hughes, J. S. Moore, *Chem.Rev.* **2001**, *101*, 3893-4011.

[32] I. Huc, *Eur.J.Org.Chem.* **2004**, 17-29.

[33] E. Yashima, K. Maeda, in *Foldamers - Structure, Properties, and Applications*, Eds.: S. Hecht, I. Huc, Wiley-VCH, Weinheim , 2007, pp. 331-366.

[34] Y. Wang, F. Li, Y. M. Han, F. Y. Wang, H. Jiang, *Chem.Eur.J.* **2009**, *15*, 9424-9433.

[35] D. Haldar, C. Schmuck, *Chem.Soc.Rev.* **2009**, *38*, 363-371.

[36] S. M. Langenegger, R. Häner, *Chem.Commun.* **2004**, 2792-2793.

[37] S. M. Langenegger, R. Häner, *ChemBioChem* **2005**, *6*, 848-851.

[38] S. M. Langenegger, R. Häner, *Bioorg.Med.Chem.Lett.* **2006**, *16*, 5062-5065.

[39] I. Trkulja, R. Häner, *Bioconjug.Chem.* **2007**, *18*, 289-292.

[40] I. Trkulja, R. Häner, *J.Am.Chem.Soc.* **2007**, *129*, 7982-7989.

[41] F. Samain, V. L. Malinovskii, S. M. Langenegger, R. Häner, *Bioorg.Med.Chem.* **2008**, *16*, 27-33.

[42] M. H. Caruthers, *Science* **1985**, *230*, 281-285.

[43] V. L. Malinovskii, F. Samain, R. Häner, *Angew.Chem.Int.Ed.* **2007**, *46*, 4464-4467.

[44] R. Häner, F. Samain, V. L. Malinovskii, *Chem.Eur.J.* **2009**, *15*, 5701-5708.

[45] V. A. Galievsky, V. L. Malinovskii, A. S. Stasheuski, F. Samain, K. A. Zachariasse, R. Häner, V. S. Chirvony, *Photochem.Photobiol.Sci.* **2009**, *8*, 1448-1454.

[46] R. Häner, F. Garo, D. Wenger, V. L. Malinovskii, *J.Am.Chem.Soc.* **2010**, *132*, 7466-7471.

[47] F. M. Winnik, *Chem.Rev.* **1993**, *93*, 587-614.

[48] K. A. Zachariasse, W. Kuhnle, A. Weller, *Chem.Phys.Lett.* **1978**, *59*, 375-380.

[49] K. Zachariasse, W. Kuhnle, *Z.Phys.Chem.* **1976**, *101*, 267-276.

[50] S. Werder, V. L. Malinovskii, R. Häner, *Org.Lett.* **2008**, *10*, 2011-2014.

[51] H. Bittermann, D. Siegemund, V. L. Malinovskii, R. Häner, *J.Am.Chem.Soc.* **2008**, *130*, 15285-15287.

[52] C. A. Hunter, K. R. Lawson, J. Perkins, C. J. Urch, *J.Chem.Soc., Perkin Trans.2* **2001**, 651-669.

[53] M. M. Green, N. C. Peterson, T. Sato, A. Teramoto, R. Cook, S. Lifson, *Science* **1995**, *268*, 1860-1866.

[54] M. M. Green, J. W. Park, T. Sato, A. Teramoto, S. Lifson, R. L. B. Selinger, J. V. Selinger, *Angew.Chem.-Int.Ed.* **1999**, *38*, 3139-3154.

[55] A. R. A. Palmans, E. W. Meijer, *Angew.Chem.Int.Ed.* **2007**, *46*, 8948-8968.

[56] K. Maeda, E. Yashima, *Top.Curr.Chem.* **2006**, *265*, 47-88.

[57] T. E. Kaiser, V. Stepanenko, F. Würthner, *J.Am.Chem.Soc.* **2009**, *131*, 6719-6732.

[58] P. Rivera-Fuentes, J. L. Alonso-Gomez, A. G. Petrovic, F. Santoro, N. Harada, N. Berova, F. Diederich, *Angew.Chem.Int.Ed.* **2010**, *49*, 2247-2250.

[59] T. F. A. de Greef, M. M. J. Smulders, M. Wolffs, A. P. H. J. Schenning, R. P. Sijbesma, E. W. Meijer, *Chem.Rev.* **2009**, *109*, 5687-5754.

[60] M. M. Green, K. S. Cheon, S. Y. Yang, J. W. Park, S. Swansburg, W. H. Liu, *Acc.Chem.Res.* **2001**, *34*, 672-680.

[61] M. M. Green, M. P. Reidy, R. J. Johnson, G. Darling, D. J. Oleary, G. Willson, *J.Am.Chem.Soc.* **1989**, *111*, 6452-6454.

[62] E. Yashima, K. Maeda, H. Iida, Y. Furusho, K. Nagai, *Chem.Rev.* **2009**, *109*, 6102-6211.

[63] F. Totsingan, V. Jain, W. C. Bracken, A. Faccini, T. Tedeschi, R. Marchelli, R. Corradini, N. R. Kallenbach, M. M. Green, *Macromolecules* **2010**, *43*, 2692-2703.

[64] N. Berova, K. Nakanishi, R. W. Woody, *Circular Dichroism - Principles and Applications*, 2nd ed. Wiley-VCH, New York **2000**.

[65] N. Berova, L. Di Bari, G. Pescitelli, *Chem.Soc.Rev.* **2007**, *36*, 914-931.

[66] G. A. Hembury, V. V. Borovkov, Y. Inoue, *Chem.Rev.* **2008**, *108*, 1-73.

[67] M. M. J. Smulders, A. P. H. J. Schenning, E. W. Meijer, *J.Am.Chem.Soc.* **2008**, *130*, 606-611.

[68] T. Ishi-i, R. Kuwahara, A. Takata, Y. Jeong, K. Sakurai, S. Mataka, *Chem.Eur.J.* **2006**, *12*, 763-776.

[69] M. M. J. Smulders, M. M. L. Nieuwenhuizen, T. F. A. de Greef, P. van der Schoot, A. P. H. J. Schenning, E. W. Meijer, *Chem.Eur.J.* **2010**, *16*, 362-367.

[70] M. M. Green, in *Circular Dichroism - Principles and Applications*, Eds.: N. Berova, K. Nakanishi, R. W. Woody, Wiley-VCH, Hoboken, NJ , 2000, pp. 491-520.

[71] D. Zhao, J.S. Moore, *Org. Biomol.Chem.* **2003**, *1*, 3471-3491.

[72] S. M. Langenegger, R. Häner, *ChemBioChem* **2005**, *6*, 848-851.

[73] M. Adrian , J. Dubochet , J. Lepault , A.W. McDowall , *Nature* **1984**, *30*, 6-32.

[74] J.R. Harris, in Methods in *Molecular Biology: Electron Microscopy Methods and Protocols*, Humana Press, Ed. J.Kuo **2007**,107-142.

4. Atomic force microscopy: A tool to study supramolecular polymerization

This work has been performed in collaboration with the group of Prof. Dr. Thomas Wandlowski:
Alexander V. Rudnev, Alina Nussbaumer, Artem Mishchenko, Vladimir L. Malinovskii, Thomas Wandlowski, Robert Häner; *manuscript in preparation*

4.1 Abstract

AFM is known to be an useful technique to image DNA molecules on a mica surface. The presented studies show that AFM can also be used for our designed supramolecular polymers. It is possible to visually screen and directly observe the formation of supramolecular polymers. AFM-technique is a valuable contribution to the previously used optical techniques in studying the here described supramolecular systems. In this chapter it is highlighted that the simple AFM measurements can give fast and reliable information upon screening of complex functional blocks for supramolecular polymerization.

4.2 Introduction

Atomic force microscope (AFM) has emerged as one of the most widely used scanning probe microscopes used for biological applications. AFM was invented in 1986 and became a very useful instrument for imaging DNA, as well as DNA-protein complexes in air and in aqueous solutions.[1, 2, 3, 4] Mica is a common surface for AFM imaging of DNA. For imaging in air, a drop of DNA-containing solution is deposited onto freshly split mica, rinsed with water and then dried thoroughly. The amount of DNA bound to the mica

surface is significantly greater when the DNA solution contains salts of divalent or other multivalent inorganic cations, which can serve as a bridge between the negatively charged DNA and the negatively charged mica surface. Studies showed that DNA in solutions is bound tightly enough to the mica surface, in case the radius of the transition metal cation is between 0.69 to 0.74 Ångstrom. Ni^{2+} for example has been used to adsorb DNA onto the mica surface.[5] Further, it was shown that with a concentration of approximately 1 mM of the cation, DNA binding is most efficient.

Because of similarities in the structure between the found supramolecular polymers and DNA, namely the negatively charged phosphate backbone, the decision was made to study the designed artificial systems with AFM using similar conditions as for DNA. Moreover, it could be shown that AFM technique breaks limits of optical methods.

Optical techniques are often insufficient to discriminate and characterize minute fractions of ordered assemblies in the presence of bulk material. For example, UV/Vis spectroscopy provides averaged spectra of all absorbing species. Structure informations on individual aggregates of different type or shape are not accessible. It also makes almost impossible the distinguishing of small fractions of ordered novel assemblies appearing in a sample. Fractions of absorbing species with distinctly different optical activity may be observed with CD spectroscopy. However, the low sensitivity, (>10 fold as compared to UV/Vis spectroscopy), requires large sample concentrations, which often hampers the identification and characterization of the active molecular building blocks.

The AFM experiments allow the direct observation of shape and dynamics of the aggregates under equilibrium. Furthermore, the microscopic investigations enabled us distinguishing between cooperative and non-cooperative aggregation, as well as to clarify the origin of the loss of supramolecular chirality in their mixtures. Therefore AFM technique provides additional informations about the structure and formation of the supramolecular polymers described previously.

4.3 Results and discussion

4.3.1 Visualization of supramolecular polymers

Figure 1 shows the AFM image of $(\mathbf{Py_7})_n$ polymers (A) and B-DNA molecules (B) (600bp DNA fragment) as a reference deposited on mica using Ni^{2+} cations as binding agent. The shown long rod-like structures, strongly confirm the previous proposed model of the formation of supramolecular polymers. The data demonstrate qualitative similarities in the shapes of $(\mathbf{Py_7})_n$ assemblies and of the DNA molecules.

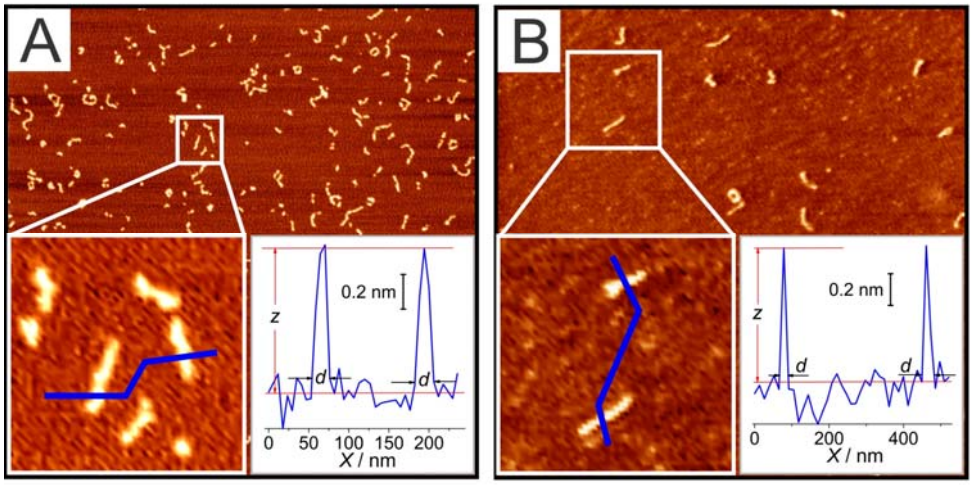

Figure 1. Tapping mode AFM images of (A) $\mathbf{(Py_7)_n}$ polymers and (B) B-DNA molecules (600bp DNA fragment) deposited on mica using Ni^{2+} cations as binding agent, 3×3 μm^2. The polymers were formed from 2.5 µM achiral oligomers $\mathbf{Py_7}$ in solution by addition of 1 M NaCl. After one month equilibration time, an aliquot of 5 µl was mixed with 10 µl of 5 mM $NiCl_2$ (final $[Ni^{2+}]$ = 3.3 mM), and subsequently deposited on mica. The DNA samples were also prepared in the presence of 1 M NaCl. Subsequently, 5 µl of the DNA solution (0.18 µg μl^{-1}) were mixed with 10 µl of 5 mM $NiCl_2$ (final $[Ni^{2+}]$ = 3.3 mM) and then deposited on mica. The insets show magnifications of panels A and B and typical cross sections of the two polymer strands.

The apparent width *d* of both polymers and DNA molecules was found to be similar and amounts to 32 ± 8 nm.

The rather high value for the experimentally determined width, (the diameter of regular B-DNA is known to be ~2 nm), is ascribed to the convolution of the AFM tip radius R with the molecular feature under study. When an object with the thickness d_{real} on a flat substrate is measured by an AFM tip of radius R and it is assumed that the minimum distance between the tip surface and the sample surface is constant, the edge of the object becomes blurred and the apparent lateral size increases by factor $2(2Rd_{real}-d_{real}^2)^{1/2}$.[6] The function linking the real diameter d_{real} with apparent width d is plotted in Figure 2. Provided that the tip radius is 10 nm (from specification of cantilevers) and the measured width of polymers d varies in the range of 24 to 40 nm, the real width d_{real} was estimated to be equal to ~2.0 to 2.9 nm.

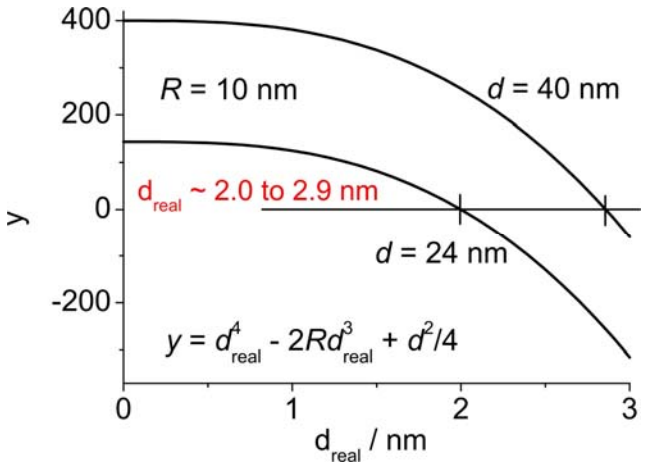

Figure 2. To estimation of the real width of polymers.

The analysis of polymer heights on different images recorded in different experiments revealed that the height varies between 0.40 nm and 0.85 nm depending on the cantilever and the scanning parameters. However, the exact diameter of double-stranded B-DNA molecules is much larger. Published data range between ~2.0 nm in solid state [7,8] and 2.2 to 2.6 nm in aqueous solution. [9] The latter accounts for the hydration shell. It should be considered that the measured height of DNA molecules adsorbed on a mica substrate by scanning probe microscopy is always less than the theoretical diameter. Possible explanations are that the salt layer [10], in which the molecules are immersed, distorts the measurements of DNA height or the distortion occurs because of the tip pressure during the tapping mode measurements. [11]

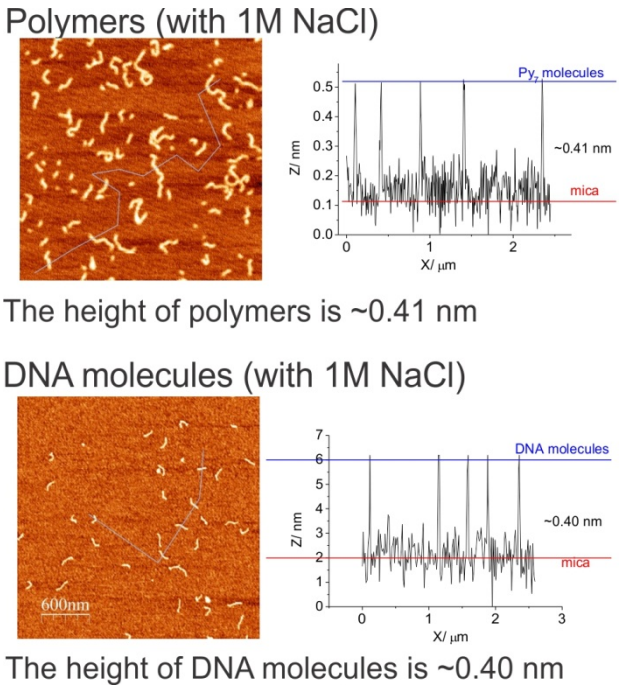

Figure 3. Comparison of the height of DNA molecules and supramolecular polymers.

Using the DNA molecules (NoLimits 600bp DNA Fragment from Fermentas Life Sciences) as a reference allowed the estimation of the real polymer height. After AFM imaging of the supramolecular polymers, we measured DNA molecules deposited also on mica with the same cantilever and the same scanning parameters (Figure 3). The ratio of polymer and DNA heights amounts to 1.0 ± 0.1. In consequence we extract the value 2.4 ± 0.4 nm as the “real” height or diameter of the polypyrene rod-like aggregates.

As previously described, the stacking within the pyrene units leading to the formation of supramolecular polymers is triggered by increasing ionic strength. The sodium cations can have a competing effect on the adsorption of the pyrene oligomers. Therefore, a detailed study has been carried out to find the right conditions for a good binding of supramolecular polymers to the mica surface. We observed no polymers adsorbed on mica in the case of low concentration of bivalent cations (Ni^{2+} ≤ 0.7 mM) (Figure 4).
The concentration of the Ni^{2+} cations was changed in order to achieve the deposition of the supramolecular polymers on the surface. With increasing concentration of Ni^{2+} from 1.3 to 3.3 the binding of the molecules increased also. The cooperative effects involved in the interactions of the adhesive lead to a stronger surface-binding of the longer

polymers. Molecular building blocks and small aggregates are significantly less strongly attached. This observation enables the detection, selection and analysis of *small fractions* of long aggregates, even in a pool of monomeric building blocks and other types of weakly associated aggregates.

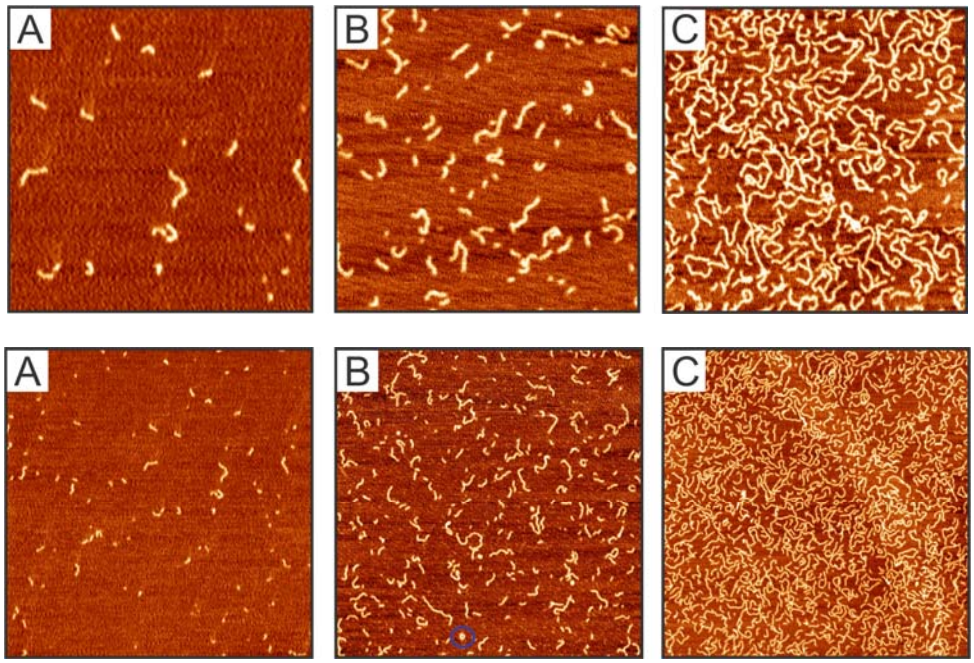

Figure 4. 1.5×1.5 and 3×3 μm^2 tapping mode AFM images (recorded in air) of $\mathbf{(Py_7)_n}$ -type supramolecular polymers initially formed in bulk solutions, and subsequently deposited on mica with Ni^{2+} as binding additive. The concentration of $\mathbf{Py_7}$ monomers was 2.3 μM. The Ni^{2+} concentration varied from 1.3 mM (A), 2.3 mM (B) to 3.3 mM (C). A ring-shaped polymer is highlighted in panel (B).

The quantitative analysis of AFM images demonstrates an exponential decrease in the number of polymers with a contour length in the range from 25 to 300 nm. Figure 5 illustrates a set of data as obtained for a $\mathbf{(Py_7)_n}$ sample on mica with 2.3 mM Ni^{2+} from 20 separate AFM images acquired at different surface spots. The exponential decay of the length distribution suggests supramolecular polymerization according to a nucleation-elongation mechanism. [12]

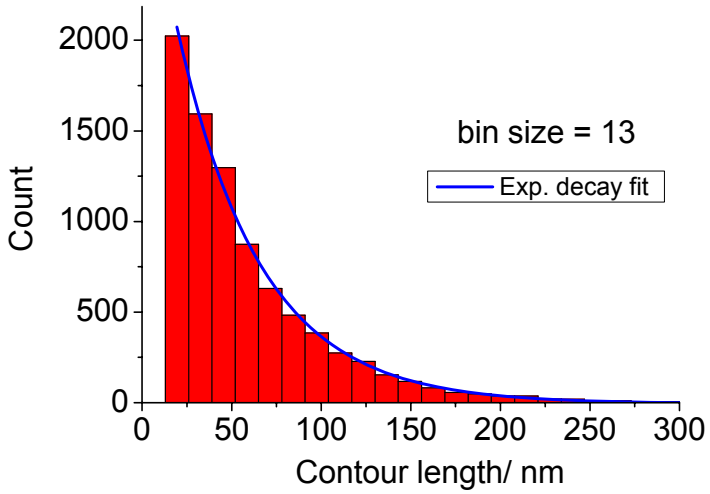

Figure 5. Contour length analysis was performed by using home-developed program in Labview software. Data were collected from 20 AFM images of supramolecular polymers formed from oligomers **Py$_7$** in bulk solution (concentration of **Py$_7$** building blocks was 7 µM) and deposited on mica using bivalent cations Ni^{2+} as binding agent. The concentration of Ni^{2+} was 2.3 mM.

Occasionally we also observed (**Py$_7$**)$_n$ polymers of circular contour. End-to-end intra-supramolecular assembly leads to ring-shaped polymeric assemblies such as marked in Figure 4B.

4.3.2 Formation of supramolecular polymers

The influence of salt on the formation of supramolecular polymers was studied with optical techniques. The appearance of vibronic structures in the absorbance spectra within time showed stacking and organization within the pyrene units with increasing ionic strength.

In Figure 6 the results of a time-dependent study of **Py$_7$** in the absence, as well as in the presence, of 1 M NaCl in the monomer-containing bulk solution are presented. Based on the above experiments, the concentration of Ni^{2+} was chosen as 2.3 mM. No linear elongated polymer chains are formed in the absence of sodium chloride, even after an extended assembly time up to 3 weeks. Figure 6A reveals only rather small, non-cooperative aggregates of undefined size and shape. Cooperative polymerization of **Py$_7$**

requires the addition of NaCl to the solution. Clearly, supramolecular polymerization of **Py_7** can be initialized in a rather controlled manner.

The time-dependent experiments revealed that the formation of rod-like **$(Py_7)_n$** polymers starts 40 minutes after adding 1 M NaCl to the **Py_7**-containing solution (Figure 6B). Increasing the equilibration time leads to a continuous increase in the number of detectable **$(Py_7)_n$** polymers (Figure 6C and 6D).

The formation of supramolecular polymers can not be detected by UV/Vis measurements after 40 minutes reaction time due to sensitivity limitations. Increasing reaction time up to 3 weeks leads finally to a detectable increasing hypochromism (previous section). This clearly shows the high sensitivity of the AFM-type detection approach for monitoring supramolecular polymerization. With AFM, individual aggregated products on the mica substrate surface which are not yet visible by optical techniques, can be already detected.

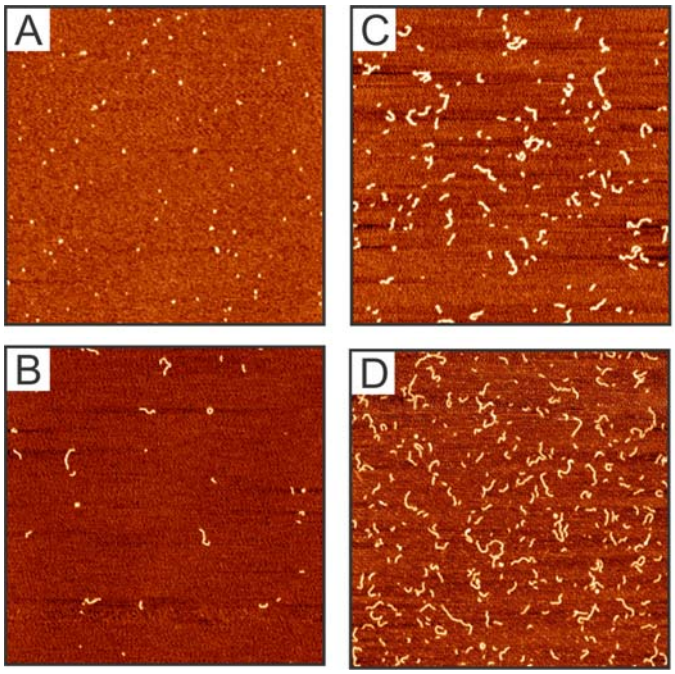

Figure 6. Tapping mode AFM images recorded in air for the assembly of **$(Py_7)_n$** on mica with 7 µM **Py_7** monomer solutions (frame size 3×3 μm^2): (A) in the absence of 1 M NaCl after 10 hours equilibration; (B) to (D) in the presence of 1 M NaCl after 40 min (B), 1 week (C) and 3 weeks (D) reaction time . The concentration of Ni^{2+} was 2.3 mM.

4.3.3 Cooperative and non-cooperative formation of polymers

Previously, oligomer **Py_7-C** is introduced, with a cytosine attached via the 5'- oxygen.
Two mechanisms can explain the findings of the "sergeant-and-soldiers" experiments: (I) a change in the aggregation process from a cooperative to a non-cooperative mechanism [12] with increasing contents of the mismatching unit **Py_7-C** or; (II) the incidence of multiple reversals in the supramolecular polymers. [13] Both mechanisms seemed reasonable, based on the original spectroscopic data.
AFM was applied to gain a picture of the proposed model. In Figure 7B, 100% of oligomer **Py_7** is deposited on the mica surface. The supramolecular polymers are visible clearly. With 10 % of the oligomer **Py_7-C**, a reduction of bound supramolecular polymers is visible. Image 7D shows no adsorbed molecules on mica surface. This suggests that mechanism (I) is more probable. Oligomer **Py_7-C** form small aggregates, which are not bound efficiently to the mica surface and as a consequence will be washed away during the washing step. Already during the process of adsorption and interaction with the mica surface, which is promoted using Ni^{2+} cations as an additive, a selection of cooperative supramolecular polymers and non-cooperative aggregates occurs.

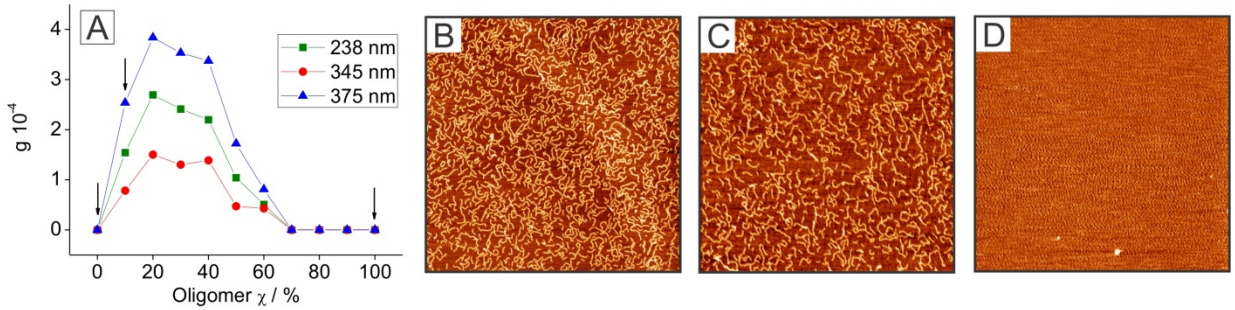

Figure 7. (A) Changes in the intensities of CD signals (as the anisotropy factor *g*) at different wavelengths in dependence on the fraction of oligomers **Py_7-C** in bulk solution. (B)-(D) 3×3 μm^2 AFM images of mica samples modified with polymers deposited from solutions containing (B) 0% of **Py_7-C** (pure **Py_7**), (C) 10% of **Py_7-C**, and (D) 100% of **Py_7-C**. These **Py_7-C** fractions are indicated by arrows in panel (A).

Further AFM studies were performed of the "sergeant-and-soldiers" of **Py_7** and **Py_7-C** at constant total concentration of pyrene blocks (typically 2.3 µM). The AFM data shown in

Figure 8 illustrate that the density of linear polymer strands decreases with increasing contents of the cytidine-modified **Py_7-C**. No rod-like polymers units were detected for samples prepared from a reaction solution with more than 60% **Py_7-C** (Figure 8E). Clearly, the nucleation step is suppressed. Thus, the attachment of a terminal cytidine nucleotide onto the pyrene oligomer changes the aggregation mechanism from cooperative (pure **Py_7**, Figure 8A) to non-cooperative (pure **Py_7-C**, Figure 8 E).

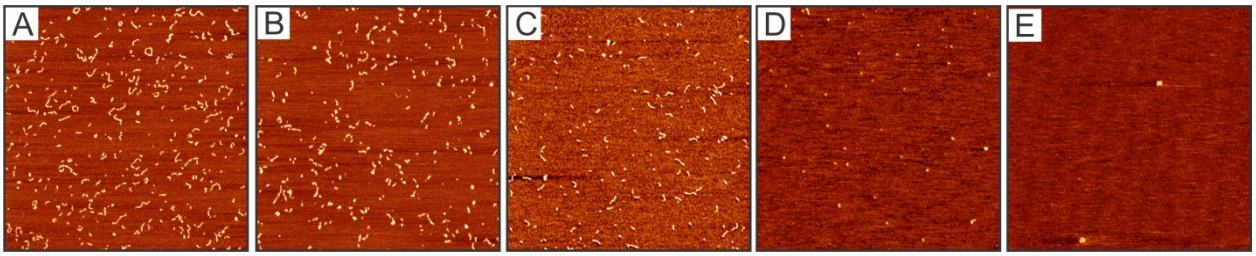

Figure 8. Tapping mode AFM images of mica samples modified with polymers formed in oligopyrene solutions containing different molar fractions of **Py_7-C** (image size 3 x 3 μm^2): (A) 0% (pure **Py_7**), (B) 20%, (C) 40%, (D) 60%, and (E) 100% (pure **Py_7-C**). The total concentration of pyrene oligomers was 2.5 µM in all samples. The ionic strength is given by the 1 M NaCl electrolyte.

4.4 Conclusions

It could be shown that the formed supramolecular polymers can be studied by atomic force microscopy (AFM). AFM is a convincing technique to visualize processes like formation of supramolecular polymers, and can be used to distinguish between the cooperative and non-cooperative mechanism in supramolecular polymerization. The obtained results are in strong agreement with the results obtained by optical techniques and the proposed model.

The images give a valuable contribution to the characterization of these supramolecular systems.

Moreover, it could be shown that AFM technique provides fast and reliable structure information, which significantly extends the detection limits of UV/Vis and CD spectroscopy.

4.5 Experimental part

Atomic force microscopy. Samples of mica (20×20 mm^2) were attached to the steel baseplate through the double scotch tape and cleaved with tape immediately before use. 5 µl of 2.5 or 7 µM oligomer solutions was mixed with 10 µl of 1-5 mM $NiCl_2$ solution (the final concentrations of Ni^{2+} are 0.7 to 3.3 mM). The mixture obtained was dropped onto mica surface and the sample was left for 8 min. Afterwards the mica surface was thoroughly rinsed with Milli Q water (> 18 MΩ cm^{-1}, 4 ppb TOC) and dried under gentle stream of 5 N Ar (Alpha Gas). AFM imaging was performed in tapping mode in air with Nanosurf FlexAFM (Nanosurf AG, Switzerland). We used cantilevers Nanosensors PPP-NCHR-W (freq. ~280kHz, tip radius ~ 10 nm).

4.6 References

[1] Y.L. Lyubchenko, *Cell Biochemistry and Biophysics* **2004**, *41*, 75-98.

[2] A.Engel, Y.L. Lyubchenko, D.Müller, *Trends Cell Biol.* **1999**, *9*, 77-80.

[3] Y.L. Lyubchenko, L.S. Shlyakhtenko, *Methods* **2009**, *47*, 206-213.

[4] H.G. Hansma, D.E. Laney, M. Bezanilla, R. L. Sinsheimer, P.K. Hansma, *Biophysical J.* **1995**, *68*, 1672-1677.

[5] H.G. Hansma, D.E. Laney, *Biophysical J.* **1996**, *70*, 1933-1939.

[6] K.-i. Umeda, K.-i. Fukui, *Langmuir* **2010**, *26*, 9104-9110.

[7] J. D. Watson, F. H. C. Crick, *Nature* 1953, *171*, 737-738.

[8] S. Arnott, D. W. L. Hukins, *Biochem. Biophys. Res. Commun.* **1972**, 1504-1509.

[9] M.Mandelkern, J. G. Elias, D. Eden, D. M. Crothers, *J. Mol. Biol.* **1981**, *152*, 153-161.

[10] F. Moreno-Herrero, J. Colchero, A.M. Baró, *Ultramicroscopy* **2003**, *96*, 167-174.

[11] G. Yunchang, Z.Xingfei, S. Jielin, L. Minqian, H. Jun, *Chinese Science Bulletin* **2004**, *49*, 1574-1577.

[12] L. Brunsveld, B. J. B. Folmer, E. W. Meijer, R. P. Sijbesma, *Chem.Rev.* **2001**, *101*, 4071-4097.

[13] M. M. Green, K. S. Cheon, S. Y. Yang, J. W. Park, S. Swansburg, W. H. Liu, *Acc.Chem.Res.* **2001**, *34*, 672-680.

5. Stereochemical control of supramolecular pyrene polymers

Alina L. Nussbaumer, Florent Samain, Vladimir L.Malinovskii and Robert Häner; *manuscript in preparation*

5.1 Abstract

Amphiphilic oligopyrenotides containing 7 pyrene units (**Py_7**) assemble into supramolecular polymers. In this chapter a comprehensive study of co-aggregates of the non-chiral **Py_7** and its mono- or di-substituted nucleotide analogs (**Py_7-N** and **N-Py_7-N'**) is presented. The data show that the formation of supramolecular polymers from oligopyrenotides **Py_7** is very sensitive to the nature of the attached, chiral auxiliary. A single natural nucleotide may be sufficient for the fine tuning of the aggregates' properties by changing the mechanism of aggregation from an *isodesmic* to a *nucleation-elongation* process, which results in a high degree of amplification of chirality in the formed supramolecular polymers. Watson-Crick complementarity does not play a significant role, since co-aggregates of oligomers modified with complementary nucleotides show no signs of supramolecular polymerization. Depending on the nucleotide, the helical sense of the polymers is shifted to an *M*-helix or a *P*-helix. The findings demonstrate the value of oligopyrenotides as oligomeric building blocks for the generation of optically active supramolecular polymers.

5.2 Introduction

Due to its self-assembling properties, DNA is probably one of the most prominent and exploited biological molecules, which is used to build multidimensional nanostructures and nanomaterials.[1,2] Possible medical and materials applications may be limited by the chemical and physical characteristics of the natural DNA building blocks. Not surprisingly, the quest is increasing for modified building blocks to give new properties to the structure, and for other modifications to gain more information about the nature of DNA. [3-5] However, precise control over the association and structural organization of the synthesized functional molecules lies still in the nature of DNA, which is often used as a scaffold in the development of novel types of materials. [6-16] Previous results from our group showed that an entirely artificial section of twelve or more pyrene 2,8-dicarboxamide units embedded in a double-stranded DNA molecule adopt a right-handed helical organization. [17] The negatively charged phosphate backbone and the DNA parts guarantee solubility in aqueous medium of the chimeric oligomers, despite the high lipophilicity of the pyrene residues. In these constructs, the DNA part facilitates the structural organization of the pyrene parts by bringing two pyrene strands in close proximity. On the other hand, these amphiphilic oligopyrenotides [18] also have their own, intrinsic structural features and form aggregates *via* directional self-assembly. [19] This observation prompted us to do further investigations reducing the DNA part to a minimum, namely one nucleotide pair, to explore if the pyrene units still adopt a defined structure and if transfer of chirality occurs from the nucleotide to the pyrene stacks. Heptapyrenotides (**Py_7**) [20] assemble into supramolecular polymers. [21-25] Doping with a cytidine modified oligopyrene (**Py_7-C**) has a significant influence on the helical aggregates via a mechanism of chiral amplification. [26-28]

In general, preferential helicity of columnar stacks can be realized through the introduction of chiral peripheral substituents of the aromatic stacking units or by use of chiral external factors, such as the solvent, ligands, or templates. [25, 29-42] In this chapter an extended study of co-aggregates of the non-chiral pyrenyl oligomer (**Py_7**) and its mono- or di-substituted nucleotide analogs (**Py_7-N** and **N-Py_7-N**') is presented. We demonstrate that a single nucleotide may be sufficient for the fine tuning of the aggregates' properties by changing the mechanism of aggregation from *isodesmic* to

nucleation-elongation, which results in a high degree of amplification of chirality in the supramolecular polymers (Scheme 1).

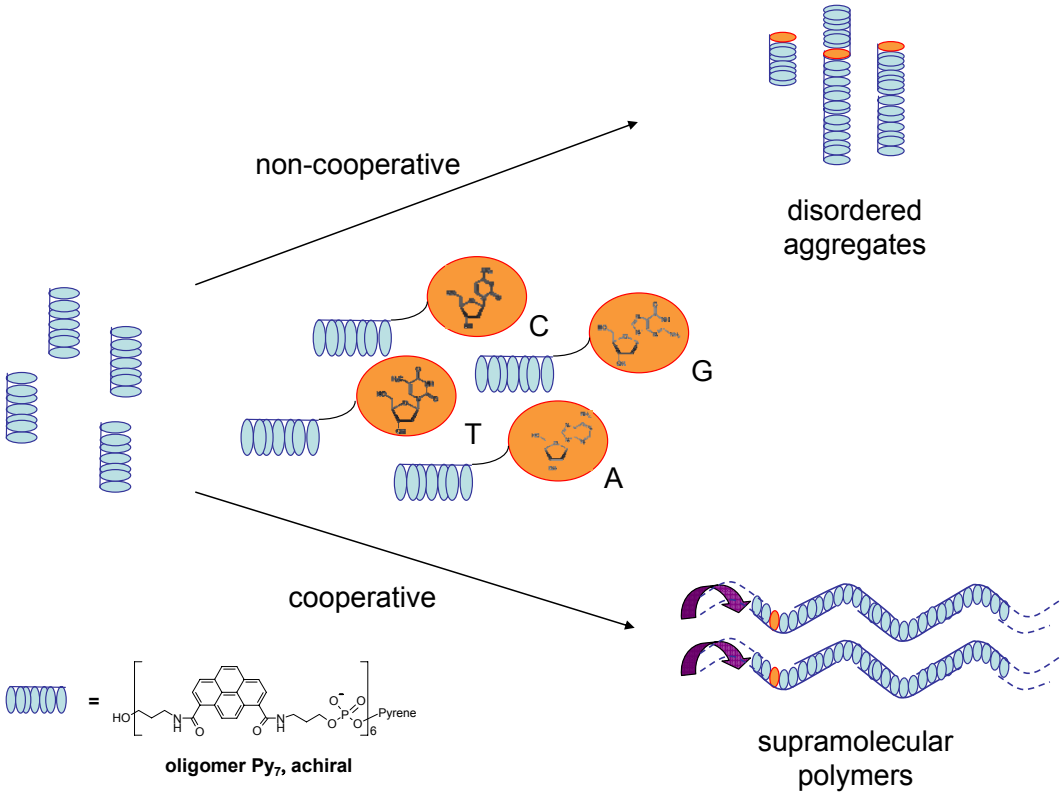

Scheme 1. Influence of a single nucleotide on the aggregation of oligomers Py_7 and the effect of amplification of chirality.

5.3 Results and Discussion

To investigate the influence of a single nucleotide on the formation of supramolecular assemblies, oligomers containing seven pyrene units and one or two of the four natural nucleotides (A,T,G,C) were synthesized (oligomers **1**-**13**, Scheme 2 and Table 1). The nucleotides were attached either via their 5'- oxygen (**2**, **5**, **8**, **11**) or their 3'- oxygen (**3**, **6**, **9**, **12**); oligomers **4**, **7**, **10** and **13** have one and the same kind of nucleotide attached on each end of the heptapyrenotide.

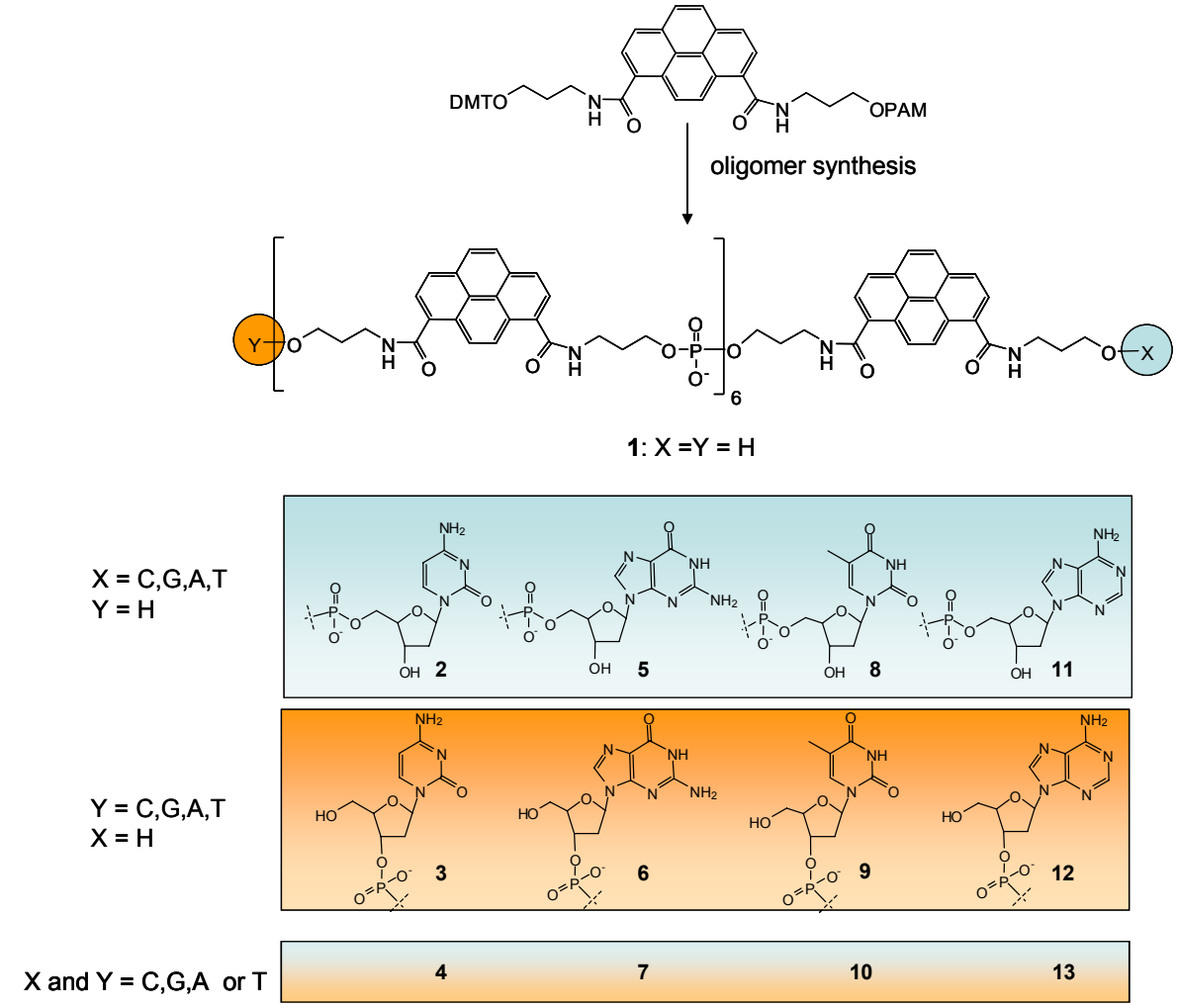

Scheme 2. Oligomers used in this study. Nucleotides are attached to the oligopyrenotide *via* their 5'- or 3'-ends.

Table 1. Pyrene oligomers used in the study; spectroscopic characteristics of self-aggregates and co-aggregates with oligomer **1**.

Nr.	oligomer	H% at nm[a] 245	284	354	polymerization process[b] self-aggr./co-aggr.		CD-type[c] self-aggr./co-aggr.		additional remarks[d]	
1	Py_7	31	43	32	*nucl.*	-	-	-		
2	Py_7-C	11	13	10	*isod.*	*nucl.*	-	*2*		
3	C-Py_7	16	23	18	*isod.*	*nucl.*	*1*	*2*		
4	C-Py_7-C	13	16	12	*isod.*	*nucl.*	-	-		
5	Py_7-G	18	26	19	*isod.*	*nucl.*	-	2^m		
6	G-Py_7	14	17	11	*isod.*	*nucl.*	*2*	-	*monomer fluoresc.*	*monomer fluoresc.*
7	G-Py_7-G	13	17	15	*isod.*	*nucl.*	*1*	2^m		*monomer fluoresc.*
8	Py_7-T	20	28	17	*isod.*	*nucl.*	*1*	-		
9	T-Py_7	13	14	12	*isod.*	*isod.*	-	-		
10	T-Py_7-T	10	12	10	*isod.*	*nucl.*	-	-		
11	Py_7-A	15	21	20	*isod.*	*nucl.*	-	2^m		
12	A-Py_7	11	15	9	*isod.*	*nucl.*	*1*	-	*monomer fluoresc.*	*monomer fluoresc.*
13	A-Py_7-A	10	12	10	*isod.*	*isod.*	-	-		

[a] Hypochromism upon aggregation; sodium phosphate buffer, pH =7.0, 1 M NaCl; 5 μM total oligomer concentration; [b] *isod. = isodesmic, nucl. = nucleation*; [c] *CD-type 1*: λ = 348 nm (+), 328 nm (-), 270 nm (-), 240 nm (+); *CD-type 2*: λ = 373 nm (+), 345 nm (-), 238 nm (-), 208 nm(-); *CD-type* 2^m: mirror image of *CD-type 2* (for further explanation see text); [d] *monomer fluoresc.* indicates that partial pyrene monomer fluorescence was observed in addition to excimer fluorescence.

The synthesized oligomers were investigated by absorbance, fluorescence and CD-spectroscopy. [13] Information about the degree of stacking of pyrenes in the oligomers is provided by UV/Vis spectroscopy. Vibronic structures are a result of reduced rotational freedom of the pyrene molecules and are observed if the pyrene molecules are stacked in an ordered way. Fluorescence spectra give an indication about the twisting of the pyrene units within stacks, which appears as a characteristic blue shift of pyrene excimer emission. The most common technique to examine chiral systems is CD-spectroscopy. In the present case, it provides information about the effect of a nucleotide on the formation of non-racemic, chiral pyrene assemblies in contrast to non-chiral aggregates with a random orientation of building blocks, or racemic mixture of chiral aggregates.
Formation of supramolecular polymers upon aggregation of **1** was described recently. [20] Self-association of the oligomers (**2**-**13**) was studied to elucidate the influence of modification (chiral aromatic molecule) on aggregation/assembly. Association of oligomers with complementary bases **2*6**, **3*5**, **4*7**, **8*12**, **9*11**, **10*13** was tested by mixing the oligomers in a 1:1-ratio in analogy to self-assembly of complementary strands in DNA. Moreover, co-aggregation of unmodified **1** with all of its base-modified derivatives **2**-**13** was investigated. The findings are described below.

5.3.1 Cytidine modified oligomers (**2**, **3** and **4**)

Figure 1 shows the normalized absorbance spectra in the range from 300-425 nm for oligomers **1**-**4** (left) and the co-aggregates **1*2**, **1*3** and **1*4**. Vibronic structures in absorbance spectra are much less pronounced in the case of self-association of the oligomers **2**-**4** (**1**>**3**>**2**>**4**). Co-aggregation of oligomer **1** with oligomers **2**-**4** shows some degree of vibronic structures. Among them co-aggregate **1*3** seems to be most ordered, but less than **1** alone (**1**> **1*3** >**1*2** >**1*4**). Hence, the best resolved vibronic structures are due to the assembly of oligomer **1**, which also exhibits the highest hypochromism upon cooling (Table 1, Figure 2)

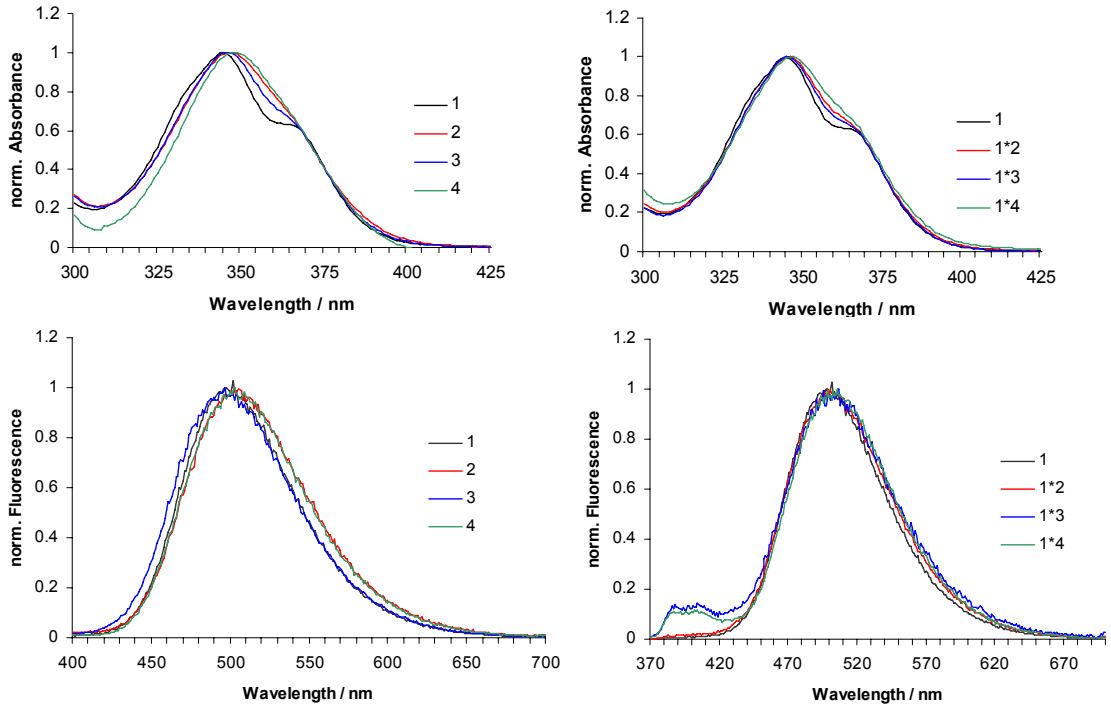

Figure 1. Normalized absorbance (top) and fluorescence (bottom) spectra of oligomers **1** (Py_7), **2** (Py_7-C), **3** (C-Py_7) and **4** (C-Py_7-C) (left) and co-aggregates of the cytidine-derived oligomers with 1 in a 1:1 ratio (right). Conditions: sodium phosphate buffer, pH =7.0, 1 M NaCl, 20°C; 5 μM total oligomer concentration.

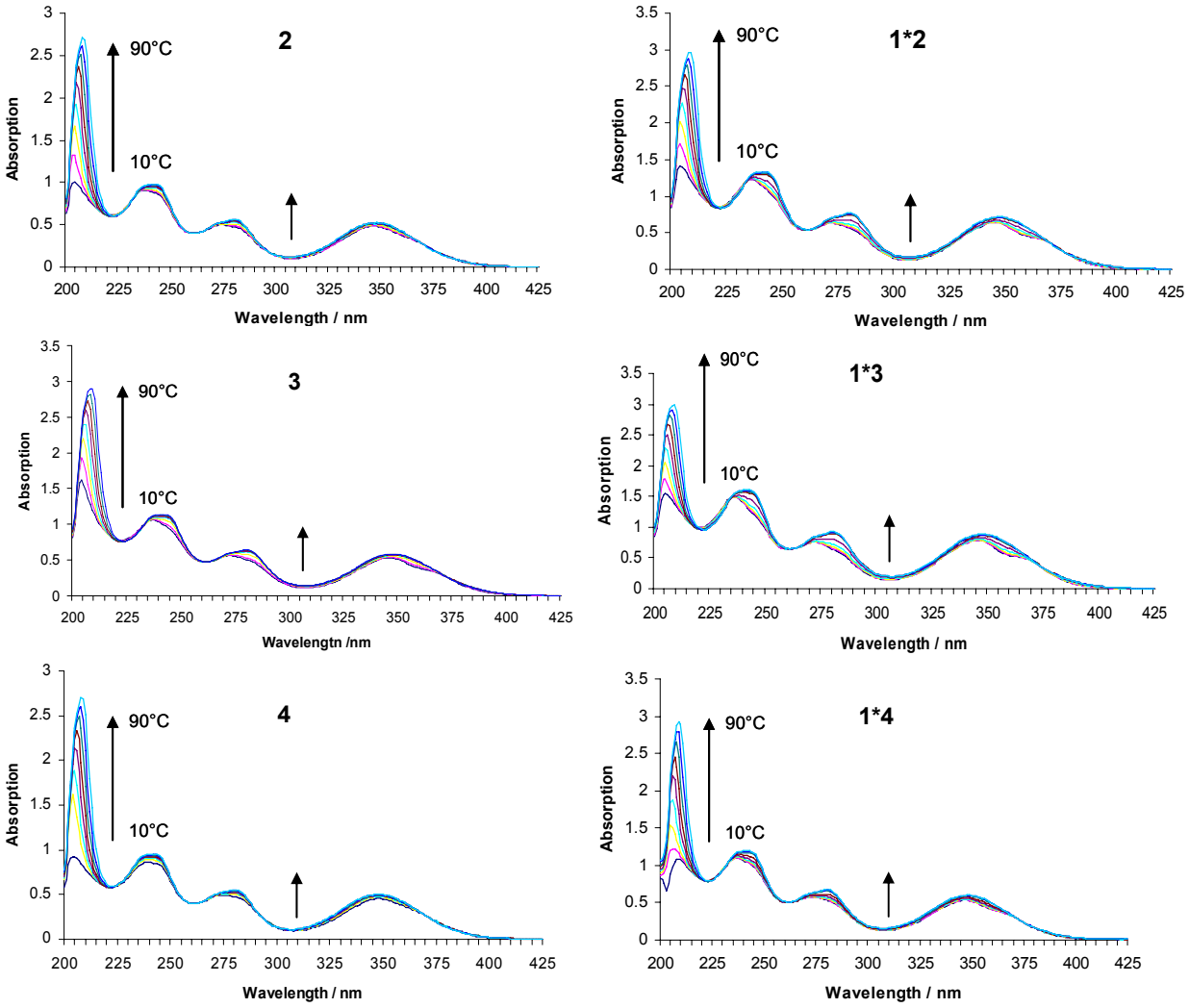

Figure 2. Temperature variable UV/Vis spectra of oligomer **2** (Py_7-C), **3**(C-Py_7), **4** (C-Py_7-C) (left) and co-aggregates with oligomer **1** in a 1:1 ratio (right). Conditions: sodium phosphate buffer, pH =7.0, 1 M NaCl**.** Total concentration of pyrenyl containing blocks: 5 µM.

The reduction of vibronic structures upon addition of one of the nucleotide-modified oligomers indicates a decrease of the fraction of ordered pyrene stacks. Self-aggregation of oligomer **2** shows the smallest values of hypochromism, meaning that attachment of a 3'-cytidine nucleotide has the biggest effect of disorganization within the pyrene stacks.

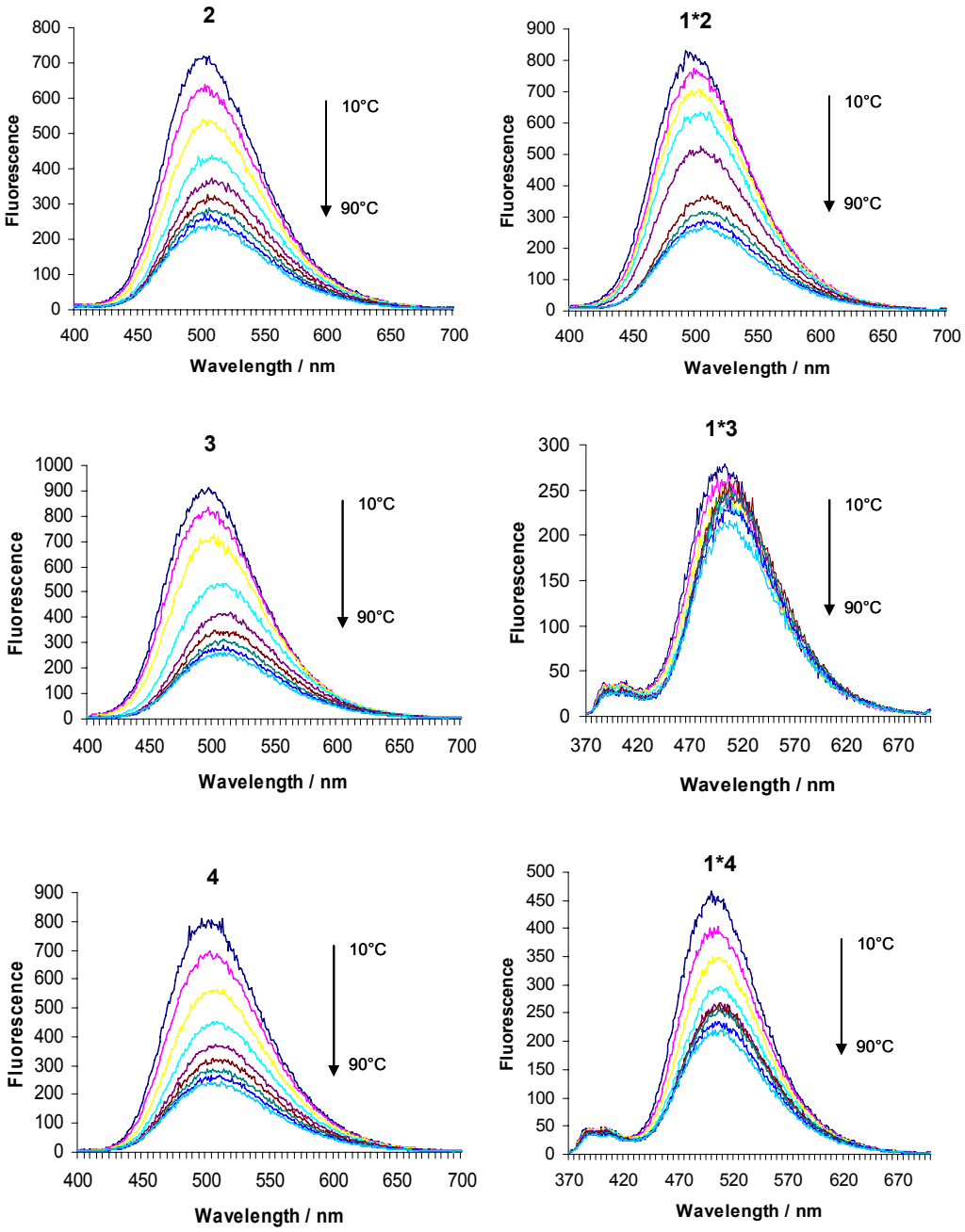

Figure 3. Temperature variable fluorescence spectra of oligomer **2** (Py_7-C), **3** (C-Py_7), **4** (C-Py_7-C) (left) and co-aggregates with oligomer **1** in a 1:1 ratio (right). Conditions: sodium phosphate buffer, pH =7.0, 1 M NaCl**.** Total concentration of pyrenyl containing blocks: 5 μM.

Temperature-dependent fluorescence spectra show a gradual loss in pyrene emission with increasing temperature (Figure 3) within self-association of oligomers **2**-**4**. For these oligomers short complexes are more probable, which gradually dissociate with increasing temperature. For co-aggregate **1*2**, a small transition can be observed between 50°C and 60°C, suggesting the formation of a more defined aggregate (Figure 3).

The bathochromic shift (10-13 nm) in pyrene emission is due to the increased conformational freedom in the melted structures. In Figure 1 (bottom) the normalized fluorescence spectra of pyrene emission at 20°C are presented. Self-association of **1** (498 nm) and **3** (497 nm) show a more pronounced blue shift than **2** (503 nm) and **4** (503 nm) relative to the excimer signals of the co-aggregates **1*2**, **1*3**, **1*4**, which occur at similar wavelength between 503-507 nm.

Based on the vibronic structures and the blue shift in pyrene emission, self–aggregates of oligomer C-Py_7 (**3**) seem to be most organized in the cytidine series. From absorbance spectra the structural organization in the co-aggregates is decreasing the following: **1**> **1*3** >**1*2** >**1*4**. The twisting of the pyrene units is in the same order as judged by the blue shift in fluorescence spectra.

Self-association of oligomer **3** shows a CD-response suggesting the formation of a chiral structure. A bisignate signal for the pyrene band is observed, centered at 340 nm, with a positive Cotton effect at λ = 348 nm, followed by a minimum at λ = 328 nm. At λ = 270 nm a negative signal appears followed by a more pronounced positive signal at 240 nm (labelled as *CD-type 1*; Figure 4 top). Co-aggregate **1*3** shows a similar CD-effect as described for **1*2**, i.e. a bisignate signal for the pyrene band centered at 360 nm with a positive Cotton effect at λ = 373 nm and a negative Cotton effect at λ = 345 nm. Two negative signals were observed at λ = 238 nm and λ = 208 nm (*CD-type 2*). Interestingly, co-aggregate **1*3** showed an even more intense signal than **1*2**. Apparently, a 5'-cytidine stabilizes the chiral aggregate even better than the 3'-cytidine, which shows that the attachment of the nucleotide is an important factor for the transfer of chirality. If the pyrene oligomer is modified with cytidine on both sides (**4**), no CD-signal was observed (Figure 4, bottom).

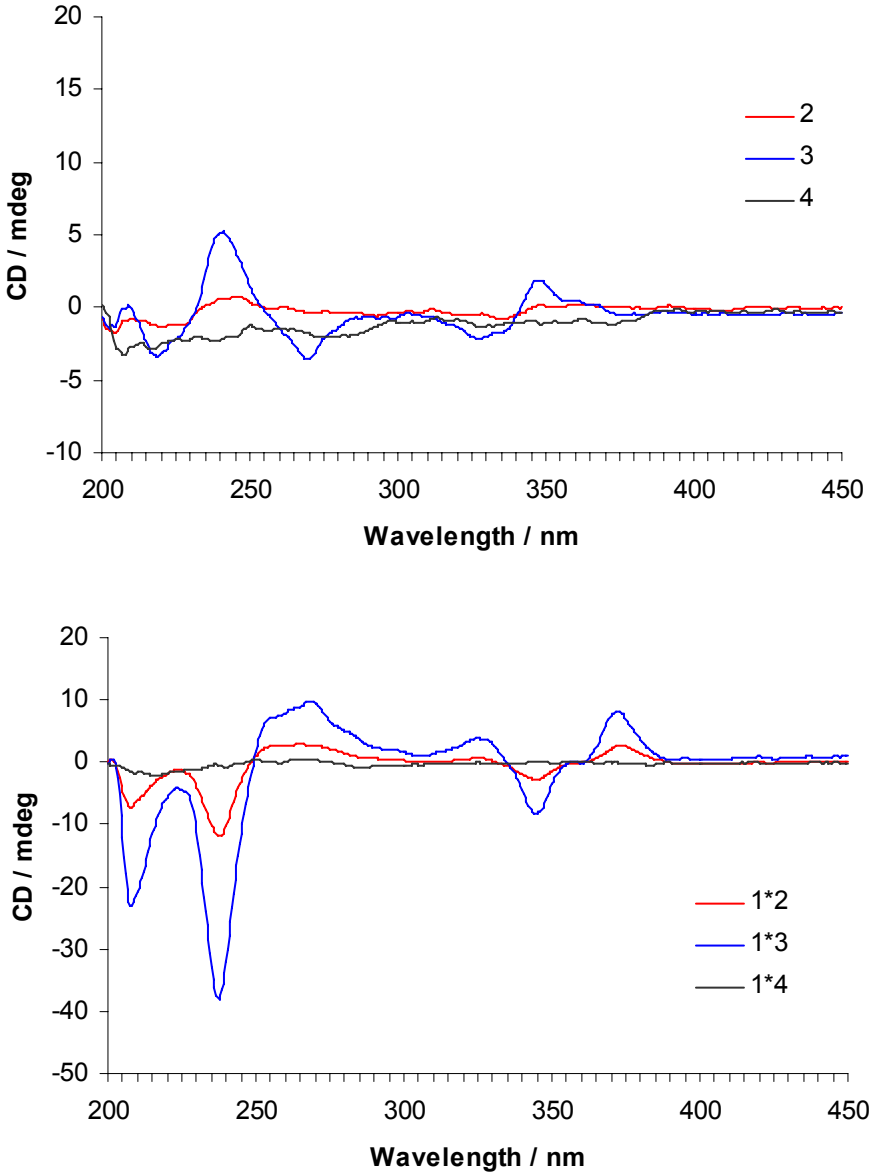

Figure 4. CD-spectra of cytidine-modified oligomers **2** (Py_7-C), **3** (C-Py_7) and **4** (C-Py_7-C); self-aggregates (top) and co-aggregates with oligomer **1** in a 1:1 ratio. Conditions: see Fig. 1.

The cooling profiles of self-aggregates of **2**-**4** fit an isodesmic model for all the three oligomers (Figure 5). If the oligomers are combined with oligomer **1** two stages are observed upon decrease of temperature: formation of a nucleus, followed by an elongation process. [43-47]

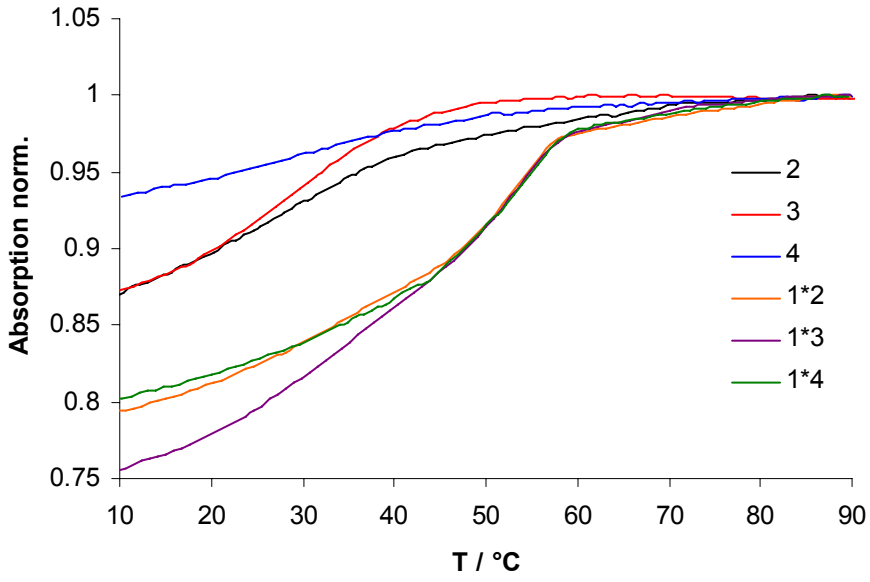

Figure 5. Cooling profiles of cytidine-modified oligomers **2** (Py_7-C), **3** (C-Py_7) and **4** (C-Py_7-C) alone and as co-aggregates with oligomer **1** in a 1:1 ratio. Conditions: 5 μM pyrene oligomer, sodium phosphate buffer pH = 7, 1.0 M NaCl.

Although CD measurements indicate a chiral structure of the self-aggregate **3**, no clear pattern of cooperativity was observed for this oligomer. Co-aggregates **1*2**, **1*3**, **1*4** all exhibit cooperativity in their cooling profiles, which is in agreement with absorbance and fluorescence spectra, although **1*4** is not CD-active (see Figure 4).

5.3.2 Guanosine modified oligomers (**5**, **6** and **7**)

Apart from oligomer **5**, absorbance spectra of self-aggregates of guanosine-modified oligomers show little vibronic structure. The intensity of the vibronic structures observed from the co-aggregates is in the following order: **1*6>1*7≈1*5** (Figure 6, 7).

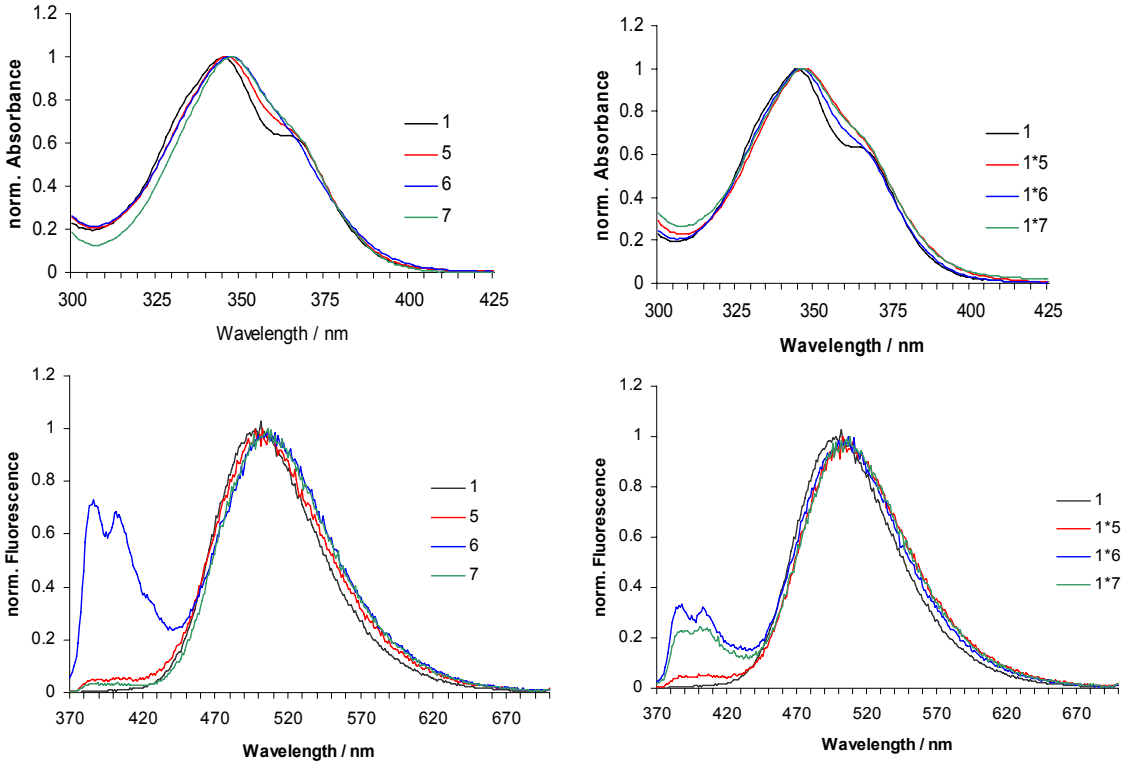

Figure 6. Normalized absorbance (top) and fluorescence (bottom) spectra of oligomers **1** (Py_7), **5** (Py_7-G), **6** (G-Py_7) and **7** (G-Py_7-G) (left) and the co-aggregates of the guanosine-modified oligomers with **1** in a 1:1 ratio (right). Conditions: see Fig. 1.

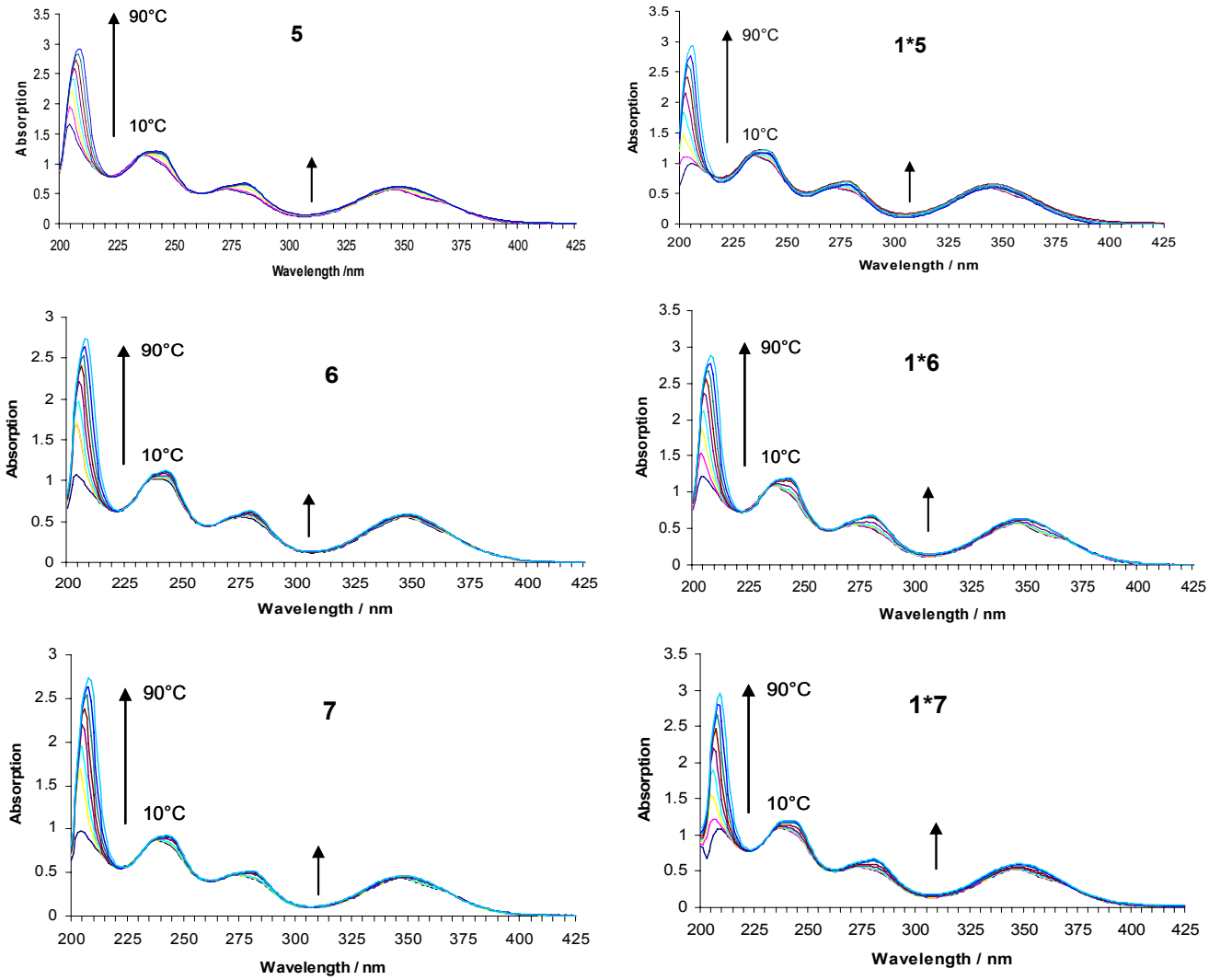

Figure 7. Temperature variable absorbance spectra of oligomer **5** (Py_7-G), **6** (G-Py_7), **7**(G-Py_7-G) (left) and co-aggregates with oligomer **1** in a 1:1 ratio (right). Conditions: sodium phosphate buffer, pH =7.0, 1 M NaCl. Total concentration of pyrenyl containing blocks: 5 μM.

Upon thermal melting, the fluorescence spectra show a gradual reduction of the pyrene emission intensities, except for **7** and co-aggregate **1*6** (Figure 8).

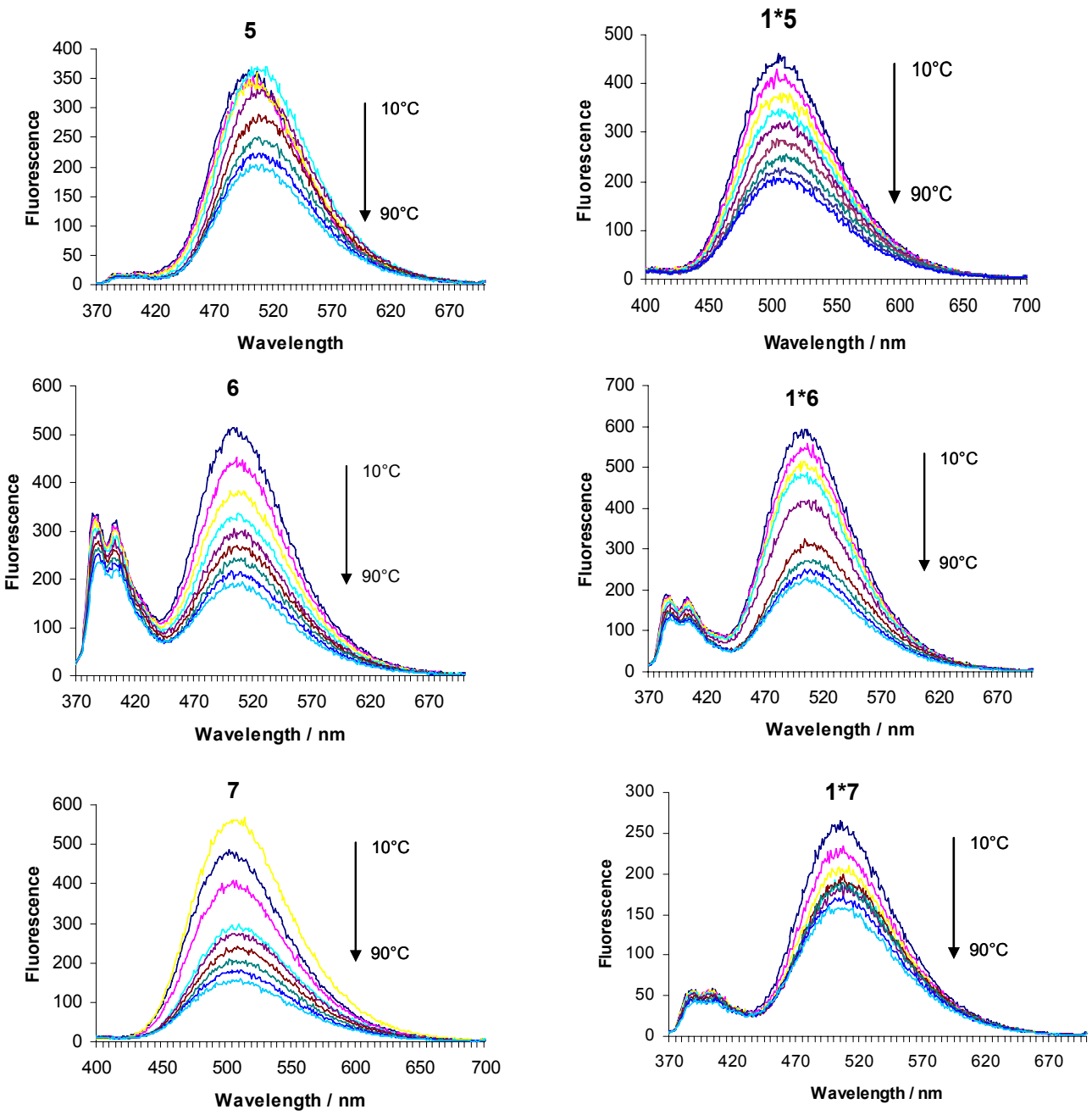

Figure 8. Temperature variable fluorescence spectra of oligomer **5**(Py_7-G), **6**, **7** (left) and co-aggregates with oligomer **1** in a 1:1 ratio (right). Conditions: sodium phosphate buffer, pH =7.0, 1 M NaCl**.** Total concentration of pyrenyl containing blocks: 5 µM.

The self-aggregate of oligomer **6** shows, in addition to excimer fluorescence, a considerable part of pyrene monomer emission (370-420 nm, Figure 6, bottom). A possible explanation could be that the nucleobase guanine, when attached at the 5'-end,

can displace one of the pyrene unit from the stack, which leads then to an unassociated pyrene unit and, thus, to monomer emission. The maxima of the pyrene excimer bands of **5**, **6**, **7**, as well in their co-aggregates with **1**, are in the narrow range of 503-508 nm.

CD-spectra reveal interesting patterns for the guanosine-modified oligomers. This nucleotide has a stabilizing effect on the chiral organization of the pyrene units if attached to the 5'-end or at both ends of the oligopyrenotide. Except for the guanosine attached at 3'-end (**5**) which doesn't lead to a preferred chiral organization, all oligomers are CD-active. Oligomer **6** alone shows the signal, which was observed for the co-aggregates **1*2** and **1*3** (*CD-type 2*), i.e. a bisignate signal for the pyrene band in the region of 345-375 nm and two negative bands at 240 nm and 206 nm. The self-aggregate of **7** exhibits *CD-type 1*. Co-aggregate **1*5** shows a quite intense CD with a bisignate signal centered again at 360 nm (negative Cotton effect at λ = 373 nm, positive Cotton effect at λ = 345 nm) and two positive signals at λ = 238 nm and λ = 208 nm. Interestingly, this corresponds to the exact mirror image of the spectrum *CD-type 2* (labeled as *CD-type 2*^{m}) described above (e.g. for the **1*3** co-aggregate). This aspect will be discussed later in more detail. The combination of **1** and **7** shows the same characteristics, though of lesser intensity. Co-aggregation of **1*6** showed no defined shape (Figure 9).

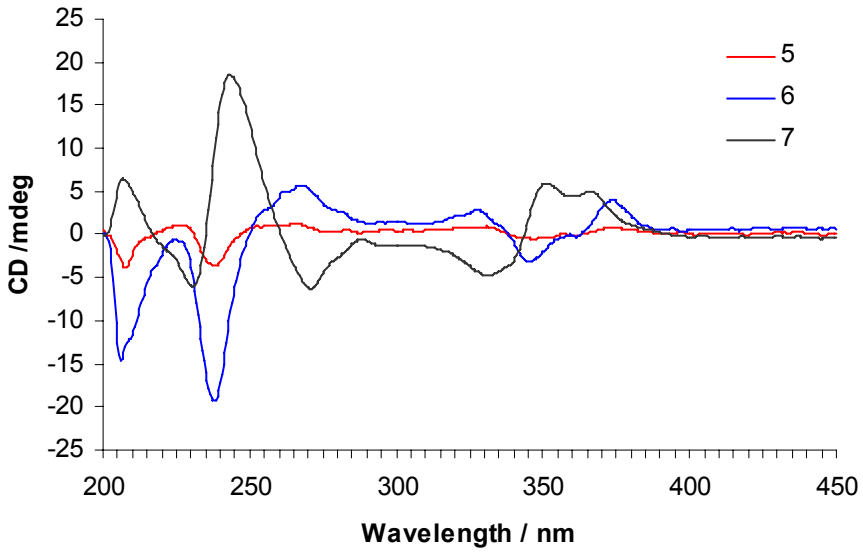

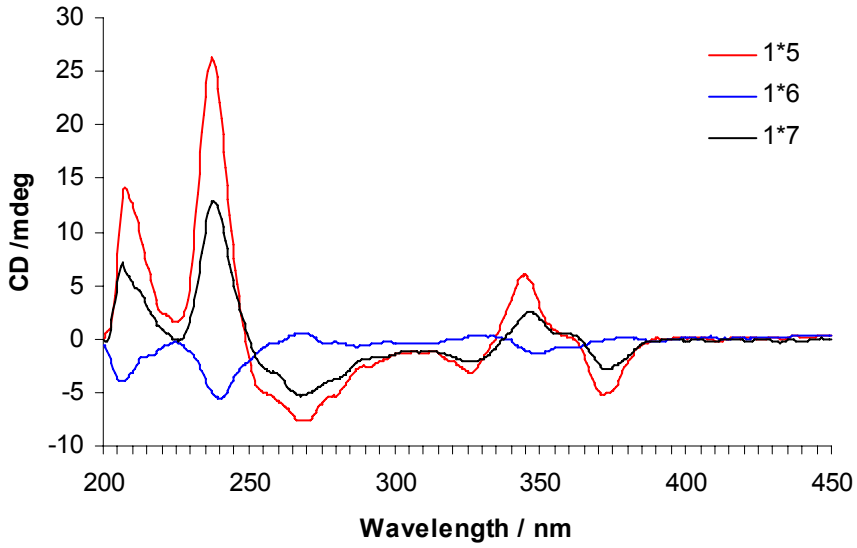

Figure 9. CD-spectra of guanosine-modified oligomers **5** (Py_7-G), **6** (G-Py_7) and **7** (G-Py_7-G); self-aggregates (top) and co-aggregates with oligomer **1** in a 1:1 ratio. Conditions: see Fig. 1.

The cooling profile clearly follows an isodesmic pattern for the self-aggregate of oligomer **7** (Figure 10). In the co-aggregates with oligomer **1**, a sharp transition in the range between 50 and 60 °C is observed, indicating the formation of a nucleus and elongation process. Considering the absorbance, fluorescence and cooling data co-aggregate **1*6** forms a defined assembly, but a preferred chirality is not observed. Co-aggregation of **1*5** or **1*7** leads to a defined assemblies with a preferred chiral sense. Oligomer **7** assembles to a defined chiral structure by an isodesmic mechanism. Formation of a nucleus was not observed for self-aggregate **6**. However, the CD curve (*CD-type 2*) suggests, that the formation of supramolecular polymers occurs.

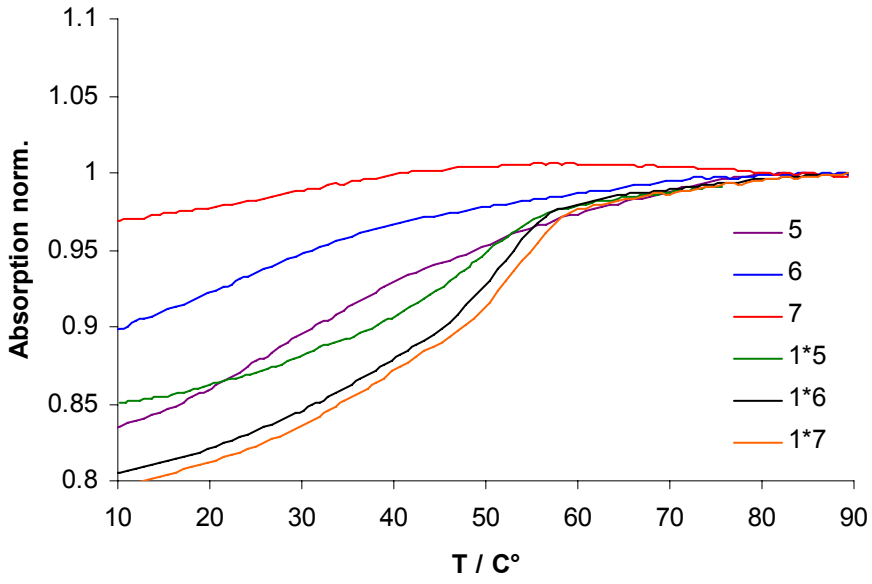

Figure 10. Cooling profiles of pyrene oligomer modified with guanosine **5** (Py_7-G), **6** (G-Py_7) and **7** (G-Py_7-G), self-aggregate or co-aggregates with oligomer **1** in a 1:1 ratio. Conditions: see Fig. 5.

5.3.3 Thymidine modified oligomers (**8**, **9** and **10**)

Self-association of oligomer **8**, but not of oligomers **9** and **10**, leads to some degree of vibronic structure (Figure 11(top), 12). Also in the co-aggregates, **1*8** exhibits the most pronounced vibronic structure. Pyrene excimer fluorescence (Figure 11 (bottom), 13) is very similar in all self- and co-aggregates of the thymidine-modified oligomers (maxima at 502-507 nm), except for the self-aggregate of oligomer **8**, which is blue shifted (498 nm).

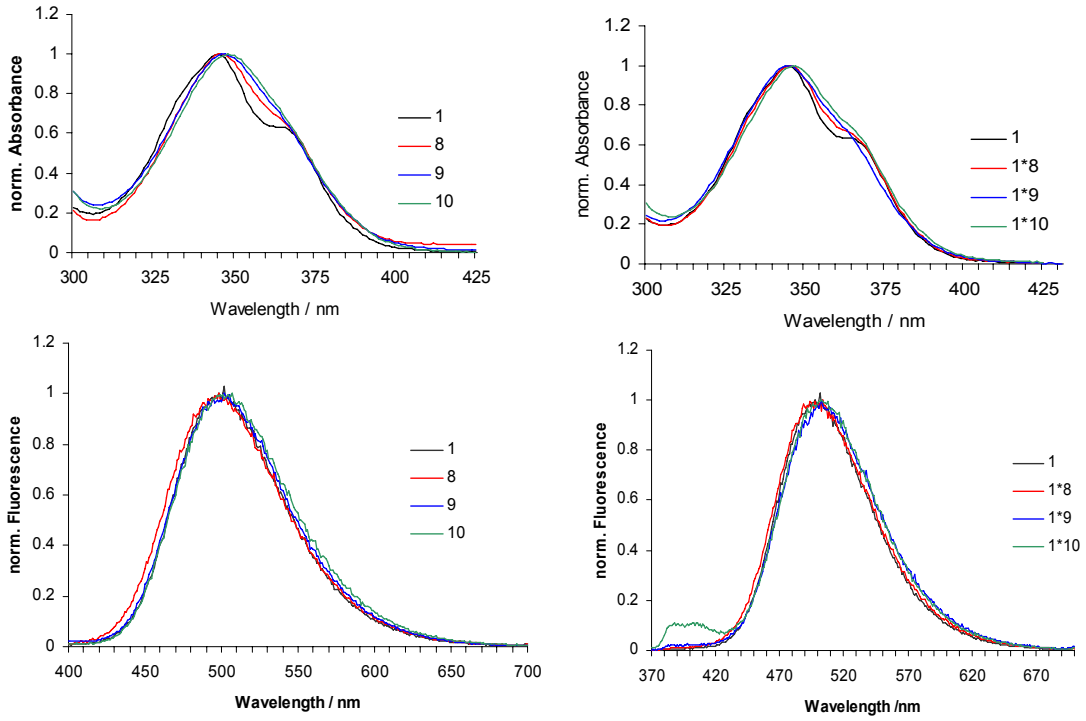

Figure 11. Normalized absorbance and fluorescence spectra of oligomers **1** (Py_7), **8** (Py_7-T), **9** (T-Py_7) and **10** (T-Py_7-T) (top) and the co-aggregates of the thymidine-modified oligomers with **1** in a 1:1 ratio (bottom). Conditions: see Fig. 1.

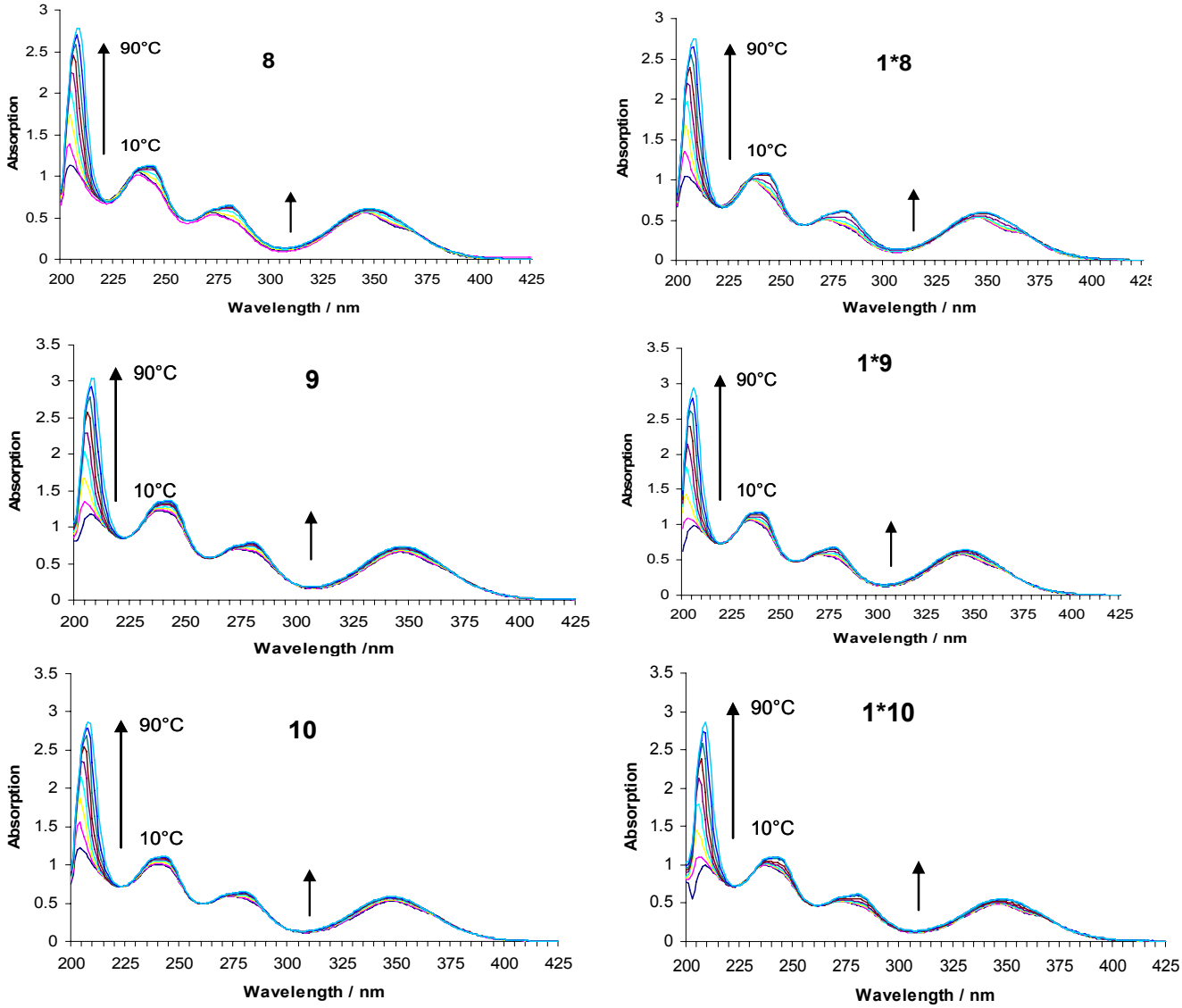

Figure 12. Temperature variable absorbance spectra of oligomer **8, 9, 10** (left) co-aggregates with oligomer **1** in a 1:1 ratio (right). Conditions: sodium phosphate buffer, pH =7.0, 1 M NaCl. Total concentration of pyrenyl containing blocks: 5 μM.

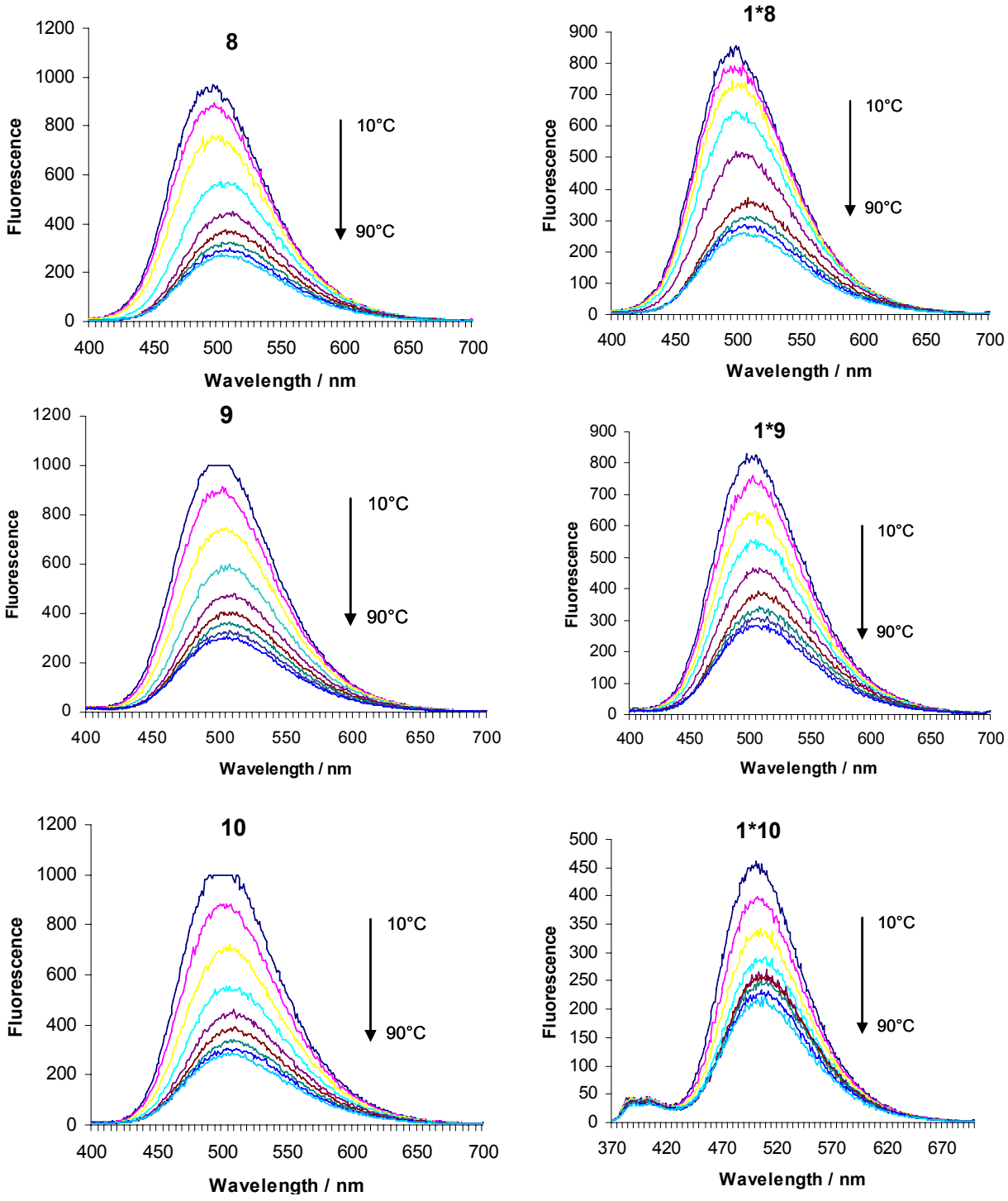

Figure 13. Temperature variable fluorescence spectra of oligomer **8, 9, 10** (left) and co-aggregates with oligomer **1** in a 1:1 ratio (right). Conditions: sodium phosphate buffer, pH =7.0, 1 M NaCl**.** Total concentration of pyrenyl containing blocks: 5 μM.

Upon self-association, only oligomer **8** shows a clear CD response (Figure 14, *CD-type 1*). The other self-aggregated oligomers (**9** and **10**) or their co-aggregates with oligomer **1** showed no distinct Cotton effects.

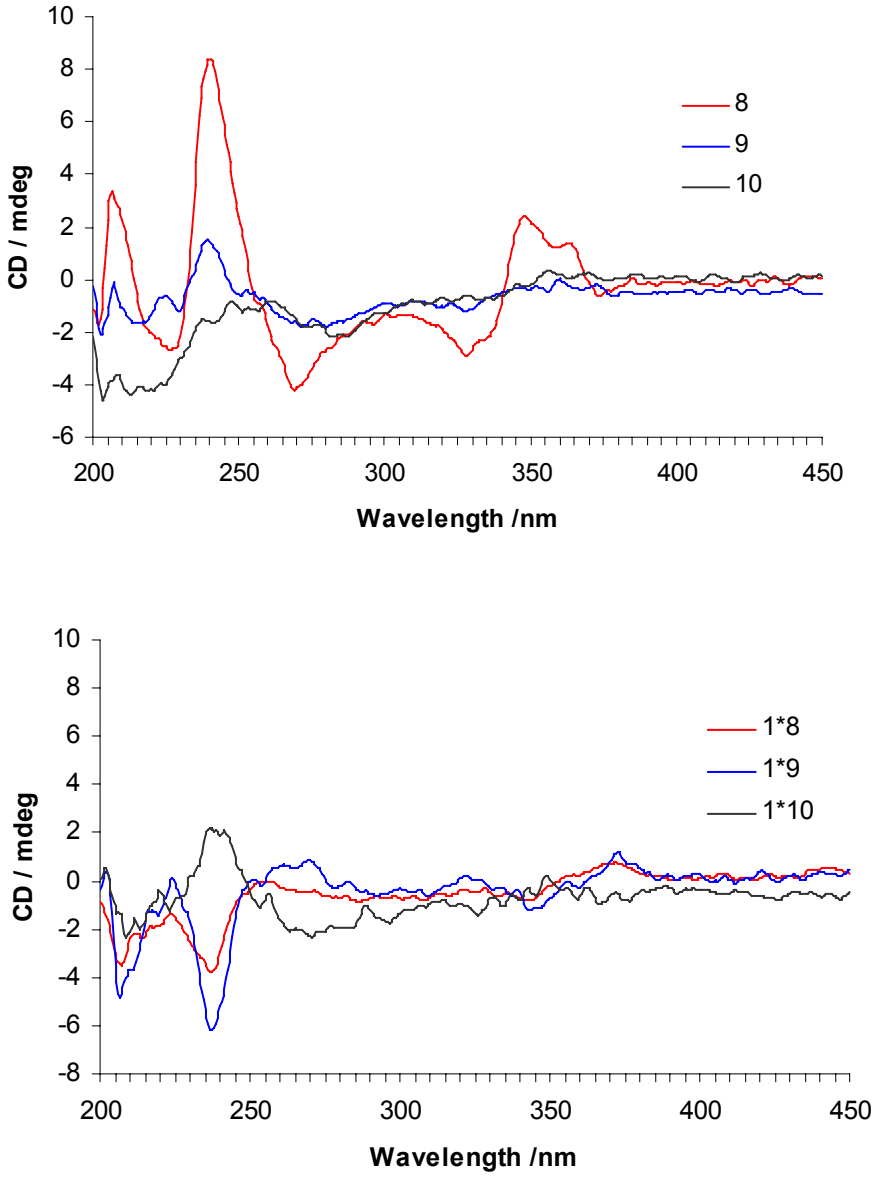

Figure 14. CD-spectra of pyrene oligomer modified with thymidine **8** (Py_7-T), **9** (T-Py_7) and **10** (T-Py_7-T); self-aggregates (top) and co-aggregates with oligomer **1** in a 1:1 ratio. Conditions: see Fig. 1.

According to the cooling profiles of co-aggregates **1*8** and **1*10** (Figure 15), the mechanism of the assembly-formation follows a nucleation-elongation process, as suggested by the sharp transition points observed at 60°C (**1*10**) and 47°C (**1*8**) upon change of temperature. A sharp transition indicating formation of a nucleus followed by elongation was not observed for co-aggregate **1*9**. Self-aggregates **8**, **9** and **10** clearly follow an isodesmic pattern.

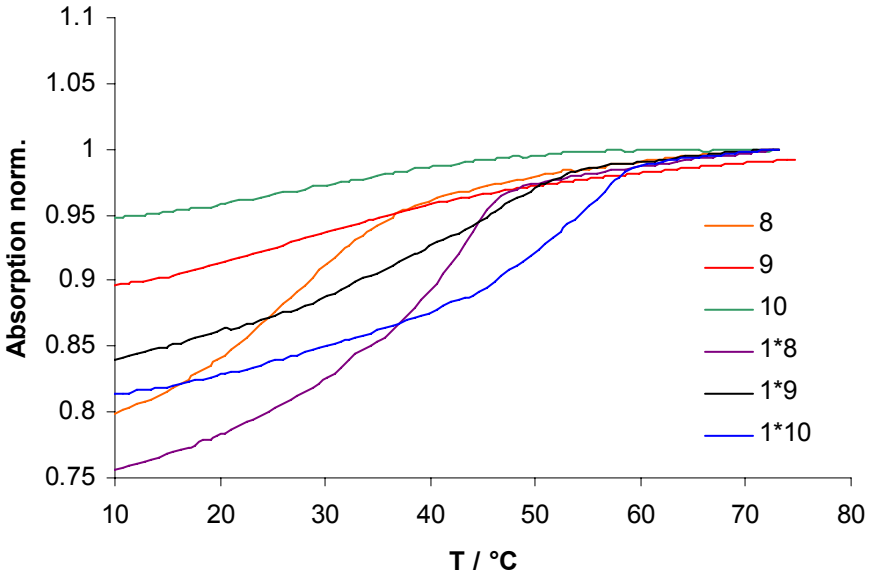

Figure 15. Cooling profiles of pyrene oligomer modified with thymidine **8** (Py_7-T), **9** (T-Py_7) and **10** (T-Py_7-T), self-aggregates and co-aggregates with oligomer **1** in a 1:1 ratio. Conditions: see Fig. 5.

5.3.4 Adenosine modified oligomers (**11**, **12** and **13**)

The self-aggregates of oligomers **11**, **12** and **13** reveal no pronounced vibronic structures in the UV/Vis spectra. In co-aggregate **1*12** they are somewhat more pronounced than in **1*11** or **1*13**. Upon self-association of oligomer **12**, some pyrene monomer emission at 370 nm-420 nm is present, similar as observed with oligomer **6**.

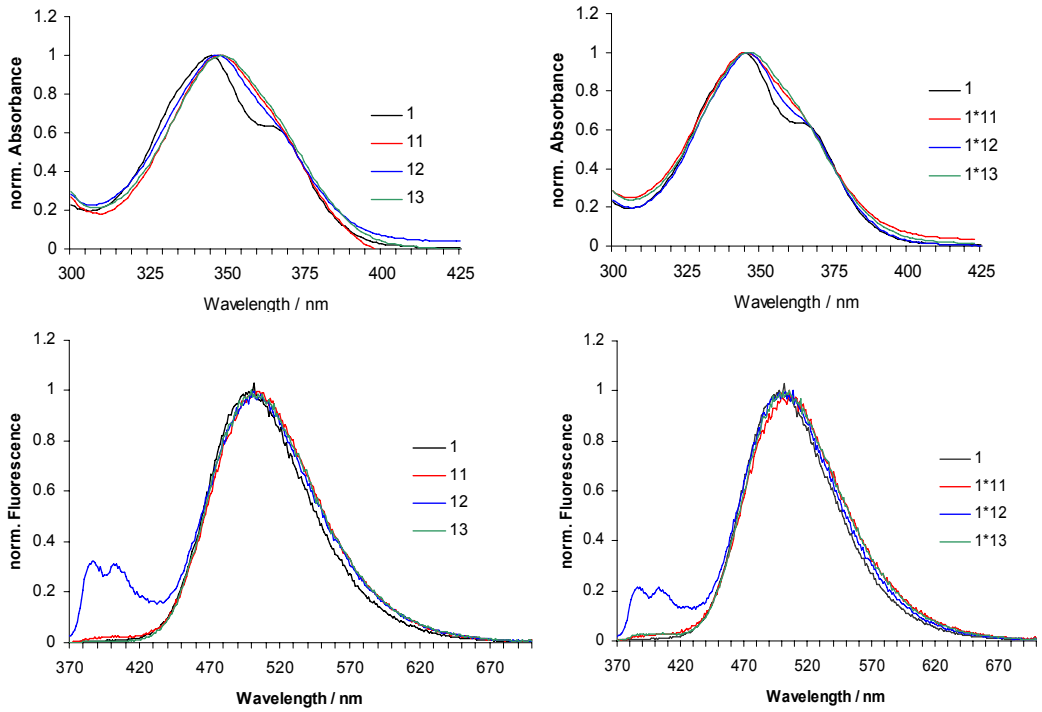

Figure 16. Normalized absorbance (top) and fluorescence (bottom) spectra of oligomers **1** (Py_7), **11** (Py_7-A), **12** (A-Py_7) and **13** (A-Py_7-A) (left) and the co-aggregates of the adenosine-modified oligomers with **1** in a 1:1 ratio (right). Conditions: see Fig. 1.

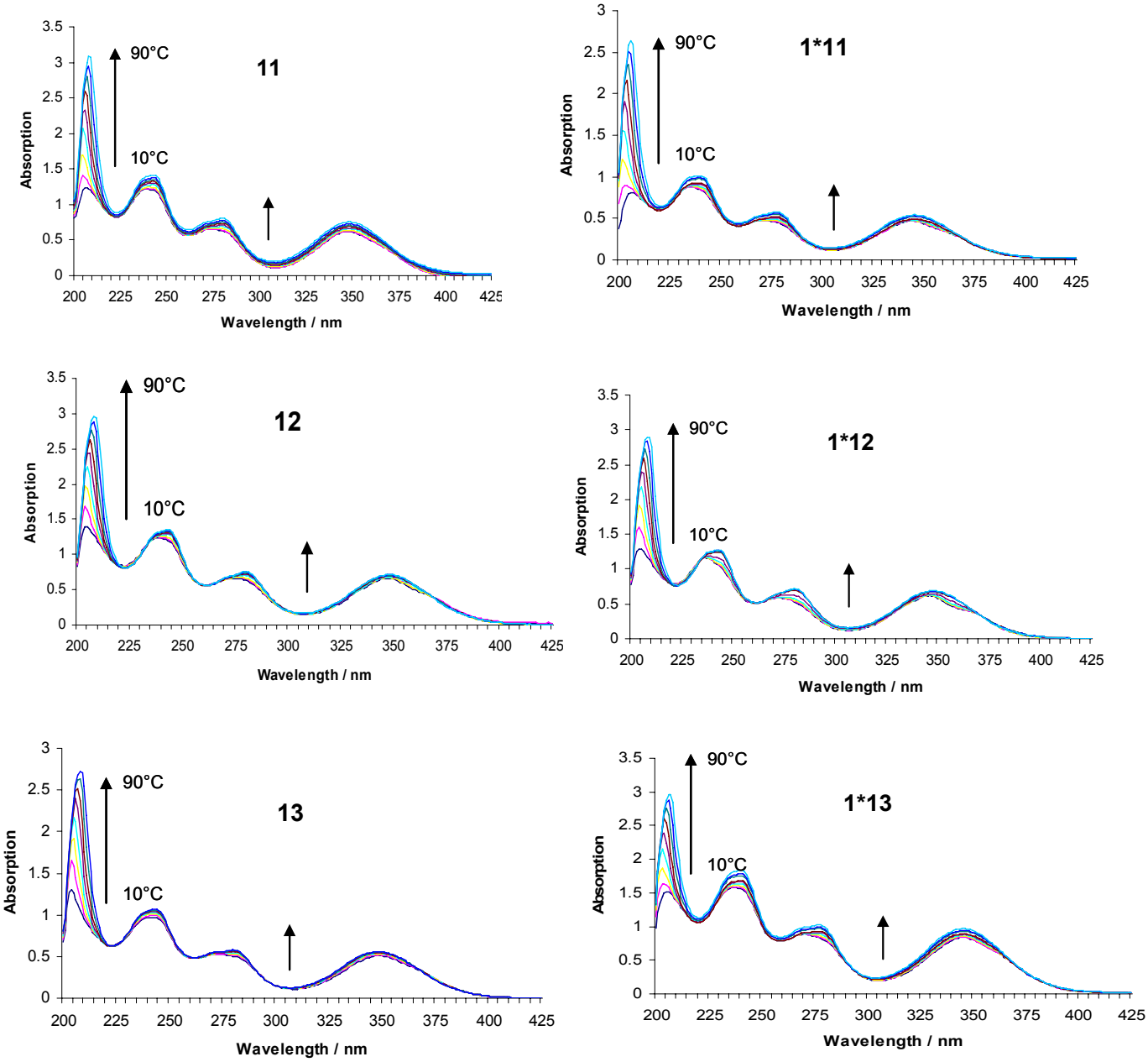

Figure 17. Temperature variable absorbance spectra of oligomer **11** (Py_7-A), **12** (A-Py_7), **13** (A-Py_7-A) (left) and co-aggregates with oligomer **1** in a 1:1 ratio (right). Conditions: sodium phosphate buffer, pH =7.0, 1 M NaCl. Total concentration of pyrenyl containing blocks: 5 μM.

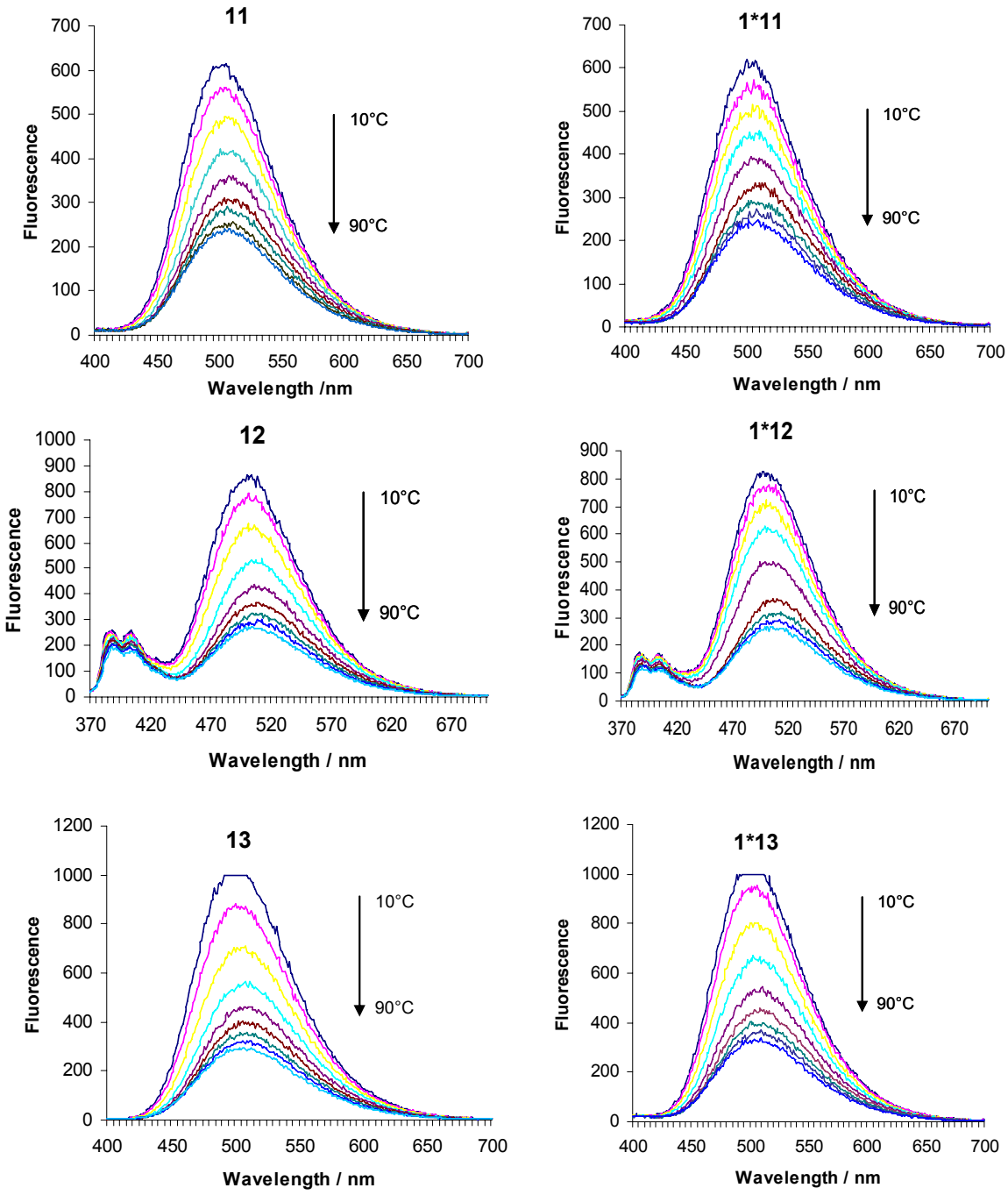

Figure 18. Temperature variable fluorescence spectra of oligomer **11** (Py_7-A), **12** (A-Py_7), **13** (A-Py_7-A) (left) and co-aggregates with oligomer **1** in a 1:1 ratio (right). Conditions: sodium phosphate buffer, pH =7.0, 1 M NaCl. Total concentration of pyrenyl containing blocks: 5 μM.

CD spectroscopy reveals no distinct signal for self-aggregates **11** and **13** (Figure 19). For oligomer **12** the presence of a signal is observed, which is not very pronounced, however. While the co-aggregates **1*12** and **1*13** show no Cotton effects, **1*11** exhibits strong CD signals.

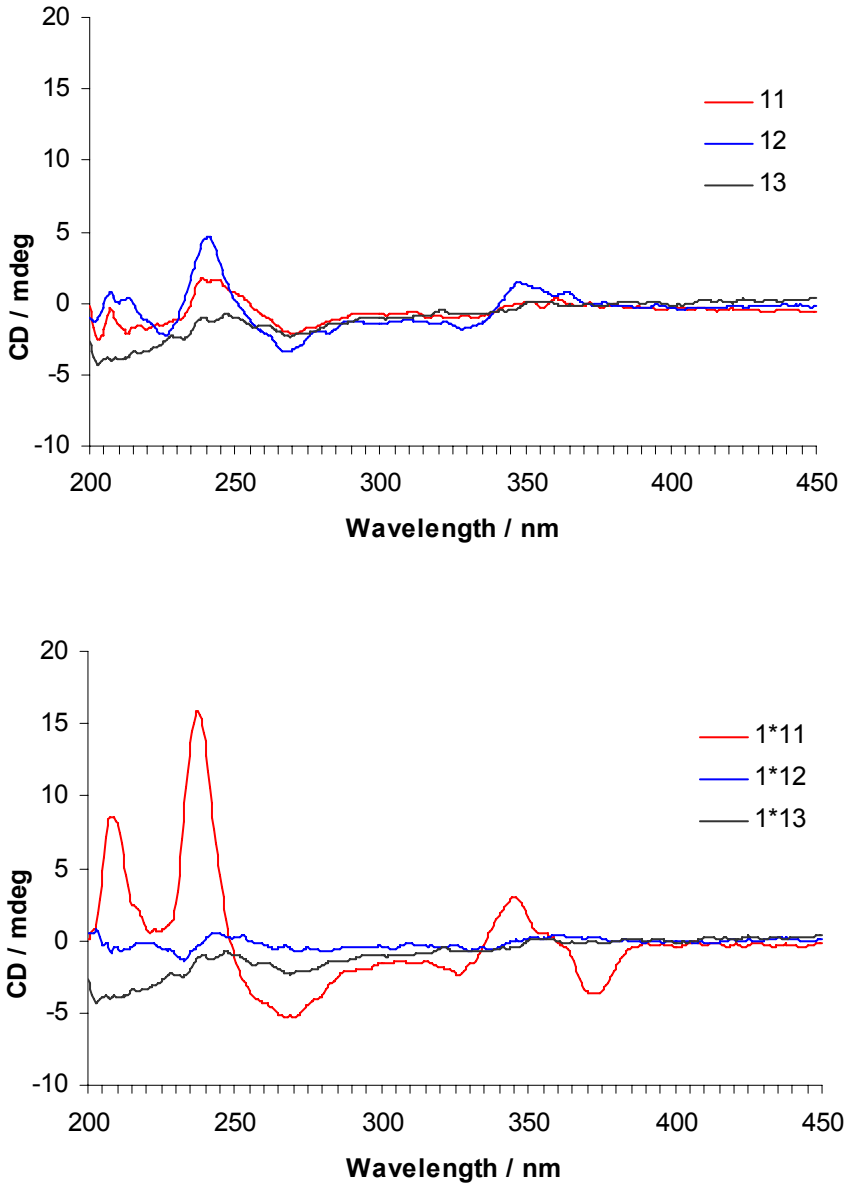

Figure 19. CD-spectra of pyrene oligomer modified with adenosine **11** (Py_7-A), **12** (A-Py_7) and **13** (A-Py_7-A); self-aggregates (top) and co-aggregates with oligomer 1 in a 1:1 ratio. Conditions: see Fig. 1.

Upon temperature change, the co-aggregates **1*11** and **1*12** (Figure 20) indicate a nucleation-elongation mechanism. For oligomer **11**, **12** and **13** alone, the assembly/disassembly process follows an isodesmic pattern.

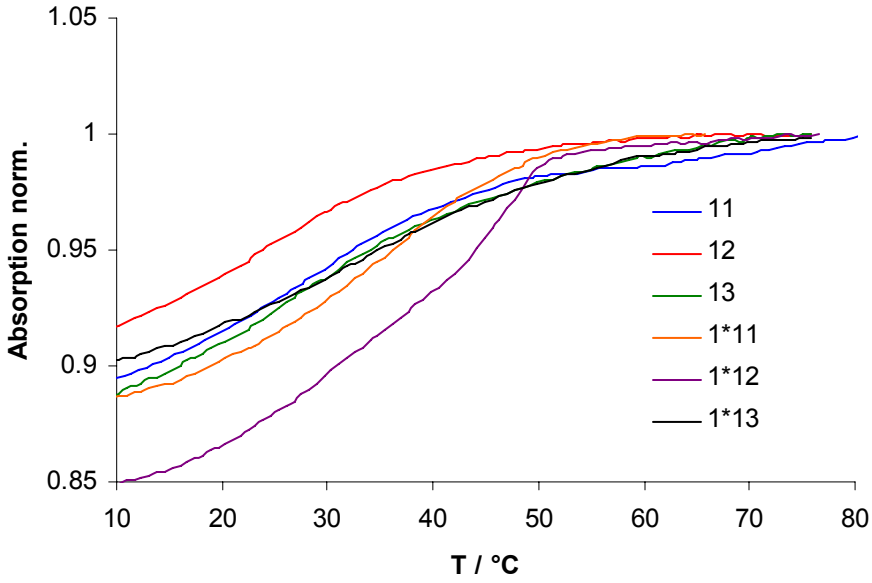

Figure 20. Cooling profiles of pyrene oligomer modified with adenosine **11** (Py_7-A), **12** (A-Py_7) and **13** (A-Py_7-A), self-aggregates and co-aggregates with oligomer **1** in a 1:1 ratio. Conditions: see Fig. 5.

5.3.5 Supramolecular polymers

Supramolecular polymers are dynamic, polymeric aggregates of monomeric units, held together by reversible and directional, non-covalent interactions. [22, 48-51] The lengths of the chains are related to the strength of the non-covalent interactions, the concentration of the monomer(s) and the temperature. Furthermore, the reversibility of non-covalent bond formation ensures the self-healing of initially formed defective sites during polymer assembly. The self-assembly process can be described by two main models. In an isodesmic process, the assembly is non-cooperative and the association is identical at any step of the polymerization process, which is characterized by a single binding constant. [43] The characteristics of a nucleated mechanism is a rather slow pre-

aggregation of a certain number of building blocks forming a nucleus (nucleation), which is then followed by a rapid process of chain propagation. [44] The latter mechanism usually takes place in the growth of ordered supramolecular polymers. [52] By changing the temperature, information can be obtained by which mechanism the self-assembly proceeds. Previously it was found that supramolecular polymerization of oligomer **1** occurs via a nucleated process. [20] The data presented above extend these preliminar studies and show that the self-association of the nucleotide-modified pyrene oligomers **2**-**13** follow an isodesmic model. In the formation of co-aggregates with oligomer **1**, however, significant differences are observed. All co-aggregations with oligomers modified by the nucleotides cytidine (**1*2**, **1*3**, **1*4**) and guanosine (**1*5**, **1*6**, **1*7**) follow a nucleated self-assembly process. Also, for the co-aggregates **1*8** (with Py_7-T) and **1*10** (with T-Py_7-T) the formation of a nucleus is observed. In the adenosine series, a nucleation process is not observed for **1*13** (A-Py_7-A), but when adenosine is attached at only one of the two sides (**1*11** and **1*12**) the formation of a nucleus is possible. Thus, it can be concluded that, even though the modified oligomers interact among themselves in a non-cooperative way, they form supramolecular polymers in combination with the heptapyrenotide Py_7 (**1**). The interaction, however, is dependent on the nature and position of the attached nucleotide. While some of the described oligomers prevent completely the formation of a nucleus (oligomers **9** T-Py_7 and **13** A-Py_7-A) most of them proceed via a nucleation process in the co-aggregation with oligomer **1**.

5.3.6 Helical chirality of polymers

Helical chirality originates from the unidirectional twist of building blocks along the propagation axis. [53] Natural helical polymers, such as DNA and proteins, are composed of enantiomerically pure, chiral building blocks. The adopted helical sense corresponds, thus, to the thermodynamically favored diastereomer. The heptapyrenotide **1**, however, is achiral. Consequently, its folding into a helical conformation will lead to a racemic mixture of right- and left-handed helices in the absence of external, symmetry breaking factors. The presence of a chiral inductor, however, may lead to the preferential formation of one type of helix. [39, 54] In the present case, the chiral inductor is a heptapyrenotide bearing one or two terminally attached nucleotides (C, G, T or A,

oligomers **2**-**13**). Oligomer **1** forms supramolecular polymers under conditions of high ionic strength in aqueous medium. The polymerization process proceeds through a nucleation step. The effect of copolymerization with all of the chiral oligomers **2**-**13** was systematically investigated. Most of the co-aggregates were found to form supramolecular polymers. The attached nucleotides, however, are not in all cases able to shift the equilibrium towards one of the two enantiomeric helices, as evidenced by the absence of a CD-signal. CD-inactive co-aggregates were observed with oligomers **4** (C-Py_7-C), **6** (G-Py_7), **8** (Py_7-T), **10** (T-Py_7-T) and **12** (A-Py_7; Figures 4, 9, 14 and 19).

Oligomers **2** (Py_7-C), **3** (C-Py_7), **5** (Py_7-G), **7** (G-Py_7-G) and **11** (Py_7-A) are most suitable to shift the equilibrium into one direction. The formation of the assemblies occurs via a nucleation-elongation process (see Figure 5, 10, 15, 20) and the appearance of a characteristic CD signal is observed. The CD curves are displayed as a whole in Figure 21. The shapes correspond to *CD-type 2* or its mirror image *CD-type-2*^{m}. Oligomers **2**, **3**, **5**, **7**, and **11** are modified with the nucleotide cytidine, guanosine or adenosine. Depending on the nucleotide the helical sense of the polymers can be shifted towards either form, i.e. **5**, **7** and **11** induce the M-helix, **2** and **3** the P-helix. Thymidine seems not to be suitable to favor one enantiomer of the supramolecular polymers.

Self-association of **6** (G-Py_7) seems to be a special case. It exhibits *CD-type 2*, just as observed with supramolecular polymers, but in the cooling-profile the formation of a nucleus was not observed. Self-aggregates of **3**, **7, 8** and **12** show a third type of signal (*CD-type 1*). The fact that the cooling follows an isodesmic pattern, strongly suggests that smaller complexes are formed rather than supramolecular polymers by these oligomers. The nature of these complexes is still under investigation.

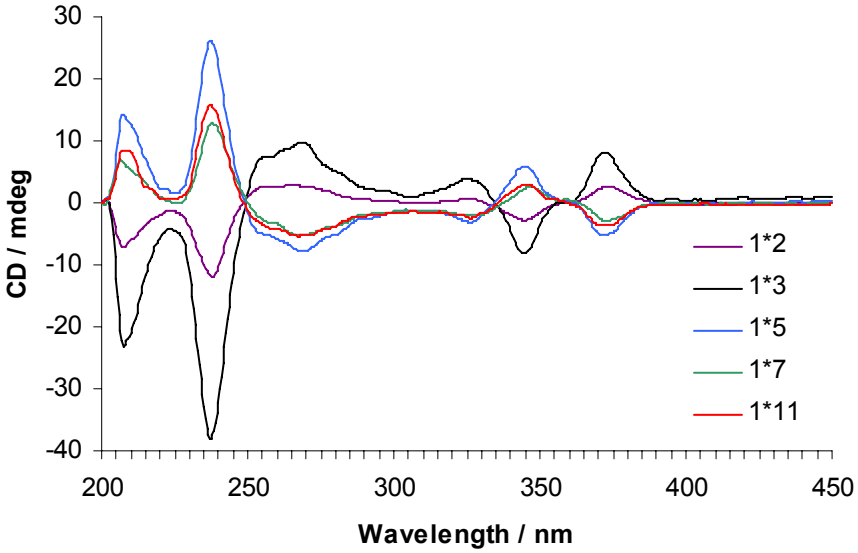

Figure 21. CD-spectra of co-aggregates between pyrene oligomers **2** (Py_7-C), **3** (C-Py_7), **5** (Py_7-G), **7** (G-Py_7-G) and **11** (Py_7-A) with oligomer **1** in a 1:1 ratio; note the mirror-inverted shape of the curves. Conditions: see Fig. 1.

5.3.7 Amplification of chirality

Amplification of chirality was first described in the pioneering work by Mark Green and co-workers studying polyisocyanates. [26,27] This phenomenon is not limited to covalently linked polymers but occurs also in non-covalent supramolecular assemblies. [25] Minute amounts of a chiral seed compound may be sufficient to render the polymers homochiral. [20,28] The fact that some of the oligomers showed very intense Cotton effects in the co-aggregates with **1** prompted us to study the amplification of chirality effect, using 10% of the corresponding chiral oligomer (Figure 22). The development of the signals was monitored over a period of 4 weeks. Growth of the CD signals and, thus, amplification of chirality, was observed with oligomers **3**, **5**, **7** and **11**.

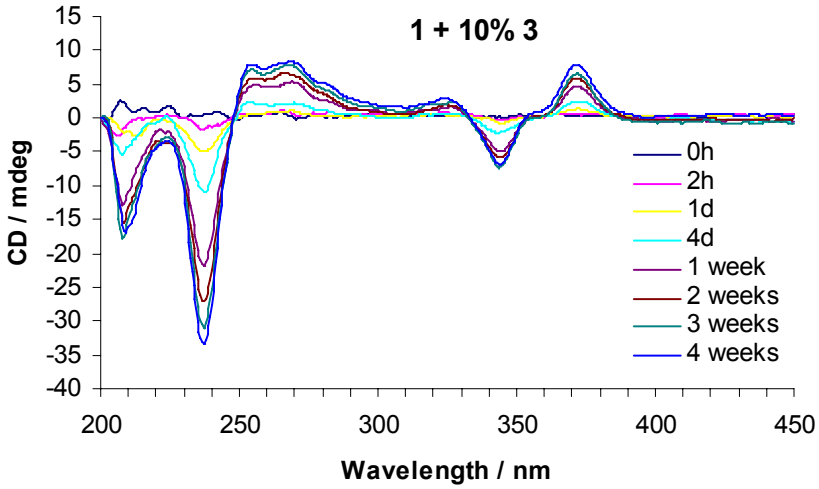
1 + 10% 3
CD / mdeg
Wavelength / nm
0h
2h
1d
4d
1 week
2 weeks
3 weeks
4 weeks

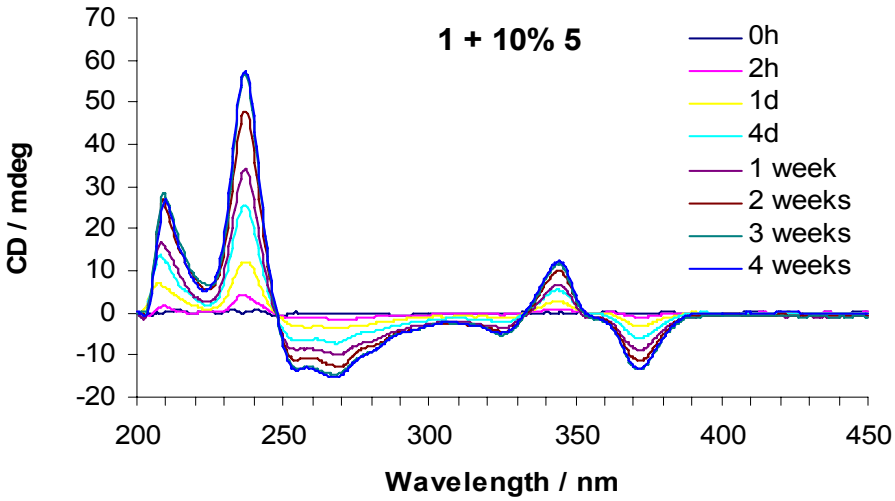
1 + 10% 5
CD / mdeg
Wavelength / nm
0h
2h
1d
4d
1 week
2 weeks
3 weeks
4 weeks

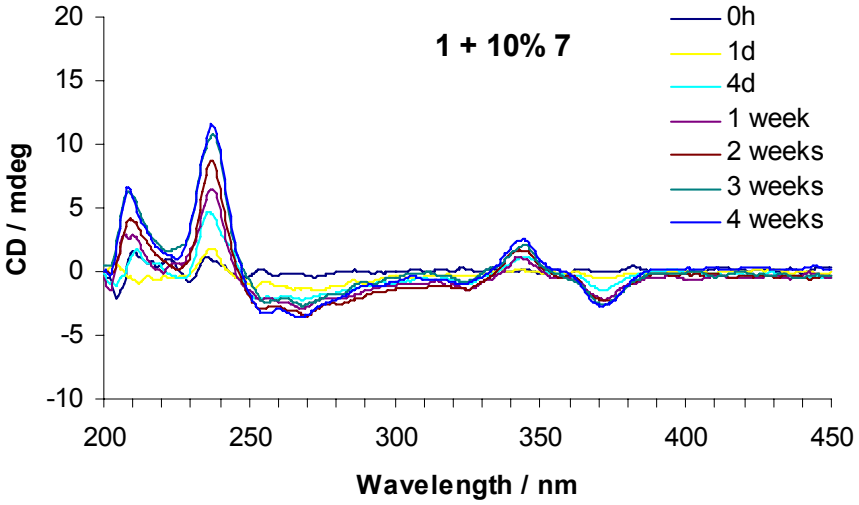
1 + 10% 7
CD / mdeg
Wavelength / nm
0h
1d
4d
1 week
2 weeks
3 weeks
4 weeks

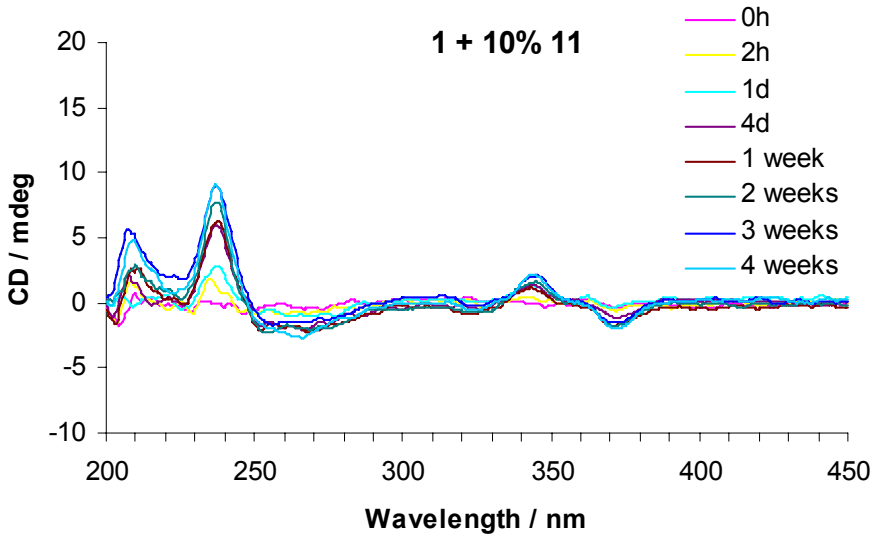

Figure 22. Amplification of chirality; oligomer **1** with 10 % of oligomers **3** (C-Py_7), **5** (Py_7-G), **7** (G-Py_7-G) and **11** (Py_7-A). Conditions: see Fig. 1.

In Figure 23, the calculated g-factor is shown for the 9:1 ratio of oligomer **1** with either oligomer **2**, **3**, **5**, **7** or **11**. Guanosine attached at the 3'-end has the highest impact on the amplification of the chirality.

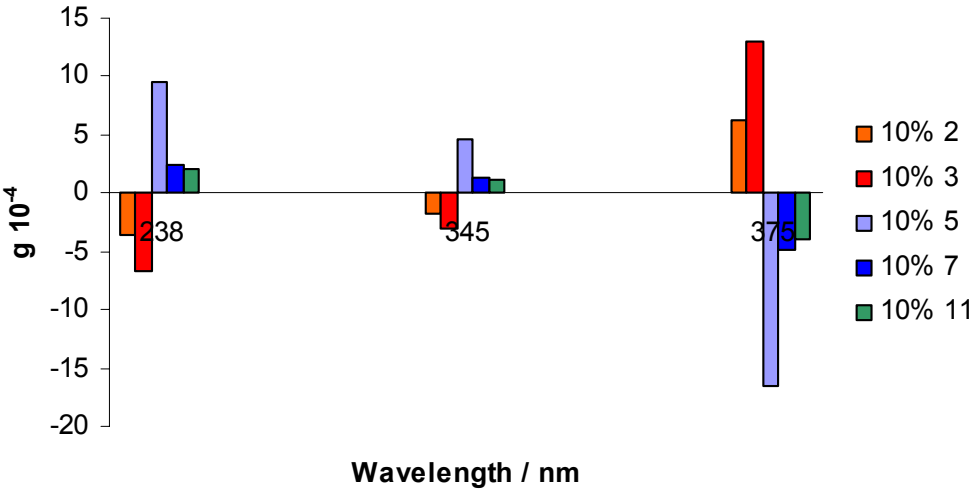

Figure 23. G-factor; oligomer **1** with 10 % of oligomers **2** (Py_7-C), **3** (C-Py_7), **5** (Py_7-G), **7** (G-Py_7-G) or **11** (Py_7-A). Conditions: see Fig. 1.

The amplitude dramatically grows with smaller amounts of chiral information. The pyrene oligomers are highly sensitive to the chiral nature of the nucleoside guanosine (Figure 23). Further, it could be shown that in the case of the nucleotide cytidine, the point of attachment has a remarkable impact on the g-factor: the amplification of chirality is much more pronounced if the nucleotide is located at the 5'-end (**3**) than at the 3'-end (**2**).

5.3.8 The effect of Watson-Crick complementary bases

Association of oligomers with complimentary bases **2*6**, **3*5**, **4*7**, **8*12**, **9*11**, **10*13** was tested by mixing the oligomers in 1:1 ratio in analogy to self-assembly of complementary strands in DNA.

In Figure 24 the absorbance spectra of co-aggregates modified with the nucleotide cytidine and guanosine are shown. Association of **2*6** and **3*5** show the same intensities of vibronic structures. If the nucleotide guanosine is attached via the 3'- oxygen, or the nucleotide cytidine seems to have no influence on the association properties, no vibronic structures are observed in the co-aggregate **4*7** (Figure 25).

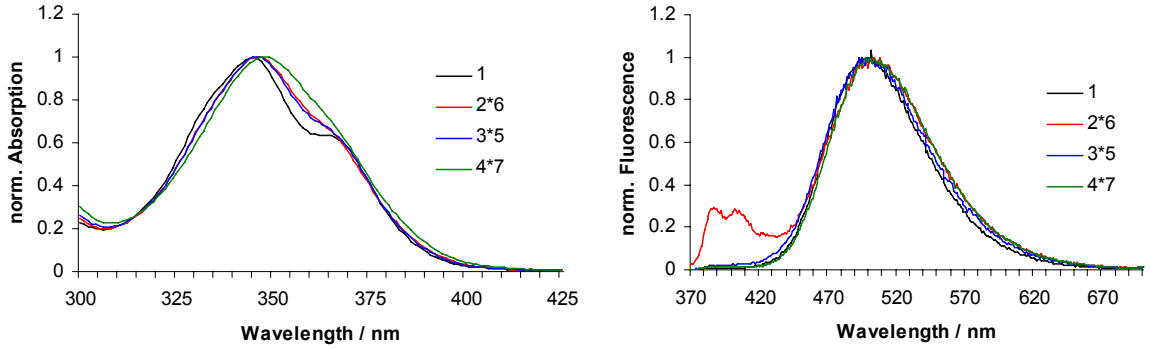

Figure 24. Normalized absorbance (left) and fluorescence (right) spectra of **2*6** (Py_7-C)* (G-Py_7), **3*5** (C-Py_7)* (Py_7-G), **4*7** (C-Py_7-C)* (G-Py_7-G). Conditions: see Fig. 1.

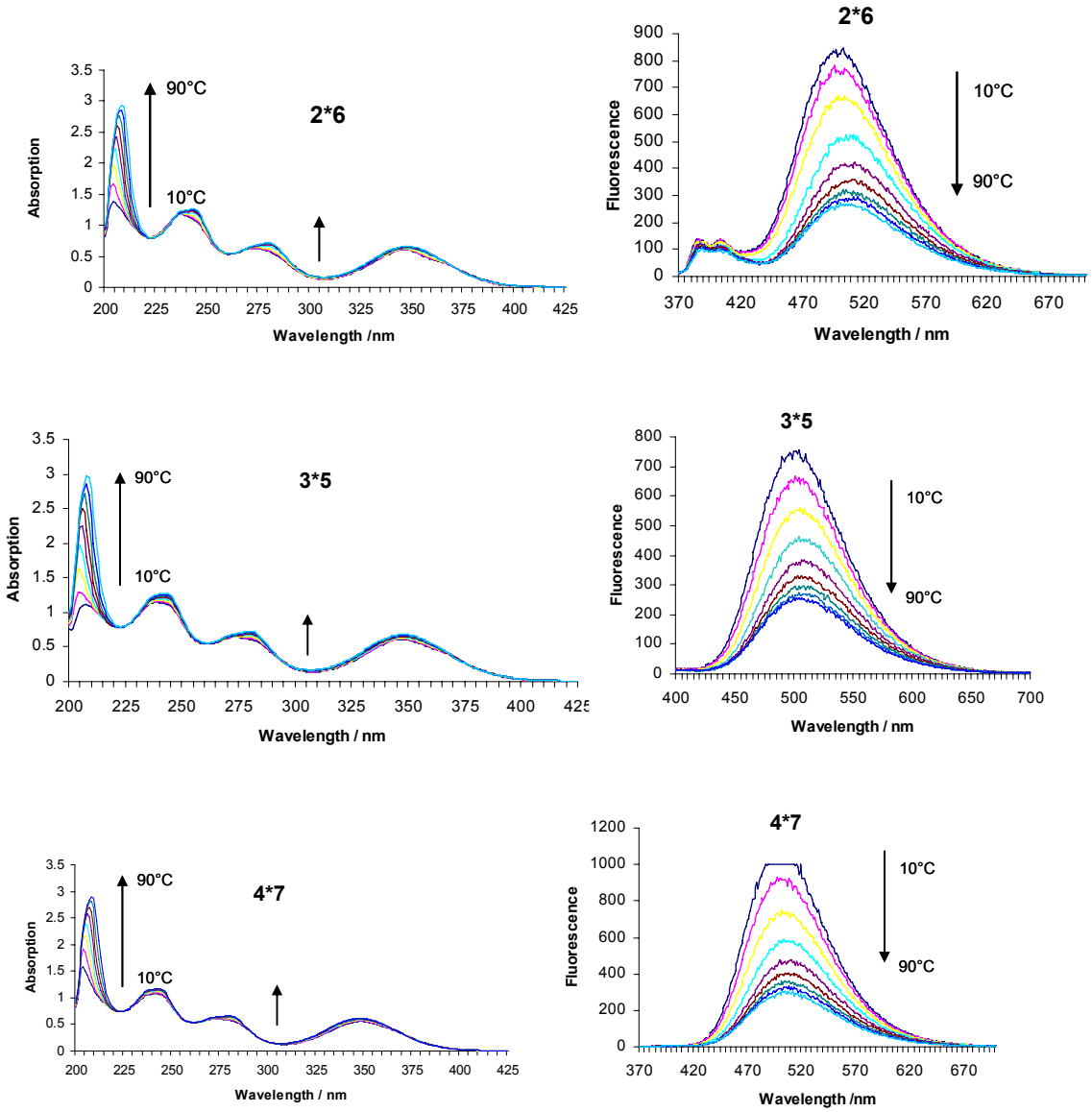

Figure 25. Temperature variable absorption spectra (left) and fluorescence spectra (right) of oligomer **2, 3, 4** and its complementary base. Conditions: sodium phosphate buffer, pH =7.0, 1 M NaCl. Total concentration of pyrenyl containing blocks: 5 μM.

Fluorescence spectra of **2*6** show monomer emission next to the pyrene excimer emission. Self-association of oligomer **6** shows the same characteristics, but with double intensity in monomer emission of pyrene. An explanation could be that also in the mixture of **2** and **6**, self-association of oligomer **6** occurs (Figure 24 and 25).

The association of **3*5** and **4*7** show weak CD-response with the same features of self-aggregate **3** and self-aggregate **7**, but with less intensity (Figure 26). Self-association of oligomer **5** and **4** don't show any CD-response. An interaction between **3** with **5** and **4** with **7** doesn't seem to be probable. Rather, self-association of the oligomers can be an explanation for the observations.

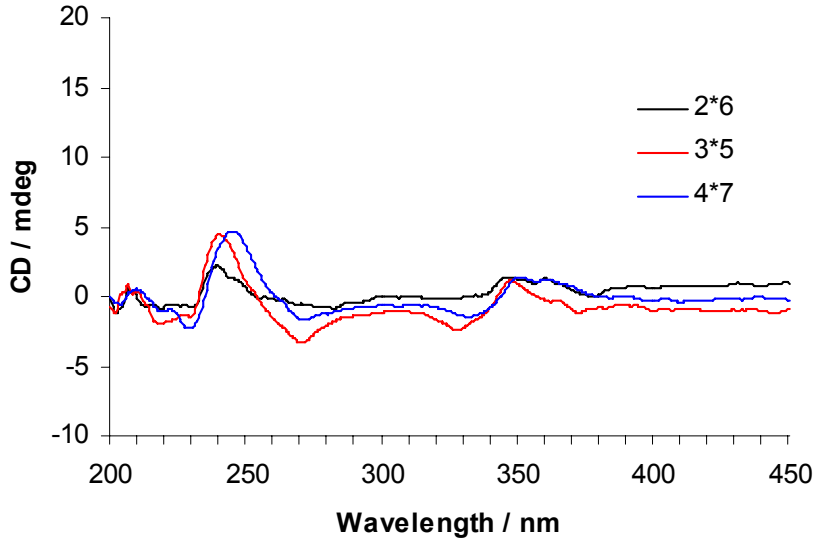

Figure 26. CD-spectra of **2*6** (Py_7-C)* (G-Py_7), **3*5** (C-Py_7)* (Py_7-G), **4*7** (C-Py_7-C)* (G-Py_7-G). Conditions: see Fig. 1.

The association of thymidine and adenosine modified oligomers show in the case of **8*12** vibronic structures (Figure 26 and Figure 27).

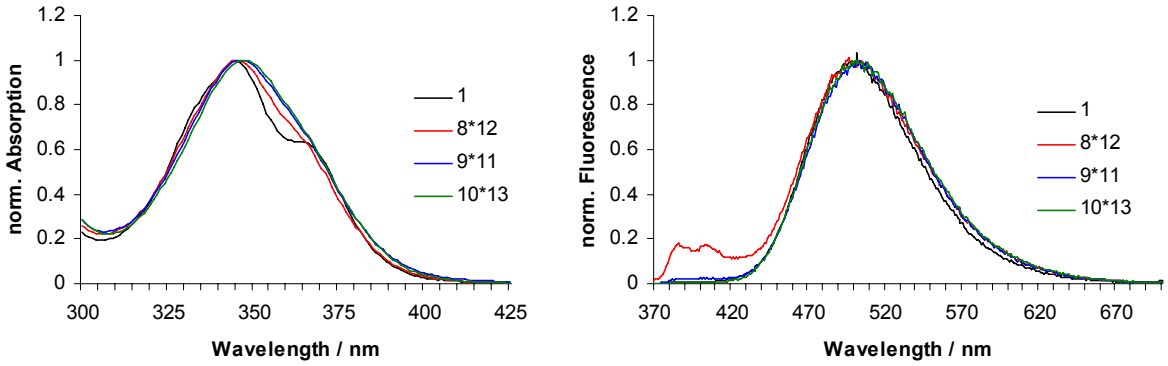

Figure 26. Normalized absorbance and fluorescence spectra of **8*12** (Py_7-T)* (A-Py_7), **9*11** (T-Py_7)* (Py_7-A), **10*13** (T-Py_7-T)* (A-Py_7-A). Conditions: see Fig. 1.

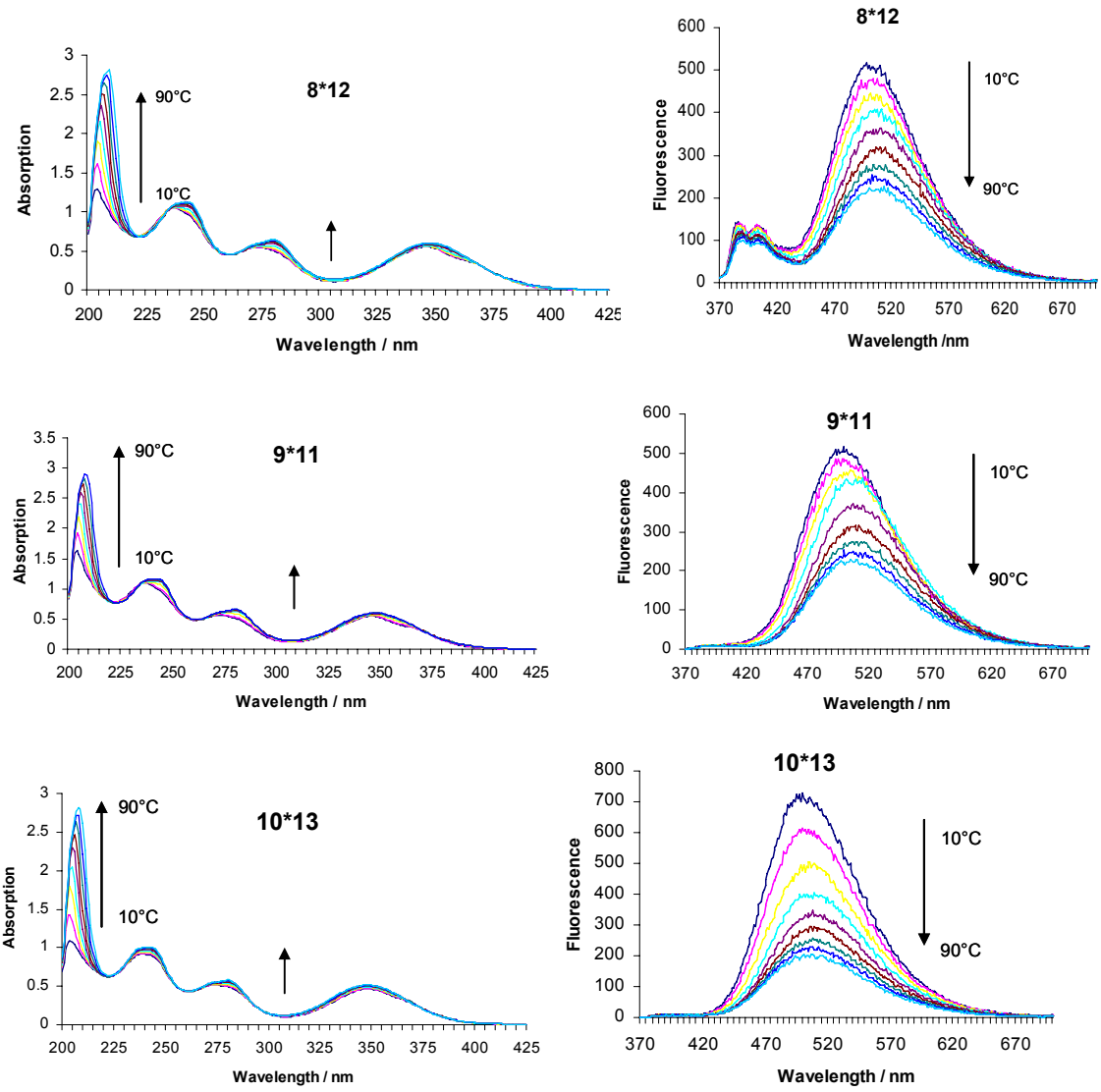

Figure 27. Temperature variable absorption spectra (left) and fluorescence spectra (right) of oligomer **8, 9, 10** and its complementary base. Conditions: sodium phosphate buffer, pH =7.0, 1 M NaCl. Total concentration of pyrenyl containing blocks: 5 μM.

Fluorescence spectra show pyrene monomer emission in the co-aggregate **8*12**, which comes from the self-association of oligomer **12**.

Only the co-aggregate **8*12** is CD-active. Self-association of oligomer **8** and **12** show both *CD-type 1*. It is most probable that the CD-signal appears from self-association of both oligomers (Figure 28).

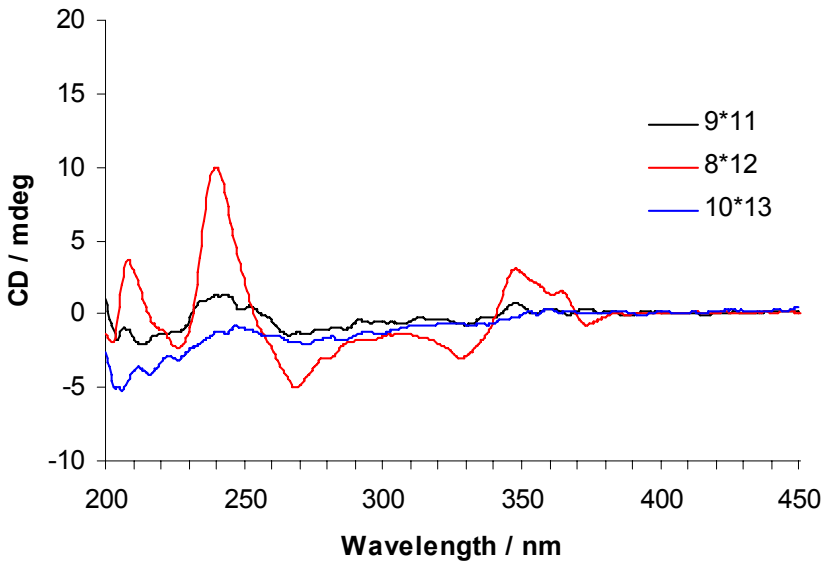

Figure 28. CD-spectra of pyrene oligomer **8*12** (Py_7-T)* (A-Py_7), **9*11** (T-Py_7)* (Py_7-A), **10*13** (T-Py_7-T)* (A-Py_7-A). Conditions: see Fig. 1.

The cooling profiles of the aggregates **2*6**, **3*5**, **4*7**, **8*12** and **10*13** follow all an isodesmic mechanism. The attached nucleotide prevents the formation of supramolecular polymers. Further is a specific interaction of the two oligomers modified with the complementary nucleotide not observed (Figure 29).

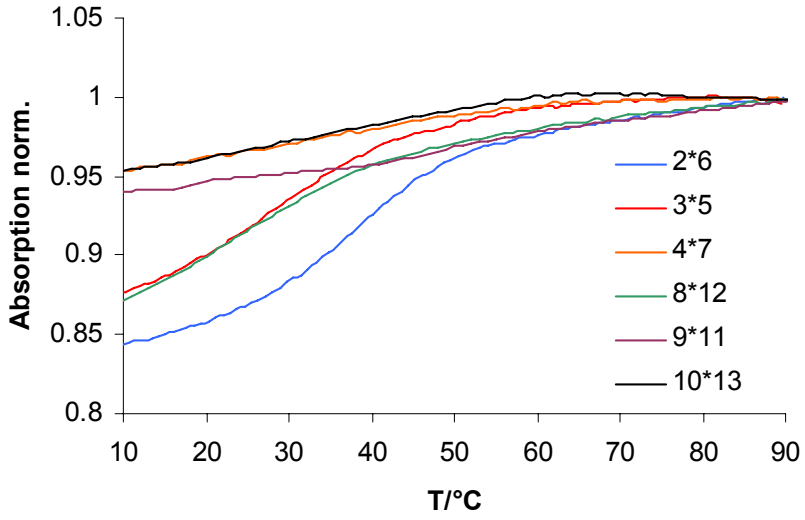

Figure 29. Cooling profile of the co-aggregates **2*6**, **3*5**, **4*7**, **8*12**, **10*13** in a 1:1 ratio. Conditions: see Fig. 3.

5.4 Conclusions

Formation of supramolecular polymers via aggregation of oligomer **1** was described in chapter 1. In this chapter, an extended study of co-aggregates of achiral heptapyrenotide (Py_7) and its nucleotide modified derivatives (Py_7-N and N-Py_7-N, **2**-**13**) are presented. Self-association of the oligomers and their co-aggregation with **1** was studied to elucidate the influence of the chiral modification on the polymerization behavior. Self-association of the modified pyrene oligomers **2**-**13** was shown to follow an isodesmic model, and the formation of long assemblies is absent. Co-aggregates with oligomers modified with cytidine (**1*2**, **1*3** and **1*4**), as well modified with guanosine (**1*5**, **1*6** and **1*7**), follow a nucleated self-assembly process, which is characteristic for the formation of supramolecular polymers. In co-aggregate **1*8** (Py_7-T) and **1*10** (T-Py_7-T), the formation of a nucleus, but not the preferential formation of one type of helical polymers, is observed. In the case of adenosine, co-aggregates with oligomer **1** and the oligomers modified with, **1*11** and **1*12** show a nucleation-elongation mechanism upon change of temperature. Within the co-aggregate of oligomer **1** with **9** (T-Py_7) and **13** (A-Py_7-A) no nucleation-elongation mechanism was observed.

The supramolecular polymers formed by aggregation of **1** are present as a racemic mixture of helical polymers. A single nucleotide present in oligomers **2**-**13** can favor one of the two enantiomeric helices in their co-aggregates with oligomer **1**. Oligomers **2** (Py_7-C), **3** (C-Py_7), **5** (Py_7-G), **7** (G-Py_7-G) and **11** (Py_7-A) induce formation of one of the enantiomers. Amplification of chirality could be observed in the presence of 10% of **2**, **3**, **5**, **7** or **11**. Co-aggregates with oligomer **4** (C-Py_7-C), **6** (G-Py_7), **8** (Py_7-T), **10** (T-Py_7-T) and **12** (A-Py_7) were not optically active. Aggregates of oligomers with complementary nucleotide **2*6**, **3*5**, **4*7**, **8*12** and **10*13** show no signs of supramolecular polymerization.

The data show that the formation of supramolecular polymers of oligopyrenotides is very sensitive to the nature of chiral auxiliaries, in this case attached natural nucleotides. A single nucleotide may be used for the fine tuning of the aggregate properties. Formation of supramolecular polymers follows a nucleation-elongation mechanism and leads to strong amplification of chirality in supramolecular polymers. Oligopyrenotides are valuable oligomeric building blocks for the generation of optical active polymeric

materials. Due to their amphiphilic nature, they may find applications as chiroptical components of molecular devices in aqueous media.

5.5 Experimental part

The required pyrene building block [55] and the oligomers were synthesized and purified according to a published procedures.[20]

Spectroscopic methods

Unless otherwise indicated, all experiments were performed in sodium phosphate buffer (10 mM, 1M NaCl, pH 7.0) for 5 μM oligomer concentration, ε_{350}= 20'000 $dm^3 \times mole^{-1} \times cm^{-1}$ was used for pyrene units.

Temperature dependent UV/VIS spectra were collected with an optic path of 1 cm over the range of 200-500 nm at 10-90 ºC with a 10 ºC interval on *Varian Cary-100 Bio*-UV/VIS spectrophotometer equipped with a *Varian Cary*-block temperature controller. The cell compartment was flushed with N_2.

Thermal melting experiments were carried out on *Varian Cary-100 Bio*-UV/VIS spectrophotometer equipped with a *Varian Cary*-block temperature controller and data were collected with Varian WinUV software at 354 nm (cooling-ramp in the temperature range of 10-90°C, temperature gradient of 0.5°C/min). Data are normalized at maximum of absorbance (at high temperature).

Temperature dependent fluorescence data were collected on a *Varian Cary Eclipse* fluorescence spectrophotometer equipped with a *Varian Cary*-block temperature controller (excitation at 350 nm; excitation and emission slit width of 2.5 nm) using 1 cm x 1 cm quartz cuvettes. *Varian Eclipse* software was used to investigate the fluorescence of the oligopyrenes at a wavelength range of 370-700 nm in the temperature range of 10-90 °C.

CD spectra were recorded on a *JASCO J-715* spectrophotometer using quartz cuvettes with an optical path of 1 cm. (Scanning speed: 100 nm/min; data pitch: 0.5 nm; band width: 1.0 nm; response: 1 sec).

The calculation of the g-factor was done with the equation G = CD(mdeg)/(32980*Abs) using the absorbance and CD values in mdeg recorded by the *JASCO-J-715*.

Amplification experiment using 10% of chiral oligomers 3, 5, 7 or 11: oligomer **1** (5 μM building block concentration) was mixed together with phosphate buffer and sodium chloride and heated to 90°C (10 mM, 1M NaCl, pH 7.0). After cooling and equilibration of 1 week, 10% (0.5 μM building block concentration) of the corresponding oligomers of **3**, **5**, **7** and **11** were added to the preformed supramolecular polymers. Data points were taken after 2 hours, 1 day, 4 days and then every week until one month had passed.

Mass spectrometry of oligomers was performed with a Sciex QSTAR pulsar (hybrid quadrupole time-of-flight mass spectrometer, *Applied Biosystems*). ESI-TOF MS (negative mode, CH_3CN/H_2O/TEA) data of compounds are presented in Table 1.

Table 1. Mass spectrometry data of synthesized oligomers (ESI-TOF MS, negative mode, CH_3CN/H_2O/TEA).

	Oligonucleotide	Molecular Formula	Calc. average mass	Found mass
1	SSS SSS S	$C_{168}H_{156}N_{14}O_{40}P_6$	3197.0	3198.0
2	(5') SS SSS SSC	$C_{177}H_{167}N_{17}O_{46}P_7$	3485.0	3485.0
3	(5') CSS SSS SS	$C_{177}H_{167}N_{17}O_{46}P_7$	3485.0	3486.6
4	(5') CSS SSS SSC	$C_{186}H_{178}N_{20}O_{52}P_8$	3773.3	3774.8
5	(5') SS SSS SSG	$C_{178}H_{167}N_{19}O_{46}P_7$	3525.1	3526.7
6	(5') GSS SSS SS	$C_{178}H_{167}N_{19}O_{46}P_7$	3525.1	3525.0
7	(5') GSS SSS SSG	$C_{188}H_{178}N_{24}O_{52}P_8$	3853.3	3853.4
8	(5') SS SSS SST	$C_{178}H_{168}N_{16}O_{47}P_7$	3500.0	3501.0
9	(5') TSS SSS SS	$C_{178}H_{168}N_{16}O_{47}P_7$	3500.0	3500.0
10	(5') TSS SSS SST	$C_{188}H_{180}N_{18}O_{54}P_8$	3801.0	3802.0
11	(5') SS SSS SSA	$C_{178}H_{167}N_{19}O_{45}P_7$	3509.0	3510.9
12	(5') ASS SSS SS	$C_{178}H_{167}N_{19}O_{45}P_7$	3509.0	3509.6
13	(5') ASS SSS SSA	$C_{188}H_{178}N_{24}O_{50}P_8$	3821.3	3821.3

5.6 References

[1] N. C. Seeman, *Acc. Chem. Res.* **1997**, *30,* 357-363.

[2] C. A.Mirkin, R. L.Letsinger, R. C. Mucic, J. J. Storhoff, *Nature* **1996**, *382,* 607-609.

[3] E. T. Kool, *Chemical Reviews* **1997**, *97,* 1473-1487.

[4] J. Wengel, *Acc. Chem. Res.* **1999**, *32,* 301-310.

[5] F. D. Lewis, R. L. Letsinger, M. R. Wasielewski, *Acc. Chem. Res.* **2001**, *34,* 159-170.

[6] N. C. Seeman, *Annu. Rev. Biochem.* **2010**, *79,* 65-87.

[7] C. K. McLaughlin, G. D. Hamblin, H. F. Sleiman, *Chem. Soc. Rev.* **2011**, *40,* 5647-5656.

[8] K. Kinbara, T. Aida, *Chem. Rev.* **2005**, *105,* 1377-1400.

[9] F. A. Aldaye, A. L. Palmer, H. F. Sleiman, *Science* **2008**, *321,* 1795-1799.

[10] T. Torring, N. V. Voigt, J. Nangreave, H. Yan, K. V. Gothelf, *Chem. Soc. Rev.* **2011**, *40,* 5636-5646.

[11] U. Feldkamp, C. M. Niemeyer, *Angew. Chem. Int. Ed.* **2006**, *45,* 1856-1876.

[12] M. Endo, H. Sugiyama, *Chembiochem* **2009**, *10,* 2420-2443.

[13] V. L. Malinovskii, D. Wenger, R. Häner, *Chem. Soc. Rev.* **2010**, *39,* 410-422.

[14] A. Ruiz-Carretero, P. G. A. Janssen, A. Kaeser, A. P. H. Schenning, J. *Chem. Commun.* **2011**, *47,* 4340-4347.

[15] A. Mammana, G. Pescitelli, T. Asakawa, S. Jockusch, A. G. Petrovic, R. R. Monaco, R.Purrello, N. J. Turro, K. Nakanishi, G. A. Ellestad, M. Balaz, N. Berova, *Chem. Eur. J.* **2009**, *15,* 11853-11866.

[16] P. P. Neelakandan, Z. Pan, M. Hariharan, Y. Zheng, H. Weissman, B. Rybtchinski, F. D. Lewis, *J. Am. Chem. Soc.* **2010**, *132,* 15808-15813.

[17] V. L. Malinovskii, F. Samain, R. Häner, *Angew. Chem. Int. Ed.* **2007**, *46,* 4464-4467.

[18] R. Häner, F. Garo, D. Wenger, V. L. Malinovskii, *J. Am. Chem. Soc.* **2010**, *132,* 7466-7471.

[19] R. Häner, F. Samain, V. L. Malinovskii, *Chem. Eur. J.* **2009**, *15,* 5701-5708.

[20] A. L. Nussbaumer, D. Studer, V. L. Malinovskii, R. Häner, *Angew. Chem. Int. Ed.* **2011**, *50,* 5490-5494.

[21] J. S. Moore, *Current Opinion in Colloid & Interface Science* **1999**, *4,* 108-116.

[22] L. Brunsveld, B. J. B. Folmer, E. W. Meijer, R. P. Sijbesma, *Chem. Rev.* **2001**, *101,* 4071-4097.

[23] J. M. Lehn, *Polymer International* **2002**, *51,* 825-839.

[24] T. F. A. de Greef, M. M. J. Smulders, M. Wolffs, A. P. H. J. Schenning, R. P. Sijbesma, E. W. Meijer, *Chem. Rev.* **2009**, *109,* 5687-5754.

[25] K.Maeda, E.Yashima, *Top. Curr. Chem.* **2006**, *265,* 47-88.

[26] M. M. Green, N. C. Peterson, T. Sato, A.Teramoto, R. Cook, S. Lifson, *Science* **1995**, *268,* 1860-1866.

[27] M. M. Green, M. P. Reidy, R. J. Johnson, G. Darling, D. J.Oleary, G. Willson, *J. Am. Chem. Soc.* **1989**, *111,* 6452-6454.

[28] A. R. A. Palmans, E. W. Meijer, *Angew. Chem. Int. Ed.* **2007**, *46,* 8948-8968.

[29] M. M. Green, A Model for How Polymers Amplify Chirality. In *Circular Dichroism - Principles and Applications*; Berova, N., Nakanishi, K., Woody, R. W., Eds.; Wiley-VCH: Hoboken, NJ, 2000; Chapter 17.

[30] H. Engelkamp, S. Middelbeek, R. J. M. Nolte, *Science* **1999**, *284,* 785-788.

[31] M. M. J. Smulders, A. P. H. J. Schenning, E. W. Meijer, *J. Am. Chem. Soc.* **2008**, *130,* 606-611.

[32] A. J. Markvoort, H. M. M. ten Eikelder, P. A. J. Hilbers, T. F. A. de Greef, E. W. Meijer, *Nat Commun* **2011**, *2,* 509.

[33] A. Lohr, F. Wurthner, *Angew. Chem. Int. Ed.* **2008**, *47,* 1232-1236.

[34] F. Garcia, L. Sanchez, *J. Am. Chem. Soc.* **2011**, *134,* 734-742.

[35] A. Lohr, F. Würthner, *Isr. J. Chem.* **2011**, *51,* 1052-1066.

[36] B. L. Feringa, R. A. van Delden, *Angew. Chem. Int. Ed.* **1999**, *38,* 3418-3438.

[37] S. J. George, Z.Tomovic, M. M. J. Smulders, T. F. A. de Greef, P. E. L. G. Leclere, E. W. Meijer, A. P. H. J. Schenning, *Angew. Chem. Int. Ed.* **2007**, *46,* 8206-8211.

[38] D. Monti, M.Venanzi, G.Mancini, C. D. Natale, R. Paolesse, *Chem. Commun.* **2005**, 2471-2473.

[39] E. Yashima, K. Maeda, H. Iida, Y. Furusho, K. Nagai, *Chem. Rev.* **2009**, *109,* 6102-6211.

[40] K. Morino, N. Watase, K.Maeda, E. Yashima, *Chem. Eur. J.* **2004**, *10,* 4703-4707.

[41] B. Isare, M. Linares, L. Zargarian, S. Fermandjian, M. Miura, S. Motohashi, N. Vanthuyne, R. Lazzaroni, L. Bouteiller, *Chem. Eur. J.* **2010**, *16,* 173-177.

[42] D. Pijper, B. L. Feringa, *Soft Matter* **2008**, *4,* 1349-1372.

[43] F. Oosawa, M. Kasai, *J. Mol. Biol.* **1962**, *4,* 10.

[44] R. B. Martin, *Chem. Rev.* **1996**, *96,* 3043-3064.

[45] D. H. Zhao, J. S. Moore, *Org. Biomol. Chem.* **2003**, *1,* 3471-3491.

[46] M. M. J. Smulders, M. M. L. Nieuwenhuizen, T. F. A. de Greef, P. van der Schoot, A. P. H. J. Schenning, E. W. Meijer, *Chem. Eur. J.* **2010**, *16,* 362-367.

[47] T. E. Kaiser, V. Stepanenko, F. Würthner, *J. Am. Chem. Soc.* **2009**, *131,* 6719-6732.

[48] A. W. Bosman, R. P. Sijbesma, E. W. Meijer, *Mat. Today* **2004**, *7,* 34-39.

[49] J. M. Lehn, *Prog. Polym. Sci.* **2005**, *30,* 814-831.

[50] G. M. Whitesides, J. P. Mathias, C. T. Seto, *Science* **1991**, *254,* 1312-1319.

[51] J. S. Lindsey, *New J. Chem.* **1991**, *15,* 153-180.

[52] T. F. A. Greef, E. W. Meijer, *Nature* **2008**, *453,* 171-173.

[53] G. A. Hembury, V. V. Borovkov, Y. Inoue, *Chem. Rev.* **2008**, *108,* 1-73.

[54] E. Yashima, *Nat Chem* **2011**, *3,* 12-14.

[55] S. M.Langenegger, R.Häner, *ChemBioChem* **2005**, *6*, 848-851.

6. Towards new DNA-based nanostructures connected via artificial sticky ends

6.1 Abstract

This chapter is about the investigation of artificial sticky ends made of pyrene units attached to a natural DNA sequence. The designed bi-segmental DNA/pyrene strands could lead to new nanostructures and geometric objects with an alternating DNA and pyrene part. The optical data presented, show that the artificial sticky ends made of 7 pyrene units recognize each other. Extented structures are formed, which precipitate in solution. Further characterization of the precipitat with AFM techniques was not yet succesful.

6.2 Introduction

DNA is well known and used to build multidimensional nanostructures and nanomaterials. [1, 2, 3] One approach to construct DNA-nanostructures is the use of sticky ends. A “sticky end” is a short single-stranded overhang, protruding from the end of a double-stranded helical DNA molecule. Two molecules with complementary sticky ends will hybridize to form a molecular complex. [4]

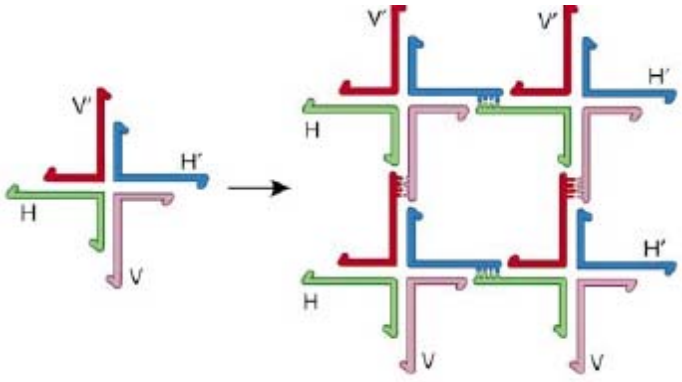

Scheme 1. Assembly of branched molecules, using complementary sticky ends H, H’ and V, V’. [4]

Nadrian Seeman and co-workers assembled four synthetic DNA strands into a four-way branched junction. Due to the incorporation of addressable sticky ends at the periphery of this four-armed building block, it was possible to construct higher-order assemblies.[4,5]

In the previous chapters, it was described that pyrene oligomers containing 7 pyrene units can form supramolecular polymers. [6]
The fact that the pyrene units interact with each other and form stable extended structures, leads to the idea of attaching to a DNA-sequence an artificial overhang made of 7 pyrene units. The interaction of the pyrene "sticky ends" with each other connects the DNA part, forming long supramolecular polymers with alternating DNA and pyrene parts.

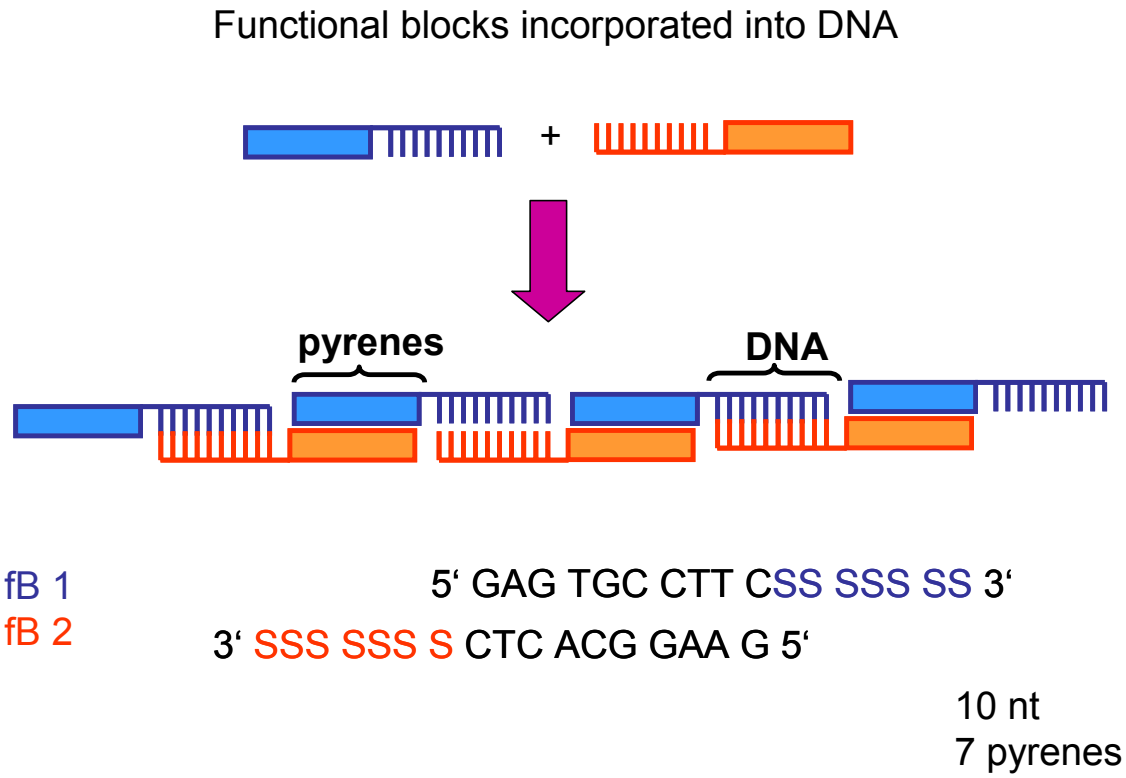

Scheme 2. Design of the DNA sequences modified with a pyrene overhang.

This chapter is about the investigation of artificial sticky ends made of pyrene units attached to a natural DNA sequence. It could lead to new nanostructures and geometric objects with an alternating DNA and pyrene part (Scheme 2). With the help of the DINAMelt web server for nucleic acid melting prediction, developed by *Nicholas R.*

Markham and Michael Zuker [7] , the DNA sequences have been designed. For the DNA part it is important that it is long enough to form stable structures, meaning at least 8 nucleotides are required. Further, the DNA stem should not form loops or other structures. [3]

For this project two complementary sequences have been designed, **fB1** and **fB2**, each with 10 nucleotides. Both sequences have an overhang containing 7 pyrene units.

6.3 Results and Discussion

Prelimary results of hybrid **fB1**/**fB2** showed CD-response at high salt concentration, namely 3M of NaCl. The next step was to perform titration experiments with increasing amounts of salt, in order to gain a deeper insight on the influence of the salt concentration on the structural organization of the designed DNA/pyrene blocks **fB1** and **fB2**. The data points were taken after the addition of sodium chloride to the samples, at 90°C and at room temperature, after an equilibration time of 30 minutes. Measurements were carried out, using UV/Vis and CD spectroscopy. In absorbance spectra (Figure 1), the appearance of vibronic structures could be observed at high salt concentration (2M and 2.5 M).

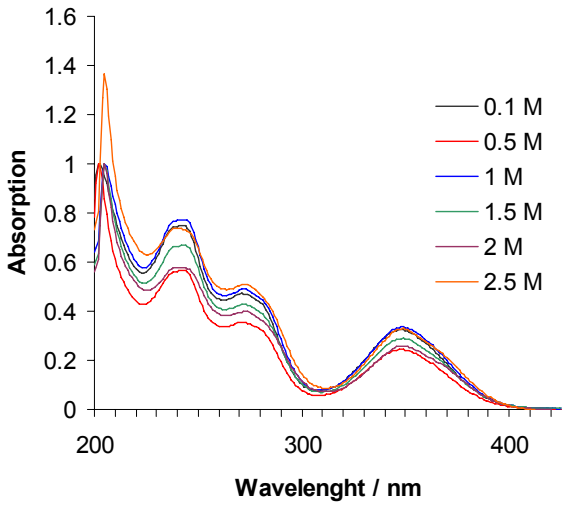

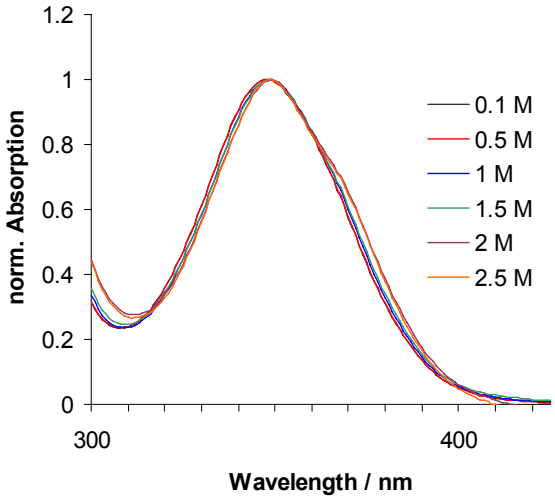

Figure 1. Absorbance spectra (top) and normalized absorbance spectra in the range of 300 nm-420 nm (bottom) of hybrid **fB1**/**fB2** (both 2.5 µm concentration, 100mM phosphate buffer) with increasing concentration of salt. The data shown here were taken after cooling to room temperature.

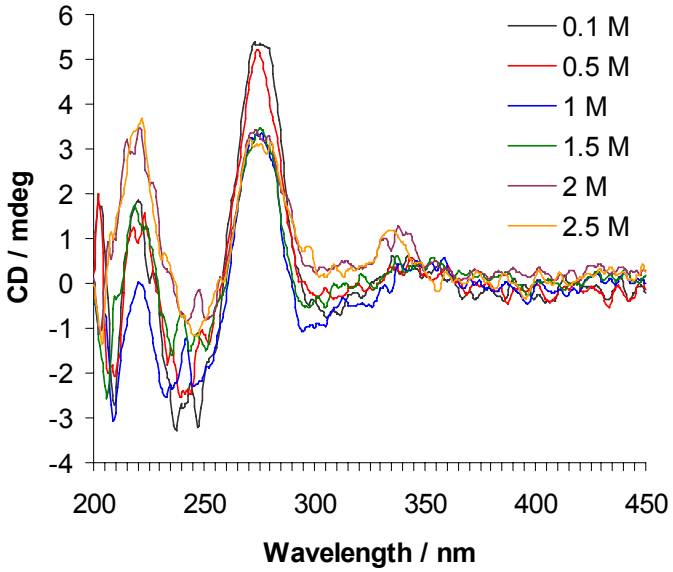

Figure 2. CD spectra of the hybrid **fB1**/**fB2** (both 2.5 µM concentration, 100mM phosphate buffer) with increasing concentration of sodium chloride. The data shown here were taken after cooling to room temperature.

In CD-spectra of the hybrid **fB1**/**fB2**, the characteristic signals of B-DNA (positive band centered near 275 nm, a negative band centered near 245 nm, and a crossover around 258 nm) are visible (Figure 2). Further, the appearance of a CD-signal at 335 nm, which is slightly increasing with increasing sodium chloride concentration, is visible. 335 nm is in the range of pyrene absorbance. The increasing sodium chloride concentration force the hydrophobic interactions of the pyrene units and a chiral ordered structure within the pyrene units is formed.

During heating of the **fB1**/**fB2** hybrid, a signal reduction in the CD spectra can be clearly observed, which can be explained by the melting of the double strand into single strands (Figure 3).

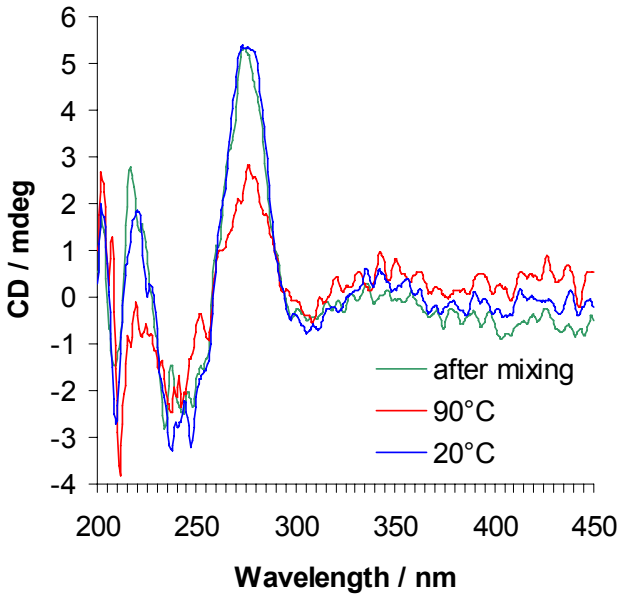

Figure 3. CD spectra of hybrid **fB1**/**fB2** (each 2.5 µM concentration, 100mM phosphate buffer, 0.1M NaCl) at 20 °C and 90°C.

The obtained results from optical techniques show clearly that within the hybrid **fB1**/**fB2**, the DNA parts interact with each other. Hybridization of the DNA strands is most probable. From absorbance spectra, stacking of the pyrene units can be confirmed at high sodium chloride concentration due to the appearance of vibronic structures. The CD-response in the region of pyrene show chiral organization.

For comparison, self-association of the two strands **fB1** and **fB2** were measured separately using 2.5 M sodium chloride. Figure 4 shows the data of self-aggregate **fB1** in

2.5 M sodium chloride obtained by UV/Vis spectroscopy, and the data obtained by CD spectroscopy are shown in Figure 6. The same experiments were performed with the self-aggregate **fB2** (Figure 5 and Figure 7). The data points were taken right after the mixing of the samples, to see if an organized structure is formed immediately. As a next step, the strands were heated then cooled, to give time for the formation of the most stable structure.

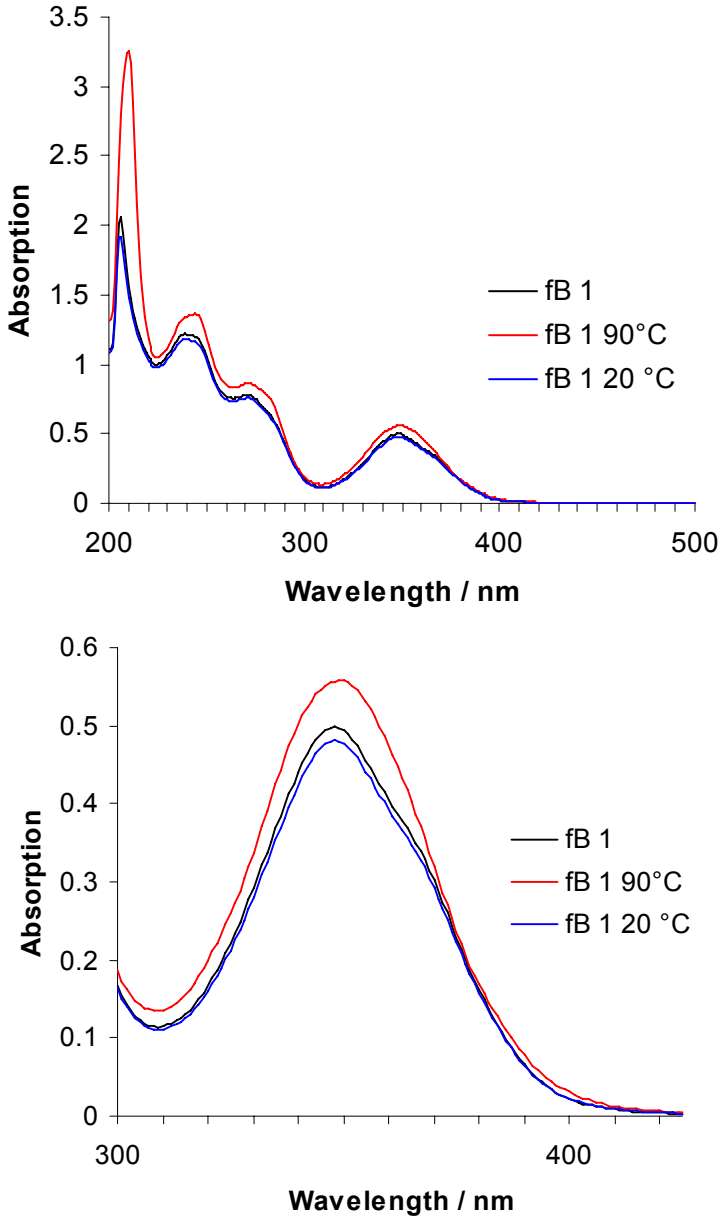

Figure 4. Absorbance spectra of **fB1** (5 μM concentration, 100mM phosphate buffer, 2.5 M NaCl) after mixing at 90°C and 20 °C.

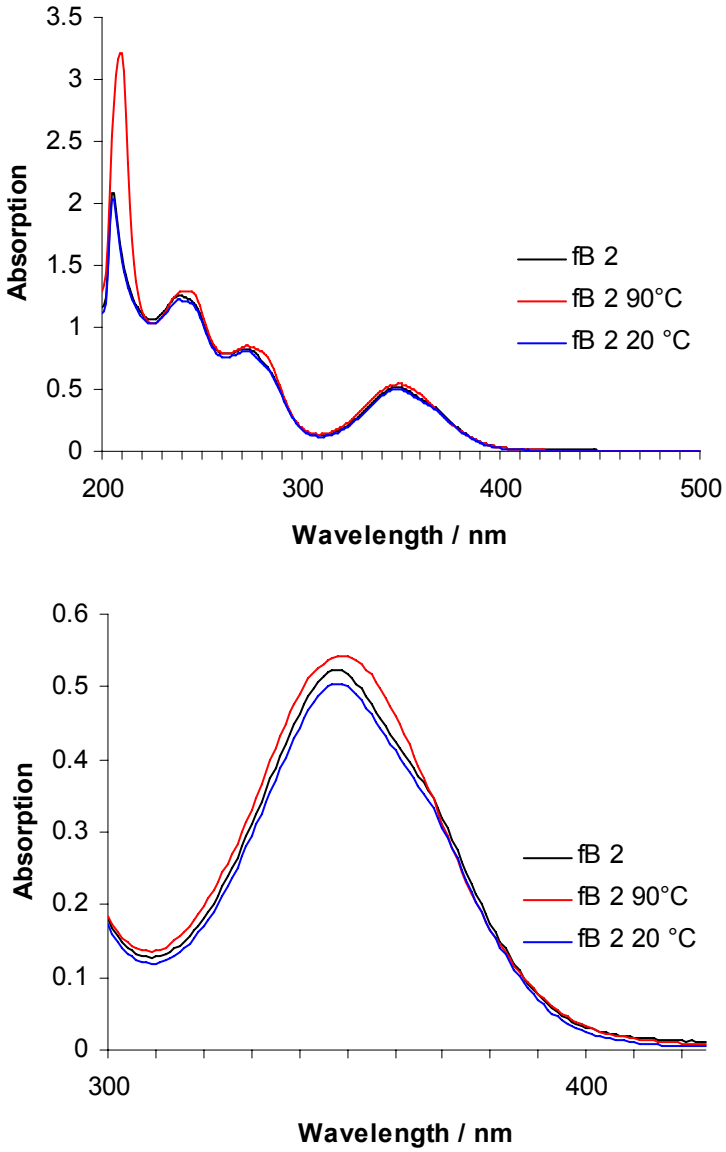

Figure 5. Absorbance spectra of **fB2** (5 μM concentration, 100mM phosphate buffer, 2.5 M NaCl) after mixing at 90°C and 20 °C.

In absorbance spectra, hypochromism can be observed upon hybridization. In **fB1** the value of hypochromism (H_{354}= 16.5%) is slightly more pronounced then in the strand **fB2** (H_{354} = 9.8%). Further, the vibronic structures are more pronounced in **fB1** than in **fB2**, suggesting that the DNA sequence might have influence on the stacking of the pyrene

units. By increasing the temperature the vibronic structures disappear, which is explained by the diaggregation of the pyrene units.

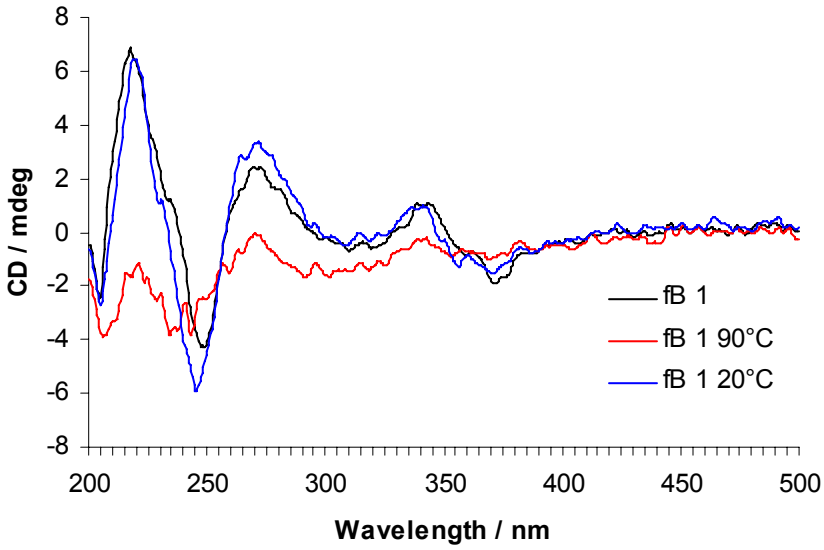

Figure 6. CD spectra of **fB1** (5 µM concentration, 100mM phosphate buffer, 2.5 M NaCl) after mixing at 90°C and 20°C.

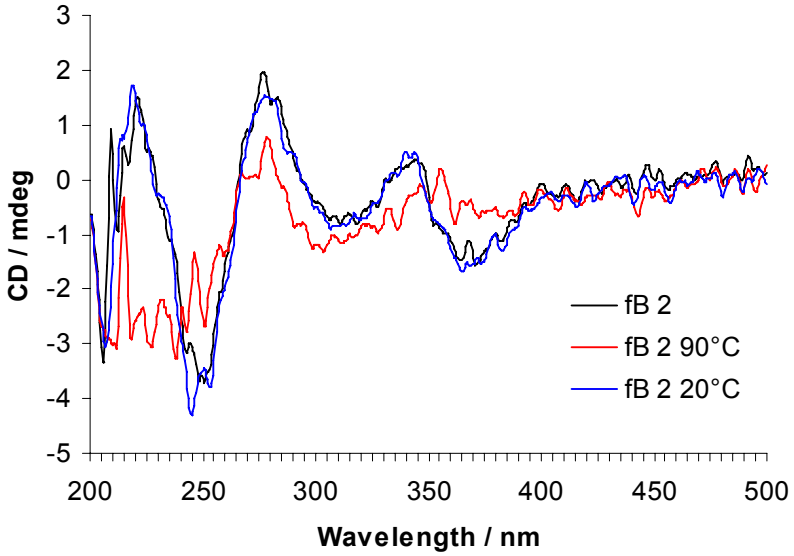

Figure 7. CD spectra of **fB2** (5 µM concentration, 100mM phosphate buffer, 2.5 M NaCl) after mixing at 90°C and 20°C.

In CD spectra a bisignate signal is observed centered at 360 nm with a minimum at 370 nm and a maximum at 345 nm. Self-association of **fB1** and **fB2** strands show the same characteristics. This observation confirms the high packing of the pyrene units, and the observed exciton-coupled CD-signal is further evidence for helical arrangement in the pyrene-stacks. In the region of DNA absorption slight changes of the band intensity in the CD spectra are observed. The intensity of the band at 275 nm is decreasing and at the same time an increase of the band at 220 nm is observed. It is clear that pyrene absorbance occurs in the same region as DNA, which makes it difficult to assign the signals to the absorbing species.

The obtained results, from the bi- and tri-segmental oligomers composed of nucleotides and non-nucleosidic pyrene units which have been published in our group recently, can be compared with the self-association of **fB1** and **fB2**. The single strands containing 7 pyrene units show, upon hybridization of two strands in the CD-spectra, a very intense bisignate signal for the pyrene band centered at 348 nm, with a positive Cotton effect at λ= 365 nm followed by a minimum at λ= 332 nm. [8, 9]

Self-association of **fB1** and **fB2** show a similar CD-response, but in this case the signal is shifted to higher wavelength with a negative Cotton effect followed by a maximum (see Figure 6 and 7). The described differences in CD-signal could be explained, that in the self-associate of **fB1** and **fB2** no hybridization of the DNA strands occure, which is a further proof that the helical arrangement is an intrinsic property of the pyrene units.

The self-association of **fB1** and **fB2** showed that the overhangs made of pyrene units recognize each other and form stable and organized hybrids. It could be proven that the principle of sticky ends consisting of pyrene units can work (Scheme 3).

Scheme 3. Self-association of strand **fB1** and **fB2**.

After two days a reduction of the UV/Vis and CD- signal of the hybrid **fB1**/**fB2** was observed. This observation could only be explained by precipitation of the hybrid **fB1**/**fB2**. It was possible to redissolve the material partially after heating (see Figure 8).

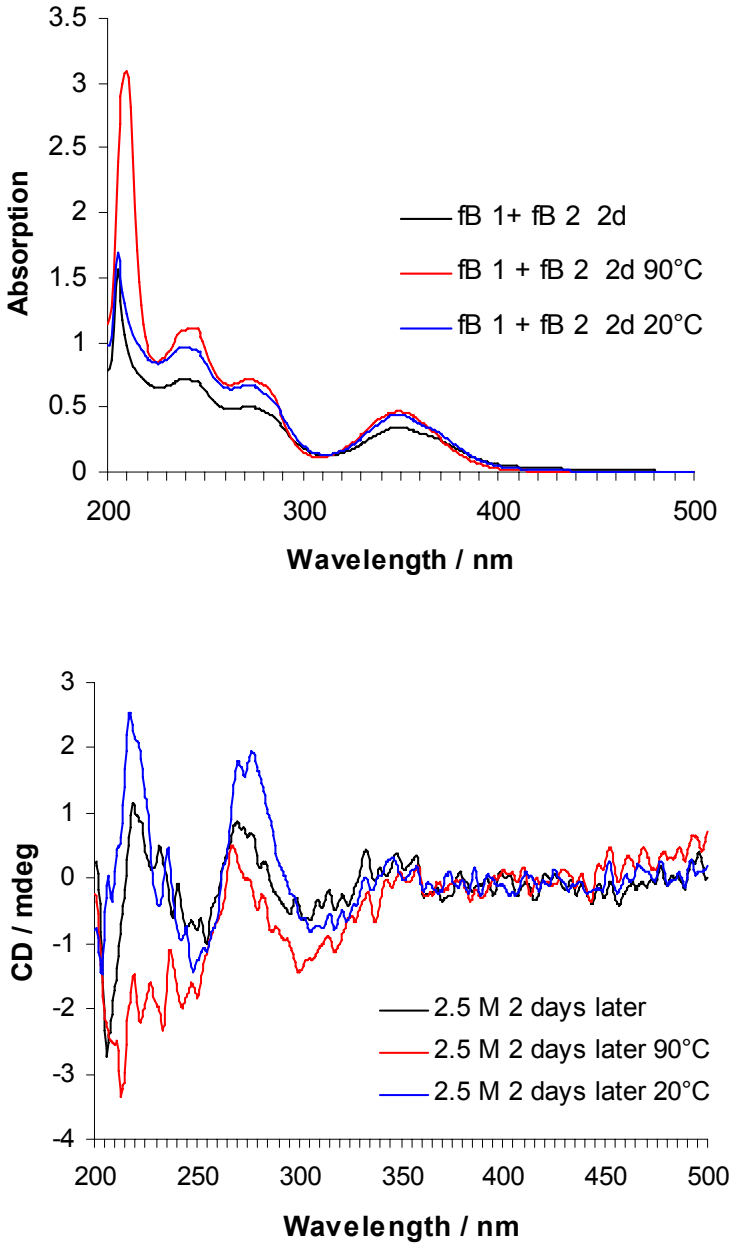

Figure 8. UV/Vis (top) and CD spectra (bottom) of fB 1 and fB 2 mixed together (each 2.5 µM concentration, 100mM phosphate buffer, 2.5 M NaCl). The data points were taken after 2 days.

As a control, the samples were mixed once again, **fB1** (5 µM) and **fB2** (5 µM) alone and as a hybrid (2.5 µM each), in 2.5 M sodium chloride. Precipitation could only be observed with the hybrid **fB1**/**fB2**.

From the obtained spectroscopic data it could be observed that the hybrid of **fB1** and **fB2** shows hybridization of the DNA part and slight helical organization in the region of pyrene absorbance at high salt concentration. The fact that precipitation in the solution occurs, confirms that a structure with higher order is formed. Self-association of the strands **fB1** and **fB2** showed the concept of sticky ends made of 7 pyrene units works and that the units recognize each other.

To get a deeper understanding of the self-associated structures, AFM measurements were performed. To start, a sodium chloride concentration of 1 M was chosen in order to prevent any precipitation. The image was performed on a mica surface. The results showed only small spots, instead of formation of long elongated structures (Figure 9).

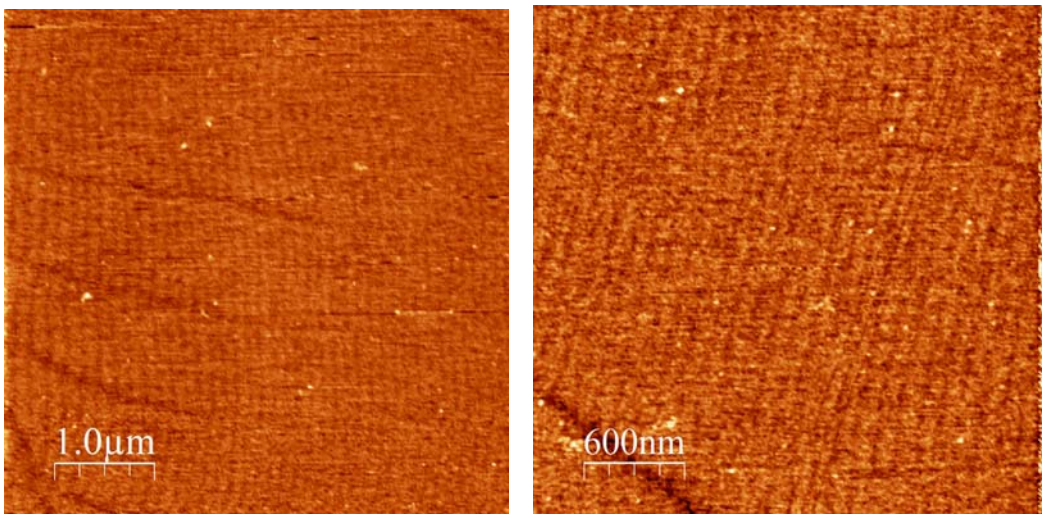

Figure 9. AFM image of **fB1**/**fB2** hybrid (each 2.5 µM concentration, 100mM phosphate buffer, 1 M NaCl). Concentration of Ni^{2+}: 5mM.

As a next step, the concentration of Ni^{2+} was increased to 10 mM in order to achieve a better binding of the synthesized molecules. The concentration of NaCl was increased as well to 2M, to force the hydrophobic interactions. (Figure 10).

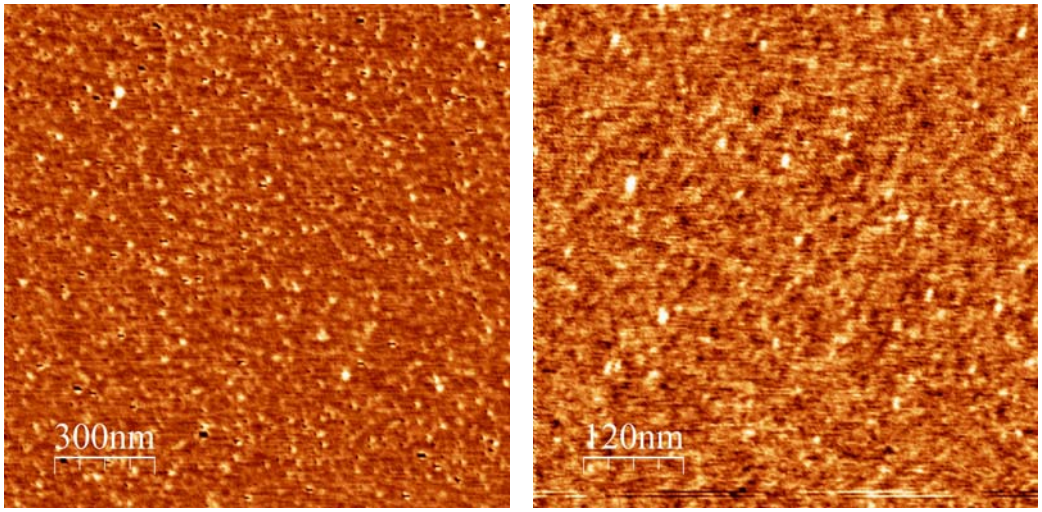

Figure 10. AFM image of **fB1**/**fB2** hybrid (each 2.5 µM concentration, 100mM phosphate buffer, 2 M NaCl). Concentration of Ni^{2+}: 10 mM, .

During this step the binding of the synthesized molecules was quite efficient. The mica surface was almost completely covered with the material, but it was not possible to see clearly organized structures. The conditions used for AFM measurements seem not to be optimal for the presented system. A sodium chloride concentration of 2M is probably required to form extented structures. If the assemblies of higher order are formed, a lower concentration than 10 mM Ni^{2+} would be more accurate in order to prevent overloading of the mica surface. It is necessary that in case precipitation occurs, meaurements are carried out using the solid material, not the solution where smaller aggregates are present.

It is possible that changes in the design of **fB1** and **fB2**, for example extension of the DNA part, could prevent the formed structures from precipitation.

6.4 Conclusions

Bi-segmental DNA/pyrene strands have been synthesized and characterized. The investigation of pyrene "sticky ends", connecting the DNA parts and leading to long supramolecular polymers with alternating DNA and pyrene parts was presented.
From the obtained spectroscopic data it could be observed that the hybrid of **fB1** and **fB2** shows hybridization of the DNA part and slight helical organization in the region of pyrene absorbance at high salt concentration. The fact that precipitation in the solution occurs, confirms that a structure with higher order is formed. Self-association of the strands **fB1** and **fB2** showed vibronic structures and a bisignate CD-signal in the region of pyrene absorbance. The data prove the concept of sticky ends made of pyrene units. To perform AFM measurements, the optimal conditions are not found yet.
Recently Asanuma and co-workers [10] published a similar system, using three cationic *p*-methylstilbazoles tethered on D-threoniols at the 5' termini as a glue connecting DNA duplexes by their interstrand cluster formation. With this approach it was possible to form nanowires.

6.5 Experimental part

Synthesis of the pyrene-DNA building block

The required strands were synthesized according to a published procedure.[11] Nucleoside phosphoramidites from *Transgenomic* (Glasgow, UK) were used for oligomer synthesis. Oligomers were prepared *via* automated oligonucleotide synthesis by a standard synthetic procedure ('trityl-off' mode) on a 394-DNA/RNA synthesizer (*Applied Biosystems*). Cleavage from the solid support and final deprotection was done by treatment with 30% NH_4OH solution at 55°C overnight. All oligomers were purified by reverse phase HPLC (LiChrospher 100 *RP-18,* 5µm, Merck), eluent *A* = $(Et_3NH)OAc$ (0.1 M, pH 7.4); eluent *B* = MeCN; elution at 30°C; gradient 5 – 45% B over 39 min.

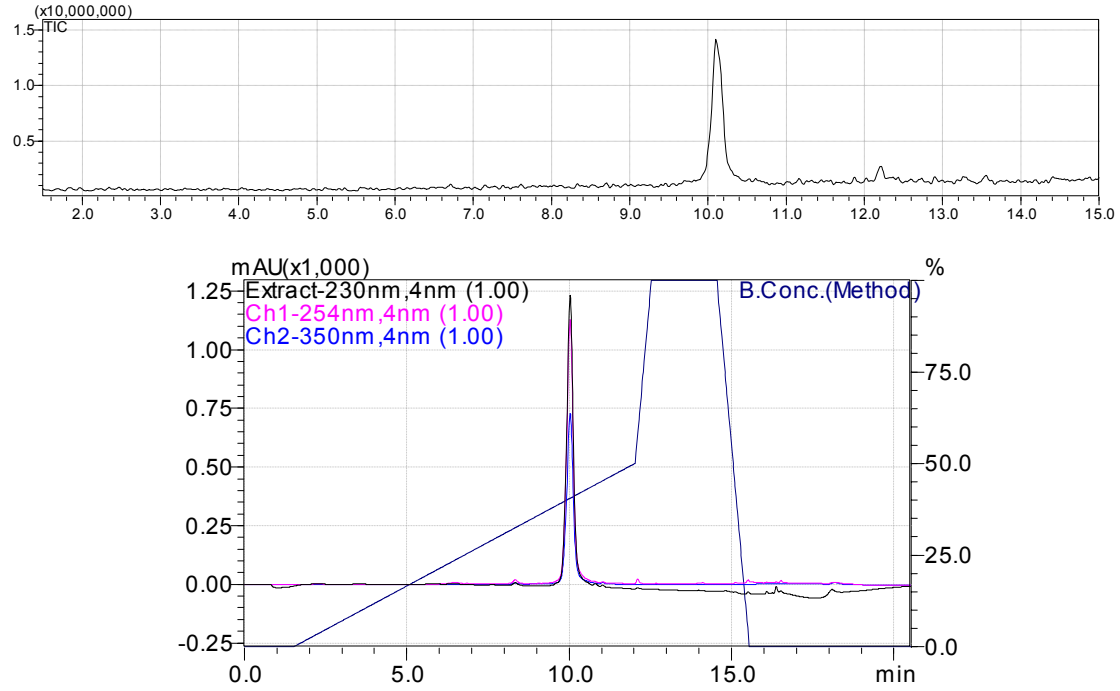

Figure 11. LC-MS data of oligomer **fB1**; total ion chromatogram (top) and chromatogram using detection wavelength at 230 nm, 254 nm and 350 nm.

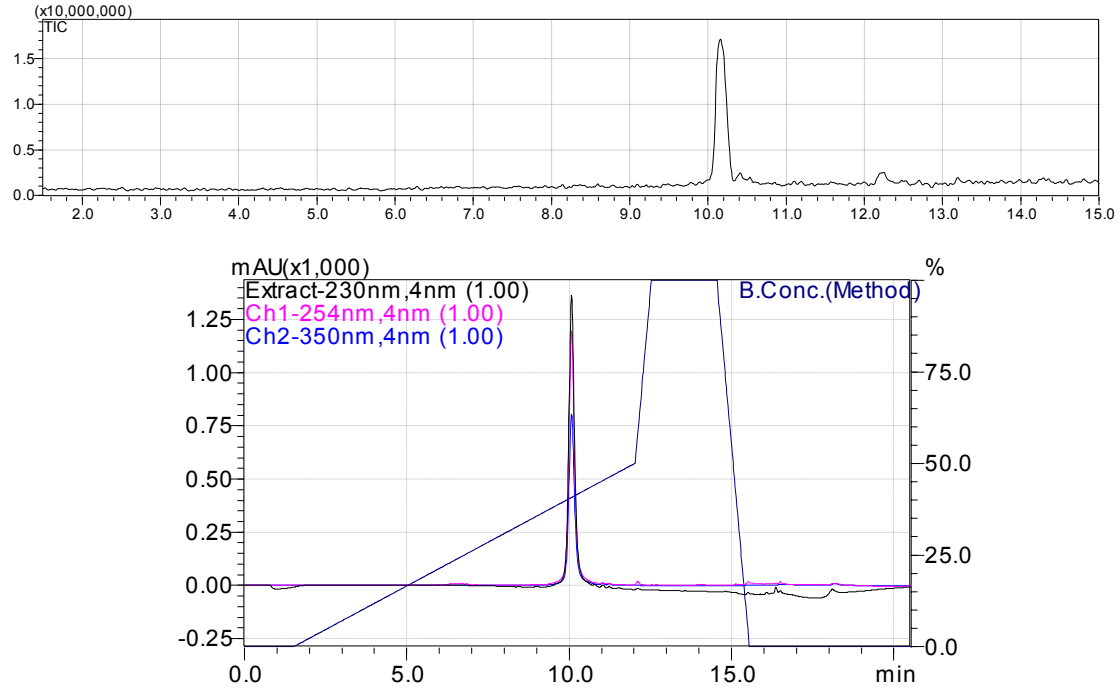

Figure 12. LC-MS data of oligomer **fB2**; total ion chromatogram (top) and chromatogram using detection wavelength at 230 nm, 254 nm and 350 nm.

Spectroscopic methods

Unless otherwise indicated, all experiments were performed in sodium phosphate buffer (10 mM, pH 7.0; NaCl concentration as indicated) for 5 µM oligomer concentration, ε_{350}= 20'000 $dm^3 \times mole^{-1} \times cm^{-1}$ was used for pyrene units.

Temperature dependent UV/VIS spectra were collected with an optic path of 1 cm over the range of 200-500 nm at 20 ºC and 90 ºC on *Varian Cary-100 Bio*-UV/VIS spectrophotometer equipped with a *Varian Cary*-block temperature controller. The cell compartment was flushed with N_2.

Titration experiments were carried out as follows: The samples **fB1** (2.5 µM) and **fB2** (2.5 µM) were mixed in 100mM phosphate buffer with the starting salt concentration of 0.1 M. The sample was directly measured after the mixing. The next step was to heat the sample to 90°C and collect the next data point. Afterwards the sample was cooled during 30 min to room temperature and measured again. The data points were taken with UV/Vis and CD spectroscopy.

CD spectra were recorded on a *JASCO J-715* spectrophotometer using quartz cuvettes with an optical path of 1 cm. (Scanning speed: 100 nm/min; data pitch: 0.5 nm; band width: 1.0 nm; response: 1 sec).

Atomic force measurements: samples of mica (20×20 mm^2) were attached to the steel baseplate through the double scotch tape and cleaved with tape immediately before use. The mica surface was treated with 20 µl of 5 mM Ni^{2+} for 1 min, then washed with water and dried with Argon. 10 µl of 5mM Ni^{2+} and 5 µl of 5 µM fB1+fB2 molecules were mixed in a vial and then added onto mica surface. After 8 minutes the mica surface was thoroughly rinsed with Milli Q water (> 18 MΩ cm^{-1}, 4 ppb TOC) and dried under a gentle stream of 5N Argon (Carbagas). For the second measurement, 8 µl of Ni^{2+} solution and 8 µl of 5 uM fB1+fB2 hybrids with 2 M NaCl were mixed in a vial and then added onto mica surface. Again, after 8 minutes the surface was rinsed with water. AFM imaging was performed in tapping mode in air with Nanosurf FlexAFM (from Nanosurf AG, Switzerland). Cantilevers Nanosensors PPP-NCHR-W (freq. ~280kHz) were used.

Mass spectrometry of oligomers was performed with a Sciex QSTAR pulsar (hybrid quadrupole time-of-flight mass spectrometer, *Applied Biosystems*). ESI-TOF MS (negative mode, CH_3CN/H_2O/TEA) data of compounds are presented in Table 1.

Table 1. Mass spectrometry data of synthesized oligomers (ESI-TOF MS, negative mode, CH_3CN/H_2O/TEA).

	Oligonucleotide	Molecular Formula	Calc. average mass	Found mass
fB 1	(5') GAG TGC CTT CSS SSS SS	$C_{265}H_{267}N_{48}O_{111}P_{16}$	6395.8	6395
fB 2	(5') GAA GGC ACT CSS SSS SS	$C_{265}H_{267}N_{55}O_{108}P_{16}$	6445.8	6445

6.6 References

[1] M. Endo, H. Sugiyama, *ChemBioChem* **2009**, *10* , 2420-2443.

[2] F. A. Aldaye, H. F. Sleiman, *Pure.Apple.Chem.* **2009**, *81*, 2157-2181.

[3] Y. H. Roh, R. C.H. Ruiz, Songming Peng, Jong B. Lee, Dan Luo, *Chem.Soc.Rev*. **2011**,

[4] N. C. Seeman, *Nature* **2003**, *421*, 427-431.

[5] N. C. Seeman, *J.Theor. Biol.* **1982**, *99*, 237

[6] A. L. Nussbaumer, Daniel Studer, Vladimir L. Malinovskii, Robert Häner *Angew.Chem.Int.Ed*. **2011**, *50*, 5490-5494.

[7] N.R. Markham, M. Zuker, *Nucl. Acids Res.*, web server issue **2005**, W577-W581.

[8] V. L. Malinovskii, F. Samain, R. Häner, *Angew.Chem.Int.Ed.* **2007**, *46*, 4464-4467.

[9] R. Häner, F. Samain, V. L. Malinovskii, *Chem.Eur.J.* **2009**, *15*, 5701-5708.

[10] H. Kashida, T. Hayashi, T. Fujii, H. Asanuma, *Chem.Eur.J.* **2011**, *17*, 2614-2622.

[11] S. M.Langenegger, R.Häner, *ChemBioChem* **2005**, *6*, 848-851.

7. Assembly of porphyrin ligands on oligopyrenotide helical scaffolds

Vladimir L. Malinovskii, Alina L. Nussbaumer and Robert Häner;
manuscript in prep.

7.1 Abstract

The cationic porphyrin **H_2TMPyP**, a classical DNA ligand, is shown to bind to supramolecular polymers (**polyPy***) that are composed of short oligopyrenotides. The spectroscopic properties of **H_2TMPyP** bound to **polyPy*** exhibit striking similarities to the complex of **H_2TMPyP** with **poly-d(AT)**, for which a groove binding mode of interaction is well established. CD effects observed at the porphyrin Soret band are consistent with the formation of a chiral supramolecular aggregate. A single cytidine nucleotide present at one end of a chiral auxiliary oligomer is responsible for inducing asymmetry in the helical assembly of achiral pyrene and porphyrin components. The findings show that artificial DNA-like polymers may be used as supramolecular templates for the assembly of functional molecules.

7.2 Introduction

The formation of chiral supramolecular assemblies is an important aspect in the development of novel types of materials[1-7] and may find its place in the growing area of nanotechnology.[8,9] In dynamic molecular systems, the occurrence of optical asymmetry may be used to control electronic signals of modular units.[10-14] DNA serves as a template for the organization of functional molecules.[15-28] Fundamental studies of DNA-ligand interactions,[29-36] stimulated in earlier days by possible medical applications, were

extended to the use of DNA as a chiral template in materials related studies.[7,15,37,38] Among the many types of compounds investigated, cationic porphyrins take an prominent place.[30,39-44] As a result, the nature of their interaction with nucleic acids is particularly well characterized.[45-48] The described supramolecular helical polymers[49] formed from anionic pyrene oligomers[50,51] show close structural similarity to DNA. This observation led to the idea to investigate their value as a supramolecular template for non-covalent ligand organization. In this chapter the assembly of a cationic porphyrin on an oligopyrenotide scaffold is described (Scheme 1).

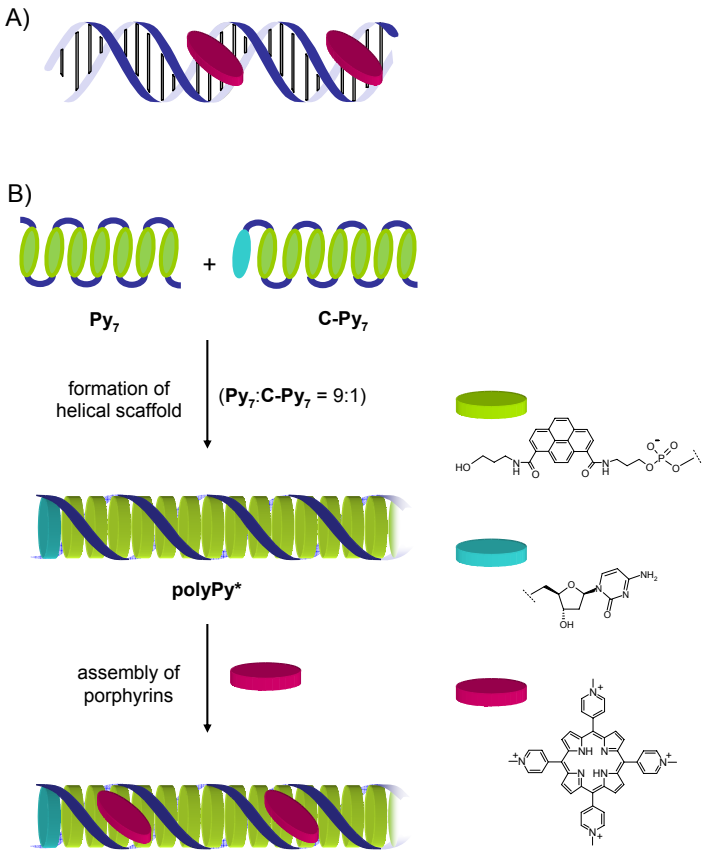

Scheme 1. Schematic illustration of A) porphyrin-DNA groove binding interaction[30,43,53] and B) porphyrin assembly on a supramolecular oligopyrenotide scaffold.

7.3 Results and Discussion

Solutions of supramolecular polymers were obtained after equilibration of a 9:1 mixture of the non-chiral heptapyrenotide **Py_7** and its chiral analog containing an additional, terminally linked nucleotide (**C-Py_7**).[49] Compound ratios, equilibration conditions and concentrations suitable for spectroscopic analysis were determined in a set of preliminary experiments. A 7 µM concentration of oligomers (corresponding to 50 µM in pyrene units) was found to be ideal and the polymerization process was considered complete within 3 weeks, after which time no further changes in the CD signals were observed. The cationic porphyrin, *meso*-tetrakis(1-methylpyridin-4-yl)porphyrin (**H_2TMPyP**) was chosen as the ligand because spectroscopic signatures of DNA interactions with this compound have been characterized in depth.[39,40,42,43,46,52-54] Additionally, **poly-d(AT)** served as DNA reference material for comparison of the obtained spectra.

UV/Vis spectroscopy provide initial evidence for interaction between **H_2TMPyP** and the pyrenotide polymer (**polyPy***). In Figure 1 the normalized absorbance spectra of **H_2TMPyP** in pure water, in 1M NaCl solution, in the presence of **poly-d(AT)** and (**polyPy***) is shown. Addition of the ligand to the solution of the polymers induces a slight red-shift (2 nm) of the Soret band. This shift correlates well with the one observed for the binding of **H_2TMPyP** to **poly-d(AT)** in the experiments ($\Delta\lambda$ = 4 nm, Table 1) and is in the range of changes described in the literature ($\Delta\lambda$ ~ 2-9 nm).[40] In contrast, a much higher red-shift ($\Delta\lambda$ >15 nm) was reported for the complex with poly-d(GC).[40]

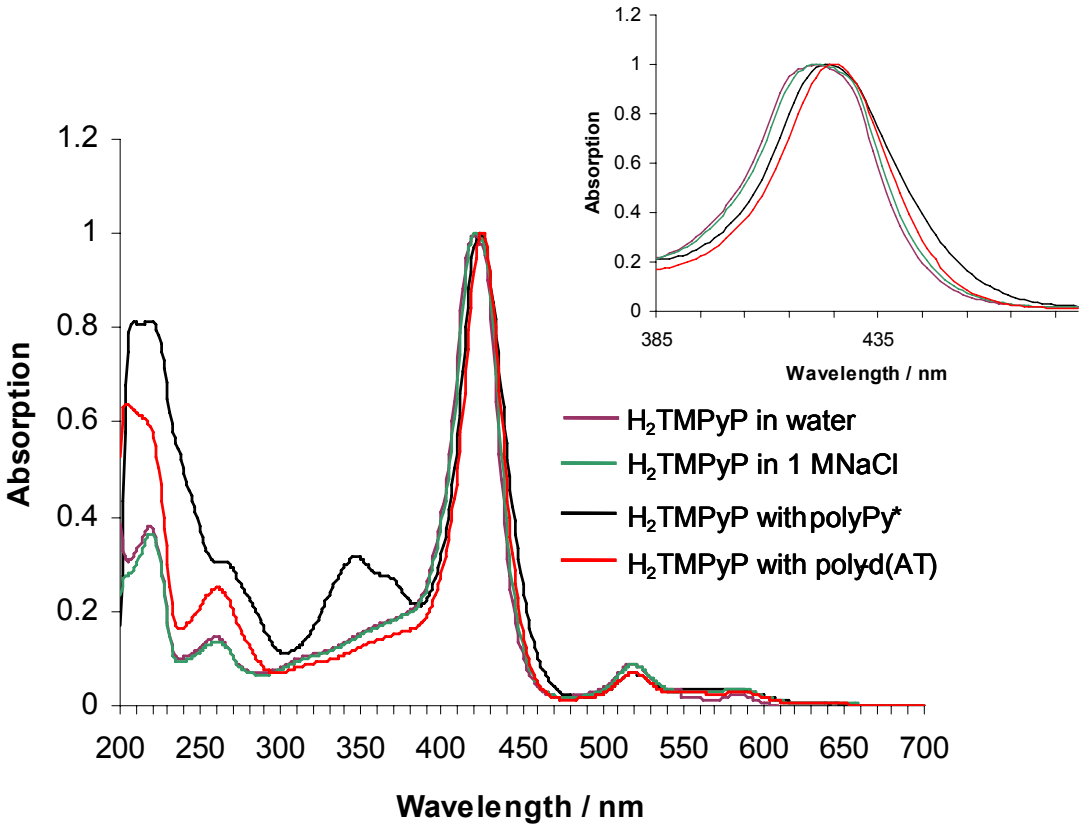

Figure 1. Normalized UV/Vis spectra of **H_2TMPyP** and its complexes with **poly-d(AT)** and **polyPy***; conditions: **20 μM** H_2TMPyP**,** sodium phosphate buffer pH =7.0, 10°C; **polyPy***: 7 μM total oligomer concentration, 1.0 M NaCl; DNA: **50** μM in base pairs, 0.2 M NaCl.

Also, the hypochromism (H, 23%) at the Soret band is in agreement with the one obtained for **poly-d(AT**) (H, 25%) whereas significantly higher values result from **poly-d(GC)** binding (H, ~40%).[40] This can be seen in Figure 2, where the relative UV/Vis absorption spectra are shown. The almost identical band shifts and hypochromisms at the Soret band upon binding of the porphyrin to **polyPy*** and **poly-d(AT)** suggest that i) **H_2TMPyP** binds to **polyPy*** and ii) the interaction resembles the one observed with **poly-d(AT)** (*outside* or *groove binding*) and not **poly-d(GC)** (*intercalation*).

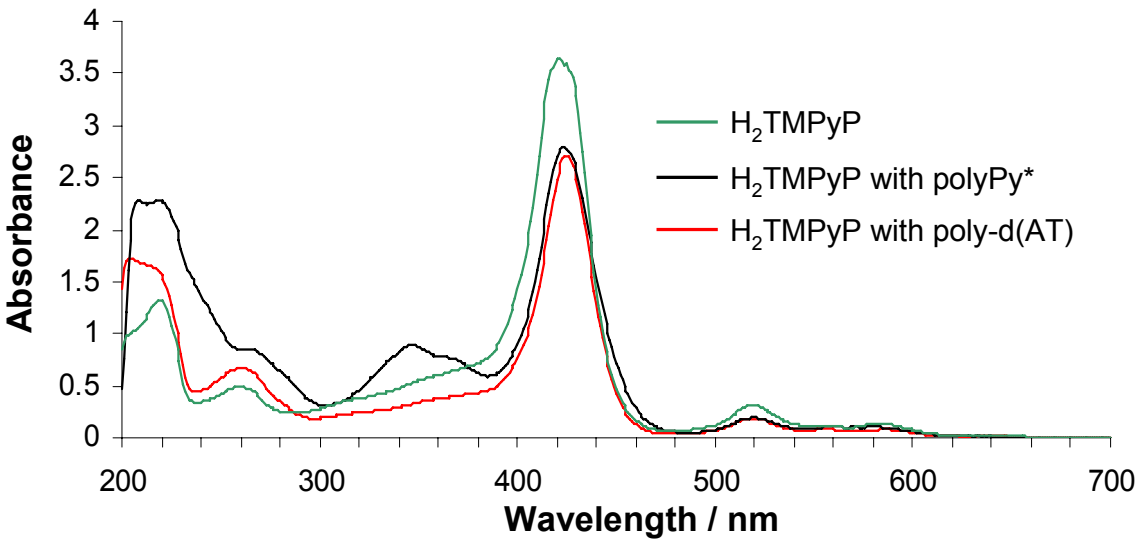

Figure 2. Relative UV/Vis absorption spectra of free **H_2TMPyP** and in the presence of **poly-d(AT)** and **polyPy***; conditions: pH = 7.0, 10°C; polyPy*: 7 µM total oligomer concentration, 1.0 M NaCl; DNA: 50 µM in base pairs, 0.2 M NaCl.

H_2TMPyP	(-)	polyPy*	poly-d(AT)	poly-d(GC)
Absorbance (λ_{max}, nm)	421	423	425	(444)[40]
H (%)		23	25	(~40)[40]
Soret band (nm) $\Delta\varepsilon$, $M^{-1}cm^{-1}$	-	416 +21	431 +35	(440)[45] (-25)[45]
Fluorescence (λ_{max}, nm)	715	630;670;715	655;715	(669;730)[41]

Table 1. Spectroscopic characteristics of **H_2TMPyP** alone and bound to **polyPy***, **poly-d(AT)** or **poly-d(GC)**. Conditions: see Fig. 1.

Fluorescence spectra are shown in Figure 3. Binding of **H_2TMPyP** to **polyPy*** leads to an increase of the blue-shifted component of the fluorescence signal (see difference

spectrum in Figure 2). The position and also the changes of the band structure are in agreement with the description of **poly-d(AT)** (groove) bound **H_2TMPyP** (Table 1).[41] Thus, the fluorescence spectra indicate again a similarity of **H_2TMPyP** complexes formed with **polyPy*** and **poly-d(AT)**, but not with **poly-d(GC)**.

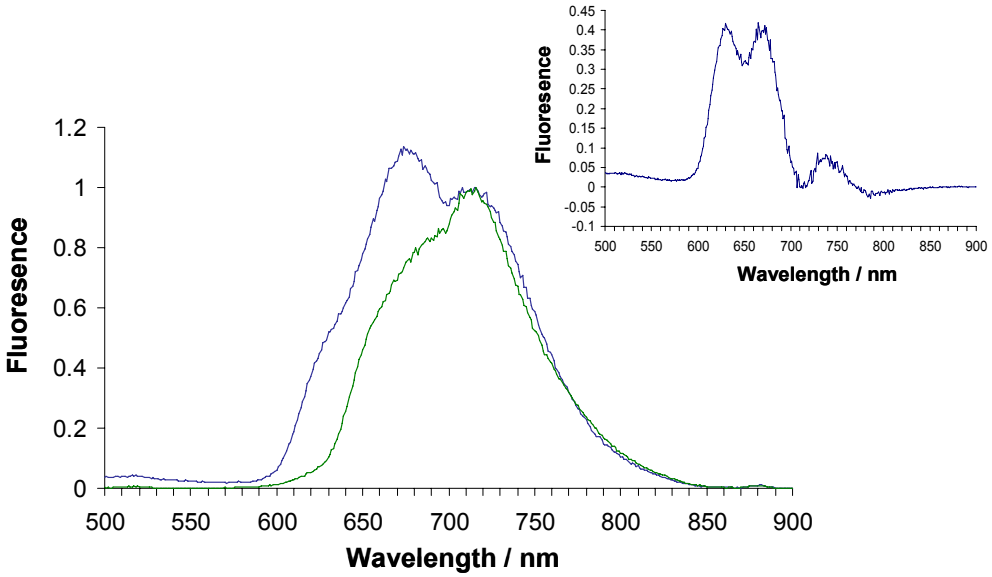

Figure 3. Normalized fluorescence spectra of **H_2TMPyP** (6 μM) in the presence (solid line) and absence (broken line) of **polyPy*** (sodium phosphate buffer, pH = 7.0, 1 M NaCl, 20°C; 7 μM total oligomer concentration corresponding to 50 μM in pyrene units; λ(ex) = 440 nm (Soret band); inset: corresponding difference spectrum.

In addition, binding of **H_2TMPyP** to **polyPy*** does not affect the structure of the supramolecular polymers since fluorescence as well as excitation spectra of pyrenes exhibit no significant changes upon complex formation. The vibronic structures are still well visible, as it is shown in Figure 4.

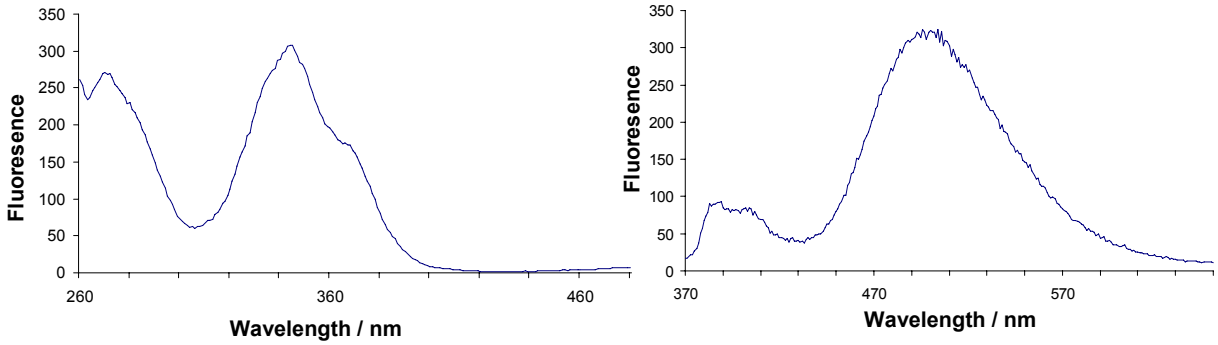

Figure 4. left: Excitation spectra (λ(em) = 500 nm) of **polyPy*** in the presence of **H_2TMPyP** (20 μM); *right*: fluorescence spectra (λ(ex) = 350 nm) in the presence of **H_2TMPyP** (20 μM) (sodium phosphate buffer, pH =7.0, 1 M NaCl, 10°C; 7 μM total oligomer concentration.

To determine the binding constant fluorescence titration experiments were performed (Figure 5 and 6).

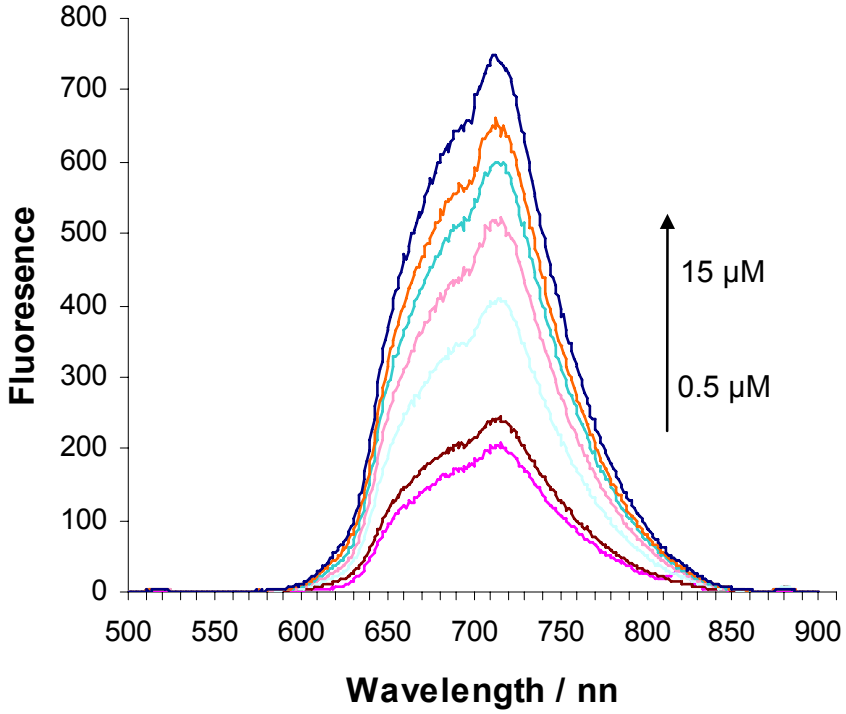

Figure 5. Fluorescence spectra of **H_2TMPyP** with increasing concentration (0.5 μM -15 μM) in the absence of **polyPy*** (7 μM total oligomer concentration corresponding to 50 μM in pyrene units); sodium phosphate buffer, pH = 7.0, 1 M NaCl, 20°C; λ(ex) = 440 nm (Soret band).

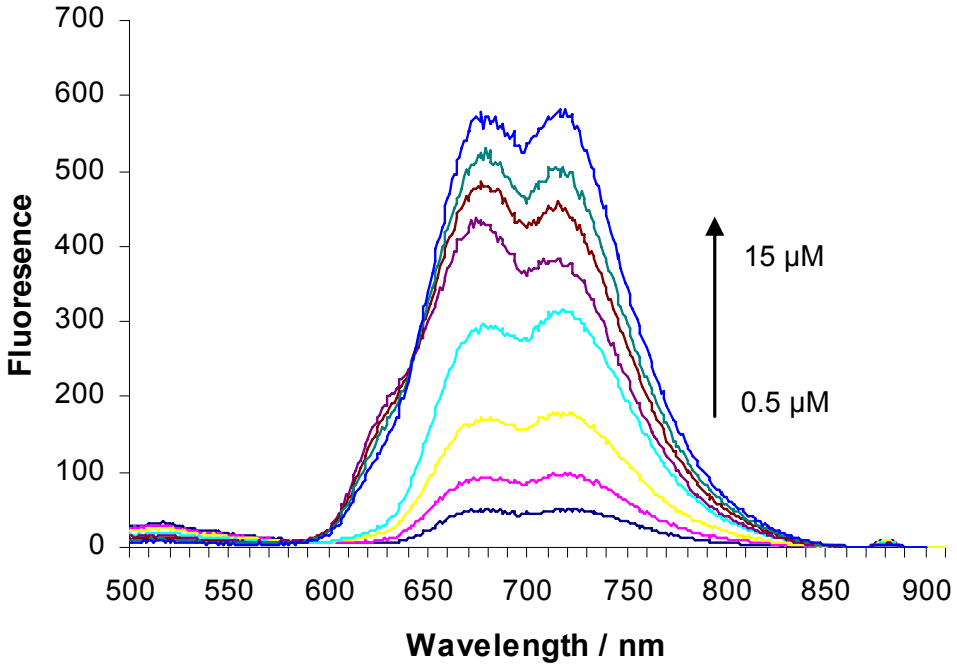

Figure 6. Fluorescence spectra of **H_2TMPyP** with increasing concentration (0.5 µM -15 µM) in the presence of **polyPy*** (7 µM total oligomer concentration corresponding to 50 µM in pyrene units); sodium phosphate buffer, pH = 7.0, 1 M NaCl, 20°C; λ(ex) = 440 nm (Soret band).

Fluorescence seemed to be the method of choice, because of the higher sensitivity compared to UV/Vis absorbance spectroscopy. It is easier to assign the detected signals of fluorescence to the bound and non-bound fraction of ligands. In Figure 5 the titration of **H_2TMPyP** in the absence of the template is shown. There is a gradual increase of fluorescence signal by an increase of the amount of ligands, but in the shape of the signals no changes are observed. In presence of the template small differences also in the shape of porphyrin fluorescence are observed. With the concentration of 6 µM of **H_2TMPyP** the biggest fraction of ligands is bound to the template.

The apparent binding constant for the **H_2TMPyP-polyPy*** interaction was found to be $1.4 \pm 0.2 \times 10^5$ M^{-1}. Fluorescence data thus show that **polyPy*** serves as a robust template for organization of the cationic porphyrins.

The position and also the changes of the band structure are in excellent agreement with the description of the **poly-d(AT)** (groove) bound **H_2TMPyP** (Table 1 and Figure 3). For the porphyrin-polyphosphate complex, the position of the bands are 667 nm and 727 nm

and so do not overlap with the observed values. This could be an indication that DNA-like grooves may well be present in artificial DNA like **polyPy***. The reduced effect in the fluorescence spectra compared to the **poly-d(AT)- H_2TMPyP** complex (Figure 3) is well known to be an effect of high salt concentration.

Thus, the fluorescence spectra indicate again a close similarity of the **H_2TMPyP** complex formed with **polyPy*** and with **poly-d(AT)** but not with **poly-d(GC)**.

When measuring the excitation spectra further interesting observations were found. Additional support for binding of **H_2TMPyP** to **polyPy*** is obtained from excitation experiments monitoring porphyrin fluorescence at 655 nm (Figure 4), which clearly show energy transfer from the pyrene scaffold to the porphyrin ligands. In addition to direct excitation at the Soret (420 nm) and Q-bands (> 500nm), substantial fluorescence also arises from pyrene excitation (250 and 350 nm bands).

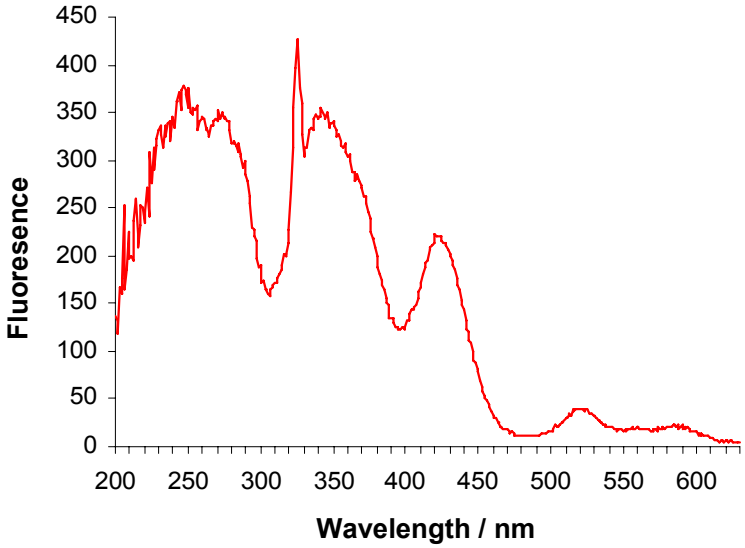

Figure 7. Excitation spectrum of **H_2TMPyP-polyPy***; conditions: λ(em) = 655 nm; pH = 7.0, 20°C, 1.0 M NaCl; **H_2TMPyP**: 4 μM; **polyPy***: 7 μM total oligomer concentration.

Also, the excitation spectra can help to distinguish between the bound and the unbound fraction of cationic porphyrins. In Figure 8 the two excitation spectra are shown using the emission wavelength at 710 nm and 650 nm. The excitation spectrum λ(em) = 710 nm shows the energy transfer to a much lesser extent. This confirms that this fraction doesn't interact with the template and, regarding this, corresponds to the unbound species.

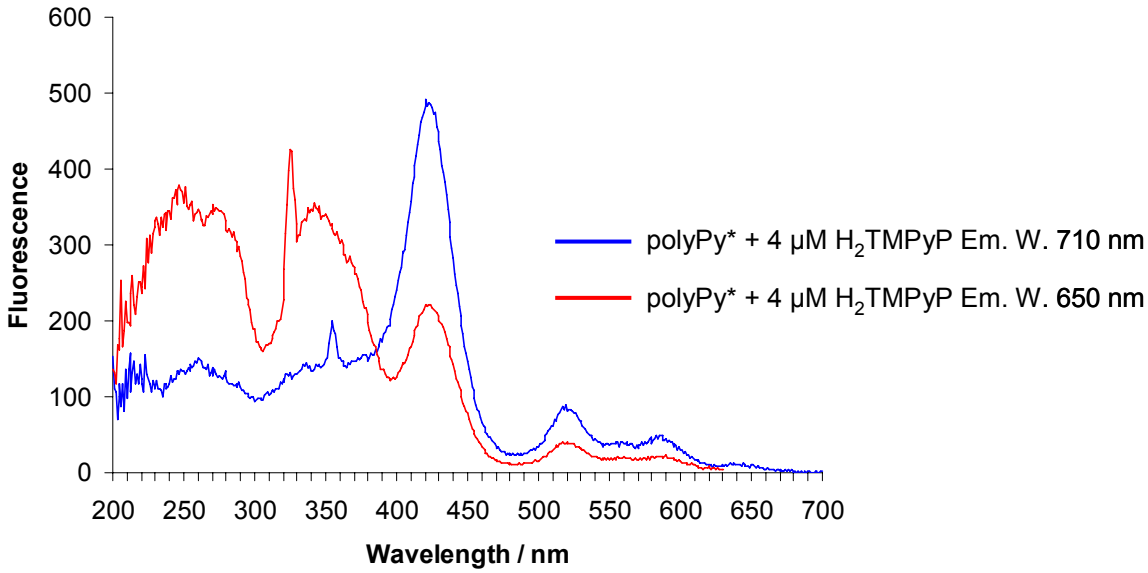

Figure 8. Comparison of excitation spectra of **H_2TMPyP-polyPy***; conditions: λ(em) = 655 nm and λ(em) = 710 nm; pH = 7.0, 20°C, 1.0 M NaCl; **H_2TMPyP**: 4 µM; polyPy*: 7 µM total oligomer concentration.

Insight into DNA-ligand interactions is provided by circular dichroism (CD) spectroscopy.[53] Distinct differences in the induced CD (ICD) signal at the Soret band allows differentiating between an *intercalative* (negative signal) and a *groove binding* (positive signal) porphyrin-DNA interaction.[43,45] The concentration dependent appearance of a positive ICD (416 nm, Δε = 21 $M^{-1}cm^{-1}$) in this region (Figure 3, top) indicates a *non-intercalative* binding of **H_2TMPyP** to **polyPy***. [55] The **H_2TMPyP/poly-d(AT)** interaction leads to a very similar spectrum (Figure 3 bottom) exhibiting also a positive ICD at the Soret band, red-shifted by 15 nm.

This shift may originate from structural differences of the two types of polymers, but may also reside, at least partly, in the difference in ionic strengths, 1 M and 0.2 M NaCl for **polyPy*** and **poly-d(AT)**, respectively. In analogy to the corresponding drug-DNA complexes, we assign the positive ICD to a inclined orientation of the bound ligands relative to the helical axis of the polymer.[55] Therefore, intercalative binding mode or outside, self-stacked aggregation, which are recognized by a negative ICD or an exciton coupled CD, respectively,[45,55] can be ruled out.

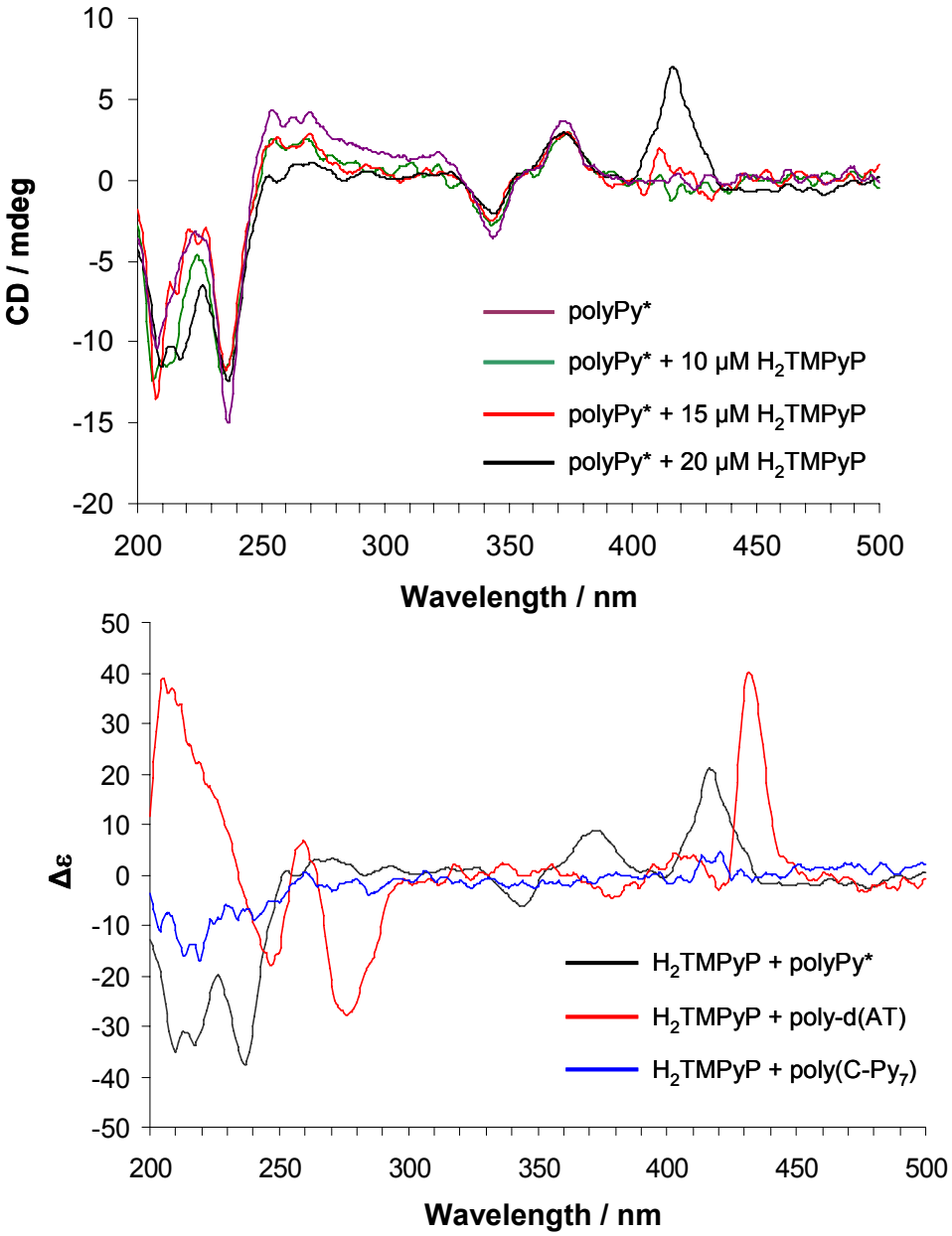

Figure 7. Top: growth of induced CD signal in the region of the porphyrin Soret band (400-430 nm) with increasing **H_2TMPyP** concentrations (7 μM **polyPy*** conc.); bottom: comparison of CD spectra of **H_2TMPyP** (20 μM) in the presence of **polyPy***, **poly-d(AT)** and **C-Py$_7$**; conditions: see Fig. 1; **C-Py$_7$**: 7 μM.

Importantly, shape and intensity of the exciton coupled CD in the pyrene region (300-400 nm) remain essentially unchanged, which again demonstrates the structural robustness of the supramolecular scaffold during complex formation. The chiral building block **C-Py$_7$**

alone, which was shown previously not to form supramolecular polymers,[49] does not lead to any porphyrin CD signals.

The spectroscopic data described above provide strong evidence for the assembly of cationic porphyrins along the helical, supramolecular oligopyrenotide scaffold. Asymmetry is effected by amplification of chirality induced by a small amount of a chiral oligomer.[49] Overall, the asymmetry arises from a single nucleotide, cytidine, which amounts to less than 1% of the whole (**polyPy***)-(**H_2TMPyP**) complex. The binding of **H_2TMPyP** to **polyPy*** occurs in a non-intercalative way and closely resembles the *groove binding* mode of interaction observed for **H_2TMPyP**/**poly-d(AT)**. It is reasonable to assume that electrostatic interactions between the polyphosphate backbone of **polyPy*** and the cationic porphyrin are the main driving force for complex formation. Moreover, the close resemblance of the spectroscopic signatures between **H_2TMPyP** complexes with **polyPy*** and with **poly-d(AT)** strongly hints at the presence of grooves in the supramolecular polymers as illustrated in Scheme 1.

7.4 Conclusions

In conclusion, it could be shown that supramolecular polymers formed of short oligopyrenotides serve as helical scaffolds for the molecular organization of cationic porphyrin ligands. The polymer-ligand aggregate resembles the well-characterized **H_2TMPyP**/**poly-d(AT)** complex. Spectroscopic data favour a model in which groove bound porphyrins are arranged along a helical, polymeric scaffold in a non-intercalative mode. The study demonstrates the value of supramolecular polymers as templates for the organization of functional molecules. Moreover, they represent alternatives to DNA scaffolds with substantially different electronic properties.

7.5 Experimental part

General procedures

The required pyrene building block [56] and the oligomers were synthesized according to a published procedures. [49]

Poly-d(AT) was purchased from LabForce Inc. A stock solution was prepared by dissolving the material in sterile, endotoxin-free physiological water provided by the supplier.Meso-5,10,15,20-Tetrakis-(N-methyl-4-pyridyl)porphine tetratosylate (**H_2TMPyP**) was purchased from Calbiochem. Purity of the material, especially absence of metals, was confirmed by NMR analysis before use of the material.

Stock solutions.

Py_7: sodium phosphate buffer (10 mM, 1M NaCl, pH 7.0); 7 µM oligomer concentration (corresponding to 50 µM concentration in pyrene units); an ε_{350} value of 20'000 $dm^3 \times mole^{-1} \times cm^{-1}$ was used for pyrene.

Poly-d(AT): sodium phosphate buffer (19 mM, 0.2 M NaCl, pH 7.0); [40] 50 µM concentration in base pairs; an ε_{262} value of 13'200 $dm^3 \times mole^{-1} \times cm^{-1}$ was used for the determination of the base pair concentration.

H_2TMPyP: an ε_{420} value of 220'000 $dm^3 \times mole^{-1} \times cm^{-1}$ was used.[3]

Preparation of the oligopyrenotide polymer solution (polyPy*). A 7 µM solution of the oligomer **Py_7** in 1 ml of buffer (10 mM sodium phosphate, pH 7.0, 1M NaCl) was heated to 80°C. After the mixture was allowed to cool to room temperature, a solution of C-Py_7 (approx. 10µl) was added so that the total amount of **C-Py_7** reached 10% of oligomer components. Equilibration was hence controlled by measurement of the CD signal in the pyrene area (around 350 nm). Constant signals were obtained after equilibration for 3 weeks at room temperature.

UV/VIS spectra were collected with an optical path of 1 cm over the range of 200-700 nm at 10ºC on *Varian Cary-100 Bio*-UV/VIS spectrophotometer equipped with a *Varian Cary*-block temperature controller.

Circular dichroism experiments. CD spectra were recorded on a *JASCO J-715* spectrophotometer at 10°C using quartz cuvettes with an optical path of 0.5 cm. (Scanning speed: 100 nm/min; data pitch: 0.5 nm; band width: 1.0 nm; response: 1 sec) with a temperature controller. All measurements were done at 10°C. Increasing amounts of a stock solution of **H_2TMPyP** were added stepwise to a solution (250 µl) of the equilibrated **polyPy*** solution prepared as described above. Concentrations of stock solutions were chosen such that the total dilution of the analyte solution did not exceed 1% by each addition of **H_2TMPyP**. CD spectra were recorded 30 min after each incremental addition of **H_2TMPyP**. The same procedure was applied to **poly-d(AT)** with a concentration of 50 µM base pairs in 19 mM phosphate buffer, pH = 7.0, and 0.2 M NaCl.[2] **Calculation of Δε.** For the calculation of Δε in M^{-1} cm^{-1} the formula
Δε =Θ(mdeg)/32980*C*l was used. [57]

Fluorescence data were collected on a *Varian Cary Eclipse* fluorescence spectrophotometer equipped with a *Varian Cary*-block temperature controller using 0.5 cm x 0.5 cm quartz cuvettes. *Varian Eclipse* software was used to investigate the fluorescence of the (**polyPy***)-(**H_2TMPyP**) complex at a wavelength range of 370-900 nm (excitation wavelength for pyrene: 350 nm; excitation wavelength for **H_2TMPyP**: 420 nm, 520 nm, 585 nm; excitation and emission slit width of 5 nm), and the excitation at a wavelength range of 200-700 nm (emission wavelength for pyrene: 500 nm; emission wavelength for **H_2TMPyP**: 715 nm; excitation slit width and emission slit width: 5 nm).

7.6 References

[1] G. M. Whitesides, J. P. Mathias, C. T. Seto, *Science* **1991**, *254*, 1312-1319.

[2] N. C. Seeman, *Annu.Rev.Biochem.* **2010**, *79*, 65-87.

[3] J. M. Lehn, *Supramolecular Chemistry - Concepts and Perspectives*, VCH, Weinheim **1995**.

[4] V. Balzani, A. Credi, F. M. Raymo, J. F. Stoddart, *Angew.Chem.Int.Ed.* **2000**, *39*, 3349-3391.

[5] R. J. Hooley, J. Rebek, *Chem.Biol.* **2009**, *16*, 255-264.

[6] E. Schwartz, S. Le Gac, J. J. L. M. Cornelissen, R. J. M. Nolte, A. E. Rowan, *Chem.Soc.Rev.* **2010**, *39*, 1576-1599.

[7] A. Ruiz-Carretero, P. G. A. Janssen, A. Kaeser, A. P. H. J. Schenning, *Chem.Commun.* **2011**, *47*, 4340-4347.

[8] T. F. A. Greef, E. W. Meijer, *Nature* **2008**, *453*, 171-173.

[9] H. C. Hesse, J. Weickert, M. Al-Hussein, L. Dossel, X. L. Feng, K. Müllen, L. Schmidt-Mende, *Solar Energy Materials and Solar Cells* **2010**, *94*, 560-567.

[10] M. A. Mateos-Timoneda, M. Crego-Calama, D. N. Reinhoudt, *Chem.Soc.Rev.* **2004**, *33*, 363-372.

[11] J. M. Lehn, *Prog.Polym.Sci.* **2005**, *30*, 814-831.

[12] A. Scarso, J. J. Rebek, *Supramol.Chir.* **2006**, *265*, 1-46.

[13] K. S. Cheon, J. V. Selinger, M. M. Green, *Angew.Chem.Int.Ed.* **2000**, *39*, 1482-1485.

[14] E. Yashima, K. Maeda, *Macromolecules* **2008**, *41*, 3-12.

[15] K. C. Hannah, B. A. Armitage, *Acc.Chem.Res.* **2004**, *37*, 845-853.

[16] J. Wengel, *Org.Biomol.Chem.* **2004**, *2*, 277-280.

[17] M. Endo, H. Sugiyama, *Chembiochem* **2009**, *10*, 2420-2443.

[18] V. V. Filichev, E. B. Pedersen, in *Wiley Encycl.Chem.Biol.*, ,*Vol*. *1*, Ed.: T. P. Begley, Wiley, Hoboken , 2009, pp. 493-524.

[19] R. Varghese, H. A. Wagenknecht, *Chem.Commun.* **2009**, 2615-2624.

[20] V. L. Malinovskii, D. Wenger, R. Häner, *Chem.Soc.Rev.* **2010**, *39*, 410-422.

[21] H. Kashida, X. Liang, H. Asanuma, *Curr.Org.Chem.* **2009**, *13*, 1065-1084.

[22] T. J. Bandy, A. Brewer, J. R. Burns, G. Marth, T. Nguyen, E. Stulz, *Chem.Soc.Rev.* **2010**, *40*, 138-148.

[23] M. E. Ostergaard, P. J. Hrdlicka, *Chem.Soc.Rev.* **2011**.

[24] W. Su, V. Bonnard, G. A. Burley, *Chem.Eur.J.* **2011**, *17*, 7982-7991.

[25] O. Khakshoor, E. T. Kool, *Chem.Commun.* **2011**, *47*, 7018-7024.

[26] S. M. Langenegger, R. Häner, *ChemBioChem* **2005**, *6*, 2149-2152.

[27] V. L. Malinovskii, F. Samain, R. Häner, *Angew.Chem.Int.Ed.* **2007**, *46*, 4464-4467.

[28] R. Häner, F. Samain, V. L. Malinovskii, *Chem.Eur.J.* **2009**, *15*, 5701-5708.

[29] R. J. Fiel, *J.Biomol.Struct.Dyn.* **1989**, *6*, 1259-1275.

[30] L. G. Marzilli, *New J.Chem.* **1990**, *14*, 409-420.

[31] O. Kennard, *Pure Appl.Chem.* **1993**, *65*, 1213-1222.

[32] T. R. Krugh, *Curr.Opin.Struct.Biol.* **1994**, *4*, 351-364.

[33] B. H. Geierstanger, D. E. Wemmer, *Annu.Rev.Biophys.Biomol.Struct.* **1995**, *24*, 463-493.

[34] S. Neidle, *Nat.Prod.Rep.* **2001**, *18*, 291-309.

[35] H. K. Liu, P. J. Sadler, *Acc.Chem.Res.* **2011**, *44*, 349-359.

[36] B. Meunier, *Chem.Rev.* **1992**, *92*, 1411-1456.

[37] G. A. Hembury, V. V. Borovkov, Y. Inoue, *Chem.Rev.* **2008**, *108*, 1-73.

[38] A. Mammana, G. Pescitelli, T. Asakawa, S. Jockusch, A. G. Petrovic, R. R. Monaco, R. Purrello, N. J. Turro, K. Nakanishi, G. A. Ellestad, M. Balaz, N. Berova, *Chem.Eur.J.* **2009**, *15*, 11853-11866.

[39] R. J. Fiel, J. C. Howard, E. H. Mark, N. Datta Gupta, *Nucl.Acids Res.* **1979**, *6*, 3093-3118.

[40] R. F. Pasternack, E. J. Gibbs, J. J. Villafranca, *Biochemistry* **1983**, *22*, 2406-2414.

[41] J. M. Kelly, M. J. Murphy, D. J. Mcconnell, C. Ohuigin, *Nucl.Acids Res.* **1985**, *13*, 167-184.

[42] U. Sehlstedt, S. K. Kim, P. Carter, J. Goodisman, J. F. Vollano, B. Norden, J. C. Dabrowiak, *Biochemistry* **1994**, *33*, 417-426.

[43] R. F. Pasternack, E. J. Gibbs, *Metal Ions in Biological Systems, Vol 33* **1996**, *33*, 367-397.

[44] R. F. Pasternack, E. J. Gibbs, D. Bruzewicz, D. Stewart, K. S. Engstrom, *J.Am.Chem.Soc.* **2002**, *124*, 3533-3539.

[45] R. F. Pasternack, *Chirality* **2003**, *15*, 329-332.

[46] D. R. McMillin, A. H. Shelton, S. A. Bejune, P. E. Fanwick, R. K. Wall, *Coord.Chem.Rev.* **2005**, *249*, 1451-1459.

[47] B. H. Yun, S. H. Jeon, T. S. Cho, S. Y. Yi, U. Sehlstedt, S. K. Kim, *Biophys.Chem.* **1998**, *70*, 1-10.

[48] S. Lee, S. H. Jeon, B. J. Kim, S. W. Han, H. G. Jang, S. K. Kim, *Biophys.Chem.* **2001**, *92*, 35-45.

[49] A. L. Nussbaumer, D. Studer, V. L. Malinovskii, R. Häner, *Angew.Chem.Int.Ed.* **2011**, *50*, 5490-5494.

[50] F. Samain, V. L. Malinovskii, S. M. Langenegger, R. Häner, *Bioorg.Med.Chem.* **2008**, *16*, 27-33.

[51] V. A. Galievsky, V. L. Malinovskii, A. S. Stasheuski, F. Samain, K. A. Zachariasse, R. Häner, V. S. Chirvony, *Photochem.Photobiol.Sci.* **2009**, *8*, 1448-1454.

[52] L. G. Marzilli, D. L. Banville, G. Zon, W. D. Wilson, *J.Am.Chem.Soc.* **1986**, *108*, 4188-4192.

[53] M. Ardhammar, T. Kurucsev, B. Norden, in *Circular Dichroism - Principles and Applications*, Eds.: N. Berova, K. Nakanishi, R. W. Woody, Wiley-VCH, New York , 2000, pp. 741-768.

[54] H. Mita, T. Ohyama, Y. Tanaka, Y. Yamamoto, *Biochemistry* **2006**, *45*, 6765-6772.

[55] M. Kubista, B. Akerman, B. Norden, *J.Phys.Chem.* **1988**, *92*, 2352-2356.

[56] S. M.Langenegger, R.Häner, *ChemBioChem* **2005**, *6*, 848-851.

[57] A.Rodger, M. A. Ismail, Introduction to Circular Dichroism. In *Spectrophotometry & Spectrofluorimetry - A Practical Approach*; Gore, M. G., Ed.; Oxford University Press: New York, **2005**; Chapter 4.

8. Porphyrin derivatives -towards non-nucleosidic building blocks for the incorporation into DNA

8.1 Abstract

Porphyrins find many applications in medicine and material science. Defined multiporphyrin arrays are attractive for the design of artificial light-harvesting systems. It is not surprising that the interest is increasing for the use of DNA as a scaffold to arrange porphyrins in a controlled fashion.
In this chapter the synthesis towards non-nucleosidic building blocks based on the porphyrin core are described. It was possible to prepare the phosphoramidite of a triazolylporphyrin for the incorporation into the DNA scaffold via standard oligonucleotide synthesis. Prelimary spectroscopic results are presented.

8.2 Introduction

Porphyrins, due to their unique aromatic structure and their excellent photochemical and photophysical properties, are ubiquitous in nature with essential biochemical functions in plants and animals. They are involved in oxygen storage, transport, oxygen activation, electron transport, light harvesting, and energy transfer. [1]
Different porphyrin derivatives find many applications, for example in medicine and in material science. Porphyrin based photosensitizers are used in photodynamic therapy (PDT), a method for cancer treatment. After excitation, when the photosensitizer returns to its ground state, electron transfer in its immediate environment can occur. The formed oxygen radicals induce cell death and tumor destruction. [2, 3] In material sciences porphyrin are used for light-harvesting systems or for electronic materials. [4]
The tetrapyrrolic macrocycles have a very strong absorption band around 400-430 nm (Soret band) with a rather high extinction coefficient ($\varepsilon \approx 10^5$) and four Q-bands between 500 and 650 nm (Scheme 1). The Intensity of the Q-bands vary depending on the

porphyrin types. In the absorbance spectra of metalloporphyrin, band I and III merge into one, band II and IV disappear, and a new band appears. [5] Consequently, from absorbance spectra, it can be easily distinguished between free base porphyrin and its metallo-derivatives.

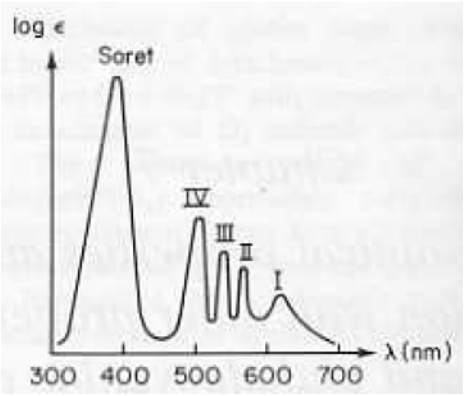

Scheme 1. Absorption spectra of porphyrin: Soret band and Q-bands (IV, III, II, and I). [5]

Porphyrins are one of the most studied DNA binding agents, and there are many reports on porphyrin-DNA interactions. However, most studies focused on interactions between free cationic porphyrins and DNA. Because of their facile tunability of the electronic properties through modification and metallation of the porphyrin core, and the possible applications in material science, DNA-porphyrin conjugates gain increasing interest. [6]

In Figure 2 selected examples of porphyrin-DNA conjugates are presented.

One of the first attempts to incorporate porphyrin into a DNA scaffold was carried out by Richert et al. [7] Alkylporphyrin linked to the phosphate groups of DNA via oxypropyl chains, was incorporated as a non-nucleosidic building block (**1A**). Another example is described by Kool et al.[8] In their approach, they coupled the porphyrin moiety on a 2-deoxy-D-ribose and incorporated the porphyrin nucleoside into DNA via phosphoramidite chemistry (**1B**).

Berova and co-workers studied the through space exciton coupling between two porphyrins covalently attached to a short DNA sequence, and the effect of covalently attached porphyrins on DNA structure and stability. The porphyrins were attached either on the 3'end (**1C**) [1,9] or the 5' end [5] (**1D**) with a short amide linker to the nucleobase.

Example (**1E**) shows a porphyrin-DNA conjugate using tetraphenylporphyrin-phosphoramidite as a non-nucleosidic building block. [10]

Stulz et al. [11] described tetraphenyl porphyrin substituted deoxyuridine used as a building block for the incorporation into DNA. Up to 11 tetraphenyl pophyrins were incorporated in a row into DNA (**1F**).

Endo et al. [12] did postmodification of DNA with porphyrin moieties to construct conformationally controlled porphyrin dimer structures (**1G**). Click chemistry was used as well for the postsynthetic modification of oligonucleotides with porphyrin molecules (**1H**).[13]

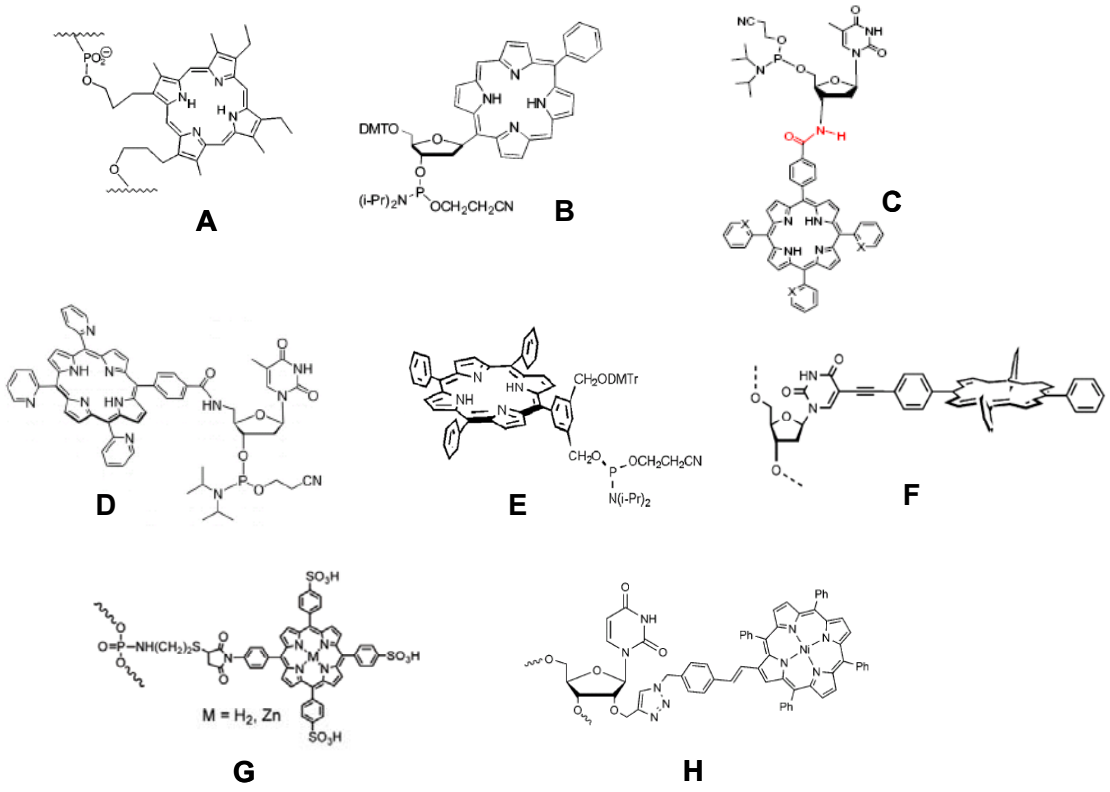

Figure 1. Selected examples of porphyrin-DNA conjugates: (**A**) [7], (**B**) [8], (**C**) [9], (**D**) [5], (**E**) [10], (**F**) [11], (**G**) [12], (**H**) [13].

Examples in which porphyrin was incorporated as a non-nucleosidic building block into DNA is found, less frequently.

The goal of this project was to synthesize a non-nucleosidic building block with a porphyrin core. For the incorporation of the porphyrin building block into DNA a triazole linker was choosen, which was already used by our group for the incorporation of pyrene into a DNA scaffold. [14]

Osuka et al. [15] described triazolyl-porphyrin, which assembled to form slipped cofacial dimers by the complementary coordination of the triazole nitrogen atom at the 3-position to the zinc center of a second porphyrin moiety (Figure 2).

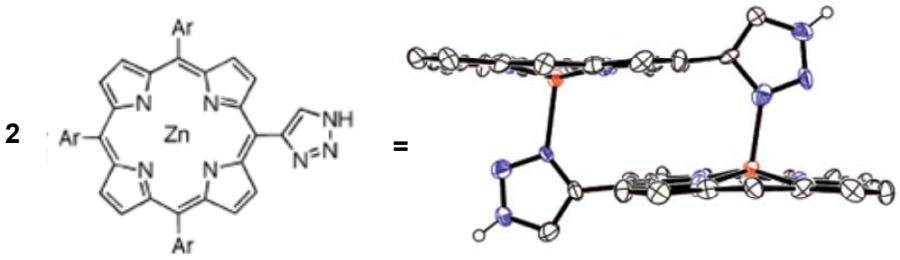

Figure 2. Slipped cofacial triazolyl-porphyrin dimers formed by complementary coordination of the triazole nitrogens. [15]

With the observations found in literature in mind, the non-nucleosidic triazolyl-porphyrin (Figure 3) was designed. Metallation of the building block could lead to further interesting structural features.

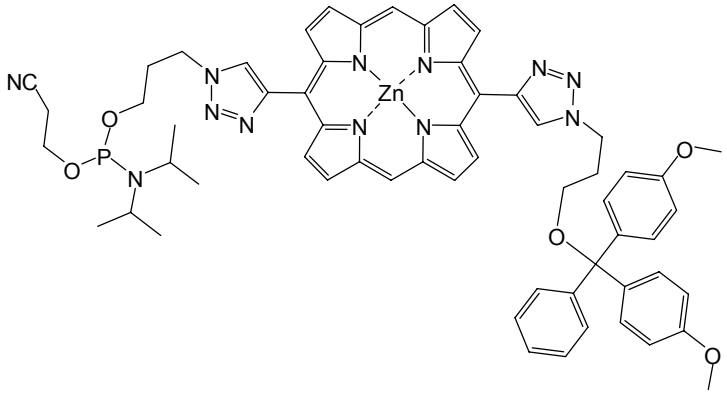

Figure 3. Designed porphyrin building block for the incorporation into DNA.

8.3 Results and discussion

8.3.1 Synthesis of the non-nucleosidic building block

Recently Lindsey et al. [16] published a strategy to synthesize Mg-porphine in satisfactory yield. The first approach was to synthesize Mg-porphine **4** in a good quantity, which can be used for further modification and attachement of suitable linkers for the incorporation into DNA using standard oligonucleotide synthesis.

Dipyrromethanes occupy a central place in porphyrin chemistry. [17] Dipyrromethan **1** was prepared in a one-flask reaction of formaldehyde and excess pyrrole using $InCl_3$ as a catalyst. The workup procedure entailed quenching with NaOH, filtration, removal of pyrrole and purification by columne chromatographie, yielding in up to 74%. After the reaction, pyrrole was recovered by distillation.

The next step was the Vilsmeier formylation of dipyrromethan **1**, affording a mixture composed of the target 1-formyldipyrromethan **2**, unreacted **1**, and 1,9-diformyldipyrromethan **3**. The crude Vilsmeier reaction mixture can be used for the next step, because **2** will self-condense and **3**+**4** also react to give Mg-porphine **4**. During the reaction to obtain **4**, polymeric material is formed as a side reaction. Because of the metalloporphine **4,** solubility is inceased and the product can be obtained with extraction from the black polymeric material (Figure 4). [16]

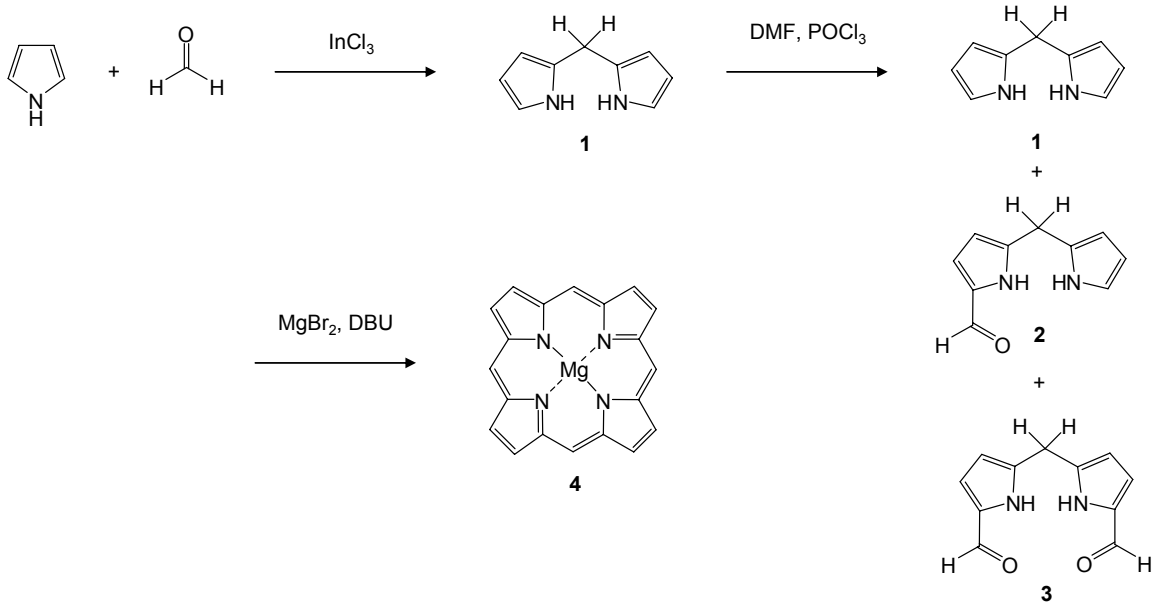

Figure 4. Synthesis of Mg-porphine via 1-formyldipyrromethan. [16, 17]

The following step was bromination of the Mg-porphine **4**. In literature, N-bromoacetamide [18] and N-bromsuccinimid [15] are used for the bromination of porphyrins.

Both conditions were tested at room temperature using dichloromethan as solvent, leading to a mixture of different isomers (Figure 5).

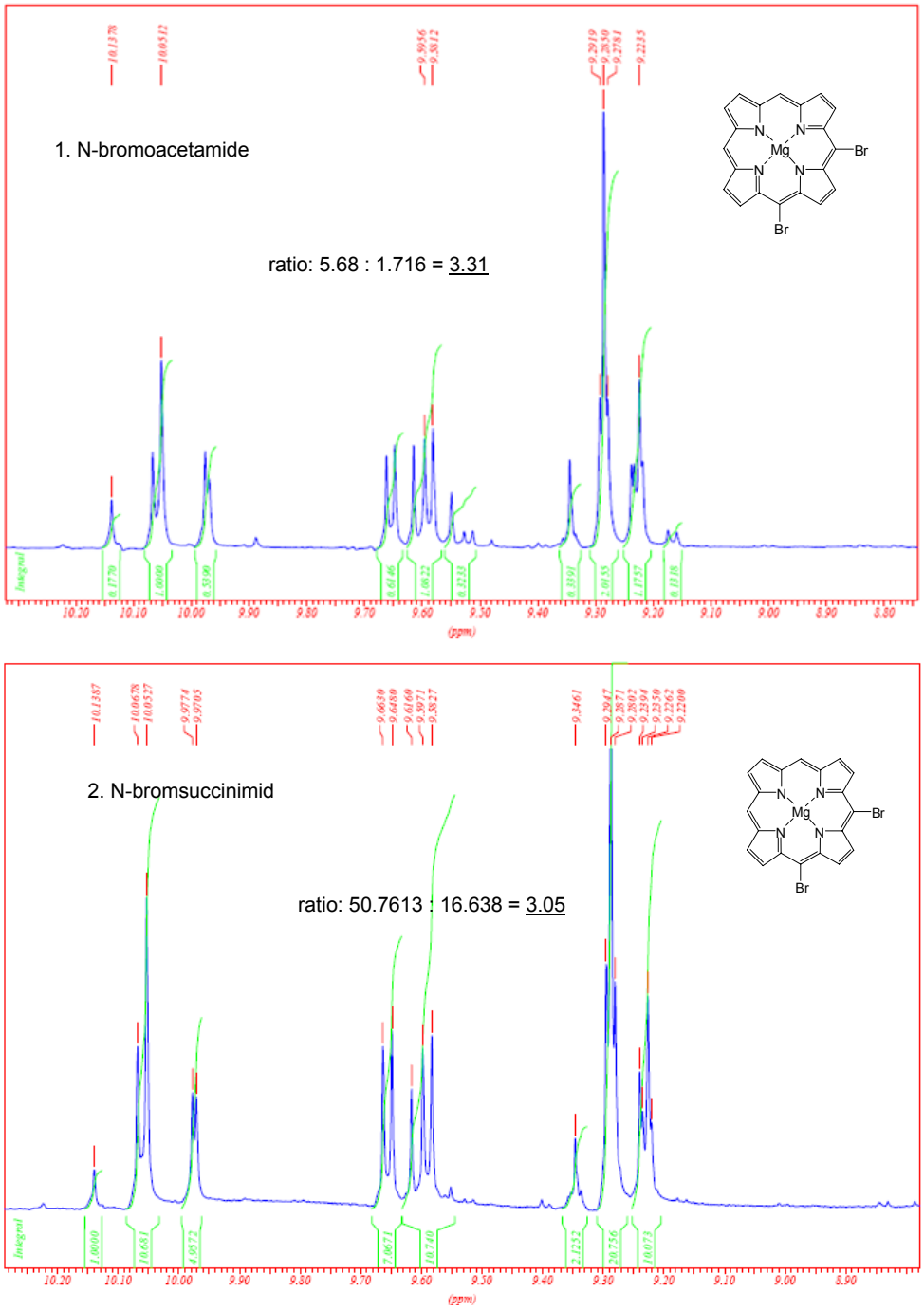

Figure 5. NMR-Spectra of the brominated porphins.

Figure 5 shows the two spectra of Mg-porphine treated with the bromination reagents. The spectra show that with N-bromoacetamid more isomers are formed. The ratio between the meso and the pyrrolic position should be 4 of a meso-dibrominated porphine. The calculated ratios are in the expected range.

Unfortunately, it was not possible to separate the different isomers of **5** with column chromatography. It was expected that, after the coupling step, the separation could be performed.

For the Sonogashira coupling, copper (I) iodide is used as a co-catalyst. It was tried to avoid using copper (I) iodide, because we were concerned that copper might insert into the porphyrin. Copper is very tightly bonded in the porphine ring and rather drastic methods are used to remove copper.[19] As a consequence, copper free coupling reaction have been developed. [20] In our hands, first attempts under these conditions showed no efficient coupling.

Alternatively, metalloporphyrin, for example Zn-porphyrin, can be used to suppress formation of the Cu-complex. Schlötzer and Fuhrhop [21] showed that the bromination of Mg-porphin occurs cleanly at the *meso*-position. As a consequence of these findings, the following strategy was proposed: (1) bromination of Mg-porphine **5**, (2) demetallation **6**, (3) Zn insertion **7** (4) coupling reaction under CuI conditions. Attempts showed that demetallation and Zn insertion should be carried out in two separate steps (Figure 6).

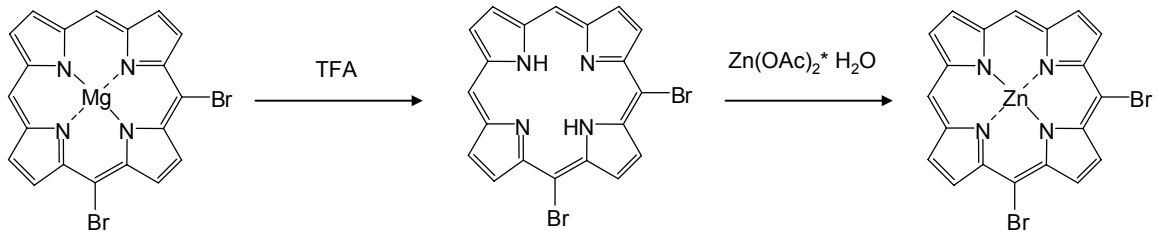

5 **6** **7**

Figure 6. Demetallation of porphin and insertion of Zn.

Demetallation was carried out in THF using trifluoroacetic acid (TFA). The product **6** was obtained by precipitation with water and followed by filtration. For Zn insertion zink acetate in THF was used to get compound **7**.

Sonogashira coupling under copper(I) iodide conditions with $Pd_2(dba)_3$, PPh_3 was performed, starting from the brominated porphine. Due to the obtained different isomers, it was not possible to get pure material with a satisfactory yield.

As a consequence the strategy was changed using the procedure described by Anderson et al. [22] to obtain directly the Zn-5,15-Bis(triisopropylsilyl)ethynylporphyrin **10** (Figure 7).

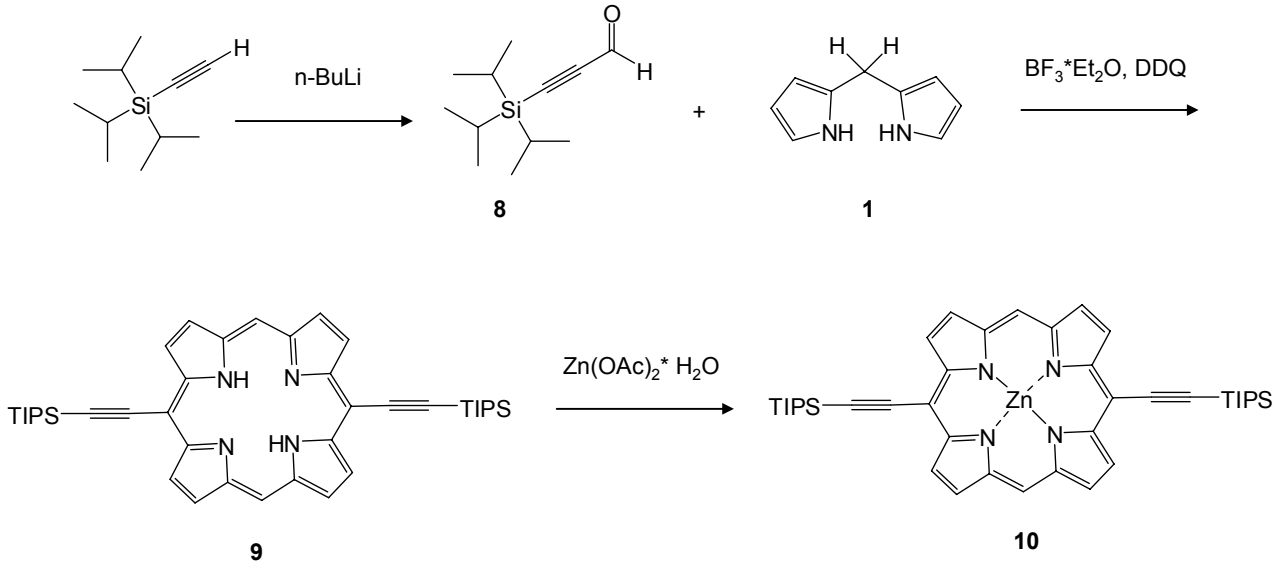

Figure 7. Synthesis of Zn-5,15-Bis(triisopropylsilyl)ethynylporphyr **10**. [22]

The formation of triisopropylsilylpropynal **8** worked very well and no purification was required. The obtained oil was used for the condensation with dipyrromethan using boron trifluoride, followed by DDQ oxidation to obtain compound **9**. Zn insertion with zink acetate gave compound **10**.

The dry deprotected compound **15** is unsoluble. This problem was overcome by *in situ* deprotection using TBAF on silica gel. The product can be filtered and the solution was directly used for the Huisgen 1,3-dipolar cycloaddition. The porphyrin dissolved in THF was treated with a 1:1 mixture of unprotected and 4,4'-dimethoxytrityl (DMT)-protected 1,3-azidopropanol (**13**, **14**), which were prepared *in situ* from a mixture from the corresponding bromides (**11**, **12**). [14] A range of reaction conditions were tested for the Huisgen 1,3-dipolar cycloaddition.

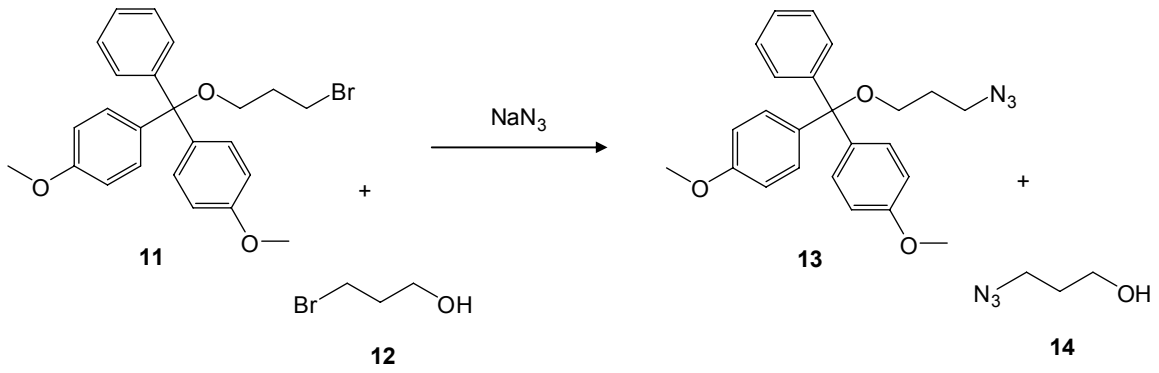

Figure 8. Formation of the unprotected and 4,4'-dimethoxytrityl (DMT)-protected 1,3-azidopropanol **14** and **13**.

Using CuCl together with sodium ascorbate became the method of choice. For the separation of the three products **16**, **17** and **18**, an aluminiumoxid column chromatography was carried out and the target compound **17** was achieved in a yield of 37% (Figure 9).

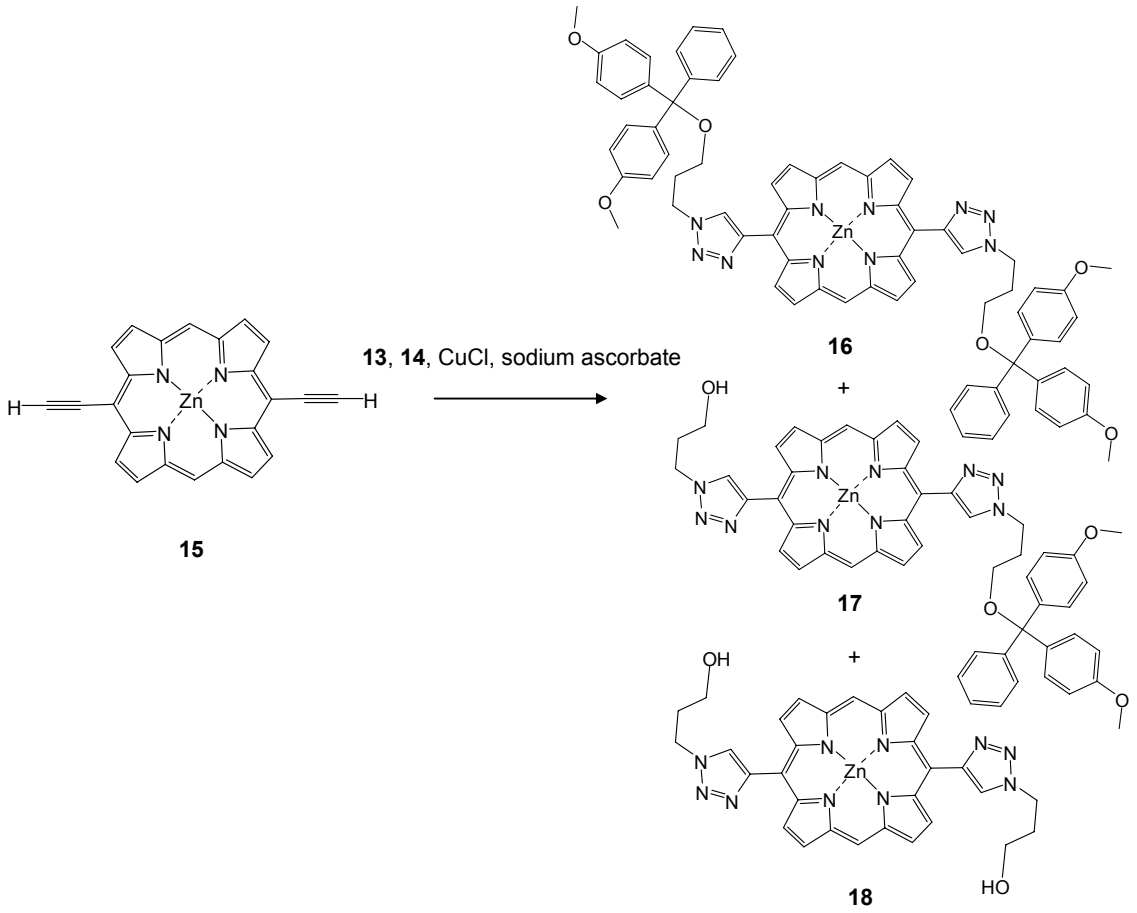

Figure 9. Synthesis of triazolylporphyrins **16**, **17**, and **18**.

The obtained alcohol **17** was further converted into the phosphoramidite **19** (Figure 10).

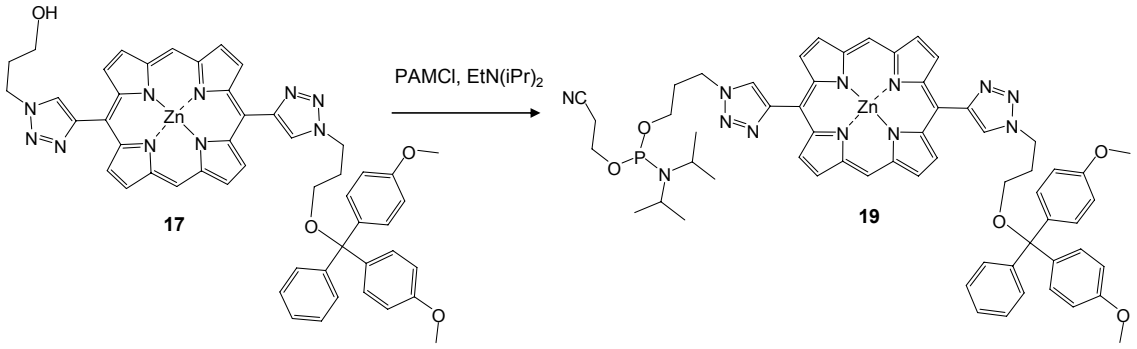

Figure 10. Synthesis of phosphoramidite **19**.

8.3.2 Spectroscopic studies of the new synthesized building blocks

First absorption measurements of the building block **18** were performed using the same conditions, which are used for DNA (10 mM phosphate buffer, 100 mM NaCl).

The absorbance spectra of the synthesized triazolylporphyrin showed interesting properties. At the temperature of 20°, three main bands in the region of 350 nm to 500nm were observed. The maxima are at 380 nm, 410 nm and 445 nm. During heating the two bands at 380 nm and 445 nm reduced, and the intensity of the Soret band at 410 nm increased. The synthesized porphyrin **18** shows strong aggregation in aqueous media (Figure 11).

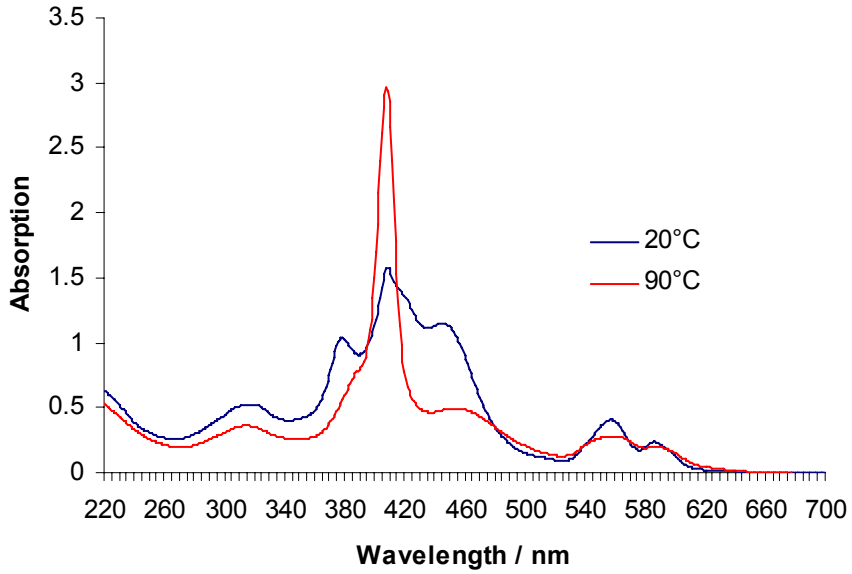

Figure 11. Absorbance spectra of the triazolylporphyrin **18**.

8.3.3 Synthesis of oligonucleotides

The following sequences have been synthesized using standard oligonucleotide synthesis.

Oligo 1:	5‘-AGC TCG GTC AZC GAG AGT GCA-3‘
Oligo 2:	3‘-TCG AGC CAG TZG CTC TCA CGT-5‘
Oligo 3:	5‘-AGC TCG GTC ZZC GAG AGT GCA-3‘
Oligo 4:	3‘-TCG AGC CAG ZZG CTC TCA CGT-5‘

Z stays for the incorporated Zn-Porphyrin. The synthesized oligonucleotides were purified by reversed-phase HPLC. The concentrations have been determined by OD measurements.

8.3.4 Spectroscopic studies of oligomer 1 and 2

Prelimary measurements have been carried out of oligomer **1** and **2**. The conditions are 1 µM oligonucleotide concentration, 10 mM phosphate buffer and 100 mM NaCl.
In UV/Vis the Soret-band of the porphyrin at 420 nm is well visible. In the range of 500 nm to 650 nm the Q-bands of porphyrin are visible. The fact that all of the four Q-bands, namely at 505 nm, 540 nm, 575 nm and at 630 nm are visible, show that during the standard oligonucleotide synthesis demetallation of the porphyrin occured. At the wavelength of 260 nm the natural part of the oligonucleotide is absorbing light. The spectra for oligomer **1** and oligomer **2** are similar (Figure 12 and 13).

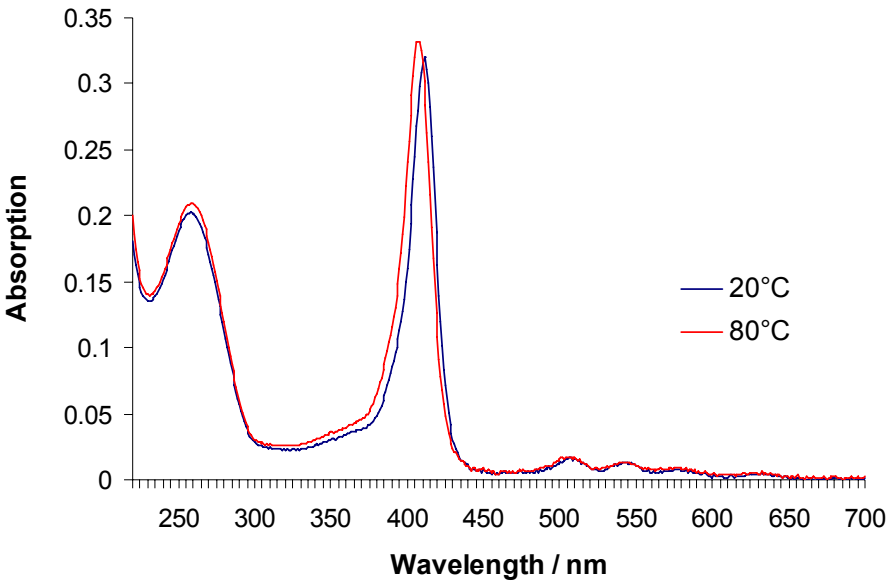

Figure 12. Absorbance spectra of oligomer **1**.

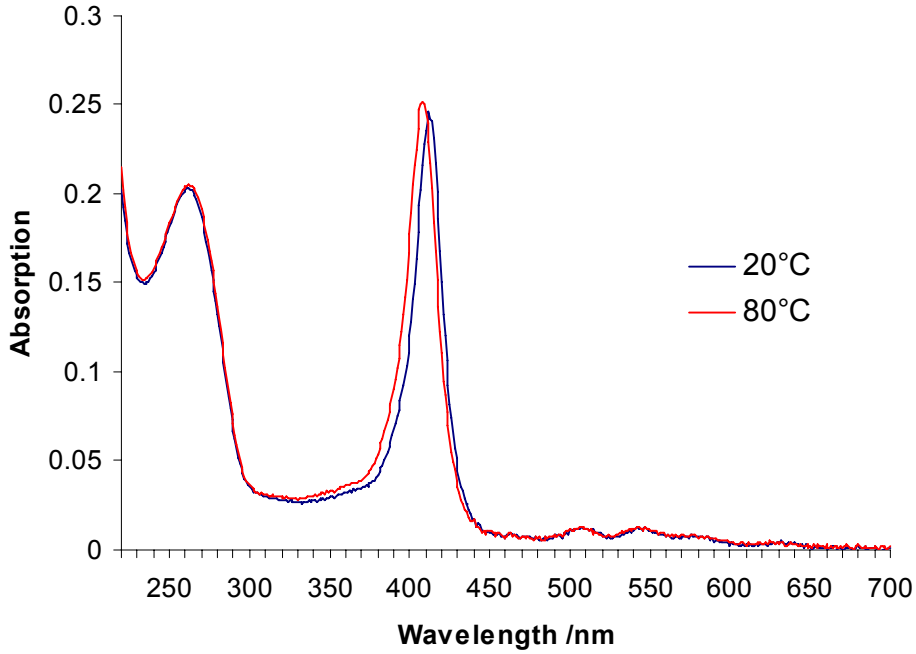

Figure 13. Absorbance spectra of oligomer **2**.

The hybrid of oligomer **1** and **2** showed low hypochromism upon temperature change. At the wavelength of 411 nm it is 4%, and in the range of 260 nm the hypochromism is around 2.5 % (Figure 14).

It was not possible to confirm the mass of the synthesized oligomers by mass spectrometry.

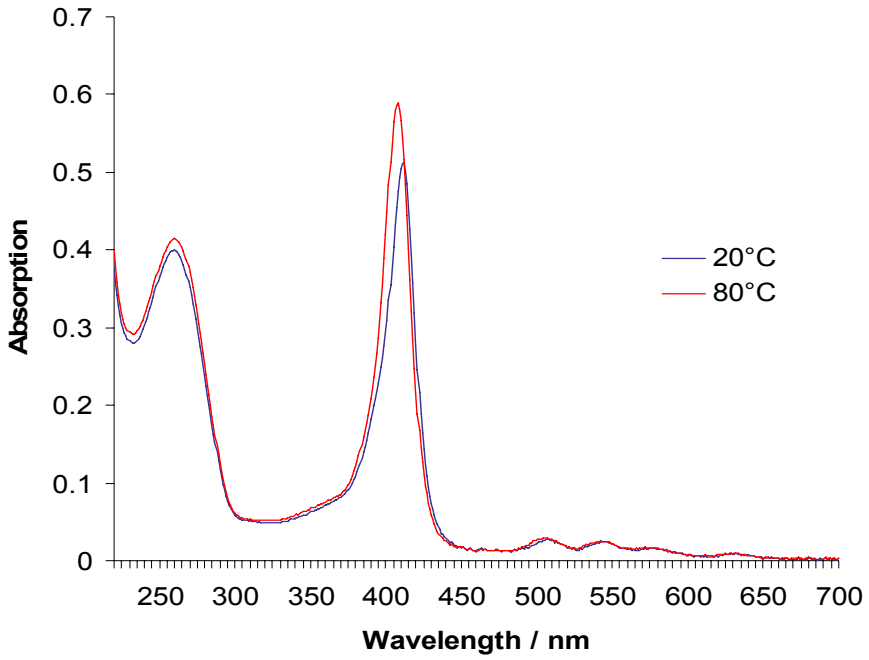

Figure 14 . Absorbance spectra of hybrid **1** and **2**.

8.3.4 Synthesis of non-nucleosidic porphyrin building block with alkynyl linker

Other attempts towards the synthesis of porphyrin derivatives, for the incorporation into a DNA scaffold, have been carried out. Figure 15 illustrates the procedure, starting from the attachement of the linker directly to the aldehyde via Pd-mediated coupling, using CuI as a co-catalyst (**20**). [23] The following condensation to the porphyrin leads directly to the dialcohol, which can be converted into DMT- and PAM-protected material.

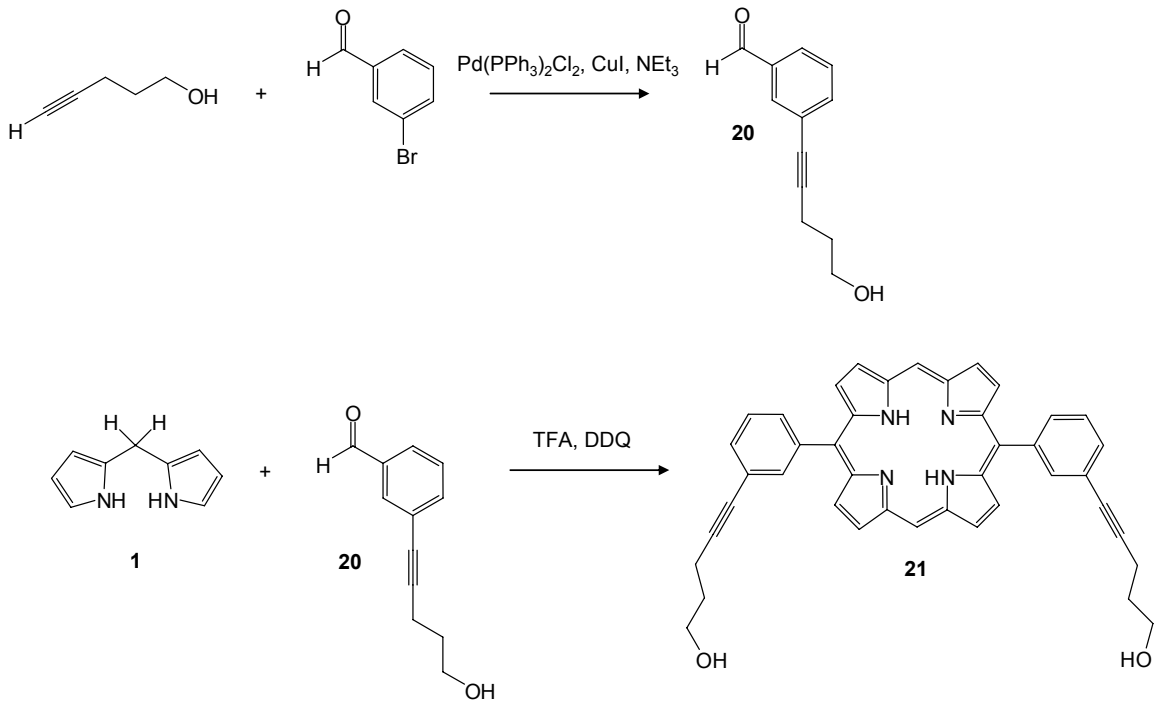

Figure 15. Towards the synthesis of non-nucleosidic porphyrin building block with alkynyl linker.

The Pd-mediated coupling gave compound **20** with a yield of 40%. The condensation leading to the porphyrin derivate was more difficult. Using boron trifluoride, the conversion to the desired product **21** was unsatisfactory. As a consequence the purification step was difficult. Extraction with a Soxhlet apparature was performed using different solvents.

In literature it is described that the meso substitution of the dipyrromethan moiety is very crucial for a successful condensation reaction. [24, 25, 26] For dipyrromethans substituted with a bulky group and dipyrromethan without meso substitution, TFA is the reagent of choice, whereas dipyrromethan substituted with a less hindered group, boron trifluoride leads to a better conversion.

The reaction using TFA as a catalyst and DDQ as the oxidizing reagent worked very well. Compound **21** was isolated after column chromatography. The next step was then DMT-protection. A range of reaction conditions were tested, but it was not possible to convert compound **21** into the (DMT)-protected derivative. NMR-studies with deuterium oxide exchange as well mass spectrometry confirmed that the hydroxy groups are present (Figure 16). Side reactions like oxidation of the alcohol can be excluded.

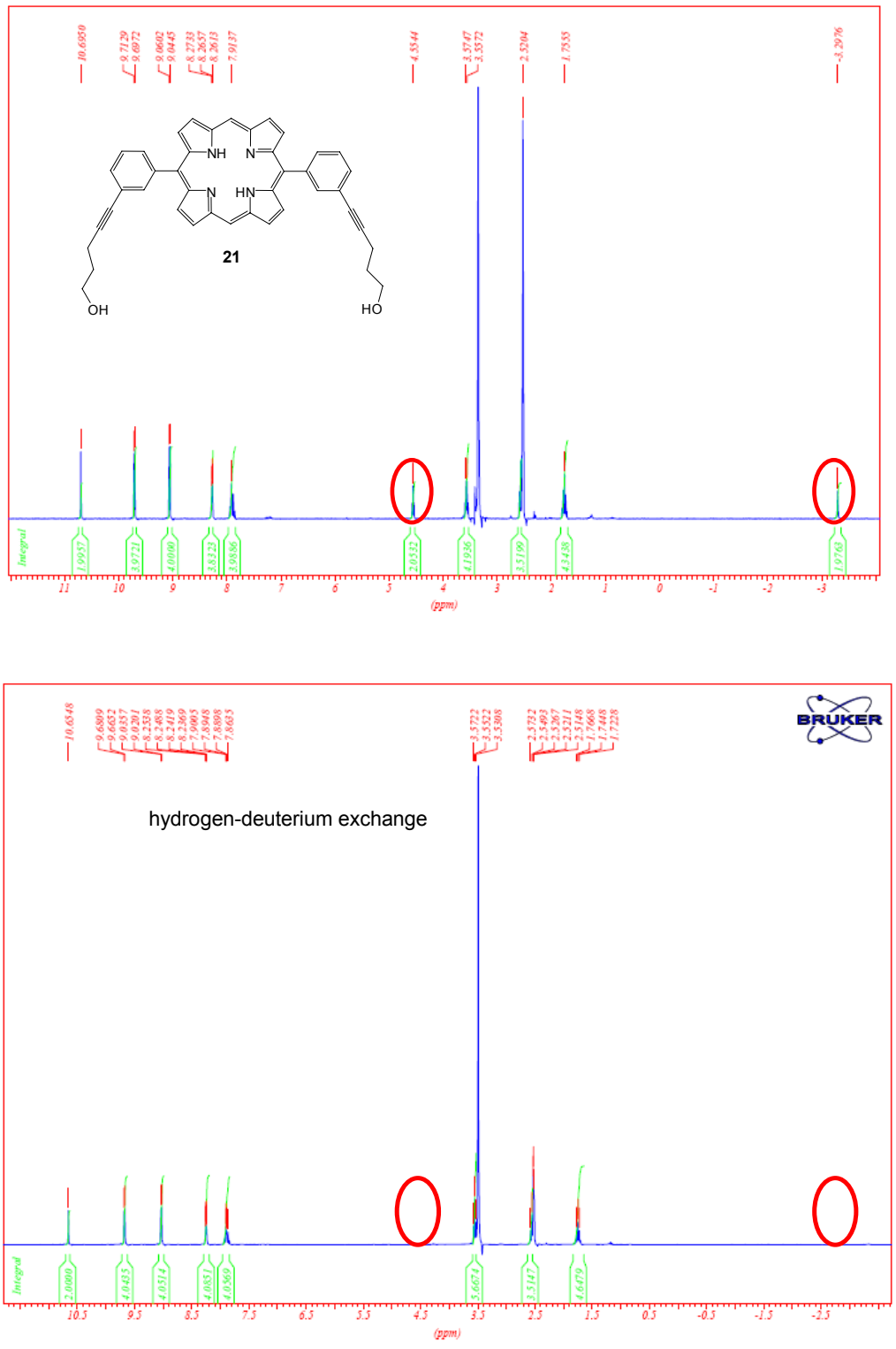

Figure 16. NMR study: deuterium oxide exchange.

8.4 Conclusions

In conclusion, 5,15-triazolylporphyrin was synthesized from the corresponding 5,15-diethynylporphyrin via a Huisgen 1,3-dipolar cycloaddition. The compound was transformed into the phosphoramidite and incorporated using standard oligonucleotide synthesis. It was not possible to confirm the exact mass of the oligonucleotides by mass specrometry. The absorbance spectra showed clearly the Soret band of the porphyrin and the band of the oligonucleotides. Extension of the coupling time during the oligonucleotide synthesis, or changing of the deprotection procedure from the solid support, might lead to better yields of the DNA-conjugates.

A second strategy for the synthesis of porphyrin with alkynyl linker was presented. The linker was directly attached to the aldehyde via Pd-mediated coupling using CuI as a co-catalyst. The following condensation to the porphyrin led directly to the dialcohol. DMT-protection was not yet possible. This strategy is shorter and could extend the library of different porphyrin derivatives for the incorporation into DNA, by using other dipyrromethan derivatives for example.

Condensation using the bromoaldehyd followed by Pd-mediated coupling with the protected DMT-linker could overcome the problem of the unreactive alcohol.

8.5 Experimental part

1. Synthesis of dipyrromethane **1** [17]

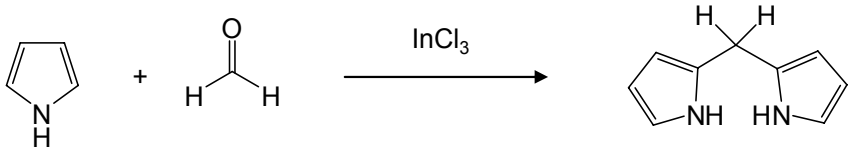

1

amount	name	data (g/mol)	mmol:	eq
1.5 g	paraformaldehyde	30.03	50	1
350 ml	pyrrole	67.09	5000	10
1.1 g	$InCl_3$	221.2	5	0.1
6 g	NaOH	40.0	150	3

A mixture of pyrrole and paraformaldehyde was degassed with a stream of argon for 15 minutes at room temperature. The reation mixture was heated at 70°C under argon until all paraformaldehyde was dissolved. The temperature of the reaction mixture was cooled to 55°C before the addition of $InCl_3$. The reaction mixture was stirred at 55°C for 3 hours under argon.

The heat source was removed and NaOH was added.

The mixture was stirred for 1 hour at room temperature and then filtered. The filtrate was concentrated and pyrrole was recovered.

The obtained crude product was purified with column chromatography (silica, 7:2:1 hexane/CH_2Cl_2/ethyl acetate).

The solid material was dissolved in hexan/CH_2Cl_2 and the volatile components were removed under vacuum until precipitation of the crystals **1**. The obtained yield was 74% of compound **1**.

TLC (hexane/CH_2Cl_2/ethyl acetate, 7:2:1) R_F =0.32.

^{1}H-NMR (300 MHz, $CDCl_3$): δ 6.65-6.63 (m, 2H), 6.17-6.14 (m, 2H), 6.05-6-03(m, 2H), 3.96 (s, 2H).

^{13}C-NMR (300 MHz, $CDCl_3$): δ 129.21, 117.46, 108.41, 106.59, 26.44.

EI-MS *m/z* = 488; MW = 146.19; $C_9H_{10}N_2$.

2. Synthesis of 1-formyldipyrromethan **2** [16]

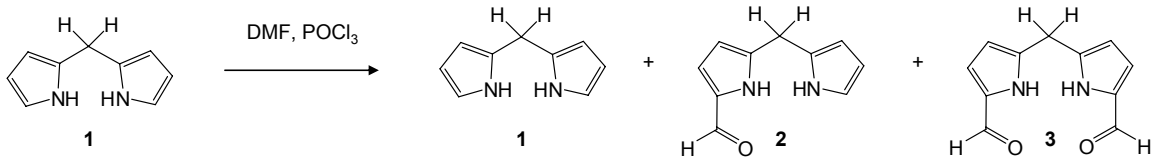

amount	name	data (g/mol)	mmol:	eq
45 ml	DMF			
6.8 ml	$POCl_3$	153.3	73	
5,4 g	dipyrromethan **1**	146.2	37	1
111.5 ml	DMF			
23.5 ml	Vilsmeier reagent	128	40.5	1

For the formation of the Vilsmeier reagent, a sample of DMF was treated with $POCl_3$ at 0°C under argon with stirring for 10 minutes. A solution of **1** in DMF at 0°C under argon was treated with the freshly prepared Vilmeier reagent, and the resulting solution was stirred for 1.5 hours at 0°C.

The reaction mixture was poured into a mixture of 2 M NaOH (300 ml) and CH_2Cl_2 (200 ml) at 0°C. The resulting blue reaction mixture was stirred for 20 minutes at 0°C until it turned orange-brown.

The organic phase was washed with NH_4Cl (200 ml), water and brine, dried with Na_2So_4 and concentrated under vacuum to give a red, oily crude product. The crude product was directly used for step 3 without purification.

TLC (CH_2Cl_2/ethyl acetate, 5:1) R_F =0.73; R_F =0.46; R_F =0.16.

3. Synthesis of Mg-porphine **4** [16]

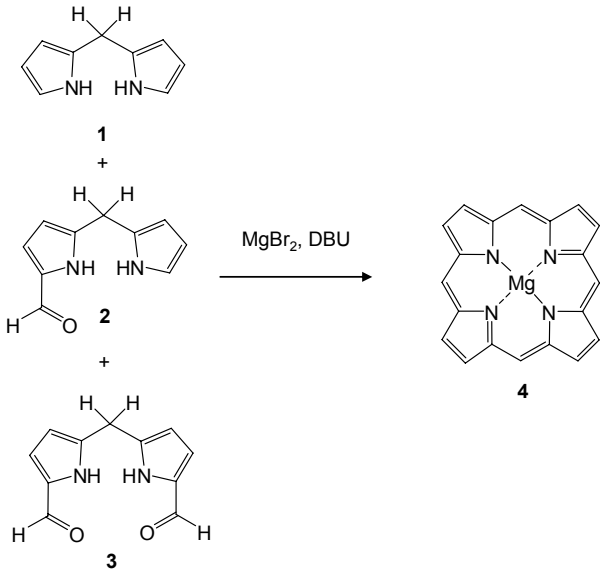

amount	name	data (g/mol)	mmol:	eq
7.5 g	**1**, **2**, **3**	174.2	43	1
410 ml	toluene			
61.4 ml	DBU	152.2	410	9.5
22.6 g	$MgBr_2$	184.1	123	3

For the formation of compound **4** the crude mixture of **1**, **2**, **3** was dissolved in anhydrous toluene in an oven-dried round-bottom flask. The resulting suspension was heated to 80°C, and DBU was added tropwise under vigourus stirring. The resulting solution was stirred for 5 minutes, during which the temperature increased from 80°C to 100°C and the mixture darkened. $MgBr_2$ was added under vigourus stirring. The reaction flask was attached to a reflux condenser and heated at 115°C overnight with exposure to air.

The toluene was removed under vacuum. The resulting residue was treated with THF (200 ml), then stirred vigorously for 20 minutes using the rotavap at 30°C, before filtering through a Buchner funnel. The extraction procedure was repeated 3-4 times. The filtrates were combined and concentrated. The resulting crude product was dissolved in diethyl ether (1L), washed with water (200 ml) and brine (5× 200 ml); if required small amounts of MeOH was added to facilitate phase separation. After evaporation of the solvent, compound **4** was obtained in a yield of 10%.

TLC (alumina; CH_2Cl_2/ethyl acetate, 5:1) R_F =0.28.

^{1}H-NMR (300 MHz, THF-d_8): δ 10.24 (s, 4H), 9.45(s, 8H).

^{13}C-NMR (300 MHz, THF-d_8): δ 159.6, 142.1, 115.3.

EI-MS *m/z* = 488; MW = 332.6; $C_{20}H_{12}MgN_4$.

4. Synthesis of triisopropylsilylpropynal **8** [22]

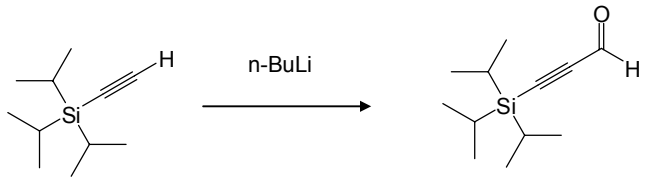

8

amount	**name**	**data (g/mol)**	**mmol:**	**eq**
22 ml	n-Buthyllithium	64.05	35.5	1
7.5 ml	Triisopropylsilylacetylene	182.38	33.43	~1
75 ml	THF			
2.45ml	DMF	73.1	35.5	1
60 ml	5% sulfuric acid	98.07		
	$NaHCO_3$			

An oven-dried reaction-flask was degassed with a stream of argon.

n-BuLi was added dropwise to a solution of triisopropylsilylacetylene in anhydrous THF at 0°C under argon. The mixture was stirred for 20 minutes at 0°C, then at room temperature for 20 minutes, then re-cooled to 0°C and DMF was added slowly with stirring. The mixture was allowed to warm to room temperature over 20 minutes before heated to reflux for 1 hour. For the addition of 5% sulfuric acid (60 ml) the reaction was again cooled to 0°C. Saturated $NaHCO_3$ solution was added until pH 5 was reached.

The reaction mixture was extracted with CH_2Cl_2 (4× 50ml) and washed with water (100 ml). The solvent was evaporated yielding the product **8** in 80%.

TLC (EtOAc/hexane, 1:3) R_F =0.23.

^{1}H-NMR (300 MHz, $CDCl_3$): δ 9.19 (s, 1H), 1.12-1.03 (m, 18H).

^{13}C-NMR (300 MHz, $CDCl_3$): δ 176.6, 104.64, 100.8.

EI-MS *m/z* = 488; MW = 210.39; $C_{12}H_{22}OSi$.

5. Synthesis of Zn-5,15-Bis(triisopropylsilyl)ethynylporphyrin **10** [22]

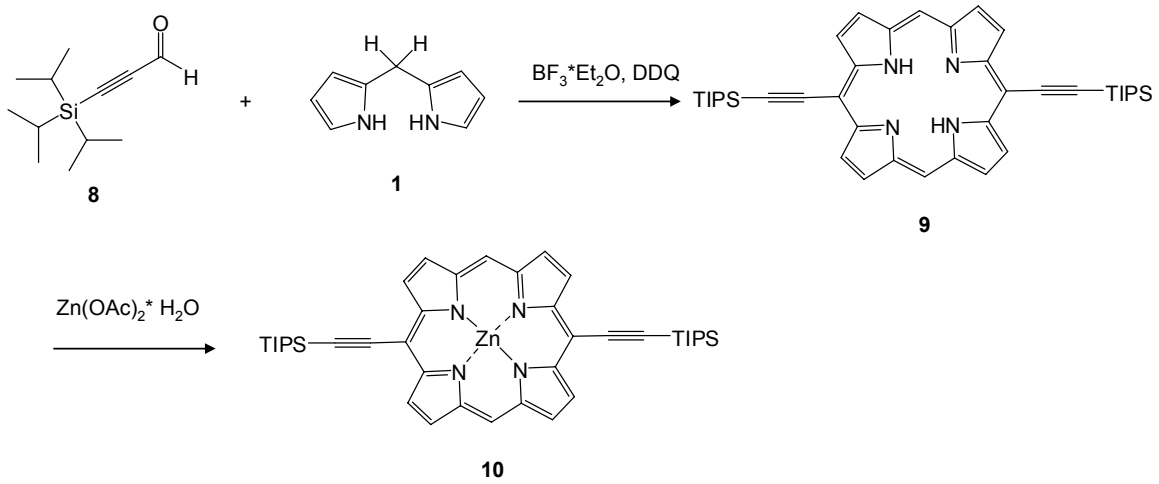

amount	name	data (g/mol)	mmol:	eq
1 g	dipyrromethane **1**	146.2	6.75	1
1.5 ml	triisopropylsilylpropynal	210.4	6.75	1
2.3 g	DDQ	227	10.1	1.5
280µl	BF_3*Et_2O	141.9	2.2	0.3
400 ml	CH_2Cl_2			
50 ml	THF			
400 mg	$Zn(OAc)_2$*H_2O	219.5	1.9	2 eq. versus **9**

Dipyrromethan and triisopropylsilylpropynal was solved in anhydrous CH_2Cl_2 and stirred under argon. BF_3*Et_2O was added dropwise. After 45 minutes DDQ was added and stirred in an open vessel during 30 min.

The reaction mixture was filtered through a bed of silicagel 2-3 times. The amount of solvent was reduced and compound **9** was precipitated with MeOH (671,1 g/mol; yield: 25%; TLC (hexane/CH_2Cl_2 1:2) R_F =0.3).

For the metallation **9** was dissolved in THF and $Zn(OAc)_2$*H_2O, solved in a small amount of MeOH, was added.The mixture was stirred for 2 hours at 30°C using the rotavap and afterwards precipitated with MeOH. Compound **10** was obtained in a yield of 90%.

TLC (hexane/CH_2Cl_2 1:2) R_F =0.33.

^{1}H-NMR (300 MHz, $CDCl_3$): δ 10.01 (s, 2H), 9.77 (d, J= 4.53 Hz, 4H), 9.28 (d, J= 4.53 Hz, 4H) 1.54-1.48 (m, 18H).

^{13}C-NMR (300 MHz, $CDCl_3$): δ 162.38, 152.28, 149.29, 132.21, 131.49, 109.75, 107.46, 100.23, 97.81, 19.35, 12.16.

EI-MS *m/z* = 488; MW = 734.45; $C_{42}H_{52}N_4Si_2Zn$.

6. Synthesis of unprotected and 4,4'-dimethoxytrityl (DMT)-protected 1,3-azidopropanol **13** and **14** [14]

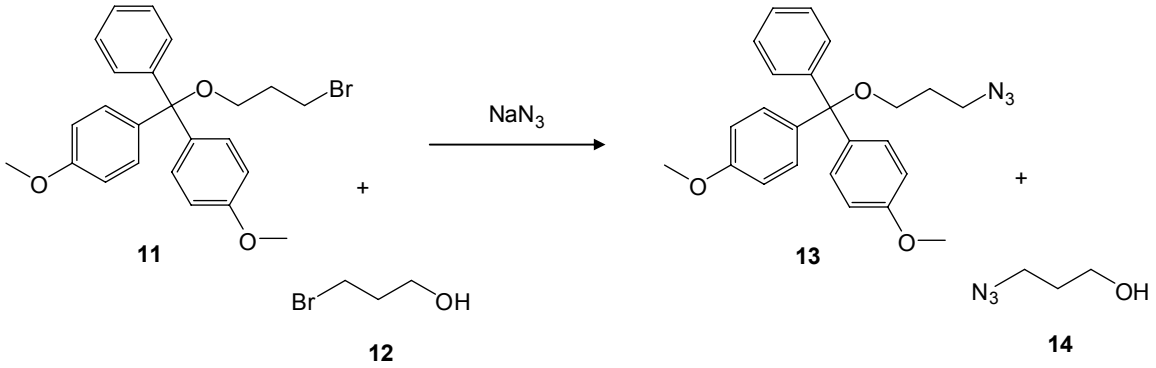

11 **12** **13** **14**

amount	name	data (g/mol)	mmol:	eq
841 mg	3-bromo-1-(dimethoxytrityloxy)-propane **11**	442.37	1.9	1
166 µl	3-bromo-1-propanol **12**	138.99	1.9	1
247.8 mg	NaN_3	65.01	3.8	2
10 ml	D_6-DMSO			

The reaction flask with D_6-DMSO was degassed with a stream. 3-bromo-1-(dimethoxytrityloxy)-propane and 3-bromo-1-propanol were treated with NaN_3 under argon. The reaction was stirred under argon and at room temperature over night.
NMR was measured directly from the reaction mixture.

^{1}H-NMR (300 MHz, DMSO-d_6): 7.37-7.20 (m, 9H), 6.89 (d, J= 9.03 Hz, 4H), 4.57-4.54 (m, 2H), 3.71 (s, 6H), 3.45-3.32 (m, 4H), 3.01-2.99 (m, 2H), 1.75-1.65 (m, 2H), 1.65-1.62 (m, 2H).

7. Insitu deprotection of Zn-5,15-bis(triisopropylsilyl)ethynylporphyrin **10** and formation of 5, 15-bistriazolylporphyrin **17**

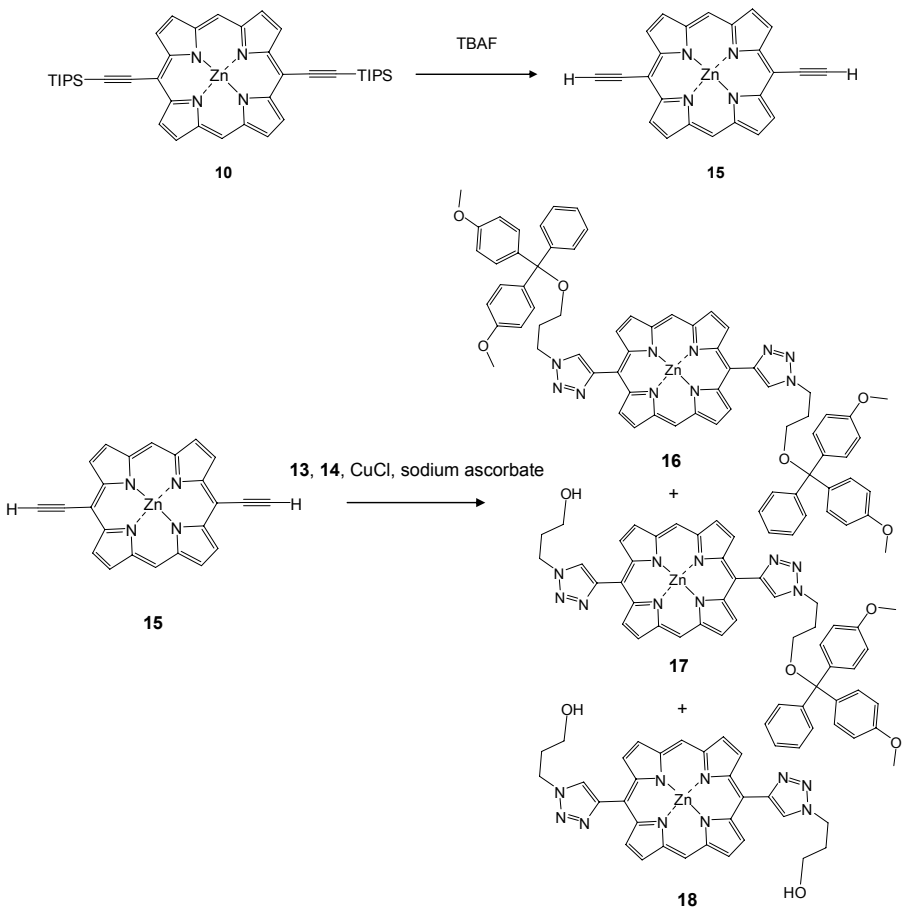

amount	name	data (g/mol)	mmol:	eq
140 mg	**10**	734.45	0.19	1
508 mg	TBAF	1.5 mmol/1g silica	0.76	4
2 ml	mixture **13**/**14**			2
15 mg	sodium ascorbate	198.11	0.076	0.4
8 mg	CuCl	98.99	0.076	0.4
4 ml	THF			

Compound **10** was dissolved in a small amount of THF. TBAF on silicagel (1.5 mmol/ 1g silicagel) was added. The solution was stirred during 30 minutes at room temperature.
Control by TLC (hexane/CH_2Cl_2 1:2) R_F =0.25. The reaction mixture was filtered to remove TBAF on silicagel and the amount of THF was reduced.
The solution of **15** in THF was degassed with a stream of argon for 15 minutes. A solution of unprotected and 4,4'-dimethoxytrityl (DMT)-protected 1,3-azidopropanol (**13** and **14**) was added together with sodium ascorbate and CuCl. The reaction mixture was heated to reflux and was stirred at 60°C over night. The reaction mixture turned from green to red.
The volumn was reduced and purification was done by column chromatography on aluminumoxid (CH_2Cl_2 + 2% MeOH).
The solvent was evaporated and the product was dissolved in a small amount of CH_2Cl_2. The product **17** was precipitated with hexane and 1% triethylamine to yield a red solid 37%.

TLC (CH_2Cl_2 + 2% MeOH) R_F =0.25.
^{1}H-NMR (300 MHz, THF-d_8): δ 10.27 (s, 2H), 9.40 (d, J=4.5 Hz, 4H), 9.21 (d, J=4.5 Hz, 4H), 8.62 (s, 1H), 8.52 (s, 1H), 7.56 (d, J=9 Hz, 2H), 7.42 (d, J=9 Hz, 4H), 7.26-7.21 (m, 2H), 7.12-7.09 (m, 1H), 6.81 (d, J=9 Hz, 4H), 4.96 (m, 2H), 4.88 (m, 2H), 4.05 (m, 1H), 3.84 (m, 2H), 3.47 (m, 2H), 2.58 (m, 2H), 2.42 (m, 2H).
^{13}C-NMR (300 MHz, THF-d_8): δ 159.57, 151.12, 150.34, 149.16, 148.97, 146.25, 136.94, 132.53, 132.46, 131.96, 131.91, 130.72, 128.9, 128.3, 128.26, 127.18, 113.64, 108.68, 106.29, 87.05, 84.53, 60.87, 59.05, 58.22, 55.03, 48.18, 47.79, 34.42, 31.82, 13.58.
EI-MS *m/z* = 488; MW = 926.35; $C_{51}H_{44}N_{10}O_4Zn$.

8. PAM protected 5,15-bistriazolylporphyrin **19**

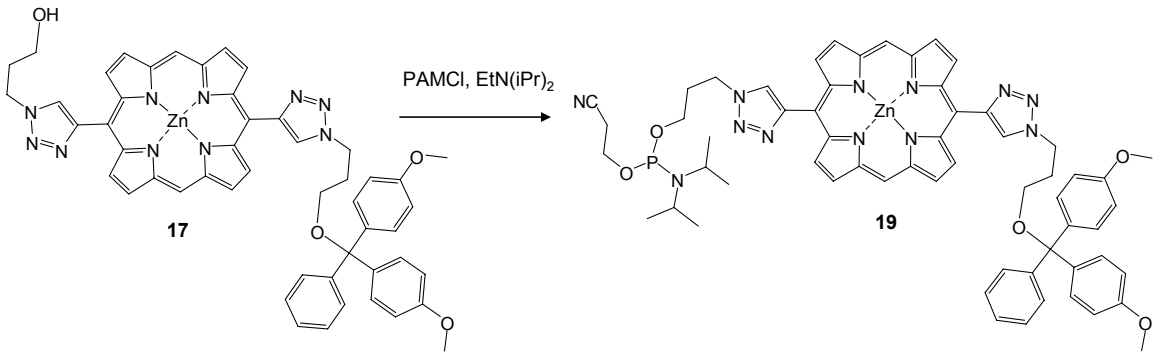

amount	name	data (g/mol)	mmol:	eq
50 mg	**17**	926.35	0.054	1
15,3 mg	PAM-Cl	236.68	0.065	1.2
0, 032 ml	Huenig's base	129.25	0.189	3.5
3 ml	CH_2Cl_2			

An oven-dried reaction-flask was degassed with a stream of argon.

PAM-Cl was added dropwise to a solution of **17** in anhydrous CH_2Cl_2 and huenig's base at room temperature under argon. The mixture was stirred for 1 hour at room temperature.

Purification was done by column chromatography on silica (ethyl acetate/ CH_2Cl_2 + 2% Et_3N 1:1). The solvent was evaporated and the product was dissolved in a small amount of (EtOAc/ CH_2Cl_2 + 2% Et_3N 1:1). The product **19** was precipitated with cyclohexane to yield a red solid 85%.

TLC (EtOAc/ CH_2Cl_2 + 2% Et_3N 1:1) R_F =0.3.

^{1}H-NMR (300 MHz, THF-d_8): δ 10.27 (s, 2H), 9.42 (d, J=4.5 Hz, 4H), 9.23 (d, J=4.5 Hz, 4H), 8.78 (s, 1H), 8.52 (s, 1H), 7.55 (d, J=9 Hz, 2H), 7.42 (d, J=9 Hz, 4H), 7.26-7.21 (m, 2H), 7.12-7.09 (m, 1H), 6.81 (d, J=9 Hz, 4H), 4.96-4.94 (m, 4H), 4.68 (m, 1H), 4.31 (m, 1H), 3.84 (m, 2H), 3.58 (m, 2H), 2.82-2.57 (m, 4H), 2.43 (s, 4H), 1.32 (m, 12H).

^{13}C-NMR (300 MHz, THF-d_8): δ 159.57, 151.3, 150.34, 149.16, 148.97, 146.25, 136.94, 132.53, 132.46, 131.9, 130.72, 128.9, 128.5, 128.26, 127.18, 113.5, 108.68, 106.29, 87.05, 84.54, 60.86, 59.05, 58.23, 55.03, 48.18, 47.79, 34.42, 31.82, 25.1, 20.3.

^{31}P-NMR (300 MHz, THF-d_8): δ 148.19.

EI-MS *m/z* = 488; MW = 1126.6; $C_{60}H_{61}N_{12}O_5PZn$.

9. Synthesis of 3-(5-hydroxypent-1-ynyl)benzaldehyde **20**

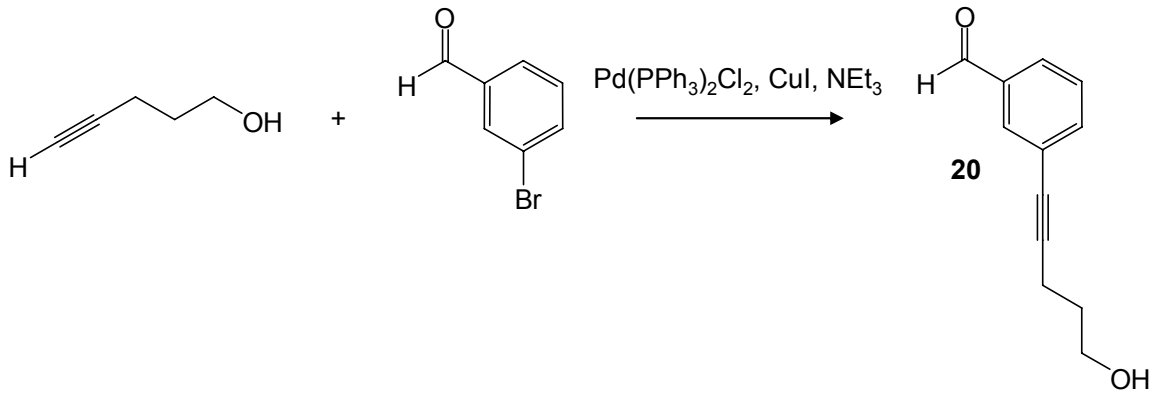

amount	name	data (g/mol)	mmol:	eq
3 ml	4-Bromobenzaldehyde	185	26	1
105 mg	$Pd(PPh_3)_2Cl_2$	702	0.15	0.006
55 mg	CuI	190	1.5	0.06
50 ml	triethylamine			
3 ml	4-pentyn-1-ol	84	31	1.2

4-Bromobenzaldehyde, $Pd(PPh_3)_2Cl_2$, and CuI were placed in a reaction flask which was thoroughly flushed with argon. Then triethylamine, followed by 4-pentyn-1-ol were added. The reaction mixture was stirred at 80°C during night. Then the mixture was cooled to room temperature, EtOAc was added and the grey precipitat was removed by filtration and the filtrate was concentrated. The product was purified by column chromatography and obtained in a yield of 40 % (Silica, EtOAc/hexane, 1:2).

TLC (EtOAc/hexane, 1:2) R_F =0.36.

^{1}H-NMR (300 MHz, $CDCl_3$): δ 9.97 (s, 1H), 7.88 (m, 1H), 7.76 (m, 1H), 7.61 (m,1H), 7.48 (m, 1H), 3.83 (m, 2H), 2.56 (m, 2H), 1.87 (m, 2H).

^{13}C-NMR (300 MHz, $CDCl_3$): δ 191.85, 137.29, 136.2, 133.05, 129.07, 128.56, 125.13, 91.38, 79.89, 61.74, 31.37, 16.05.

EI-MS *m/z* = 488; MW = 188.2; $C_{12}H_{12}O_2$.

10. Synthesis of 5, 15-bis 3-(5-hydroxypent-1-ynyl)phenylporphyrin **21**

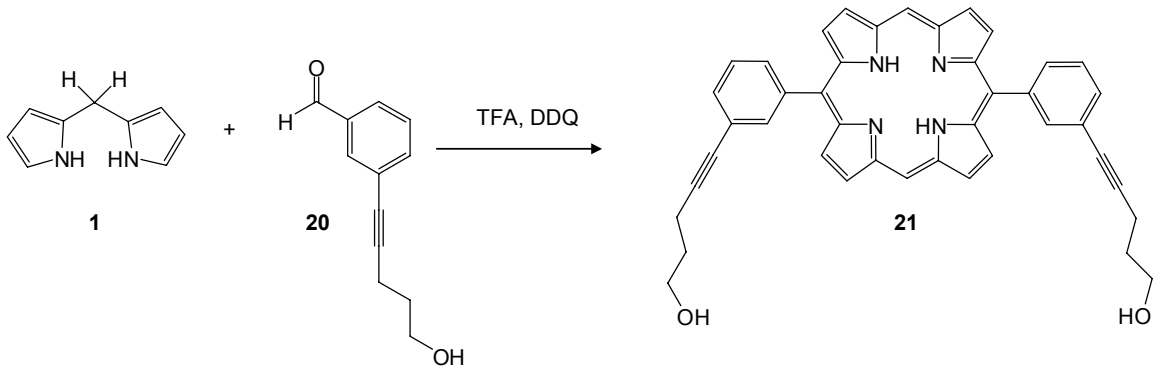

amount	name	data (g/mol)	mmol:	eq
0.5 g	**1**	146.2	3.42	1
0.64 g	**20**	188.2	3.42	1
0.45 ml	TFA	114	6.05	1.7
300 ml	CH_2Cl_2			
0.77 g	DDQ	227.0	3.42	1

Dipyrromethane **1** and 3-(5-hydroxypent-1-ynyl)benzaldehyde **20** were dissolved in CH_2Cl_2 (300 ml) in a reaction flask. TFA was added tropwise. The reaction mixture was stirred at room temperature during 2 hours. DDQ was added and the reaction mixture was stirred at room temperature during night.

The reaction mixture was filtered over a bed of aluminaoxide using CH_2Cl_2 + 4% MeOH to wash the product out of the aluminaoxide. The filtrate was concentrated and purified by flash chromatography on aluminaoxide.

The solvent was reduced and the precipitate was filtered to obtain compound **21** in a yield of 20%.

TLC (CH_2Cl_2 + 4% MeOH) R_F =0.3.

^{1}H-NMR (300 MHz, $CDCl_3$): δ 10.62 (s, 2H), 9.68 (d, J=4.71 Hz, 4H), 9.03 (d, J=4.68 Hz, 4H), 8.25 (m, 4H), 7.90 (m, 4H), 3.57 (m, 4H), 2.57 (m, 4H), 1.76 (m, 4H).

^{13}C-NMR (300 MHz, $CDCl_3$): δ 140.88 , 136.99, 134.09, 132.88, 131.04, 130.76, 127.74 , 122.43 , 117.72 , 106.00 , 91.29 , 80.52 , 59.49 , 31.55 , 15.53.

EI-MS *m/z* = 488; MW = 626.7; $C_{42}H_{34}N_4O_2$.

8.6 References

[1] M. Balaz, A.E. Holmes, M. Benedetti, G. Proni, N. Berova, *Bioorg. Med. Chem.* **2005**, *13*, 2413-2421.

[2] X.Zheng, R.K. Pandey, *Anti-cancer Agents in Medicinal Chemistry* **2008**, *8*, 241-268.

[3] M. Wainwright, *Anti-cancer Agents in Medicinal Chemistry* **2008**, *8*, 280-291.

[4] Ch.M. Drain, A. Varotto, I. Radivojevic, *Chem. Rev.* **2009**, *109*, 1630-1658.

[5] B.D. Berezin, *Coordination compounds of porphyrins and phthalocyanines* Wiley, **1981**.

[6] A.Mammana, T. Asakawa, K. Bitsch-Jensen, A.Wolfe, S. Chaturantabut, Y. Otani, X. Li, Z. Li, K. Nakanishi, M. Balaz, G. A. Ellestad, N. Berova, *Bioorg. Med. Chem.* **2008**, *16*, 6544-6551.

[7] K. Berlin, R.K. Jain, M.D. Simon, C. Richert, *J.Org.Chem* **1998**, *63*, 1527-1535.

[8] Moeales-Rojas, H. ; Kool, E. T. *Org.Lett.* **2002**, *4*, 4377-4380.

[9] M. Balaz, A.E. Holmes, M. Benedetti, P.C. Rodriguez, N. Berova, K. Nakanishi, G. Proni, *JACS* **2005**, *127*, 4172-4173.

[10] T. Murashima, K. Hayata, Y. Saiki, J. Matsui, D. Miyoshi, T. Yamada, T. Miyazawa, N. Sugimoto, *Tetrahedron Lettters.* **2007**, *48*, 8514-8517.

[11] L. A. Fendt, I.Bouamaied, S.Thöni, N.Amiot, E.Stulz, *JACS* **2007**, *129*, 15319-15329.

[12] M. Endo, M. Fujitsuka, T. Majima, *J.Org.Chem.* **2008**, *73*, 1106-1112.

[13] A.W.I. Stephenson, N. Bomholt, A.C. Partridge, V. V. Filichev, *ChemBioChem* **2010**, *11*, 1833-1839.

[14] S. Werder, V.L. Malinovskii, R. Häner, *Org. Lett.* **2008**, *10*, 2011-2014.

[15] C.Maeda, S.Yamaguchi, C.Ikeda, H.Shinokubo, A. Osuka, *Org.Lett.* **2008**, *10*, 549-552.

[16] D. K. Dogutan, M. Ptaszek, J. S Lindsey, *J.Org.Chem* **2007**, *72*, 5008-5011.

[17] J. K. Laha, S.Dhanalekshmi, M.Taniguchi, A. Ambroise, J. S. Lindsey, *Organic Process Research & Development* **2003**, *7*, 799-812.

[18] D-F. Shi, R. T. Wheelhouse, *Tetrahedron Letters.* **2002**, *43*, 9341-9342.

[19] J.W.Barnes, G. D. Dorough, *JACS* **1950**, *72*, 4045-4050.

[20] R. W. Wagner, T.E. Johnson, F.Li, J. S. Lindsey, *J.Org. Chem*.**1995**, *60*, 5266-5273.

[21] R. Schlözer, J.-H. Fuhrhop, *Angew. Chem*. **1975**, *10*, 388-389.

[22] T. E. O. Screen, K. B.Lawton, G. S.Wilson, N.Dolney, R. Ispasoiu, T.Goodson, S. J. Martin, D. D. C.Bradley, H. L. Anderson, *J.Mater. Chem*.**2001**, *11*, 312-320.

[23] P.D. Rao, S. Dhanalekshmi, B. J. Littler, J.S. Lindsey, *J.Org. Chem*. **2000**, *65*, 7323-7344.

[24] J.S. Lindsey, *Acc.Chem.Res.* **2010**, *43*, 300-311.

[25] G.R. Geier III, B. J. Littler, J.S. Lindsey, *J. Chem. Soc. Perkin.Trans.* **2002**, *2*, 701-711.

[26] B. J. Littler, Y. Ciringh, J.S. Lindsey, *J.Org. Chem*. **1999**, *64*, 2864-2872.

9. Conclusions

The studies presented in this work showed that a DNA stem is not required for the structural organization of pyrene units, which are linked via a flexible phosphodiester backbone. The performed experiments showed that the achiral oligomers containing 7 pyrene units have an intrinsic property to self-assemble into directional, well-defined aggregates.

Evidence for the formation of supramolecular polymers was found by the observation of amplification of chiraltiy within the pyrene stacks by adding a small amount of pyrene oligomer containing a single 2'-deoxycytidine **Py_7-C**. Exciton-coupled CD spectra revealed a helical nature of the polypyrene aggregates. The helical chirality is the result of a twisted arrangement of stacked pyrene units along the propagating helical axis. Without chiral source, they are present as a racemic mixture.

Temperature dependent measurements showed that **Py_7** assemble via a nucleation-elongation mechanism. The observed effects mentioned above support the model of cooperative interaction within the pyrene oligomers leading to rod-like assemblies.

Further, the influence of nucleotides on the aggregation of **Py_7** was studied. Mono- and di-substituted nucleotide analogs (**Py_7-N** and **N-Py_7-N**, **N=** A, G, T, C) have been synthesized for this purpose. The results showed that a single nucleotide may be sufficient for the fine tuning of the aggregates' properties by changing the mechanism of aggregation from *nucleation-elongation* to *isodesmic*.

It could be shown that the attached nucleotides can shift the equilibrium of the formed racemic supramolecular polymers towards one of the two enantiomeric helices. Oligomers **2** (Py_7-C), **3** (C-Py_7), **5** (Py_7-G), **7** (G-Py_7-G) and **11** (Py_7-A) induce formation of one of the enantiomers, which was detected by CD-spectroscopy. The data show that the formation of supramolecular polymers of oligopyrenotides is very sensitive to the nature of chiral auxiliaries, in this case attached natural nucleotides. Watson-Crick complementarity play no significant role, since co-aggregates of oligomers modified with complementary nucleotides showed no signs of supramolecular polymerization.

In addition to the data obtained from UV/Vis, fluorescence and CD spectroscopy, gel mobility experiments and electron microscopy support a model in which pyrene

oligomers form helical, supramolecular polymers through interstrand stacking interactions.

Further AFM measurements were carried out and proved to be a very useful technique for further investigation of the properties of supramolecular polymers, like structure and their mechanisms of self-assembly. Small fractions of long aggregates, even in a pool of monomeric building blocks and other types of weakly associated aggregates, could be detected with the AFM technique, whereas optical techniques reach the limits of detection.

Based on the thickness of ca. 2.4 nm, obtained by AFM measurements, we can propose that the **Py_7** oligomers form a quasi-one dimensional helical structure. The negatively charged phosphate backbones support a moderate stiffness of the rod-like aggregates and seem to prevent interhelical aggregation. With an inner core of stacked aromatic units and a phosphate backbone on the outside, the **Py_7** polymers might be regarded as structural relatives of nucleic acids.

Further, it could be shown that the designed supramolecular polymers can be used as a template for the organization of ligands. This was tested using the H_2TMPyP ligand, which is well known to interact with DNA, as it is described in literature. The spectroscopic data showed similar characteristics like the interaction of H_2TMPyP with poly-d(AT). This could be regarded as a further proof for structural similarities between DNA and the described supramolecular polymers.

Compared to other systems which form supramolecular polymers and are presented in the introduction, the system described here is build up with a new type of oligomeric building blocks forming supramolecular polymers. The preferential helicity of the supramolecular polymers is realized through the introduction of natural nucleotides attached to the pyrene oligomers. It represents another class of molecules and is different from the approach of other systems, using chiral peripheral substituents at the aromatic stacking units.

10. Outlook

The formation of supramolecular polymers by oligomers containing 7 pyrene units is an interesting and unexpected observation. Still there are questions which are not yet answered, concerning the formation of the polymers. The influence of temperature on the kinetics of the formation of the polymers could be an interesting topic for further experiments. Concentration limits for the formation of supramolecular polymers are not yet known. The results obtained show that the ionic strength has a strong impact on the organization of the hydrophobic interaction and also on the formation of supramolecular polymers.

The experiments were all carried out using 1M sodium chloride. The investigation of different sodium chloride concentrations in order to detect the limit of stacking interactions could be interesting. In relation to the binding of functional molecules, a lower salt concentration could be explored to increase the interaction to the supramolecular polymers. In literature it is reported from experiments that the binding constant of cationic porphyrins to DNA decrease by increasing salt concentration. Stronger interaction could also enhance the observed energy transfer effects. Other ligands could be tested in order to expand the suitability of the described supramolecular polymers concerning the templating behavior.

The “sergeant-and-soldiers” experiments, and the observed amplification of chirality, showed the high sensivity of the supramolecular polymers on their chiral environment. Their application as a chiral sensor could be further tested, for example, by using chiral solvents or by the addition of chiral compounds and ligands instead of the modified pyrene-oligomers.

For this system 2,8-dicarboxamide pyrene units have been used. The use of other aromatic compounds could be intersting also. For example pyrene with alkynyl linkers, porphyrins, perylenediimides, and others could be used. If so, could the formation of supramolecular polymers still be observed? Could different synthesized oligomers be mixed?

An interesting investigation would be to find aromatic compounds which show selective recognition. Does recognition of different aromatic compounds occur similar to those we find in DNA and its bases? In addition to the DNA-like supramolecular polymers described in this work, artificial codes based on, for example, differences in aromatic

stacking properties could be of interest and could lead to artificial DNA-like assemblies with recognition properties.

9. Appendix

9.1 Abbreviations

DNA	deoxyribonucleic acid
A	adenosine
G	guanosine
T	thymidine
C	cytidine
CD	circular dichroism
H_2TMPyP	tetrakis(4-N-methyl-pyridyl)porphine
nm	nanometer
Fe(III)	iron (III)
Co(III)	cobalt (III)
Mn(III)	manganese (III)
Zn(III)	zinc (III)
TTF	tetrathiafulvalene
TEM	transmission electron microscopy
CEP	2-cyanoethyl-*N*,*N*-diisopropylphosphoramidite
DMT	4,4'-dimethoxytrityl
UV/Vis	ultraviolet visible
I	intensity
NaCl	sodium chloride
em	emission
conc.	concentration
LD	linear dichrosim
LC-MS	liquid chromatography/ mass spectrometry
ESI-TOF	electrospray ionization/ time-of-flight
AFM	atomic force microscopy
Ni	nickel (II)
isod	isodesmic

nucl.	nucleation
PDT	photodynamic therapy
Mg	magnesium
$InCl_3$	indium chloride
NaOH	sodium hydroxyde
Cu	copper
THF	tetrahydrofuran
TFA	trifluoroacetic acid
$Pd_2(dba)_3$	tris(dibenzylideneacetone)dipalladium(0)
PPh_3	triphenylphosphine
DDQ	2,3-Dichloro-5,6-dicyano-1,4-benzoquinone
TBAF	tetra-n-butylammonium fluoride
CuCl	copper (I) chloride
OD	optical density
HPLC	high-performance liquid chromatography
CuI	copper(I) iodide
NMR	nuclear magnetic resonance
CH_2Cl_2	dichloromethane
DMF	dimethylformamide
$POCl_3$	phosphorus oxychloride
NH_4Cl	ammonium chloride
R_F	retention Factor
DBU	1,8-Diazabicyclo[5.4.0]undec-7-ene
$MgBr_2$	magnesium bromide
MeOH	methanol
n-BuLi	n-Butyllithium
$NaHCO_3$	sodium hydrogencarbonate
BF_3*Et_2O	boron trifluoride
TLC	thin layer chromatography
NaN_3	sodium Azide
Et_3N	triethylamine
$Pd(PPh_3)_2Cl_2$	bis(triphenylphosphine)palladiumchloride
$CDCl_3$	deuterated chloroform
D_6-DMSO	deuterated dimethyl sulfoxide

Curriculum Vitae

First name: Alina Laura

Family name: Nussbaumer

Date and place of birth: 28.8.1984, Bern, Switzerland

Address: Kirchweg 10, 3122 Kehrsatz, Switzerland

E-Mail: alina.nussbaumer@ioc.unibe.ch

Education:

1991-2000	Primary and secondary school in Kehrsatz, Switzerland
2000-2003	High school, Köniz Lerbermatt, Switzerland
2003	High school degree with main focus in biology and chemistry

2003-2006 Undergraduate studies in Biochemistry at the Department of Chemistry and Biochemistry, University of Bern, Switzerland

Degree: Bachelor of Science in Biochemistry and Molecular Biology

Supervisor: Prof. Dr. Ch. Leumann,

Thesis title: “Synthesis towards [5.3.0.0] Tricyclo-DNA”

2006-2007 **Master degree**: Molecular Life Sciences with main focus in Biochemistry and Chemical Biology

Supervisor: Prof. Dr. R. Häner,

Thesis title: “Synthesis and biological activity of methoxysubstituted furopyranones in human cancer cells”

Department of Chemistry and Biochemistry, University of Bern, Switzerland

February 2008-current

Ph.D. Thesis in Chemistry and Molecular Sciences
"Self-assembly of oligopyrenotides – from DNA to supramolecular polymers"
Supervisor: Prof. Dr. Robert Häner,
Department of Chemistry and Biochemistry, University of Bern, Switzerland

Teaching and Scientific experience

2008 Supervisor of a Master student in organic chemistry, University of Bern

2008-2010 Supervisor of apprentice in chemistry 3rd year, University of Bern

2008-2011 Practical supervisor 1st and 3rd year students in organic chemistry, University of Bern

Publications:

1. "**Amplification of chirality by supramolecular polymerization of pyrene oligomers**"
   Alina L. Nussbaumer, Daniel Studer, Vladimir L.Malinovskii and Robert Häner;
   Angew.Chem.Int.Ed. **2011**, *50*, 5490-5494
   This article was featured in CHIMIA **2011**, *65*, No.9 as an interesting publication of Swiss origin.

2. "**Oligopyrenotides: Chiral nanoscale templates for chromophore assembly**"
   Vladimir L. Malinovskii, Alina L. Nussbaumer and Robert Häner
   manuscript in preparation

3. "**Stereochemical control of supramolecular pyrene polymers**"
   Alina L. Nussbaumer, Florent Samain, Vladimir L. Malinovskii and Robert Häner
   manuscript in preparation

4. "**Cooperative and non-Cooperative assembly of oligopyrenotides resolved by atomic force microscopy** "
Alexander V. Rudnev, Vladimir L. Malinovskii, Alina Nussbaumer, Artem Mishchenko, Thomas Wandlowski, Robert Häner
manuscript in preparation

Skills and techniques:

Synthesis of organic compounds, automated DNA synthesis
Purification and characterization of products: NMR, MS, HPLC, PAGE,
Fluorescence, UV/Vis and CD spectroscopy

Software
ChemOffice, IsisDraw, Microsoft Office, Scifinder, Beilstein

Languages:

German: Native speaker
English: Advanced level/Fluent
French: Advanced level
Italian: Basic level